CHARACTERIZATION OF THE CELL WALL INTEGRITY MAPK PATHWAY IN *FUSARIUM GRAMINEARUM*

DIANEVYS GONZALEZ-PEÑA FUNDORA
Master in Microbiology, University of Havana, 2011

A thesis submitted
in partial fulfilment of the requirements for the degree of

DOCTOR OF PHILOSOPHY

in

BIOMOLECULAR SCIENCE

Department of Chemistry and Biochemistry
University of Lethbridge
LETHBRIDGE, ALBERTA, CANADA

CHARACTERIZATION OF THE CELL WALL INTEGRITY MAPK PATHWAY IN *FUSARIUM GRAMINEARUM*

DIANEVYS GONZÁLEZ-PEÑA FUNDORA

Date of defence: July 4th, 2022

Dr. N. A. Foroud	Research Scientist	Ph.D.
Dr. N. Thakor	Professor	Ph.D.
Thesis Co-Supervisors		
Dr. I. Kovalchuk	Professor	Ph.D.
Thesis Examination Committee Member		
Dr. D. Yevtushenko	Professor	Ph.D.
Thesis Examination Committee Member		
Dr. A. Laroche	Research Scientist	Ph.D.
Thesis Examination Committee Member		
Dr. E. Schultz	Professor	Ph.D.
Internal External Examiner		
Department of Biology, University of Lethbridge		
Dr. A. Di Pietro	Professor	Ph.D.
External Examiner		
Universidad de Córdoba, Spain		
Dr. M. Gerken	Professor	Ph.D.
Chair, Thesis Examination Committee		

Abstract

In the fungal phytopathogen *Fusarium graminearum*, the core of the mitogen-activated protein kinase (MAPK) cascade known as the cell wall integrity (CWI) pathway is formed by Bck1 (MAPKKK), Mkk1/2 (MAPKK) and Mgv1 (MAPK). Rlm1 is the only target that has been suggested for Mgv1. The objective of this thesis was to generate and characterize *F. graminearum* transformants that produce a high abundance of a phosphorylated Mgv1 protein that could be used in future assays for screening its candidate targets. *MGV1 in locus* constitutive overexpression increased the amounts of the Mgv1 phosphorylated protein, and did not cause phenotypical changes. *MKK1*^{197E,203E} *in locus* constitutive overexpression inhibited the expected continuous Mgv1 phosphorylation, and negatively affected mycelial growth and virulence. In addition, *MKK1*^{197E,203E}_OX strains showed increased resistance to osmotic stress, and higher abundance and phosphorylation of another MAPK (Hog1), opening questions regarding the cross-talk between the CWI and the HOG MAPK pathways.

Acknowledgements

I would like to express my deepest gratitude to my supervisor Dr. Nora Foroud for providing an awesome topic, and for her guidance and encouragement throughout all these years. I am very grateful to also had Dr. Nehal Thakor as a co-supervisor, whose suggestions and comments were greatly appreciated, as well as the fruitful discussions that were frequently held in his lab meetings. It has been a great learning experience working in both lab groups.

Thanks to the committee members: Dr. André Laroche, Dr. Igor Kovalchuck and Dr. Dmytro Yevtushenko for their advice, corrections and suggestions for improving my performance during this tenure. And thanks to all their lab members that were extremely helpful when I needed to use their locations and devices for some of the experiments.

Thanks, Dr. Elizabeth Schultz and Dr. Antonio Di Pietro, for kindly accepting being the external examiners of the thesis, and for the discussion generated during the final examination.

Thanks to my current and past labmates: Dr. Anas Eranthodi, Dr. Daria Ryabova, Clinton Dovell, Connor West, Mika Vivar, Marshall Smith, Daniel Gaudet, Janelle Veenendaal, Kristi Turton, Jocelyn Heather, Reyhaneh Pordel, Dr. Ravinder Goyal, Susan Stasiuk, Youngyoung Lee and Rexelle Asis. It has been a pleasure working with you! My indebtedness to Anas for sharing his knowledge, kindness, and patience with me during all these years!

I am grateful to Dr. Thakor's lab members, and especially to Divya Sharma, Dr. Joseph Ross, Keiran Vandendungen, Rachana Muley, Keith Aubrey, Kamiko Bressler, Prakash Chukka, Nirujah Balasingam and Veda Hegde, for their technical discussions and advice.

My sincere appreciation to my colleagues and friends at AAFC-Lethbridge for their constant support and professional assistance: Michele Cradduck, Gabriella Araujo, Eric Amundsen, Michele Frick, Salina Kaphle, Tara Vucurevich, Dr. Fengying Jiang, Kimberly Burton-Hughes,

Dr. Gaganpreet K. Dhariwal, Dr. Raman Dhariwal, Dr. Mohamed Hafez, Dr. Priti Maheshwari and Dr. Andriy Bilichak. Thanks to Dr. Rodrigo Ortega, Gale Chen and Dr. Nathaniel Zhin-Loong for the bioinformatics support, and Dr. Timothy Schwinghamer for the statistical advice. A big thanks to the AAFC greenhouse staff for taking care of my precious plants.

Thanks to Dr. Chris Rampitsch, Dr. Gopal Subramaniam, Dr. Kristina Shostak, Dr. Michelle Loewen, and Dr. Loewen's Ph.D. students Pooja Sridhar and Tanya Sharma for their collaboration in different projects, and their professional discussions and suggestions.

I would like to acknowledge the University of Lethbridge for their continuous support. Thanks to the University librarian Rumi Graham, who offered an awesome assistance with matters of references and copyright, to Susan Hill for her help with departmental subjects, and to the School of Graduate Studies (S.G.S.) staff for their guidance. My full gratitude to Karis Dykstra, Graydon Burbank and Claire Brodrick, for their great work as international student advisors.

I am very grateful for the funds received from the Canadian Phytopathological Society, as well as those received through the University of Lethbridge, such as the Alberta Innovates - Technology Futures Graduate Student Scholarship, the S.G.S. Fellowship Award, the S.G.S. International Tuition Award, the Coca-Cola Award, and the Graduate Assistantships. It was an honour receiving these scholarships/awards.

It has been awesome also sharing this time with the AAFC-Latin club friends: Diana Wilches, Danisa Bescucci, Maximo Lange, Dr. Hector Cárcamo, Dr. Sara Andrés, Dr. José Ortiz, Dr. Carlos Romero, and the one and only: Jose Barbieri. Gracias a todos!

Last, but not least, a huge thanks to my family; my lovely husband Yanier, my mum Rosa, and my sister Dianelys for all their support, patience and encouragement through these years; without you, this journey will not have been possible. Love you all!

Table of Contents

List of Tables

List of Figures

List of Abbreviations

3-ADON	3-acetyldeoxynivalenol
15-ADON	15-acetyldeoxynivalenol
AAFC	Agriculture and Agri-Food Canada
ANOVA	Analysis of variance
ATP	Adenosine triphosphate
BCK1	Bypass of C kinase
Bd21	*Brachypodium distachyon* 21
BIN2	brassinosteroid-insensitive 2
BME	β-mercaptoethanol
BPB	Bromophenol blue
BSA	Bovine serum albumin
cAMP	Cyclic adenosine monophosphate
CDK	cyclin-dependent kinase
cDNA	Complementary deoxyribonucleic acid
CFW	Calcofluor white
CHS	Chitin synthase
CMC	Carboxymethylcellulose medium
CR	Congo red
CWI	Cell wall integrity
DEG	Differentially expressed genes
DNA	Deoxyribonucleic acid
DON	Deoxynivalenol
dpi	Days post inoculation
EDTA	Ethylenediaminetetraacetic acid
ERK	Extracellular signal-regulated kinase
FA	Fusaric acid
FHB	Fusarium head blight
FPP	Farnesyl pyrophosphate
gDNA	Genomic deoxyribonucleic acid
GEF	Guanine exchange factor
GPCR	G-protein-coupled receptor
GPMK1	*Gibberella* pathogenicity mitogen-activated protein kinase 1
GSK3	Glycogen kinase synthase 3/Shaggy-like kinase
GTP	Guanosine-5'-triphosphate
GYEP	Glucose, yeast extract, peptone medium
HOG	High osmolarity glycerol
HPLC	High performance liquid chromatography
HRP	Horseradish peroxidase
HSD	Honestly significant difference
LDS	Lithium dodecyl sulfate
MAPK	Mitogen-activated protein kinase
MAPKK	Mitogen-activated protein kinase kinase
MAPKKK	Mitogen-activated protein kinase kinase kinase

MCM1	Minichromosome maintenance 1
MeOH	Methanol
MGV1	Mycelial growth and virulence 1
MIG1	MADS-box protein required for infectious growth 1 gene
MKK1	Mitogen-activated protein kinase kinase 1
MOPS	3-(N-morpholino)propanesulfonic acid
NaCl	Sodium chloride
NPN	Non-preferred nutrient
NRP	Non-ribosomal peptide
NRPS	Non-ribosomal peptide synthetase
OA	Oxalic acid
ORA	Over-representation analysis
OX	Overexpression
PAK	p21-activated kinase
PAS	Per-Arnt-Sim
PCA	Principal component analysis
PCR	Polymerase chain reaction
PDA	Potato dextrose agar
PDB	Potato dextrose broth
PKC1	Protein kinase C
PKS	Polyketide synthase
PN	Preferred nutrient
PVDF	Polyvinylidene difluoride
qPCR	Quantitative polymerase chain reaction
RCF	Relative centrifugal force
RNA	Ribonucleic acid
rpm	Revolutions per minute
RT	Reverse transcriptase
RT-qPCR	Reverse transcription-quantitative polymerase chain reaction
SBF	*SWI4/6* cell cycle box (SCB) binding factor
SDS	Sodium dodecyl sulfate
Slt2	Suppressor of the LyTic phenotype 2
SNA	Synthetic nutrient agar
SRF	Serum Response Factor
Ste	Sterile
TBS	Tris-buffered saline
TBST	Tris-buffered saline-Tween20
TF	Transcription factor
USER	Uracil-Specific Excision Reagent
WSC	Cell wall integrity and stress response component
WT	Wild-type
Y2H	Yeast two-hybrid
YPD	Yeast peptone dextrose

Chapter 1. Literature review

1.1. Introduction

Wheat is a cereal widely consumed by humans and animals. It is cultivated around the world because of its high nutritional value, the plasticity of its grain for being processed into several products and its adaptability to different environments (Shewry, 2009). Common wheat (*Triticum aestivum* L.) and durum wheat (*Triticum durum* Desf) are among the most cultivated wheat varieties. Global wheat production was estimated at 772 million metric tons in 2017, where Canada was positioned in seventh place, having produced around 30 million metric tons (https://worldpopulationreview.com/country-rankings/wheat-production-by-country) (statcan.gc.ca).

Fusarium head blight (FHB) is a devastating fungal disease that affects cereal crops, including wheat, barley (*Hordeum vulgare* L.) and oat (*Avena sativa* L.). *Fusarium species* are the causal agents, and some of them produce trichothecene mycotoxins, such as deoxynivalenol (DON), that negatively affect the quality of the kernels, which can shrink and change its colour. Grains contaminated with mycotoxins are unsuitable for human and animal consumption, since trichothecenes are harmful for mammals in a dose-dependent manner. Globally, including Canada, the economical losses caused by FHB are highly significant.

F. graminearum is one of the primary causative agents involved in FHB, though other species are also involved (Wegulo *et al*., 2015; Dweba *et al*., 2017; Valverde-Bogantes *et al*., 2020). For example, *F. graminearum* has been the most frequently observed FHB causative agent in North America and other places around the world (Goswami and Kistler, 2004). In Canadian provinces, while *F. graminearum* had the highest frequency among the *Fusarium* species

identified as causing FHB, other species, such as *F. poae*, *F. avenaceum* and *F. culmorum* are becoming increasingly problematic in Western Canada (Canadian Plant Disease Survey, 2020; Hafez et al., 2022).

1.2. *Fusarium graminearum* features and taxonomy

Fusarium graminearum Schwabe (1839) is an ascomycete that has *Gibberella zeae* (Schwein.) Petch, (1936) as its teleomorph. Ascomycetes are also known as "sac fungi" because of its defining feature to form "ascus" (which means "sac" in Greek) in most of their species. Inside the ascus, their sexual spores (ascospores) are formed. The taxonomy of *F. graminearum* can be found in the web Mycobank (https://www.mycobank.org/) as:

Kingdom: Fungi
Subkingdom: Dikarya
Division: Ascomycota
Subdivision: Pezizomycotina
Class: Sordariomycetes
Subclass: Hypocreomycetidae
Order: Hypocreales
Family: Nectriaceae
Genus: *Fusarium*
Species: *F. graminearum*

The genus *Fusarium* is characterized by a septated hyaline mycelium and the formation of three types of asexual structures: microconidia, macroconidia and chlamydospores; however, only macroconidia and sometimes chlamydospores are formed in *F. graminearum*.

F. graminearum macroconidia are multicellular, hyaline, half moon shaped spores with usually 3-5 septa, and a foot cell from which is attached to the phialide (Harris, 2005). When conditions are favourable, the macroconidia germinates primarily from the apical cells in a

bipolar pattern (Harris, 2005). Factors, such as relative humidity, temperature, pH, availability of nutrients and light, can interfere with this process (Beyer *et al*., 2004).

Chlamydospores are globose structures with a thick and multilayer cell wall that ensures survival of fungi under stress conditions. They are formed from macroconidia, germinated macroconidia or hyphae, where a single macroconidia can produce more than one chlamydospore (Li *et al*., 1998). When the environmental conditions are optimal for germination, the germ tube emerges from the inner cell wall of the chlamydospores, and previous studies have shown that some chlamydospores formed by *F. graminearum* were able to infect wheat plants even after 500 days in the soil (Nyvall, 1970).

F. graminearum is the asexual stage (anamorph) of this fungus, while *G. zeae* is the sexual phase (teleomorph). *G. zeae* is an homothallic species, which means it does not require the presence of another mating type to form sexual structures. Ascospores are sexual, hyaline and with 3 septa structures, grouped in 4-8 inside the ascas in the perithecia. Perithecia are dark spherical resistant structures overwintering in plant debris or soil from season to season that provides ascopores as inoculum source for new infections.

1.3. *F. graminearum* life cycle and FHB symptoms

F. graminearum is considered the main causal agent of FHB in North America and other places (Goswami and Kistler, 2004; McMullen *et al*., 2012). This pathogen can infect wheat heads at any stage, from anthesis (presence of florets) until the phase where kernels are completely filled (Alisaac *et al*., 2021). During anthesis, the most susceptible plant stage to infection, the opened florets and the extruded anthers offer an easy fungal penetration point and a source of nutrients for spore germination (Del Ponte *et al*., 2007). As a result of the infection, florets may become sterile, grains will be atrophied and/or not completely filled, the spike

becomes bleached, and purple or pinkish coloration could appear in spikelets and rachis due to the presence of the perithecia structures and mycelia (Sutton, 1982; McMullen *et al*., 2012). This pathogen is also able to penetrate plant tissues through natural openings, such as stomata (Pritsch *et al*., 2000; Nguyen *et al*., 2016), or through injured tissue (Cuzick *et al*., 2008; Yin *et al*., 2018a).

Crop residues from previously infected materials are the main source of *F. graminearum* inoculum. The fungal structures are harboured in the stalks, stems, dried leaves and soil until new hosts and environmental conditions are favourable to their germination. Temperature and humidity are key factors in the development and spread of *Fusarium* inoculum that causes FHB disease. Hyphal fragments and reproductive structures, such as ascospores, macroconidia, and chlamydospores are considered the main inoculum source, which are highly produced under warm and high humidity conditions (Sutton, 1982). The temperatures required for the development of these structures usually ranges from 5 to 35°C, but the optimum are around 25-32°, depending on the structures (Sutton, 1982). Once the environmental conditions are optimal, perithecia release the ascospores, which will become the main inoculum source for the next season (Son *et al*., 2012). Ascospores are primarily dispersed by the wind, and often during the nights when humidity levels are high (Sutton, 1982).

1.4. Brief history of FHB outbreaks

FHB is caused by *Fusarium* species, such as *F. graminearum, F. poeae, F. avenaceum, F. asiaticum, F. culmorum, F. meridionale, F. pseudograminearum* and *F. langsethiae* (Wegulo *et al*., 2015; Dweba *et al*., 2017; Valverde-Bogantes *et al*., 2020) with some of these species grouped into the *F. graminearum* species complex (FGSC) (van der Lee *et al*., 2015; Walkowiak *et al*., 2016). *Fusarium* population is dynamics and the main causal agent can change over the

time and space due to fluctuations in environmental conditions, changes in their hosts due to variations in crop productions in different regions, and introduction of imported FHB causal agents, among other factors (Valverde-Bogantes *et al*., 2020).

FHB was first described in England in 1884 by W.G Smith, and was later described in North America by F. D. Chester in 1890 and J. C. Arthur in 1891 (reviewed in Wegulo *et al*. (2015)). Weather conditions, such as warm temperatures and high humidity levels have been associated with several epidemics of FHB in wheat that have been reported since the early 1900s in Canada (Sutton, 1982). Sutton (1982) describes the period of 1927-1980 as a term characterized by sporadic epidemics of FHB in almost every place in Canada with wheat crops. In 1980, there was a severe outbreak in Ontario, Quebec and the Maritime Provinces affecting winter and spring wheat cultivars. Rain delayed the harvest for 2-4 weeks and the grain was not completely dry, which caused sprouting in the spikes, which also showed pinkish mycelium, with grains containing DON mycotoxin (Sutton, 1982).

In the first decade of the 21st century, it was shown that the strains that produce the mycotoxin 15-acetyl DON (15-ADON), which were the predominant chemotype in Western Canada, had shifted to the 3-acetyl DON (3-ADON) chemotype (Ward *et al*., 2008), while in other regions, such as Southwestern Ontario, 15-ADON continued to be the main chemotype (Tamburic-Ilincic *et al*., 2015). This change in some provinces concerned farmers and researchers, since the 3-ADON tends to produce more DON than the endemic 15-ADON chemotypes (Ward *et al*., 2008; Puri and Zhong, 2010), and causes more disease, depending on the infected wheat cultivar (Puri and Zhong, 2010; Foroud *et al*., 2012). However, Ward *et al*. (2008) did not observe a difference in pathogenesis between 3-ADON and 15-ADON isolates after spray inoculation. According to Puri and Zhong (2010), these apparently contradictory

outcomes could be the results of a different method of plant inoculation (point *vs* spray). In addition Serajazari *et al*. (2019), also showed that no difference in wheat infection regarding chemotype was observed in resistant cultivars carrying the *Fhb1* quantitative trait *locus* (which showed less symptoms than the other cultivars) when the plants were point inoculated. However, 3-ADON producing isolates were about 18 % more aggressive than 15-ADON when spray inoculated, confirming the significance of the type of inoculation when studying the interaction with the cultivar and the *F. graminearum* chemotype.

1.5. Secondary metabolites

Secondary metabolites (SMs) are low-molecular weight compounds produced by microorganisms and plants. They are unessential for the survival of the organism that produces it, but they play an evolutionary role in adaptation to different ecological niches. SMs are diverse and can provide significant advantages due to their diverse properties as antibiotics, siderophores or mycotoxins, which will allow the producer to compete for nutrients in diverse environments, as well as to colonize and establish in new spaces or tissues (Fleming, 1929; Proctor *et al*., 1995a; Kramer *et al*., 2020). Some of the most significant groups of secondary metabolites in fungi, and in particular in *F. graminearum*, are non-ribosomal peptides (NRPs), polyketides and terpenes.

1.5.1 Non-ribosomal peptides (NRPs)

Non-ribosomal peptides (NRPs) are diverse compounds synthesized by multi-modular non-ribosomal peptide synthetases (NRPSs). NRPSs possess different modules with catalytic domains that will both initiate the formation and continue the elongation of the peptide chain. The substrate is recognized by the adenylation (A) domain which is involved in the recognition and activation of the starter amino acid. A peptide acyl carrier domain (T or PCP) transfers the aminoacyl to the condensation (C) domain where the peptide bond is formed (reviewed in

Hansen *et al*. (2012)). Other domains that might be present in the module are the epimerization (E), a thioesterase (TE) and a reductase (R) domain. Some NRPs are antibiotics, siderophores, pigments or toxins and they can help to facilitate pathogenesis in certain microorganisms. For example, gramillins and fusaoctaxin A are the product of the gene clusters *NRPS8* and *NRPS5*/*NRSP9*, respectively, and both peptides are considered virulence factors in *F. graminearum* (Bahadoor *et al*., 2018; Jia *et al*., 2019).

1.5.2 Polyketides

Polyketides are a large and diverse group of secondary metabolites produced by many microorganisms, including *Fusarium* species. Polyketides are derived from a molecule consisting of a ketone and methylene groups, and its biosynthesis is similar to that of fatty acids biosynthesis, and involves the activity of polyketide synthases (PKSs). These compounds posses wide uses in different industries (Ridley and Khosla, 2009). For instance, antibiotics (tetracycline and azithromycin), antifungals (amphotericin and nystatin), and a cholesterol lowering agent (lovastatin) are some of the many examples of the use of these compounds in medicine. Some polyketide examples in *F. graminearum* are the pigment aurofusarin, the mycotoxin zearalenone, and fusarin C (Table 1.1).

Table 1.1. List of Polyketide synthases (PKS), based on Hansen *et al*. (2015).

Polyketide synthases (PKS)	Metabolite	References
PKS1		
PKS2		
PKS3	black/purple perithecial pigment (Fusarubins)	(Gaffoor *et al*., 2005; Frandsen *et al*., 2016)
PKS4	Zearalenone	(Kim *et al*., 2005b; Gaffoor and Trail, 2006)
PKS5		
PKS6	Fusaristatin A	(Sørensen *et al*., 2014)
PKS7		
PKS8	Gibepyrones and Prolipyrone B	(Westphal *et al*., 2018b)
PKS9 (FSL1)	Fusarielins	(Sørensen *et al*., 2012)
PKS10	Fusarins	(Gaffoor *et al*., 2005)
PKS11		
PKS12	Aurofusarin	(Frandsen *et al*., 2006)
PKS13	Zearalenone	(Kim *et al*., 2005b; Gaffoor and Trail, 2006)
PKS14	Orcinol	(Jørgensen *et al*., 2014)
PKS15		
PKS52		

1.5.3 Terpenes (Trichothecenes and *TRI* genes)

Trichothecenes are a group of toxic secondary metabolites produced by certain species of Fungi. These toxins bind to the A-site in the peptidyl transferase center of the 60S ribosome, thereby inhibiting protein synthesis in eukaryotic systems (Cundliffe *et al*., 1974; Garreau de Loubresse *et al*., 2014). Structurally, the trichothecenes are sesquiterpenoids with multiple fused rings. They possess a double bond in the position 9-10, and a 12, 13-epoxide group that is essential for toxicity ((Wei and McLaughlin, 1974), reviewed in (Kimura *et al*., 2007; Foroud *et al*., 2019)). Functionality varies at positions C3, C4, C7, C8, C15 with more than 200 types having been identified (reviewed in (Kimura *et al*., 2007; Foroud *et al*., 2019)). Based on specific structural features, trichothecenes are divided into 4 main types: type A, B, C and D, with

Fusarium species producing type A and B trichothecenes (Kimura *et al*., 2007; Foroud *et al*., 2019).

Type A trichothecenes, which carry a single bond at position C8, comprises a group of toxins, such as diacetoxyscirpenol (DAS), HT-2 toxin, NX-2, NX-3 and T-2 toxin. Exposure to T-2 toxin can result in "alimentary toxic aleukia" (ATA), a syndrome characterized by leukopenia (decrease in the number of white blood cells), bleeding disorders, vomiting, diarrhea, skin inflammation, gastroenteritis, subcutaneous hemorrhaging and ataxia (Pinto *et al*., 2013). This condition can be fatal and it is suggested to be the cause of the Athens plague in the 5th century B.C, as well as a number of deaths in the Soviet Union between 1932 and during WWII, after contaminated grains were ingested by the population of the region (Schoental, 1994).

Type B trichothecenes are differentiated from type A by the presence of a keto group at C8. Type B comprises toxins, such as nivalenol (NIV), DON, 3-ADON and 15-ADON, with DON being the most commonly found in grains (Sobrova *et al*., 2010; Edite Bezerra da Rocha *et al*., 2014). DON has been described as "vomitoxin" due to the symptoms observed in humans after contaminated food has been ingested. It can also cause diarrhea, leukocytosis, hemorrhage and neuronal damage (reviewed in Foroud *et al*. (2019)). In addition DON, is considered a virulence factor carried out by *Fusarium* species which facilitates the infection of the host plants (Proctor *et al*., 1995a; Desjardins *et al*., 2000).

The biosynthesis and regulation of trichothecene mycotoxins is controlled by a group of genes known as *TRI* genes. They are mainly grouped in clusters, as is common for the biosynthetic and regulatory genes of secondary fungal metabolites, and they are distributed on four *loci*. The main cluster is known as the *TRI* core gene cluster (*TRI3* to *TRI14* in *F. sporotrichioides*), a two-gene cluster is formed by *TRI1 and TRI16*, while two genes, *TRI101* and

TRI15, are positioned in independent *loci* (Kimura and Yamaguchi, 1999; Alexander *et al*., 2004; Brown *et al*., 2004; Foroud *et al*., 2019). The name and function of the genes are summarized in Table 1.2.

Table 1.2. Genes associated with trichothecene biosynthesis and regulation.

Gene	Function	Localization
TRI1	Cytochrome P450 monooxygenase	*TRI1-TRI16*
TRI3	Acetyltransferase	*TRI* core cluster
TRI4	Cytochrome P450 monooxygenase	*TRI* core cluster
TRI5	Sesquiterpene cyclase or terpene synthase	*TRI* core cluster
TRI6	Zinc-finger DNA-binding protein, Transcription factor	*TRI* core cluster
TRI7	Acetyltransferase	*TRI* core cluster
TRI8	Esterase	*TRI* core cluster
TRI9	Unknown	*TRI* core cluster
TRI10	Transcription factor	*TRI* core cluster
TRI11	Cytochrome P450 monooxygenase	*TRI* core cluster
TRI12	Transport pump	*TRI* core cluster
TRI13	Cytochrome P450 monooxygenase	*TRI* core cluster
TRI14	Unknown	*TRI* core cluster
TRI15	Cys_2-His_2 zinc finger protein, Transcription factor	*TRI15*
TRI16	Acetyltransferase	*TRI1-TRI16*
TRI101	Trichothecene 3-O-acetyltransferase gene	*TRI101*

Pioneer studies in trichothecenes involved the purification of the enzyme trichodiene synthase and isolation of the encoding *TRI5* (also known as *TOX5*) gene in *F. sporotrichioides* (Hohn and Vanmiddlesworth, 1986; Hohn and Beremand, 1989). This enzyme, a sesquiterpene cyclase, catalyzes the cyclization of farnesyl pyrophosphate (FPP) into trichodiene, the first step in the trichothecene biosynthesis pathway (Figure 1.1). Trichodiene is transformed into isotrichotriol in four steps catalyzed by Tri4, a cytochrome P450 monooxygenase. The next two isomerization steps lead to the formation of isotrichodermol, which forms the base trichothecene

structure (Foroud *et al*., 2019). From all these steps, tri5 is the enzyme often used as a marker to study the differences between trichothecene-producing and non-trichothecene producing isolates, including the trichothecene role on plant-host response or in the pathogen virulence (Proctor *et al*., 1995a; Doohan *et al*., 1999; Desjardins *et al*., 2000; Chen *et al*., 2011).

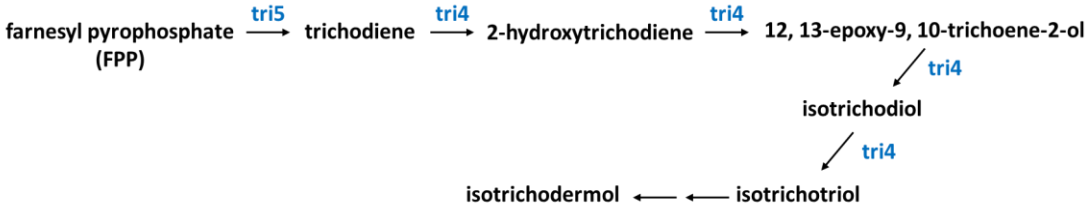

Figure 1.1. First steps in the trichodiene biosynthesis. Farnesyl pyrophosphate (FPP) is converted into trichodiene by the enzyme trichodiene synthase (Tri5). A cytochrome P450 monooxygenase (Tri4) is involved in the four next steps that lead to isotrichotriol, which is then isomerized into isotrichodermol.

TRI6 has been considered a global transcription regulator that controls genes associated with several cellular process, such as signal transduction, cellular metabolism and transport, and cell rescue and virulence, among others, in *Fusarium* species, such as *F. graminearum* (Seong *et al*., 2009; Nasmith *et al*., 2011). The regulatory function of *TRI6* is associated with *TRI10*, and it was discovered by genetic disruption of the encoding genes, which revealed that other *TRI* genes were either no longer expressed or their expression reduced (Proctor *et al*., 1995b; Tag *et al*., 2001). Furthermore, *TRI10* was also found to regulates the expression of the other *TRI* genes, in part, by the regulation of *TRI6* (Tag *et al*., 2001). In *F. sporotrichioides TRI10* acts upstream of the cluster that encodes for *TRI6*, and both genes seem to be necessary not just for the regulation of *TRI* gene expression, but also for self-protection against trichothecenes (Tag *et al*., 2001). It was suggested *TRI10* activation upregulates *TRI6*, which in turns downregulates *TRI10*.

Therefore, even though *TRI6* is not required for *TRI10* transcription, it is needed to limit *TRI10* expression in a feedback loop (Tag *et al*., 2001).

In nutrient-rich conditions *TRI6* auto-regulates its expression through binding to its own promoter (Nasmith *et al*., 2011). It was also found that under these nutrient-rich conditions, *TRI6* bound to the promoter of *TRI* genes suppressing their expression and suggesting that could act as a negative regulator of the trichothecene pathway, since *TRI* genes activation are modulated by nitrogen-deficient conditions (Nasmith *et al*., 2011).

1.6. Fungal Mitogen-activated protein kinases

Kinases are enzymes that activate/deactivate other proteins through the transference of a phosphate group. It is estimated that a 30 % of cellular proteins are phosphorylated (reviewed in (Turrà *et al*., 2014)), and in higher eukaryotes, 1 % of predicted genes encode protein kinases (reviewed in (Wang *et al*., 2011; Turrà *et al*., 2014)). Through this reversible process of protein activation/deactivation, the cell is guided to different responses in relation to development, metabolism, abiotic/biotic stresses, among others. In eukaryotic organisms, a family of serine/threonine protein kinases, known as mitogen-activated protein kinases (MAPK), are one of the most studied signal transduction pathways. MAPKs regulate gene expression, protein localization, cell division, metabolism, programmed cell death, among other processes (Roux and Blenis, 2004; Chen and Thorner, 2007; Raman et al., 2007).

MAPKs have been well conserved through evolution. They function as a three-tiered cascade, where a MAPK kinase kinase (MAPKK) phosphorylates a MAPK kinase (MAPKK), which in turns phosphorylates a MAPK. Phosphorylation of the activation loop within the MAPKs will lock the kinase domain, and trigger a conformational change that will turn the

enzyme into an active form. In the case of MAPKKKs and MAPKKs, the activation loop is formed by the amino acids serine or threonine, but for MAPKs is serine and tyrosine.

There are three main kinases in the MAPK subgroup, characterized by different phosphorylation motifs, that mediate the MAPK pathways in multi-cellular organisms: the extracellular signal-regulated kinases (ERK), the c-Jun amino-terminal kinases or stress-activated protein kinase (JNK/SAPK) and the p38 (Davis, 1994; Lee *et al*., 1994; Johnson and Lapadat, 2002; Zhang and Liu, 2002). ERKs have a TEY activation loop motif, while JNK and p38 have TPY and TGY activation loops, respectively. In filamentous fungi, three MAPK pathways have been identified where two of them have ERK-like MAPKs and the third a p38-like MAPK.

Many of the studies in fungal MAPK have been performed in *Saccharomyces cerevisiae* (Lee *et al*., 1993; Watanabe *et al*., 1995; Kamada *et al*., 1996; Gray *et al*., 1997; Chen and Thorner, 2007; Alvaro and Thorner, 2016) since it was the first eukaryotic organism with the complete genome sequenced and it is a model organism for eukaryotic research. However, even though the components and functions of the MAPK cascades in yeast are shown to be highly conserved in the Fungi Kingdom, significant differences are present between filamentous fungi and yeast.

In *S. cerevisiae*, five MAPK pathways regulate different, and perhaps overlapping processes: cell wall integrity, high osmolarity, pheromone/mating response, filamentous growth, and spore wall assembly (Figure 1.2) (reviewed in (Chen and Thorner, 2007; Hamel *et al*., 2012)). The last two pathways listed have also been described as “invasive growth” and “ascospore formation” (reviewed in (Zhao *et al*., 2007; Jiang *et al*., 2018), or “hyphal growth” and “ascospores formation” pathways (reviewed in Zheng *et al*. (2000)).

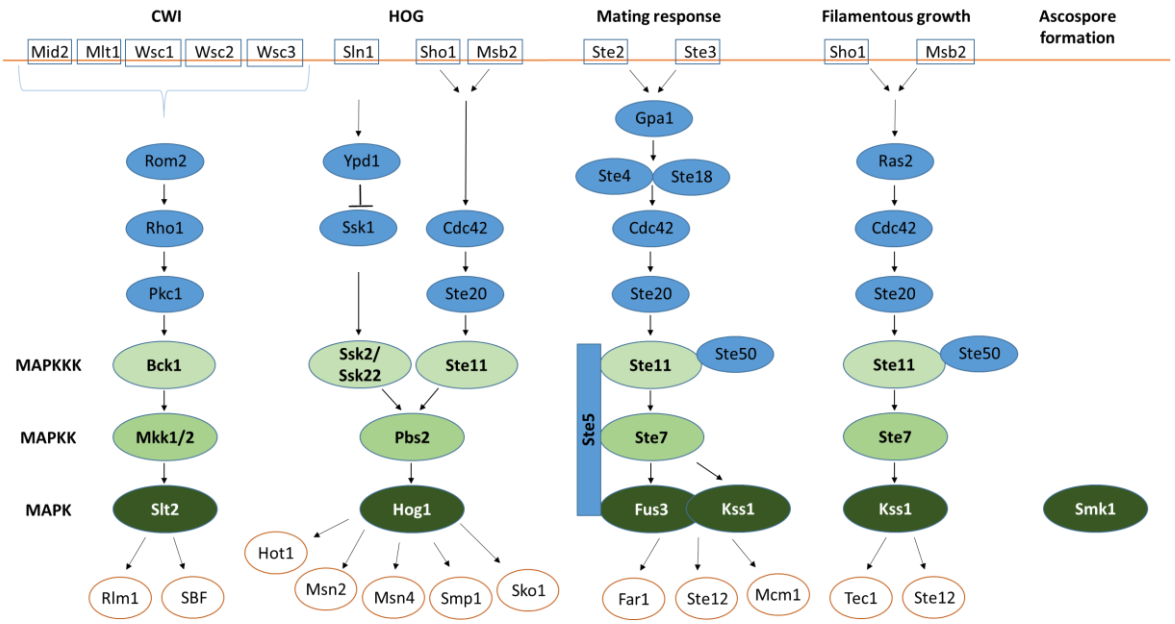

Figure 1.2. Components of the five MAPK pathways in *S. cerevisiae*: CWI (cell wall integrity), HOG (high osmolarity glycerol), pheromone/mating response, filamentous/invasive growth, and ascospore formation or spore wall assembly.

The homologs of individual MAPKKKs/MAPKKs/MAPKs sometimes have unique names in different species, making it difficult to identify to which pathway they belong. For this reason, a unified nomenclature has been proposed to avoid ambiguity in the protein name designation (Hamel *et al*., 2012). The nomenclature advises the usage of a 3-letter acronym of the species name preceding the name of the protein in the model *S. cerevisiae*. For example, the homologous of the *S. cerevisiae* MAPK Slt2 (Suppressor of the LyTic phenotype 2) would be named Fgr-Slt2 in *F. graminearum,* instead of Mgv1 (Mycelia growth and virulence 1). In my thesis, I will employ the accepted common name for individual MAPKs, while sometimes making reference to the unified nomenclature to alleviate ambiguity.

1.6.1 High Osmolarity Glycerol (HOG) pathway

The HOG pathway in fungi is activated under osmotic stress, and as result, glycerol is accumulated in the cell to maintain turgor pressure (reviewed in Jiang *et al*. (2011)). In *S.*

cerevisiae, Sho1 (synthetic high osmolarity sensitive1), Sln1 and Msb2 (mucin-like membrane protein) are receptors in the Hog1 pathway (Maeda *et al*., 1995; O'Rourke and Herskowitz, 2002; Hayashi and Maeda, 2006). This cascade can be activated by either of the two branches (Sln1 or Sho1/Msb2), depending on the stress, and they converge on Pbs2 (Maeda *et al*., 1994; Maeda *et al*., 1995; Wang *et al*., 2018). For example, cold stress (0°C) triggers the *S. cerevisiae* HOG cascade in an Sln1-dependent manner, while DMSO, a compound that rigidifies the cell membrane, is activated by both Sln1 and Sho1 (Hayashi and Maeda, 2006). Unexpectedly, the homolog of Sho1 does not seem to be involved in osmotic stress response in *F. graminearum* (Qin *et al*., 2015).

The core HOG cascade is formed by Ste11(or Ssk2/Ssk22)-Pbs2-Hog1 (Figure 1.2). In *F. graminearum*, cross-talk with another pathway was suggested after a reduction in Hog1 (described as FgOs2 in Yun *et al*. (2014)) phosphorylation was observed in a mutant with a deleted *MKK1*, the putative MAPKK of the cell wall integrity (CWI) cascade (Yun *et al*., 2014). The nature of this interaction is not completed understood. In *F. graminearum*, in addition to the core components of the HOG cascade, another protein kinase, namely Sch9, was found to interact with Hog1 (Gu *et al*., 2015). The authors proposed that Sch9 interacts with Hog1 after a co-immune precipitation (Co-IP) assay showed both proteins were pulled out together, and the deletion of Sch9 increased susceptibility to osmotic stress (Gu *et al*., 2015). The *Botrytis cinerea* homolog of Sch9, was also identified as a competitor to Mkk1 for the phosphorylation of Rim15 (Per-Arnt-Sim (PAS) kinase) in the CWI pathway. Since it has been observed that Mkk1 deletion negatively affects Hog1 phosphorylation in *F. graminearum* (Yun *et al*., 2014), Sch9 may be a key in the interaction between Mkk1 and Hog1 in this plant pathogen.

1.6.2 ERK-like (Kss1/Fus3 and Slt2) pathways

In the late 1980's, based on the results of a study of mouse cells exposed to insulin, Ray and Sturgill (1988) proposed that a kinase that phosphorylates the microtubule-associated protein 2 (named "MAP-2", where "M" stands for microtubule instead of mitogen) would be named as a "MAP kinase". This protein of 42 kDa was transiently phosphorylated on tyrosine by a diverse group of tested mitogens, suggesting a significant role in the events required for the transition of the cell from G0 into the cell cycle (Rossomando *et al*., 1989). This microtubule-associated protein kinase was then characterized as an extracellular signal-regulated kinase (ERK1), which showed high similarities to Kss1 and Fus3 from yeast (Boulton *et al*., 1990; Boulton *et al*., 1991a). Other ERK-like proteins were later identified, also involved in cell growth signalling (Boulton *et al*., 1991b), and the term changed to mitogen-activated protein kinase (MAPK); however, this term is now considered a misnomer due to the discovery of other members of the group that activate diverse processes in the cell, such as a response against biotic and abiotic stress, cell wall integrity, sporulation and pathogenesis, among others. In *S. cerevisiae*, Fus3, Kss1 and Slt2 MAPKs are ERK-like proteins.

1.6.2.1 The Kss1/Fus3- pathway

In *S. cerevisiae*, the pathways of filamentous, pseudohyphal or invasive growth, and the pheromone/mating response are separate cascades that in filamentous fungi are converged into one: the Kss1/Fus3 (referring to the MAPKs in the cascade). This pathway is mainly associated with the formation of invasive structures and pathogenesis, and for that reason it is referred to by some authors as the pathogenesis cascade (Perez-Nadales and Di Pietro, 2015). Some processes regulated by the pathway include mycelial growth, conidiation, conidia germination, endoglucanase production, appressoria formation, and plant infection (Kojima *et al*., 2002; Zhao

et al., 2011; Perez-Nadales and Di Pietro, 2015; Qin *et al*., 2015). Even though the function of this cascade is well conserved among plant pathogenic fungi, depending on the species, the function of the pathway and of each components might vary as well.

The G-coupled receptors Ste (sterile), such as Ste2 and Ste3, activate the Kss1/Fus3 pathway in *S. cerevisiae* (Burkholder and Hartwell, 1985; Hamel *et al*., 2012; Alvaro and Thorner, 2016). These receptors are known as pheromone sensing proteins in *S. cerevisiae* and are involved in chemotropism in yeast and filamentous fungi (Hamel *et al*., 2012; Turrà *et al*., 2015; Sridhar *et al*., 2020). After the ligand binds, the inhibitory Gα subunit is released, which in turns stimulates Gβ and Gγ subunits. A protein complex is then created with the association of Gβγ subunits, the Ste20 (p21-activated kinase (PAK)), and the scaffold protein Ste5, which together activates the Ste11 (MAPKKK), starting the Ste11-Ste7-Kss/Fus3 (MAPKKK-MAPKK-MAPK) cascade activation (Hamel *et al*., 2012).

Other receptors, such as Sho1 and Msb2, known as osmosensors, have been also associated with the activation of this pathway in filamentous fungi (Perez-Nadales and Di Pietro, 2015; Qin *et al*., 2015) with partially overlapping functions that promote invasive growth and plant infection (Perez-Nadales and Di Pietro, 2015). Sho1 is a receptor for the Kss1/Fus3 pathway in filamentous fungi, and has different functions depending on the species. Even though Sho1 is known as a sensor of the osmotic stress pathway (HOG) in *S. cerevisiae* (Maeda *et al*., 1995), in *F. graminearum* and *Fusarium oxysporum*, Sho1 is not involved in this response. In turn, Sho1 is important in the Kss1/Fus3 homolog cascade (Gpmk1 and Fmk1, respectively) (Perez-Nadales and Di Pietro, 2015; Qin *et al*., 2015), and in the *F. graminearum* CWI pathway (Qin *et al*., 2015). Sho1 interacts with the module Ste50-Ste11-Ste7; it recruits Ste50 and Ste7 to the membrane and Ste50 physically interacts with Ste11 and Ste7.

The MAPK of this pathway is involved in pathogenesis through the regulation of vegetative hyphal fusion, root adhesion, host penetration and colonization, cell wall degrading enzymes, such as pectinolytic enzymes (Di Pietro *et al*., 2001; Prados Rosales and Di Pietro, 2008; Turrà *et al*., 2014; Perez-Nadales and Di Pietro, 2015; David *et al*., 2017). Two main proteins are the identified downstream components of this pathway: Ste12, a transcription factor (TF) that regulates mating-responsive genes and cell cycle arrest, and Far1, a cyclin-dependent kinase (CDK) inhibitor (reviewed in (Hamel *et al*., 2012)).

1.6.2.2 The Slt2- Cell wall integrity (CWI) pathway

The CWI pathway is activated for the reassembly of the cell wall during the developmental stages of the microorganism or in response to cell wall damage. Such damage may be caused by a variety of abiotic stresses (i.e. heat or hypo-osmotic shock) or as a result of the host's response in plant-pathogen interactions (Verna *et al*., 1997; Zu *et al*., 2001; Fujioka *et al*., 2007; Levin, 2011; Yun *et al*., 2014; Zhang *et al*., 2017). This cascade is also involved in pathogenesis and virulence, among other functions (Hou *et al*., 2002; Jeon *et al*., 2008; Luo *et al*., 2012; Li *et al*., 2014; Yun *et al*., 2014; Zhang *et al*., 2015; Cristina and Concepcion, 2016). Some of the events in which the components of this cascade interfere at are the regulation of: *i*) secondary metabolite production, including those that can act as virulence factors facilitating the infection of the host; *ii*) the expression of genes associated with the formation of reproductive structures and its germination after chemical attraction to the host; *iii*) formation of invasive structures; *iv*) the integrity of the vegetative structures.

Even though the CWI pathway is well conserved in fungi, some components vary in function in different species. This literature review shows some specificities regarding the

components of the pathway in *S. cerevisiae*, and different fungal plant pathogen species, with emphasis on *F. graminearum* (Figure 1.3).

(a)

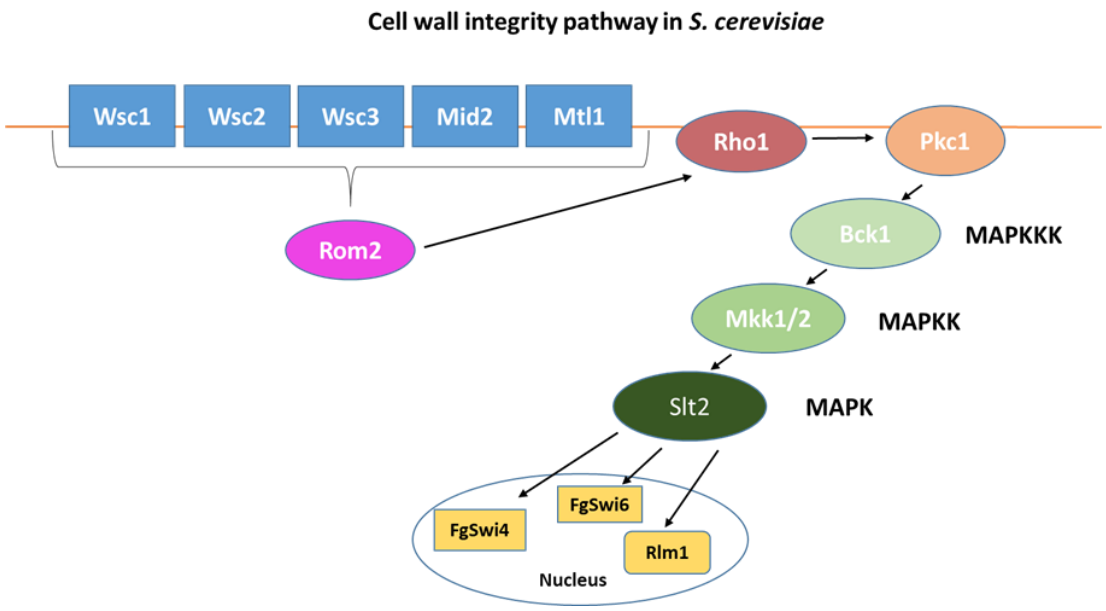

(b)

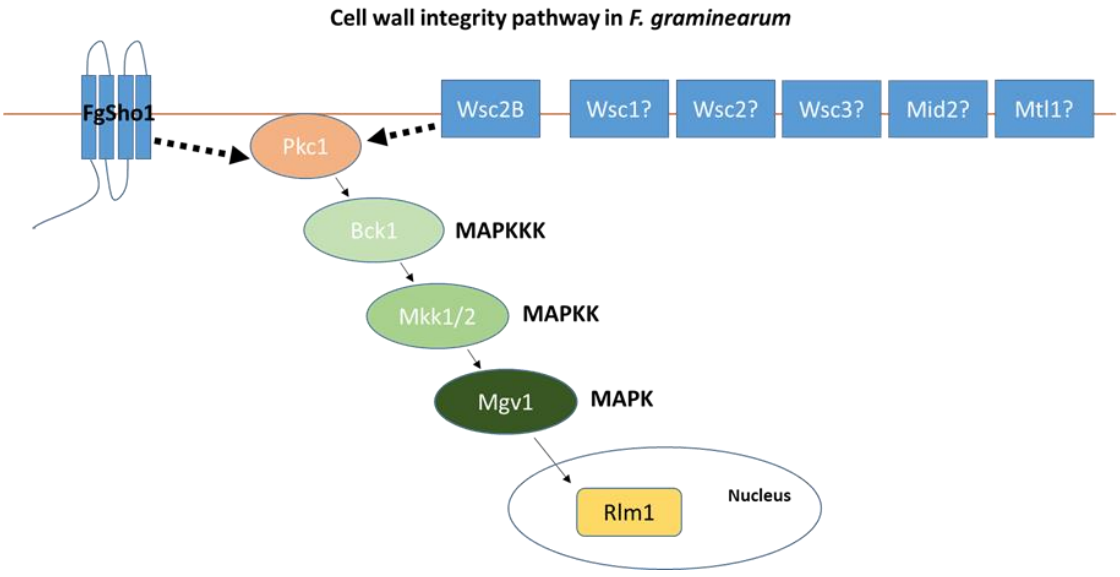

Figure 1.3. Cell wall integrity pathway (a) in *S. cerevisiae*, and (b) in *F. graminearum*. A) In *S. cerevisiae*, after the stimulus is detected by the receptors (blue rectangles) in the cell membrane, they interact with Rom2 which phosphorylates Rho1. Rho1 then phosphorylates Pkc1, which then triggers the activation of the core components of the CWI MAPK cascade: MAPKKK-MAPKK-MAPK. Slt2 interacts with different TFs, such as the Sbf complex and Rlm1. B) In *F. graminearum*, the Wsc2B and Sho1 are the only receptors that have been associated with the CWI pathway, and even though they might interact with Rom2 for Rho1 activation, and then Rho1 should led to Pkc1 phosphorylation, that has not been shown. As in *S. cerevisiae*, the *F. graminearum* Pkc1 phosphorylates Bck1, and in turn, Bck1 will phosphorylate Mkk2, which in turn will phosphorylate Mgv1. Even though it is known that MAPKs phosphorylate several targets, Rlm1 is the only one downstream component that has been identified in *F. graminearum*.

1.6.2.2.1 Upstream components in the CWI pathway

In *S. cerevisiae*, the classical upstream elements of the CWI pathway are the receptors Wsc1, Wsc2, Wsc3, Mtl1 and Mid2 (Gray *et al*., 1997; Ketela *et al*., 1999; Lodder *et al*., 1999; Zu *et al*., 2001). Wsc1 (cell wall integrity and stress response component) was first identified as Hcs77, an integral membrane protein that regulates CWI pathway and is involved in resistance to heat shock (Gray *et al*., 1997). Searching for inhibitors of the RAS (RAS-cAMP pathway, required for heat shock protection and cell cycle progression) activity or its targets, researchers screened genes that suppressed heat shock sensitivity in the cells. Thus, the Wsc family of cell sensors was identified and described, with Wsc1 (Hsc77), Wsc2 and Wsc3, as some of its components (Verna *et al*., 1997).

In *S. cerevisiae,* after a stimulus is detected by the Wsc receptors, they interact with Rom2, a guanine exchange factor (GEF) which in turns phosphorylates the small GTP-binding protein Rho1. GTP-bound Rho1 phosphorylates and activates Pkc1 (protein kinase C), a component of the CWI pathway (Nonaka *et al*., 1995; Kamada *et al*., 1996). As result of Pkc1 activation, Bck1 (Bypass of C kinase), the MAPKKK of the core proteins (Bck1-Mkk1/2-Slt2) in the CWI pathway are phosphorylated (Lee and Levin, 1992; Nonaka *et al*., 1995).

In *F. graminearum* the only member of the Wsc family cell wall sensor that has been identified as part of the CWI cascade is Wsc2B (Xu *et al*., 2019). In *F. graminearum*, the deletion of the *S. cerevisiae* orthologues Wsc1, Wsc2 and Wsc3 did not show an effect on CWI or hyphal growth (Xu *et al*., 2019). The results suggested that the function of these sensors may vary among fungal species (Xu *et al*., 2019), and/or that gene redundancy exists, such that some of these genes might have overlapping functions.

The transmembrane protein Sho1 has been identified as another sensor for the CWI pathway since its deletion increased sensitivity to cell wall stress compounds in *F. graminearum* and *F. oxysporum* (Perez-Nadales and Di Pietro, 2015; Qin *et al*., 2015), and decreased the phosphorylation of the *F. graminearum* Mgv1, the MAPK in this cascade (Qin *et al*., 2015). Sho1 has been previously recognized as the receptor of the HOG pathway and the pheromone response cascade in *S. cerevisiae* (Kss1/Fus3 in filamentous fungi) (O'Rourke and Herskowitz, 1998). However, in *F. graminearum*, it has been shown that Sho1 is not involved in the osmotic stress response (Qin *et al*., 2015), but interacts instead with the GPMK1 cascade, where it contributes to virulence, conidiation, cell wall stress response and in the DON biosynthesis (Qin *et al*., 2015).

In recent studies, the Ste2 receptor, which is often associated with the GPMK1 pathway, was found to participate in the CWI cascade in *F. oxysporum* and *F. graminearum* (Turrà *et al*., 2015; Vitale *et al*., 2019; Sridhar *et al*., 2020). Ste2, along with Ste3, is a seven-pass transmembrane domain G-protein-coupled receptor (GPCR) and a known sensor of the pheromone mating type pathway in *S. cerevisiae* (Dohlman *et al*., 1991; Alvaro and Thorner, 2016; El-Defrawy and Hesham, 2020). It has been demonstrated that Ste2 plays a significant role in chemotropism mediated by the CWI pathway, towards pheromones and plant compounds in *F.*

oxysporum (Turrà *et al*., 2015), while in *F. graminearum* it has been shown to act towards wheat secreted peroxidases (Sridhar *et al*., 2020).

1.6.2.2.2 CWI core proteins (Bck1-Mkk1-Slt2)

The CWI cascade has a protein core formed by a MAPKKK (Bck1), redundant MAPKKs (Mkk1/Mkk2) and a MAPK (Slt2) in *S. cerevisiae* (Lee and Levin, 1992; Lee *et al*., 1993; Levin, 2011). This cascade is well conserved among fungal species, but some of its other components and functions might vary. In different fungi, the core components of this cascade have been associated with the proper development of reproductive or invasive structures formed towards the invasion and infection establishment (Yun *et al*., 2014; Yin *et al*., 2018b).

In *B. cinerea*, mutants with deleted *BCK1* or *MKK1* were unable to phosphorylate Bmp3 (Bci-Slt2), even if the strains were exposed to Congo red (CR), which is an activator of the pathway (Yin *et al*., 2018b). In addition, it was observed that *Δmkk1* displayed a slower mycelial growth, less conidiation and higher sensitivity to cell wall and osmotic stresses, but was less impaired in virulence than the other two mutants *Δbck1* and *Δbmp3*. In *F. graminearum*, individual deletion of each of the core MAPK components from the CWI pathway strongly affect the development of the fungus in mycelial growth, perithecium formation and plant infection (Hou *et al*., 2002; Wang *et al*., 2011; Yun *et al*., 2014). Even though these genes play significant roles in the cell, and their absence negatively affect the cell development, they are not essential for cell survival.

The *F. graminearum MKK1* gene shares 53 % sequence identity with *MKK1/2* of *S. cerevisiae* (Yun *et al*., 2014), and has been found to interact with Mgv1 (Wang *et al*., 2011). The deletion of *MKK1* has been shown to negatively affect the phosphorylation of Mgv1, which combined with the previous results, suggests that Mkk1 functions upstream of Mgv1 in the CWI

cascade (Yun *et al*., 2014). The same study also revealed reduced phosphorylation of Hog1 in *Δmkk1* mutant, suggesting there is cross-talk between the CWI and HOG cascades. Nevertheless, this cross-talk is not yet completely understood.

In *F. graminearum*, *MGV1* is a single copy gene that encodes a protein of 416 amino acids, and shares 51.2 % sequence identity with *SLT2* from *S. cerevisiae* (Hou *et al*., 2002). In addition, it is 86 % identical to Mps1 (Mgr-Slt2) of *M. grisea* (first Slt2 homologue identified in filamentous fungi (Xu *et al*., 1998)) (Hou *et al*., 2002). Analyses of specific MAPK mutants have demonstrated that Mgv1 in *F. graminearum* plays important roles in different processes, including vegetative mycelial development as well as pathogenesis development (Hou *et al*., 2002). Deletion of *MGV1* resulted in reduced virulence and mycotoxin accumulation, but these effects could be associated with the observed fitness reduction (Hou *et al*., 2002). In addition, deletion of the *MGV1* gene generates a phenotype that is female sterile (Hou *et al*., 2002).

In other fungal pathogens, such as *B. cinerea*, there is a second downstream component of Mkk1: the Per-Arnt-Sim (PAS) kinase Rim15, which also physically interacts with the Ser/Thr protein kinase, Sch9 (Yin *et al*., 2018b). It was suggested that Mkk1 may hinder the phosphorylation of Rim15 mediated by Sch9, since Rim15 seems to have preference for Mkk1 (Yin *et al*., 2018b). Thus, Mkk1 negatively regulates and activates Rim15 by impeding its phosphorylation via Sch9 (Figure 1.4).

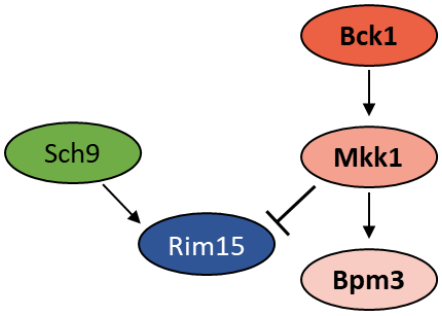

Figure 1.4. Representation of the core-components of the CWI pathway in *B. cinerea* and the interacting Mkk1 partner, the kinase Rim15.

1.6.2.2.3 Functional downstream components of Slt2 in the CWI pathway

In *S. cerevisiae*, the main downstream components of Slt2 are Rlm1 (a MADS-box transcription factor) and the Sbf (Swi4/6 cell cycle box (SCB) binding factor) complex (Watanabe *et al*., 1995; Dodou and Treisman, 1997). In several fungal pathogens, Rlm1, as well as the Sbf complex, regulate the expression of genes associated with cell wall formation and its reinforcement, as well as the cell cycle. However, it was observed that none of the orthologues to these proteins was a major regulator of cell wall-related genes in *Aspergillus nidulans*, and only *α-1,3-GLUCAN SYNTHASE* genes (*AGSA* and *AGSB*) were regulated by RlmA (orthologous to Rlm1). The authors suggested that other downstream MpkA (Ani-Slt2) factors might be involved (Fujioka *et al*., 2007). In some filamentous fungi, it has been observed that only one of the orthologues to the *S. cerevisiae* Slt2 downstream target is involved in the CWI pathway. For instance, in *F. oxysporum* the only downstream target of Slt2 that has been identified is the TF, Swi6 (Ding *et al*., 2020), while in *F. graminearum* this TF has not been proven as an Mgv1 target, even though Swi6 is involved in mycelial growth, sexual development, DON production and virulence (Liu *et al*., 2013), similar to Mgv1 (Hou *et al*., 2002). So far, the only Mgv1 downstream element that has been identified in *F. graminearum* is Rlm1 (Yun *et al*., 2014), even

though, as a MAPK, a myriad of targets is expected to be found. In fact, a predicted protein kinase network suggested more downstream targets for Mgv1 than for the other MAPKs Hog1 and Gmpk1 (Wang *et al*., 2011). In addition, in the same study, the kinase Kin4 was identified as a possible interacting partner of Mgv1 after performing Co-immunoprecipitation (Co-IP) assay. Other researchers have proposed additional Mgv1 targets in *F. graminearum*, based on the sequences that can be phosphorylated by this MAPK (Rampitsch *et al*., 2010), information that could be used as starting point for screening those putative Mgv1-interacting components.

1.6.2.2.3.1 RLM1

Rlm1 is a transcription factor that belongs to the family of MADS-box which are transcriptional regulators that share the conserved motif that encodes the MADS DNA-binding domain in eukaryotic organisms. The MADS name refers to the first four proteins identified that contains this sequence, and stands for: MCM1 (minichromosome maintenance 1) from *S. cerevisiae*, AGAMOUS from *A. thaliana*, DEFICIENS from *Antirrhinum majus*, and SRF (Serum Response Factor) from *Homo sapiens* (Schwarz-Sommer *et al*., 1990). The MADS-box family tends to form a multicomponent complex recruiting other TFs and this interaction with other proteins plays a significant role in target gene regulation (Shore and Sharrocks, 1995; Mead et al., 2002).

In *S. cerevisiae*, there are four MADS-box TFs that can be classified in two groups: Mcm1 and Arg80 (type I), and Rlm1 and Smp1 (type II) (Dodou and Treisman, 1997; Alvarez-Buylla *et al*., 2000; Jamai *et al*., 2002; Jung *et al*., 2002; de Nadal *et al*., 2003). Rlm1 is the MADS-box functional downstream component of Slt2 (Watanabe *et al*., 1995; Watanabe *et al*., 1997). Smp1 is a downstream component of Hog1, while Mcm1 is associated with the pheromone and invasive growth pathway (Kss1/Fus3) (Watanabe *et al*., 1995; Watanabe *et al*.,

1997; Jung *et al*., 2002; de Nadal *et al*., 2003). Arg80 is a regulatory TFs involved in Arginine metabolism in yeast (Jamai *et al*., 2002).

In *A. nidulans, F. graminearum, M. grisea* and *Neurospora crassa* there are two MADS-box TFs, each one homologous to *RLM1* and *MCM1* from *S. cerevisiae.* In *M. grisea*, *MIG1* (MADS-box protein required for infectious growth 1 gene) has been identified as the orthologue of *RLM1*, and its interaction with Mps1 (Mgr-Slt2) was demonstrated by yeast two-hybrid (Y2H) assay (Mehrabi *et al*., 2008). In *F. graminearum*, the MADS-box domain is present in 2 genes: FGSG_08696 (*MCM1*) and FGSG_09339 (*RLM1*), and using Y2H assay it was demonstrated that Mgv1 (Frg-Slt2) interacts with Rlm1, but not with Mcm1 (Yun *et al*., 2014). In *F. oxysporum* f. sp. *cubense*, *RLM1* is the only MADS-box described so far, which seems to have a highly conserved sequence (more than 98 %) among other *Fusarium* species, such as *F. verticillioides* and *F. fujikuroi* (Ding *et al*., 2020).

Rlm1 has been shown to regulate at least 25 genes associated with cell wall formation in *S. cerevisiae* (Jung and Levin, 1999). Among those genes there are *CHITIN SYNTHASES* (*CHS*), a family of genes involved in the formation and translocation of chitin, and *GLUCAN SYNTHASES* (*AGS1*, *FKS1*, *FKS2*), involved in glucan formation (Jung and Levin, 1999). Glucans and chitin are significant components of the fungal cell wall, representing 50-60 % and 10-20 %, respectively, of the cell wall dry weight in filamentous fungi (reviewed in Garcia-Rubio *et al*. (2020)). However, in *A. nidulans*, RlmA is not considered a major component regulated by the CWI cascade since some of the genes involved in cell wall formation, including *CHS*, were not differentially regulated compared to the WT (Fujioka *et al*., 2007).

In *F. oxysporum* f. sp. *cubense*, Rlm1 might positively regulates the chitin content and the relative expression of seven *CHS* genes, since four of these genes have a promoter with a putative

RLM1-binding domain, which contributes to the significant role of this TF in cell wall formation and integrity (Ding *et al*., 2020). This could explain why the deletion of *RLM1* resulted in down-regulation of the eight *CHS* genes evaluated in *F. graminearum* (Yun *et al*., 2014). Interestingly, downregulation of some *CHS* genes was also observed when *MKK1* (the MAPKK in the CWI cascade) was deleted in *F. graminearum*, but in the presence of Congo red (an activator of the CWI pathway) some of the genes were indistinctly differentially expressed in both strains (Yun *et al*., 2014). These results might suggest a more complex interaction between the components in this MAPK pathway, and with the genes that are under the regulation of each of its components. In addition, Rlm1 appears to regulate genes in a species-dependent manner, since it was observed that in *A. nidulans*, RlmA does not seem to regulate *CHS* genes, but it does regulate the *α-1,3-GLUCAN SYNTHASES* genes, *AGSB* (positively) and *AGSA* (negatively) (Fujioka *et al*., 2007).

Rlm1 also appears to be involved in the regulation of the secondary metabolite and pigment aurofusarin (Yun *et al*., 2014). This was suggested after a *F. graminearum* colony with a deletion in the *RLM1* gene showed a less pigmented phenotype than the WT strain, and genes involved in the biosynthetic pathway of aurofusarin were downregulated (Yun *et al*., 2014). Interestingly, this pigment was also less produced in a *F. graminearum Δmkk1* mutant, where the same biosynthetic genes tested in the *Δrlm1* mutant were downregulated. Thus, it could be hypothesized that the effects observed in the *Δmkk1* strain could be related to the resulting downregulation of *RLM1*, leading to a less pigmented colony and a reduction in the expression of pigment biosynthesis genes. However, *RLM1* expression was not analyzed in *Δmkk1,* and so a positive or negative *RLM1* regulation by Mkk1 (through Mgv1) was not established. Hence, there are some remaining questions about how the elements in the CWI pathway regulate aurofusarin production.

1.6.2.2.3.2 SBF complex

Sbf is a heterodimer complex formed by the proteins Swi4 and Swi6, where Swi4 is the DNA binding part of the complex and Swi6 has a regulatory function (Iyer *et al*., 2001; Liu *et al*., 2013). Mbf (Mlu1 cell cycle box [Mcb] Binding Factor) is another heterodimer complex formed by Swi4 and with Mbp1), and along with Sbf, they are involved in the regulation of gene expression during the G1/S transition phase. In *S. cerevisiae*, Sbf is considered a key controller of budding, and membrane and cell wall formation, while Mbf has a significant role in the regulation of genes associated with DNA replication and repair (Iyer *et al*., 2001). The structure of the Sbf and Mbf complexes are different among yeast and fungal plant pathogens. Also, all the components of the Sbf and Mbf complexes have not been identified in plant pathogen species.

In *Magnaporthe oryzae*, Mps1 (Mor-Slt2) interacts with Swi6, a protein coded by a single gene with high level of similarity with other *SWI6* in ascomycetes, such as *N. crassa*, *G. zeae*, *Podospora anserina*, and more distant to *S. cerevisiae* (Qi *et al*., 2012). In *F. oxysporum* Swi6 is the only Slt2 downstream component identified (Ding *et al*., 2020), while in *F. graminearum*, Swi6 and Mbp1 have been identified (Liu *et al*., 2013), but have not been proven to be the downstream targets of Mgv1. In *F. graminearum*, an homologue of the *S. cerevisiae SWI4* has not been found other than the *SWI6* and *MBP1* sequences (Liu *et al*., 2013). The authors suggested that the Sbf/Mbp complex in this microorganism might function differently from that in *S. cerevisiae*, forming just one type of Swi6/Mbp1 complex that regulates the transcription at the G1/S transition and the meiosis. *SWI6* sequence in *F. graminearum* contains motifs that were similar to the yeast *SWI6* and *SWI4*, and for that reason, the authors suggested a Swi4 protein might not be necessary since the Swi6/Mbp1 putative complex in *F. graminearum* may have a dual function like the Mbf and the Sbf complexes found in *S. cerevisiae* (Liu *et al*., 2013).

As part of the CWI pathway, Swi4, Swi6 and Mbp proteins are supposed to be involved in the regulation of genes associated with the cell wall formation and integrity. In *M. oryzae*, the *SWI6* deletion increased the chitin content, as well as transcript levels of *CHS* genes (Qi *et al*., 2012). In other plant pathogenic fungi, such as *F. graminearum* and *M. oryzae*, Swi6 is also involved in several processes, including hyphal growth, pigmentation, conidia formation and pathogenesis (Qi *et al*., 2012; Liu *et al*., 2013).

1.6.2.2.4 Virulence associated with secondary metabolite production and the CWI pathway

The components of the CWI cascade are not only involved in pathogen virulence through their role in reproductive and infection structures formation, since this pathway seems to regulate some secondary metabolite production. Some secondary metabolites are considered virulence factors or compounds that enhance the chance of host infection. For instance, *RLM1* deletion generated a less virulent strain, which could be related to the fact that Rlm1 positively regulates three beauvericin biosynthetic genes in *F. oxysporum* f.sp. *cubense*, but not directly, since putative Rlm1-binding domains were not found in their promoter regions (Ding *et al*., 2020). In addition, the production of the polyketide-derived secondary metabolite Fusaric acid (FA), considered a virulence factor in *Fusarium* species (Brown *et al*., 2015; Ding *et al.*, 2018) appears to be under the control of the transcription factor Rlm1 (Ding *et al*., 2020).

In DON-producing species, a correlation between the production of the metabolite and the virulence has been widely studied. DON is considered an important virulence factor for *Fusarium* spp. that facilitates plant infection, and the deletion of the *TRI5* gene affects strain virulence, depending on the host (Proctor *et al*., 1995a; Harris *et al*., 1999; Desjardins *et al*., 2000; Maier *et al*., 2006). It has been shown that even when DON might not be necessary for initial infection, it has a significant role on disease spread in wheat heads (Bai *et al*., 2002; Maier *et al*., 2006). The

deletion of *MKK1, MGV1* or *RLM1* significantly reduced the virulence of *F. graminearum* on wheat spikes, and the DON accumulation on wheat kernels were undetectable for Δ*mkk1* and Δ*mgv1,* and around 80 % less than the WT for *Δrlm1* (Hou *et al*., 2002; Yun *et al*., 2014). However, it was observed that Δ*mkk1,* Δ*mgv1* and *Δrlm1* showed a reduced colony diameter, with a stronger effect in Δ*mkk1* and Δ*mgv1* (Yun *et al*., 2014), thus opening the question of whether the reduced virulence could be associated with the reduced mycelial growth or with a combination of both conditions. Nevertheless, *TRI5* was 90 % down-regulated for *Δmkk1* and half down-regulated for *Δrlm1* (Yun *et al*., 2014). Moreover, in the same pathogen, the deletion of *SWI6* negatively affected mycelial growth and DON production in culture media, as well as pathogenesis in wheat coleoptiles and spikes (Liu *et al*., 2013).

Oxalic acid (OA) is a secondary metabolite produced by some fungi and plays a major part in pathogenesis. This compound facilitates the establishment of the plant infection due to the acidification of the media which enhances hydrolase activity from the fungus. A study in *B. cinerea* seems to be the first report that shows how the CWI pathway regulates the biosynthesis of OA (Yin *et al*., 2018b). The deletion of the *BCK1*, *MKK1* or *BMP3* (*BCI-SLT2*) genes reduced the virulence of the strains. Interestingly, a higher OA production was observed in *Δmkk1* but not in *Δbck1* or *Δbmp3*, since Mkk1 inhibits the transcription of oxaloacetate acetylhydrolase. The acidification of the extracellular media was in accordance with an observed increase in laccase, peroxidase and protease activity in *Δmkk2* mutant, an expected result since these enzymes have a higher activity at pH 3-4.5 in *B. cinerea.* (Yin *et al*., 2018b). Nonetheless, in *M. oryzae*, *MKK1* deletion caused a decrease in acid production, suggesting the relationship between Mkk1 and OA could be a species-specific trait (Yin *et al*., 2018b). The author proposed a model where the oxalic acid biosynthesis was negatively regulated by Mkk1 *via* impeding phosphorylation of

Rim15, mediated by Sch9 in *B. cinerea* (Yin *et al*., 2018b). In *F. graminearum,* an OA non-producing, but DON-producing species, *SCH9* deletion affected DON accumulation, virulence and conidiation on wheat spikes and corn silks (Chen *et al*., 2014). Since *SCH9* deletion resulted in similar phenotypic problems in *M oryzae,* it was suggested that this protein plays a conserved role in the regulation of the size of conidia and plant infection (Chen *et al*., 2014), and in secondary metabolite production (Yin *et al*., 2018b).

1.6.2.2.5 Cell wall and osmotic stress compounds

Cell wall and membrane stressing chemicals, such as Congo red (CR), calcofluor white (CFW) or sodium dodecyl sulfate (SDS), among others, are frequently used to study the role of proteins in cell wall and membrane formation or integrity. CFW is a fluorescent compound that, similar to CR, binds to chitin and interferes with its polymerization and with the linkage to other cell wall components, such as β-1,3 and β-1,6 glucans (reviewed in (de Groot *et al*., 2001)). In addition, they both seem to inhibit glucan synthases. The components of the CWI pathway and their role against these stresses have been widely researched. The results suggest that the cellular response to these compounds are species-specific, and that the gene expression and activity of the CWI cascade components towards these stress agents will differ among fungi (Yun *et al*., 2014; Yin *et al*., 2018b).

Cell wall stress compounds trigger the transcription of genes that function in the remodeling of the cell wall. As expected, the deletion of receptors *SHO1* or *MSB2* that function in the CWI pathway caused an increase in the sensitivity to CFW (200 ug/mL) and CR (600 ug/mL) in *F. oxysporum*, but the double mutant (*Δsho1-msb2*) was even more sensitive to CFW but not to CR (Perez-Nadales and Di Pietro, 2015).

In *B. cinerea*, the deletion of each of the core proteins of the CWI cascade increased the sensitivity of the mutants *vs* CR, glucanases and Glucanex (a mixture of enzymes with glucanase activity), with a higher impact observed on *Δmkk1* (Yin *et al*., 2018b). In *F. graminearum*, Mkk1 and Rlm1 also seem to be important for resistance to CR, CFW, cellulases, lysozymes or snailase, and when the genes encoding these proteins were deleted, the hyphae was well digested by the three former compounds, and abundant protoplasts were released (Yun *et al*., 2014). In addition, the conidia germination of *Δmkk1* in CR showed a swollen and shorter germ tube than in *Δrlm*1 and the WT, which were similar to each other (Yun *et al*., 2014). Conversely, in *M. grissea*, the *Δmig1* mutant was resistant to lysing enzymes, and just a few protoplasts were released (Mehrabi *et al*., 2008). Interestingly, the deletion of *RLM1* in *F. oxysporum* f. sp. *cubense* promoted resistance to CR but did not change the effect of CFW (Ding *et al*., 2020). In *A. nidulans Δrlma* was more sensitive to CFW than the WT, but the response to micafungin, an inhibitor of the *β*-1,3 glucan synthase, was not different between strains (Fujioka *et al*., 2007). In *A. niger*, *Δrlma* was more sensitive than the WT to CFW, but the addition of sorbitol partially remediated the CFW inhibition (Damveld *et al*., 2005).

In *M. grisea*, an *MPS1* (Mgr-Slt2) deletion mutant was sensitive to cell wall degrading enzymes (CWDE), since many protoplast were quickly released after cells were treated with Novozyme234. However, this mutant was not temperature-sensitive for growth, unlike the *S. cerevisiae Δslt2*. The *Mps1* deletion mutant was resistant to plasmolysis after being challenged with 1 M KCl suggesting it was not osmotically sensitive (Xu *et al*., 1998; Mehrabi *et al*., 2008).

In *S. cerevisiae*, deletion of *MPK1* or *RLM1* caused different sensitivity to caffeine, but *Δrlm1* was more resistant; however, 1 M sorbitol rescued the deficiency of the strains to resist this compound (Watanabe *et al*., 1995). In *F. graminearum*, the deletion of *RLM1* induced

upregulation of *CHS* genes when the strain was in presence of CR (Yun *et al*., 2014). This could be associated with the observed increase in phosphorylation of its upstream functional component, Mgv1, but interestingly, when *MKK1* was deleted the opposite effect was observed for most of the *CHS* genes (Yun *et al*., 2014).

1.7. Conclusions and thesis objectives

During the last 30 years, numerous data have been provided about the components and functions of the elements of the fungal CWI pathway, as well as the cross-talk among the MAPK cascades, but most of these reports come from *S. cerevisiae*. In other fungi, such as *F. graminearum*, many questions remain unanswered. For instance, since it is known that MAPKs have myriad of targets, which other downstream components, in addition to Rlm1, could be identified? In order to pursue this line of inquiry, the original goal of this project was to generate a strain from which a significant amount of a phosphorylated Mgv1 protein could be purified and used to screen Mgv1 candidate targets, previously identified by Rampitsch *et al*. (2010). To that end, one objective of the thesis was to generate *MGV1_OX* transformants that could be used for significant Mgv1 production. However, higher Mgv1 production will not guarantee high levels of Mgv1 phosphorylation that will allow to screen Mgv1 targets. Thus, the idea of generating an *MKK1* (putative upstream Mgv1 in the MAPK cascade) overexpressing phosphomimetic, that could provide a continuous phosphorylated Mgv1, was incorporated. Consequently, **the main objective of this thesis** was to **generate and characterize *F. graminearum* transformants overexpressing either the MAPK (*MGV1*) or a putative Mkk1 phosphomimic (*MKK1*^{197E,203E})**.

The thesis is organized into three technical chapters: one chapter for Mgv1 (Chapter 2) and two chapters for Mkk1 (Chapters 3 and 4), in order to study the effect of these changes in *F. graminearum*.

Chapter 2 *In locus* overexpression and characterization of the *Fusarium graminearum* *MITOGEN-ACTIVATED PROTEIN KINASE, MGV1*

2.1 Introduction

Mitogen-activated protein kinases (MAPKs) are a subfamily of kinases, a class of enzymes involved in post-translational modification of target proteins through the addition of a phosphate group(s) at specific residues. Phosphorylation induces a conformational change in the protein which affects, for instance, their interaction with other proteins or their localization. The MAPKs function in a cascade formed by a three-protein core: a MAPK kinase kinase (MAPKKK), a MAPK kinase (MAPKK) and a MAPK. The MAPKKKs are phosphorylated and activated in response to certain stimuli, and will subsequently phosphorylate and activate a MAPKK, which in turn will phosphorylate and activate a MAPK (Chen and Thorner, 2007; Goyal *et al*., 2018). MAPKs have a myriad of targets, such as transcription factors that can regulate gene expression in response to the stimulus detected (reviewed in (Chen and Thorner, 2007; Zhao *et al*., 2007; Turrà *et al*., 2014; David *et al*., 2017)).

Fusarium graminearum Schwabe is a causal agents of Fusarium head blight (FHB), a devastating disease that affects cereal crops worldwide (Wegulo *et al*., 2015; Dweba *et al*., 2017; Valverde-Bogantes *et al*., 2020). In *F. graminearum*, as in other filamentous fungi, there are three MAPK pathways which are named based on the main processes in which they are involved or from which it was originally identified (Zhao *et al*., 2007; Turrà *et al*., 2014; Jia and Tang, 2015). The three pathways are the cell wall integrity (CWI), the high osmolarity glycerol (HOG), and the virulence/filamentous growth/mating response. They are also sometimes named according to the MAPK member of each cascade, which *in F. graminearum* are Mgv1 (mycelial growth and

virulence 1), Hog1 (high osmolarity glycerol 1) and Gpmk1 (*Gibberella* pathogenicity MAPK1), respectively (Hou *et al*., 2002; Jenczmionka *et al*., 2003; Zheng *et al*., 2012; Jia and Tang, 2015).

In *F. graminearum*, the CWI pathway is composed of the MAPKKK-MAPKK-MAPK module Bck1-Mkk1/2-Mgv1 (Hou *et al*., 2002; Wang *et al*., 2011; Yun *et al*., 2014). It has been reported that the deletion of any of the three proteins that form the core in the *F. graminearum* CWI cascade negatively affects mycelial growth, perithecia formation and wheat infection (Hou *et al*., 2002; Wang *et al*., 2011; Yun *et al*., 2014). As implied by the pathway name, this cascade is also involved in the tolerance to cell wall stress compounds, such as Congo red (CR) and calcofluor white (CFW) (Yun *et al*., 2014).

The CWI cascade in *F. graminearum* seems to regulate the production and/or accumulation of secondary metabolites, such as trichothecenes and polyketides (Hou *et al*., 2002; Yun *et al*., 2014). Mgv1 and Mkk1 have been previously associated with the production of the trichothecene deoxynivalenol (DON) (Hou *et al*., 2002; Yun *et al*., 2014). DON is a sesquiterpenoid secondary metabolite that belongs to the type B trichothecene family of mycotoxins and is produced by some *Fusarium* species. It is considered a virulence factor as it is required for fungal spread into the wheat rachis and across maize ears (Proctor *et al*., 1995a; Harris *et al*., 1999; Bai *et al*., 2002; Jansen *et al*., 2005). The enzyme trichodiene synthase (Tri5) catalyzes the first step of DON biosynthesis, converting farnesyl pyrophosphate into trichodiene (Proctor *et al*., 1995a). This gene has frequently been used as a measure of how different conditions might affect the DON biosynthetic pathway and or virulence associated with this process (Proctor *et al*., 1995a; Kumaraswamy *et al*., 2012; Yun *et al*., 2014). *MGV1* and *MKK1* deletion mutants were shown to produce less DON in wheat spikelets (Hou *et al*., 2002; Yun *et al*., 2014); however, since *Δmgv1* and *Δmkk1* mutants are also strongly compromised in general fitness on solid media (Hou *et al*.,

2002; Yun *et al*., 2014), the effect of these genes on DON production might be overestimated, which suggests more studies are necessary to explore the connection between these pathways.

In addition to trichothecenes, *F. graminearum* produces other secondary metabolites, including polyketides and non-ribosomal peptides (NRPs) (Kim *et al*., 2005a; Frandsen *et al*., 2006; Sieber *et al*., 2014; Bahadoor *et al*., 2018). The genes encoding the enzymes involved in the biosynthesis and regulation of secondary metabolites are often present in clusters. In *F. graminearum,* Sieber *et al*. (2014) found a strong gene expression correlation of 20 gene clusters of unknown metabolites that may play a role in virulence. Additionally, they found a significant correlation in expression among 28 gene clusters, including those corresponding to the biosynthesis of trichothecenes, butenolide and aurofusarin.

Aurofusarin and gramillins are examples of polyketide and NRPs secondary metabolites, respectively. The aurofusarin pigment is a naphthoquinone polyketide compound found in *Fusarium* species that is cytotoxic, and for example, induces oxidative stress to human colon cells (Kim *et al*., 2005a; Frandsen *et al*., 2006; Jarolim *et al*., 2018; Westphal *et al*., 2018a). The deletion of the MAPKK in the CWI cascade, *MKK1*, negatively affected the expression of the aurofusarin biosynthetic pathway genes in *F. graminearum* (Yun *et al*., 2014). Gramillins (A and B) are cyclic lipopeptide metabolites corresponding to the NRP group and that have been recently identified as the products of the NRPS8 gene cluster and as virulence factors of *F. graminearum* in maize but not in wheat (Bahadoor *et al*., 2018). Furthermore, it has been shown that this biosynthetic gene cluster is co-induced with the *TRI* (trichothecene) genes (Bahadoor *et al*., 2018). It is unknown if Mgv1 overexpression can affect the biosynthesis and accumulation of these other secondary metabolites (NRPs and polyketides).

In the model fungus *Saccharomyces cerevisiae*, the yeast orthologue of Mgv1 is known as Slt2, and the Sbf complex and the transcription factor Rlm1 are downstream targets (Watanabe *et al*., 1995; Dodou and Treisman, 1997). The Sbf complex is a heterodimer formed by the Swi4 and Swi6 proteins, where Swi4 binds to the DNA and Swi6 is a transcription cofactor (Iyer *et al*., 2001; Liu *et al*., 2013). ScSwi6 also forms a complex with ScMbp1, named Mbf. Unlike yeast, in *F. graminearum*, the heterodimer formed by Swi6 and Mbp1 is suggested to carry out the function of both Sbf and Mbf complexes (Liu *et al*., 2013); however, an interaction between Mgv1 and Swi6 has not been investigated in this plant pathogen.

Rlm1 is a MADS-box TF involved in the regulation of at least 25 genes associated with cell wall formation in *S. cerevisiae* (for example, chitin and glucan synthases) (Jung and Levin, 1999); however this function might vary among other fungi, such as *A. nidulans*, where Rlm1 does not regulate a significant group of these genes (Fujioka *et al*., 2007). In *F. graminearum*, Rlm1 has been identified as a downstream target of Mgv1, and it's deletion slightly affects mycelial growth but strongly reduces conidia formation (Yun *et al*., 2014). In addition, a *Δrlm1* mutant showed increased sensitivity to cell wall degrading compounds and a reduction in virulence in wheat heads (Yun *et al*., 2014).

Outside of the core MAPK cascade for Mgv1, Rlm1 is one of two proteins, the other being the kinase Kin4, that have been shown to interact with Mgv1 in *F. graminearum* (Wang *et al*., 2011; Yun *et al*., 2014). MAPKs have multiple targets, and in this case, the *F. graminearum* Mgv1 protein is thought to have a greater number of downstream targets than either Hog1 or Gmpk1 (Wang *et al*., 2011). A number of candidate Mgv1 targets were identified in a phosphoproteomics study, based on the consensus sequence Pro-X-Ser/Thr-Pro present in the detected phosphopeptides (Rampitsch *et al*., 2010). The identification of new targets for Mgv1

will help to understand how the known components of the CWI cascade are involved in the regulation of several cellular processes (i.e. mycelial growth, virulence, secondary metabolite production, resistance to cell wall stresses). Since only Rlm1 and Kin4 have been shown to interact with Mgv1, but it is expected that Mgv1 possesses more targets (Rampitsch *et al*., 2010; Wang *et al*., 2011), **the long term objective of this thesis is to identify other proteins that interact with and function downstream of Mgv1.** For this purpose, **the short-term objective of this chapter is to generate and characterize *MGV1* overexpressing transformants that could be used in future research to purify high amounts of phosphorylated Mgv1 protein for screening previously identified candidate targets of Mgv1**.

2.2 Materials and methods

2.2.1 *F. graminearum* strains, growth conditions and spore production

The *F. graminearum* wild-type (WT) strain, GZ3639, and an *MGV1* disruption mutant (Δ*mgv1*; received from Dr. Rajagopal Subramaniam from AAFC-Ottawa, and previously generated by Rampitsch *et al*. (2011)) were used in this study. Mycelium was propagated from spores or a mycelial plug plated on the centre of a potato dextrose agar (PDA) Petri dish and incubated at 27°C for up to five days. For macroconidia production, either mycelial plugs of 7 mm of diameter collected from the border of four-day old PDA plates or 10^5 spores were used to inoculate 100 mL of carboxymethylcellulose (CMC) medium (1.0 g L^{-1} NH_4NO_3, 1.0 g L^{-1} KH_2PO_4, 0.5 g L^{-1} $MgSO_4{\cdot}7H_2O$, 1.0 g L^{-1} of yeast extract, 15.0 g L^{-1} of CMC sodium salt (high viscosity)) in 250-mL flasks. The spore suspension was incubated at 180 rpm, 27°C for five to seven days. The culture was then poured through autoclaved lab towels (Wypall*60, 35401-02), and the filtrate containing the macroconidia was then collected by centrifugation at 4,000 rpm

(3220 x g) for 10 min at 22°C in a swinging bucket rotor. The macroconidia were washed by centrifugation (as described above) three times with distilled water. Spores were counted using an haemocytometer, and macroconidial suspensions stored at 4°C for further use.

2.2.2 Generation of *F. graminearum* transformants overexpressing *MGV1*

F. graminearum WT genomic DNA (gDNA) was isolated from the actively growing region of four-day old mycelium on PDA plates, using the DNeasy® Plant Mini Kit (Qiagen, 69106). A fragment of the *MGV1* (FGSG_10313) gene and its upstream region were each amplified from gDNA using primer pairs P1-P2 and P3-P4, respectively. Primer sequence and related information can be found in Table 2.1. Adaptors were added to the amplicons *via* a second PCR using primers P5-P6 for the gene and P7-P8 for the upstream region. The fragments were then integrated into the pRF-HU2E vector, developed by Frandsen *et al.* (2008). This vector enables ubiquitous and constitutive *in locus* expression of a gene of interest driven by the *A. nidulans PGPDA* promoter, and contains a hygromycin resistance marker (*HPH*) for differential selection. The *MGV1* fragment was inserted immediately downstream of the *PGPDA* promoter, therefore the native *MGV1* promoter was displaced from the gene allowing *PGPDA* to drive it's expression. The construct was first inserted into *Agrobacterium tumefaciens* cells (Invitrogen, LBA4404) through electroporation, placing a Gene Pulser cuvette (BIORAD) into an electroporator (Easyject electroporator, Equibio Ltd.), set at 1800 V, 335 R and 15 µF. The transformed colonies were subsequently incubated with *F. graminearum* spores in the presence of 0.2 mM acetosyringone, which increases the virulence of *Agrobacterium* cells. The T-DNA region of the Ti plasmid from *Agrobacterium* was incorporated into the genome of *F. graminearum* WT strain through homologous recombination (Figure 2.1).

Table 2.1. Primers used to generate *F. graminearum* transformants. Adaptor sequence font colour is orange, while the font for 6xHis-tag is purple.

Primer #	Primer name	5'-3' Sequence (Tm in °C)	Purpose
1	Fg10313_F4	GGCGACCTACAAGGACGG (58.1)	Amplification of *MGV1* gene
2	Fg10313_R1248	TCTTCGAGAAGCATCCAGGC (57.1)	
3	Fg10313_PromF_ 5UTR863	CTTGGCAAGATTCAGCCCTA (54.9)	Amplification of *MGV1* upstream region
4	Fg10313_PromR_ 5UTR11	TTTCCCAAGTTGGTTGGGT (54.7)	
5	Fg10313_OE_NHis_ F1+ adapt	**GGACTTAAU**ATG**CACCATCACCATC ACCAT**GGCGACCTACAAGGA (67.8)	Amplification of *MGV1* gene + adaptors + NHis-tag
6	Fg10313_OE_R1251 + adapt	**GGGTTTAAU**TTATCTTCGAGAAGCAT CCAGG (59)	
7	Fg10313_Prom_F5_ UTR863+ adapt	**GGTCTTAAU**CTTGGCAAGATTCAGCC CTA (60)	Amplification of *MGV1* upstream region + adaptors
8	Fg10313_Prom_R5_ UTR11+ adapt	**GGCATTAAU**TTTCCCAAGTTGGTTGG GT (60.1)	
9	Fg10313_Prom_F_ T2a	TTTGTCGATCCCGCATCAT (54.4)	Verification of the cassette containing the *MGV1* upstream region in the *MGV1_OX* transformants
10	RF2	TCTCCTTGCATGCACCATTCCTTG (59.8)	
11	RF3	TTGCGTCAGTCCAACATTTGTTGCCA (61.7)	Verification of the cassette containing *MGV1* in the *MGV1_OX* transformants
12	Fg10313_R_T3a	CTGCCCTCTCAACCCATTTA (54.6)	
13	Hyg588U	AGCTGCGCCGATGGTTTCTACAA (61.3)	Verification of *HPH* (hygromycin resistance marker)
14	Hyg588L	GCGCGTCTGCTGCTCCATACAA (62.3)	
15	Mgv1_Seq1_F	AGTCCCTGGTAGGCAGCTTT (58.5)	*MGV1* Sequencing in the *MGV1_OX* transformants
16	Mgv1_Seq1_R	AAGTGCTGGAGCAGCTTGAT (57.1)	
17	Mgv1_Seq2_F	CCAGAACACTTTCTCTGTGCTGC (58.3)	
18	Mgv1_Seq2_R	GCCACAGTTATTTTCGATCACA (53.5)	
19	Mgv1_Seq3_F	CTTTGCGGTCTCAAGTACATCC (55.8)	
20	Mgv1_Seq3_R	ATCCAAAATCATACCACGCATC (53.5)	
21	Mgv1_Seq4_F_May	TACGTCCGCAACCTACCTTT (58.1)	
22	Mgv1_Seq4_R_May	CTGCCCTCTCAACCCATTTA (54.6)	
23	Mgv1_Seq5_F	CGGACTTGAGCAGGATCTTC (55.3)	
24	Mgv1_Seq5_R	ACAAGGTTAAGGGGCGATTT (54.5)	
25	β-Tub_F	GTTCTGGACGTTGCGCATCTG (59)	*β-TUBULIN* used to normalize expression of other genes (Copy number and RT-qPCR)
26	β-Tub_R	TGATGGCCGCTTCTGACTTCC (59.7)	
27	Fg_EF_F	CCTCGCTACTATGTCACCGT (56.2)	*EF-1α* used to normalize expression of other genes (Copy number and RT-qPCR) and to check DNA contamination on RNA samples
28	Fg_EF_R	CAAGGGTGTAGGCAAGGAGA (56.6)	
29	MGV1	ATGGAGTGTGATTTGGCTGC (55.9)	Expression analysis of

30	MGV1	TGGATGTACTTGAGACCGCA (55.9)	*MGV1* (Copy number and RT-qPCR)
31 **32**	TRI5_F_741 TRI5_R_817	TGTCACCTGCCATGAGATCA (58.7) TCCGAGAAGACAGCAACCAT (59)	Expression analysis of *TRI5*
33 **34**	TRI6_F2 TRI6_F2	TCTTTGTGAGCGGACGGGACTTTA ATCTCGCATGTTATCCACCCTGCT	Expression analysis of *TRI6*
35 **36**	CHS1A_F_1734 CHS1A_R_1831	TGCTTGGTTCTCTCTCGGTT (56.2) GGAGTACCTGTGTCACCGAA (56.4)	Expression analysis of *CHITIN SYNTHASE1A*
37 **38**	CHS5_F_4910 CHS5_R_4999	ACGGTCTGCAAGCCATTATC (55.4) TAAAGAGGCAGACCGAAGGA (55.4)	Expression analysis of *CHS5*
39 **40**	CHS6_F_241 CHS6_R_331	CGTGCTGAAGATGGATGTGT (55.2) TTGTAAATGGATGCGGGAAT (52.3)	Expression analysis of *CHS6*
41 **42**	PKS12_F_1799 PKS12_R_1888	ACGATGGAGCAGACGGATAC (56.5) CCCAGAATGACACCGAGAAT (54.5)	Expression analysis of *PKS12*
43 **44**	GIP1_F_1225 GIP1_R_1298	GAACACCTTCCCCCTTATCC (54.9) ACTGCCAAGCACTCTTCCAT (56.9)	Expression analysis of *GIP1* (laccase)
45 **46**	AURF_F_1328 AURF_R_1406	TCGTCAAAGCATCAGAGTGG (54.9) CCAAAAGTTCCATCCCTTCA (52.7)	Expression analysis of *AURF*
47 **48**	AURJ_F_1017 AURJ_R_1103	TCTTTGAGGCACAGCCAAC (55.7) GGGACGAGATTACCCAGGAT (55.9)	Expression analysis of *AURJ*
49 **50**	AURR1_F_1015 AURR1_R_1116	GGAAGTGAGCCGTCAAGTCT (56.9) CCCCATCTTACCCAACTCG (55.1)	Expression analysis of *AURR1*
51 **52**	AURR2_F_514 AURR2_R_605	ACCTTTTCTGAGCCGACATC (55) GCCAAACCTGCTACGACACT (57.7)	Expression analysis of *AURR2*
53 **54**	FGSG_09339_F1qPCR FGSG_09339_R1qPCR	CGCTCTGTCACCTTTTTGAAGCGA (59.8) CGACATCTACGGAGCAGAGGACGG (62.5)	Expression analysis of *RLM1*
55 **56**	Gpmk1_F1_qRT-PCR Gpmk1_R1_qRT-PCR	GACATTCAGAAGCCCCGAAG (55.8) ATCCTGTGTGCGGATGACAC (57.6)	Expression analysis of *GPMK1* (MAPK)
57 **58**	Hog1_F1_qRT-PCR Hog1_R1_qRT-PCR	TTATTGACTTCGCGCCCTCT (56.5) TTGAGGTCACGGTGGACAAC (57.4)	Expression analysis of *HOG1* (MAPK)
59 **60**	FGSG_11812_F1 FGSG_11812_R1	GTTCGAAGTTGCTCGACACA (55.5) TCGGGAGAAACACCTGAATC (54.4)	Expression analysis of *KIN4*

a)

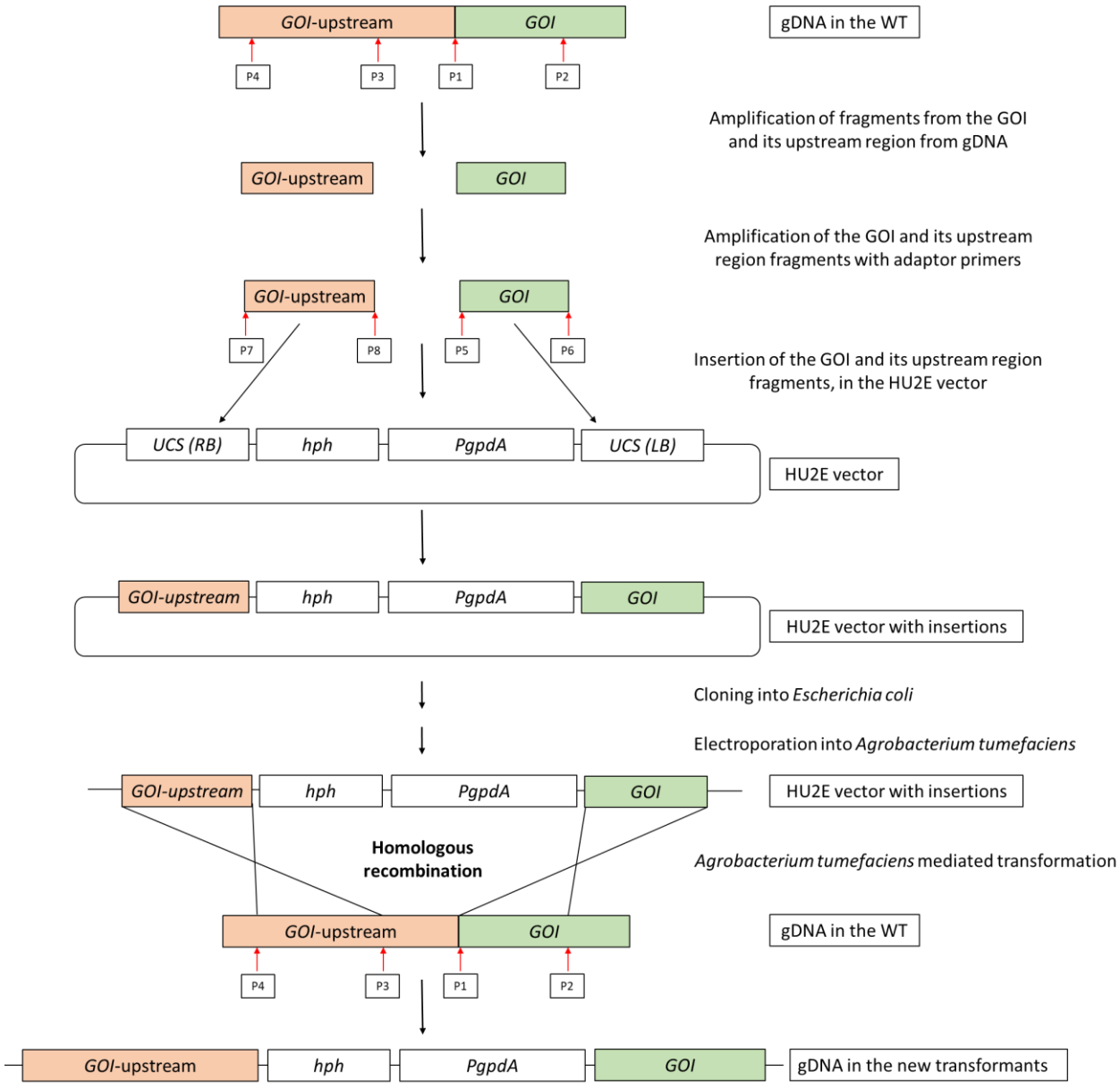
GOI-upstream
GOI
gDNA in the WT
P4
P3
P1
P2
Amplification of fragments from the GOI and its upstream region from gDNA
Amplification of the GOI and its upstream region fragments with adaptor primers
P7
P8
P5
P6
Insertion of the GOI and its upstream region fragments, in the HU2E vector
UCS (RB)
hph
PgpdA
UCS (LB)
HU2E vector
HU2E vector with insertions
Cloning into Escherichia coli
Electroporation into Agrobacterium tumefaciens
Homologous recombination
Agrobacterium tumefaciens mediated transformation
gDNA in the new transformants

b)

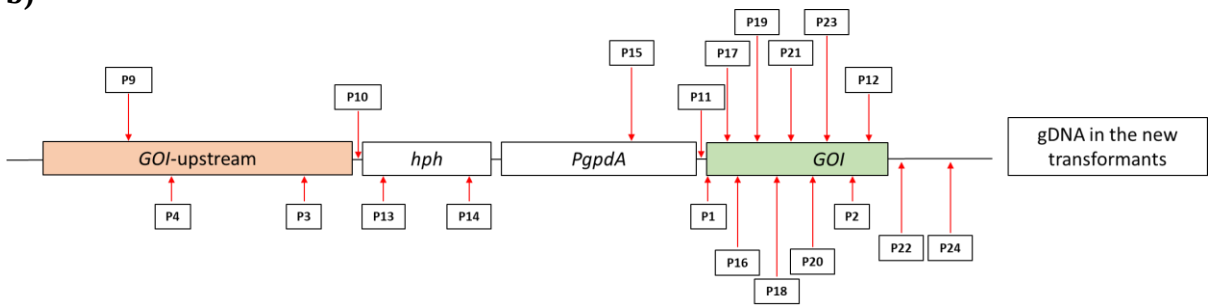
P9
P10
P15
P19
P23
P17
P21
P11
P12
GOI-upstream
hph
PgpdA
GOI
gDNA in the new transformants
P4
P3
P13
P14
P1
P2
P16
P20
P22
P24
P18

Figure 2.1. Scheme representing the generation of an *in locus* overexpressing strain developed through the USER cloning methodology. a) The HU2E vector contains a strong promoter (PGPDA) and the hygromycin resistant gene (HPH). GOI, UCS, LB, RB and P stands for: gene of interest, USER cloning sites, left border, right border, and primer, respectively. b) Position of the primers used for developing and screening the *MGV1_OX* transformants. The regions between primers P4-P3 and P1-P2 were amplified from the gDNA of the WT strain, and then inserted into the vector, which was subsequently used for homologous recombination.

Positive colonies growing on PDA medium containing 150 µg mL^{-1} hygromycin were screened by PCR. To perform the PCR, approximately 2 mg of mycelium was weighted in a scale (Sartorius Analytic AC 120 S), placed into a 1.5 mL tube with 50 µL of 10X TE (TRIS-EDTA) buffer (pH 8), and cooked in a microwave oven at maximum power for 1 min. The sample was left to rest for 2 min at room temperature, followed by a spin step for 5 min at 9,200 x *g* in a microcentrifuge. The supernatant was diluted 100 fold and used as a template for three 10 µL PCRs, each one with of the following primer sets: P9-P10, P11-P12 and P13-P14 (Table 2.1, Figure 2.1). Primers P9 and P12 are located outside of the regions used for homologous recombination; thus, they do not amplify sequences that are within the insertion cassette, and can be used to confirm that the cassette was properly inserted into the genome for *in locus* expression. Correct integration of the construct was also verified by a combination of PCRs (Primers P15-P24) and sequence analysis of the amplicons. Sequencing was carried out by the Genome Québec service lab (Montréal, Québec, Canada). New colonies were named *MGV1_OX*.

2.2.3 *MGV1* copy number in *MGV1_OX* transformants

To estimate how many copies of the construct were incorporated into the *MGV1_OX* transformants, a series of steps were performed. First, *MGV1* and the housekeeping genes *β-TUBULIN* (FGSG_09530) and *EF-1α* (FGSG_08811) were amplified from gDNA from the WT strain. The amplicons were purified and used as a template to generate a standard curve by

quantitative PCR (qPCR). gDNA was also extracted from *MGV1_OX* transformants and qPCRs were performed to detect *β-TUBULIN* and *EF-1α*, and the CT values obtained were used to estimate the concentration of the amplicons with the equation obtained from the standard curve. Finally, copy number was determined and normalized by the amount of amplification products from the housekeeping genes. The details for these steps are presented below.

The primer pairs P25-P26, P27-P28 and P29-P30, listed on Table 2.1, were used to amplify the genes *β-TUBULIN*, *EF* and *MGV1*, respectively, from the WT gDNA. Phusion DNA polymerase, a high-fidelity enzyme, was used in a 10 µL PCRs for each gene. An initial step at 98°C (30 sec) was followed by 35 cycles of 98°C (10 sec), X°C (X is defined according to the primer pair used, Table 2.2) (30 sec) and 72°C (90 sec), followed by a final extension step at 72°C (10 min) and held at 4°C. The products obtained from the PCRs for *β-TUBULIN*, *EF* and *MGV1*, were 110, 184 and 104 bp in size, respectively. The amplicons were gel purified (QIAquick Gel extraction kit- QIAGEN, # 28704) and their concentrations were measured. The purified products were used as templates for qPCRs.

Table 2.2. Annealing temperatures used in the experiments.

Primers	Annealing Temp (°C)	Purpose
P25-P26	58.5	PCR
P27-P28	56	PCR
P29-P30	55.5	PCR
P25-P30	55	qPCR for Copy number
P25-P28, P31-P34, P39-P44, P49-P50, P55-P60	54	RT-qPCR
P25-P28, P35-P38, P51-P54	55	RT-qPCR

A qPCR was carried out in 20 µL reactions containing 10 µL PerfeCTa® SYBR® Green SuperMix Low ROX (Quantabio), 0.6 µL each primer (P25-P30, Table 2.1) and 5 µL of the gel purified template. Serial dilutions of $1{:}10^2$, $1{:}10^3$, $1{:}10^4$, $1{:}10^5$ and $1{:}10^6$ were carried out for each

gene in order to obtain a standard curve. The reaction cycle started with a hold stage of 50°C (2 min) and then 95°C (10 min). The PCR stage consisted of 40 cycles of 95°C (15 sec) followed by 56°C (60 sec). The parameters for the melt curve stage were as follows: 95 °C (15 sec), 60°C (60 sec) and 95°C (15 sec). Three technical repetitions were included for each reaction. CT values from the WT serial dilutions were used to obtain the most fit equation between the CTs and the concentrations.

gDNA was extracted from *MGV1_OX* transformants and used as templates in the qPCRs with the same three sets of primers mentioned above and the same cycle conditions. The CT values obtained from *MGV1_OX* gDNA were extrapolated into the equation previously obtained, in order to get the concentration of those fragments. Copy number of the genes of interest in the transformants was calculated as the concentration of the fragments divided by the copy number of the WT strain (control). For *MGV1* copy number, the value was normalized to *β-TUBULIN* or/and *EF-1α.*

2.2.4 Confirmation of *MGV1* overexpression by RT-qPCR

Reverse transcription-quantitative PCR (RT-qPCR) was used to determine whether the *MGV1* gene was overexpressed in the transformants. Strains were grown on PDA plates for RNA extraction. Each biological replication consisted of a pool of mycelia obtained from three PDA Petri plates. Total RNA was extracted from four-day old mycelium cultured on PDA using the RNeasy® Plant Mini Kit (QIAGEN,74904), with an on-column DNase digest using RNase-free DNase I (QIAGEN, 79254). RNA concentration and purity was measured using Qubit® RNA BR assay kit (ThermoFisher, Q10210) and Agilent RNA 6000 Nano Kit with the Agilent 2100 Bioanalyzer, respectively. RNA (2.2 µg) was further treated with DNase I, RNase-free (ThermoFisher, EN0521), to eliminate any residual DNA contamination. A PCR was performed

using the clean RNA as a template, to ensure the absence of contaminating DNA. cDNA was generated in 21 µL reactions with the First-Strand cDNA synthesis kit (Invitrogen, 18080-051), containing SuperScript® III RT (200 units μL^{-1}) after 1 µg of RNA was combined with Oligo$(dT)_{20}$ (50 µM), dNTP mix (10 mM), 5X First-strand buffer, DTT (0.1 M), 1 µL RNase OUT, and 1 µL RNase H.

The qPCR component of the RT-qPCR was carried out in 10 µL reactions containing 5.0 µL PerfeCTa® SYBR® Green SuperMix Low ROX (Quantabio), 0.3 µL each primer (P25-P30, Table 2.1), and with 4.4 µL of diluted (1:20) cDNAs. Optima water and no reverse-transcriptase (NRT) samples were used as negative controls. The reaction cycle is described in section 2.2.3. Three technical repetitions were performed for each of the three biological replications and for the negative controls. A standard curve was used to normalize *MGV1* expression to the housekeeping genes (*β-TUBULIN* and *EF-1α*) in the *MGV1_OX* and in WT strains, and to estimate the relative gene expression of *MGV1* using QIAgen's Relative Expression Software Tool (REST© V2.0.13) that tests for significance between two groups using a Pair Wise Fixed Reallocation Randomisation Test ©.

2.2.5 Immunodetection of Mgv1 in *MGV1_OX* transformants

Total protein was extracted from four-day old mycelium that grew on three PDA plates of *MGV1_OX* or the WT parental strain. The mycelium was ground to a powder in liquid nitrogen using a mortar and pestle. The protein was then solubilized from the powder in a MAPK extraction buffer (1 M NaCl, 50 mM NaF, 1 mM phenylmethylsulfonyl fluoride (PMSF), 1 mM Na_3VO_4, protease inhibitor cocktail (Thermofisher, Halt™ Protease Inhibitor Cocktail, EDTA-free, 100 µL per 10 mL buffer), 0.2 % *β*-mercaptoethanol (BME) and 50 mM sodium phosphate buffer, pH 8) at a ratio of 10 mL extraction buffer per g of fresh tissue.

Following a 1 h incubation at 4°C with gentle agitation, the extracts were centrifuged at 10,000 rpm (13,751 x g) at 4°C. The supernatant was collected and pushed through a 0.45 µm syringe filter. Samples were incubated with Bradford reagent (Sigma) for 20 min and absorbance was measured at 595 nm. Protein concentration was calculated against a standard curve generated with 0.1 to 1.0 mg mL^{-1} of Bovine serum albumin (BSA).

For immunoblotting, 10 µg of total protein was combined with 5 µL of 4 x LDS (Lithium dodecyl sulfate) buffer (Invitrogen, NP0008) and 1 µL BME into a final volume of 20 µL. Samples were heated for 10 min at 70°C and were then loaded onto 12-well Bolt™ 4-12 % Bis-Tris-Plus gels (Invitrogen, NW04122BOX). Electrophoresis was carried out at 150 V for 1.5 h using Bolt™ MOPS SDS Running Buffer (Invitrogen, B000102). Gels were run in duplicate, where one was stained with Coomassie Brilliant Blue R-250 (EMD, 3340) to visualize the resolved proteins, and the other was used to transfer proteins onto Polyvinylidene difluoride (PVDF) membranes (BIORAD, 1620174). Protein transfer was carried out by electrophoresis at 100 V for 1.5 h in transfer buffer (25 mM Tris, 192 mM glycine, pH 8.3) with 20 % methanol at room temperature, followed by staining with Pierce™ reversible protein stain kit for PVDF membranes (ThermoScientific, 24585) to verify uniformity of transfer. The membrane was blocked with 3 % BSA on Tris-buffered saline (TBS) for 1 h, and was subsequently probed overnight at 4°C with 10 mL of the primary antibody anti-phospho p44/42 MAPK (ERK1/2) (Table 2.3) diluted in 5 % BSA-TBST (TBS with Tween20 (0.05 %)). After the membrane was washed with TBST, it was incubated for 1 h at room temperature with 12 mL of Goat anti-rabbit-HRP conjugated secondary antibody from BIORAD (Table 2.3) and Precision Protein™ StrepTactin-HRP conjugated (1:10,000, BIORAD, 1610381) in 3 % BSA-TBST. SuperSignal™ West Pico PLUS Chemiluminescent Substrate was used to develop the bands in the blot.

Table 2.3. Antibodies used in Western blotting.

Antibodies	Catalog	Type of Antibody	Source	Dilution	Company
anti-phospho-p44/42 MAPK (ERK1/2)	9101S	Primary	Rabbit	1:1000	Cell Signal
anti-p44/42 MAPK (ERK1/2)	9102S	Primary	Rabbit	1:1000	Cell Signal
anti-MAP Kinase (ERK1/ERK-2)	M5670	Primary	Rabbit	1:1000	Sigma
anti-phospho-P38 MAPK	9211S	Primary	Rabbit	1:1000	Cell Signal
anti-P38 MAPK	9212	Primary	Rabbit	1:1000	Cell Signal)
anti-α Tubulin YOL 1/34	SC-53030	Primary	Rat	1:1000	Santa Cruz).
anti-Actin	ab1428	Primary	Mouse	1:1000	abcam
anti-rabbit-HRP conjugated	ab6721	Secondary	Goat	1:3000	abcam
anti-rat-HRP conjugated	ab97057	Secondary	Goat	1:10,000	abcam
anti-mouse-HRP conjugated	ab205719	Secondary	Goat	1:3000	abcam
anti-rabbit-HRP conjugated	170-6515	Secondary	Goat	1:3000	BIORAD
anti-mouse-HRP conjugated	170-6516	Secondary	Goat	1:3000	BIORAD
anti-rat-HRP conjugated	5204-2504	Secondary	Goat	1:3000	BIORAD

2.2.6 Mycelial growth and reproductive structures

Mycelial growth of the *MGV1_OX* transformants and the WT strain was first measured on PDA plates, which were inoculated with a 7-mm plug of mycelia and cultured as described in section 2.1. The growth diameter was measured every 24 h from eight plates per strain, until the mycelia reached the edge of the plate. The experiment was repeated twice.

Macroconidial spore germination was measured for each of the *MGV1_OX* transformants and the WT strain. Three 90-mm Petri dishes (replicates) containing SNA (synthetic nutrient

agar/Spezieller Nährstoffarmer Agar) medium were marked with 0.7 cm x 0.7 cm squares, and 8 squares were inoculated with approximately 30 macroconidial spores (3 µL of 10^4 macroconidia mL^{-1}). Plates were incubated at 27°C, and germination was observed in each square using a light microscope (Leica DM500) at 100X magnification. Germinated macroconidia, when the germ tube exceeded the size of the conidia, were counted at 3, 6 and 8 h post inoculation. Data was reported as percentage of macroconidial germination, and analysed by one-way ANOVA (Analysis of Variance) and the means were compared using Tukey test, $p \leq 0.05$.

To determine whether the transformants were able to form perithecia, three plates containing carrot agar and a 7-mm diameter mycelial plug of each of the *MGV1_OX* transformants and WT were incubated at 27°C for four days. On the fifth day, the mycelia were completely removed and 1.0 mL of 2.5 % Tween60 was added to surface of the plate and rubbed using a Drygalski spatula. Plates were then kept at 25°C under continuous light (176.5 µmol m^{-2} s^{-1}). After 48 h, if mycelia reappeared, 1.0 mL of 2.5 % Tween60 was added again, and the rub was repeated. Plates were returned to 25°C with continuous light, and perithecia appeared within three to five days of incubation. Perithecia were observed under the microscope (Leica DM500) at 100 X magnification and the cover slide was pushed to break them open and to corroborate the presence of ascospores inside those structures.

2.2.7 Wheat and *Brachypodium distachyon* disease assay

FHB assays were carried out on Roblin (susceptible to FHB) and Penhold (moderately resistant to FHB) Canadian wheat cultivars. The experiments were performed in a greenhouse with a 16 h photoperiod at 22°C day/18°C night. Two plants were seeded per 2 L pot (13.5 cm of diameter and 17.5 cm height) containing Cornell mix (Boodley and Sheldrake, 1972). During the anthesis stage, one spike per plant was point inoculated with 1000 spores of WT or *MGV1_OX*

transformants in 10 µL of sterile water containing 0.2 % of Tween20. After inoculation, plants were kept in a misting chamber with a 16 h photoperiod at 25°C day/night, and relative humidity of 95 %, with a light intensity of 253 µmol m^{-2} sec^{-1}. Plants were returned to the greenhouse after three days. The number of diseased spikelets per spike was analysed at 7, 12 and 18 days post inoculation (dpi) by counting the number of diseased spikelets below the inoculated spikelet, and including the inoculated one. The experiment was repeated three times over the course of four weeks. Mean values of five plants per inoculum were calculated for each repetition using one-way ANOVA, followed by Tukey's HSD test ($\alpha = 0.05$).

Brachypodium distachyon (Bd21) plants were seeded into pots (34 x 19 cm) with Vermiculite. The disease assay was carried out in a growth cabinet with a 20 h photoperiod at 25°C. During the anthesis stage one spike per plant was inoculated at the fifth spikelet from the top with 3 µL of macroconidial suspension ($1x10^5$ spores mL^{-1}) of WT, *MGV1_OX1* and *MGV1_OX2* strains. After inoculation plants were held in a misting growth cabinet at 95 % humidity. After three days, plants were returned to the first growth cabinet. The number of infected spikelets in each spike was counted at 3 and 5 days post inoculation. Three replicates with 10 plants for each treatment were performed. Mean values of 30 plants (10 plants per replicate) were calculated, and confidence level analysis with $\alpha = 0.05$, was carried out. Pictures were taken 6 days after inoculation.

2.2.8 Transcriptomic analysis of *F. graminearum* strains in DON-inducing media

Transcriptomics of *MGV1_OX*, the *Δmgv1* and WT strains, was carried out at AAFC-Ottawa by Drs. Kristina Shostak and Gopal Subramaniam. A detailed methodology is presented in the PhD dissertation, Shostak (2020). For this experiment, *F. graminearum* cultured from spores was grown in preferred nutrient (PN) for 24 h (28ºC, 160 rpm) and then transferred to non-preferred

nutrient (NPN) media to induce DON production. Since in NPN media the nutrients are limited, this condition is known to induce DON production, and this method of DON-induction is described herein as DON-inducing condition #1. Mycelia were harvested 24 h after transfer to NPN and used for RNA-seq (Shostak, 2020) or shipped to Lethbridge where I carried out immunoblotting as described in section 2.2.5, using primary antibodies that recognized the phosphorylated and unphosphorylated forms of the three MAPKs: Mgv1, Hog1 and Gpmk1 (Table 2.3).

RNA-seq was carried out on samples grown under DON-inducing condition #1. Details are presented in Shostak (2020). Briefly, RNA-seq was perfomed using Illumina NovaSeq 6000 platform at the Centre d'expertise et de services Génome Québec. Differential expression analysis was carried out using DESeq2, with the threshold fold change ≥ 2 and the FDR-adjusted p-value ≤ 0.05 (Shostak, 2020). A subset of differentially regulated genes identified in the RNA-Seq dataset was confirmed by Dr. Shostak by RT-qPCR, using the methods presented in Shostak (2020). Relative expression analysis of the RT-qPCR data using Pfaffl method with *EF1α* (FGSG_08811) and *β-TUBULIN* (FGSG_09530) as reference genes was performed. I carried out statistical analysis of the data using Student's t-test with $\alpha = 0.05$.

2.2.9 Analysis of secondary metabolism in *MGV1* deletion and overexpression strains

DON accumulation and metabolomic analysis of the *MGV1_OX* transformants, together with the *Δmgv1* and WT strains, were carried out at AAFC-Ottawa by Drs. Kristina Shostak and Gopal Subramaniam, as described in the PhD dissertation Shostak (2020). The methods are briefly described here.

2.2.9.1 15-acetylated DON (15-ADON) accumulation in axenic cultures

A two-stage liquid media protocol (DON-inducing condition #2) was utilized for trichothecene induction (modified from (Miller and Blackwell, 1986)). A suspension of 10 μL containing 2 x 10^4 spores was inoculated into Falcon Multiwell 6-well culture tray (Cat #35304) containing four mL of first stage growth media at pH 7.0. Each well contained an autoclaved nylon net filter (100 μm NY1H type from Millipore Ref# NY1H02500). The trays were sealed with parafilm and affixed to an orbital shaker, for 24 h in the dark, at 170 rpm. After 24 h, the liquid was removed using a sterile transfer pipette without disturbing the filter with the mycelial growth, and it was re-suspended in sterile water to remove traces of first stage media. This step was repeated, and the mycelia/filter was then re-suspended in 4 mL of second stage media, pH 4.0 (Miller and Blackwell, 1986). The mycelium was grown in second stage under same conditions described above and the supernatant was collected after 48 h.

Mycelial solids were collected and dried under vacuum for 24 h before weighing. A nylon filter was used as a blank measurement. Sample supernatant was first filtered (0.2 μm) and combined 450 μL sample + 150 μL MeOH in the HPLC vial (see Preparation of Culture Filtrate – below). Trichothecenes were analyzed on a Shimadzu prominence LC-20AD (Mandel) with 100 μL injection on a Shimadzu SIL-20A HT prominence auto sampler. Samples were run on a Restek Pinnacle DB C18 Column (5 um, 150 x 4.6 mm Cat # 9414565) using a 22.5 % isocratic MeOH:H_2O flow over 20 min at a rate of 1 mL min^{-1}. Trichothecenes were monitored by UV 220 nm.

2.2.9.2 Metabolomic profile of *F. graminearum* transformants

Macroconidia were produced in CMC media and used as the inoculum for all cultures at concentration of 5 x 10^3 spores mL^{-1}. The strains were cultured in GYEP (glucose, yeast extract,

peptone medium) for 24 h, followed by a wash step and growth in DON-induction medium (DON-inducing condition #3), previously described (Miller and Blackwell, 1986). *F. graminearum* WT, Δ*mgv1* and *MGV1_OX6* spores were inoculated in liquid GYEP media and incubated in the dark at 28° C for 24 h with constant shaking at 170 rpm. Following 24 h growth, cultures were split into four 15 mL cultures, and were incubated while stationary on a ~10° incline in the dark at 28° C for 3 to 9 days. Samples were collected at 3, 6, 9, and 12 days, and metabolites were extracted by shaking the mycelial mats in 25 mL of acetonitrile, as described by Shostak (2020). Three biological replications were also collected from cultures on days 3 and 6 for immunoblotting to determine whether Mgv1 was activated under these conditions. In addition, the blots were probed with antibodies that recognize the other two MAPKs, Hog1 and Gpmk1, to determine the activation status of the other MAPK pathways. Immunoblotting was carried out as described in section 2.2.5, and antibodies used are listed on Table 2.3.

2.2.10 Macroconidia germination and mycelial growth in culture media with cell wall and osmotic stress agents

To determine whether the overexpression of *MGV1* could improve the resistance of the *MGV1_OX* transformants to cell wall stress agents, spore suspensions (5 µL of 1 x 10^5 and 1 x 10^4 macroconidia mL^{-1}) were used to inoculate yeast peptone dextrose (YPD) agar supplemented with 0.01 % (100 µg mL^{-1}) sodium dodecyl sulfate (SDS), 200 µg mL^{-1} calcofluor white (CFW) or 500 µg mL^{-1} Congo red (CR). Pictures were taken after two days. The experiment was repeated but on PDA plates, instead of YPD, and 10 µL of 1 x 10^4 macroconidia mL^{-1} was used as inoculum. To analyze the effect of *MGV1* overexpression on the HOG pathway, the osmotic stress agent, NaCl (1 M or 58.44 mg mL^{-1}), was also included as a treatment. Mycelial growth was measured five days after inoculation and five plates per treatment were included.

The experiment was repeated using plates inoculated with a 7-mm diameter mycelial plug (obtained from the border of a four-day old colony) instead of spores. In addition, the *Δmgv1* mutant was included in the assay as a negative control of the Mgv1 pathway. Three plates per treatment were incubated at 27°C and the mycelial diameter was measured every 24 h for five days. The percentage of inhibition caused by the stressing agents was calculated from four-day old colonies with the formula: ((C-T)/C)*100, where C represents the diameter of the colony for one strain in the control treatment (PDA) while T represents the diameter of the colony for the same strain in PDA supplemented with the stress agent. Pictures were taken 6 days after inoculation. For each assay, data were analysed using a one-way ANOVA and the means were compared using Tukey's HSD test ($\alpha = 0.05$).

2.2.11 Immunodetection of MAPKs in presence of Congo red

Eight 50-mL conical tubes containing 20 mL of potato dextrose broth (PDB) were inoculated with 2 x 10^4 spores of *MGV1_OX* transformants or WT, and 16 tubes with *Δmgv1* (due to its slow growth). After 40-42 h of incubation at 180 rpm and 27°C, 80 µL of CR solution at 25 mg mL^{-1} were added to half of the tubes, for a final concentration of 100 µg mL^{-1} of CR, and 80 µL of autoclaved Optima water was added to the other half (control). Samples were returned to the shaking incubator for 45 min. Mycelium was collected in autoclaved paper towel (described in section 2.1) after filtration from the media, and was washed with 100 mL of autoclaved Nano pure water. Mycelium was transferred to liquid nitrogen and stored at -80°C until the tissue was ground for protein analysis, as described in sections below. The experiment was replicated three times.

To evaluate the effect of long-term exposure to CR on the Mgv1 pathway, 250-mL flasks containing 100 mL of PDB were inoculated with 10^5 spores of *F. graminearum* WT, *MGV1_OX*

or *Δmgv1* strains. The flasks were kept at 27°C, shaking at 180 rpm, and different concentrations of CR (50, 100 and 150 μg mL^{-1}) were added after 40 h of incubation. Treated and untreated samples were collected 6, 12 and 24 h after exposure to CR, as described in the previous paragraph. A pool of three flasks per treatment per strain was considered one replication. The experiment was replicated three times.

2.2.12 Differential expression of genes associated with the CWI pathway, with or without Congo red

RT-qPCR was used to compare the expression of specific genes among *MGV1_OX* and the WT parental strain. Total RNA was extracted from mycelium of strains grown on PDA (as described in section 2.2.3) or grown in 250-mL flasks with 100 mL PDB supplemented with 0, 50, 100 and 150 μg mL^{-1} of CR, as outlined in section 2.2.11. Mycelia from strains grown on PDB were harvested at 6, 12 or 24 h after CR (or water, as a negative control) treatments, as described in section 2.2.11. RT-qPCR was performed as described in section 2.2.2 with the primers that are listed on Table 2.1 and the reverse transcriptase SuperScript® IV RT. Names and accession numbers of genes used in this chapter are listed in Supplementary Table 2.1.

2.3 Results

2.3.1 Generation of transformants that overexpress *MGV1 in locus*

Following transformation for *in locus* overexpression of *MGV1*, ten colonies with similar morphology were grown on a selective media containing hygromycin. Four random colonies (*MGV1_OX1*, *MGV1_OX2*, *MGV1_OX6* and *MGV1_OX8*) were selected for further analysis. The correct position of the overexpression cassette in the *F. graminearum* genome was confirmed by a series of PCRs using the primers listed on Table 2.1, as schematized in Figure 2.1. The

presence of the N-6xHis-tag after the initiation codon, and the sequence of the whole insertion cassette was corroborated through sequencing (Génome Québec) of the amplicons obtained with the primer sets P15-P24 (Supplementary Figure 2.1). After performing qPCR it was confirmed the new transformants had the same *MGV1* copy number as the WT (Figure 2.2). The overexpression of *MGV1* compared to WT was confirmed in each of the four transformants by RT-qPCR (Figure 2.3).

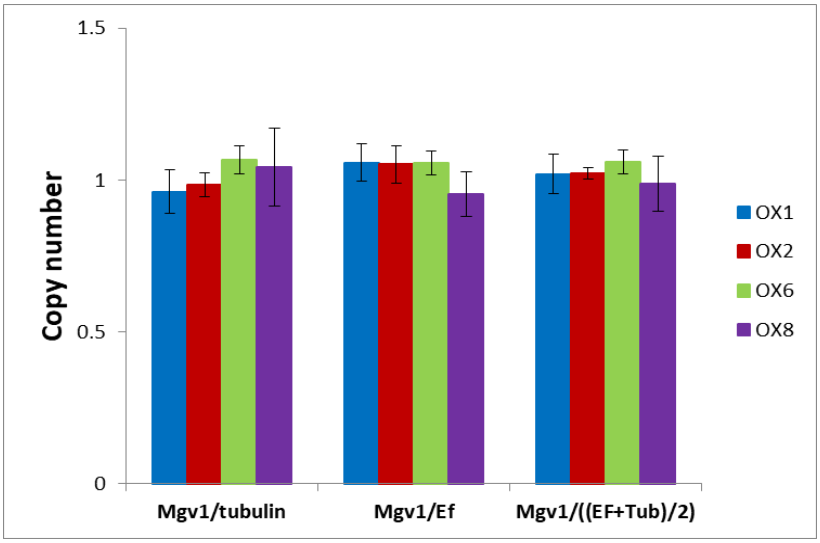

Figure 2.2. Copy number of *MGV1* analyzed by qPCR. Values of the *MGV1_OX* transformants were normalized against housekeeping genes *EF-1α* and *β-TUBULIN*, and with WT. Data was processed using REST© software that uses a pair wise fixed reallocation randomisation test © for comparing the expression ratios of the transcripts (α= 0.05). Bars represent the standard errors. No statistical differences were observed between the *MGV1_OX* strains and the WT.

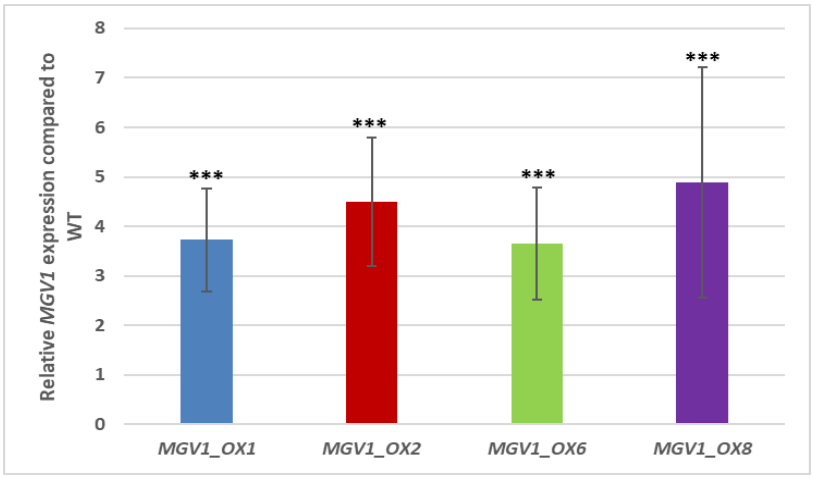

Figure 2.3. Relative expression of MGV1 in the MGV1_OX transformants compared to WT. Mycelia were collected from PDA plates, five days after inoculation. Relative expression compared to WT was calculated using REST© software that uses a pair wise fixed reallocation randomisation test © for comparing the expression ratios of the transcripts. Asterisks represent statistical differences at $p \leq 0.05$ (*), $p \leq 0.01$ (**), and $p \leq 0.001$ (***). Bars represent the standard errors of three biological replicates and three technical replicates (n=9). CT-values were normalized with the housekeeping genes: EF-1α and β-TUBULIN.

To determine if increased gene expression resulted in increased protein accumulation, immunoblotting was performed using anti-ERK like antibodies. Two bands at the expected sizes of the *F. graminearum* phosphorylated MAPKs ERK1/2-like (Mgv1 and Gpmk1) were observed (Figure 2.4). The Mgv1 protein is composed of 416 aa and has a predicted molecular weight of 46.9 kDa (47.8 kDa with the N-6x-His-tag modification), while Gpmk1 is around 41.17 kDa. *MGV1_OX6* showed a more intense band corresponding to a phosphorylated form of Mgv1 compared to the other *MGV1_OX* transformants and the WT.

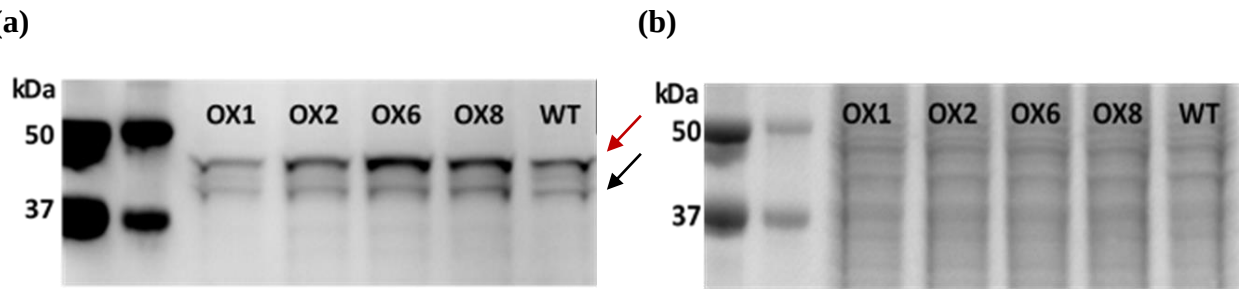

Figure 2.4. (a) Blot representing the ERK1/2-like proteins in *F. graminearum*: Mgv1 and Gpmk1. Mgv1 (red arrow) size is estimated as 46.9 kDa in the WT, and about 47.8 kDa in *MGV1_OX6* due to the N-6xHis-tag, while Gpmk1 (black arrow) is around 41.2 kDa. **(b)** Total protein observed in the blot before blocking with 3 % BSA, and developed with PierceTM reversible protein stain kit for PVDF membranes. First and second lanes are protein markers.

2.3.2 Mycelial growth, macroconidia germination and perithecia formation are not affected by the overexpression of *MGV1*

The mycelial growth of the four transformants overexpressing *MGV1* was similar to the WT, and there was no statistically significant difference in the diameter of the colonies among them (Figure 2.5). All of the strains showed a cottony white-creamish pattern with a similar growth rate. The transformants and the WT started to reach the edge of the PDA plate four days after inoculation.

(a)

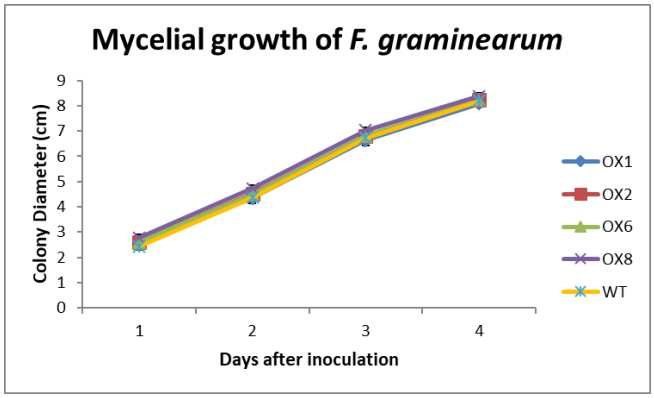

(b)

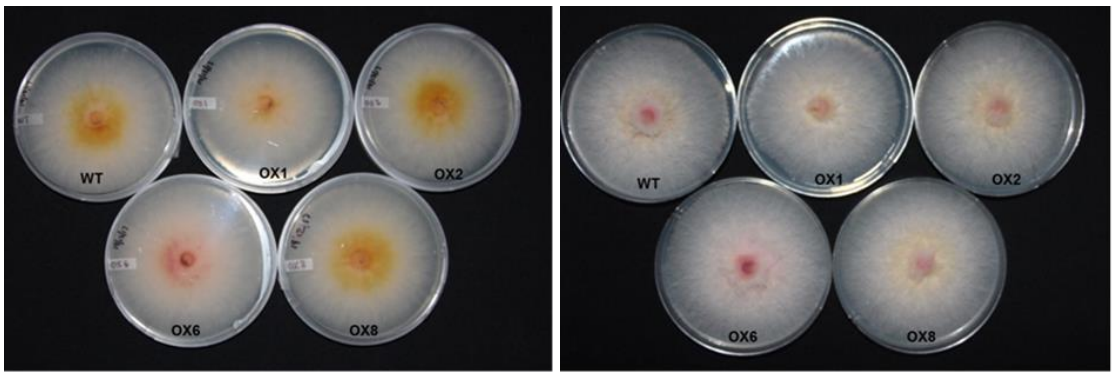

Figure 2.5. Mycelial growth of *F. graminearum* transformants overexpressing *MGV1*, and the WT. (**a)** Colony diameter every 24 h after inoculation. Bars represents the confidence level at 95 %. (**b)** Bottom (left) and top (right) of the plates four days after inoculation.

The asexual reproductive structure of *F. graminearum* are macroconidial spores, which are one of the most important inoculum sources for FHB disease. In this assay, the effect of overexpressing *MGV1* on the germination of macroconidia was analyzed. Macroconidia were considered germinated when their length was surpassed by the length of the germ tube. The macroconidia germination rate was similar among the WT and the *MGV1_OX* transformants at 3, 6 and 8 h post Petri dish inoculation (Figure 2.6). After 3 h of incubation, less than 5 % of the macroconidia were germinated, while at 8 h the number increased to more than 70 %.

(a) **(b)**

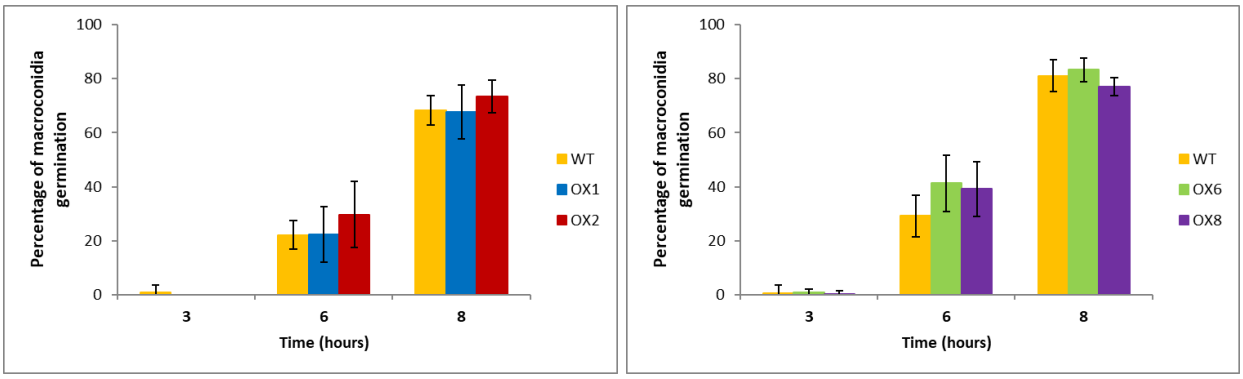

Figure 2.6. Percentage of macroconidia germination at 27°C after different incubation times, in a Petri plate containing: (**a)** WT, *MGV1_OX1* and *MGV1_OX2*; (**b)** WT, *MGV1_OX6* and *MGV1_OX8*. Three plates were used as replication in each case. Data was analyzed through one-way ANOVA, followed by Tukey's HSD test ($\alpha = 0.05$). Error bars represent the standard deviation.

F. graminearum is a homothallic species, which means it can form sexual structures without the presence of another mating type. Perithecia formation started to appear five days after the plates were scraped with Tween60, in all the plates inoculated with the WT and *MGV1_OX* transformants. Ten days after the plates were scraped, perithecia were put on slides and a glass coverslip was used to break the structure and to observe the release of asci and ascospores. Ascospores release was observed for all transformants and WT strains (Figure 2.7).

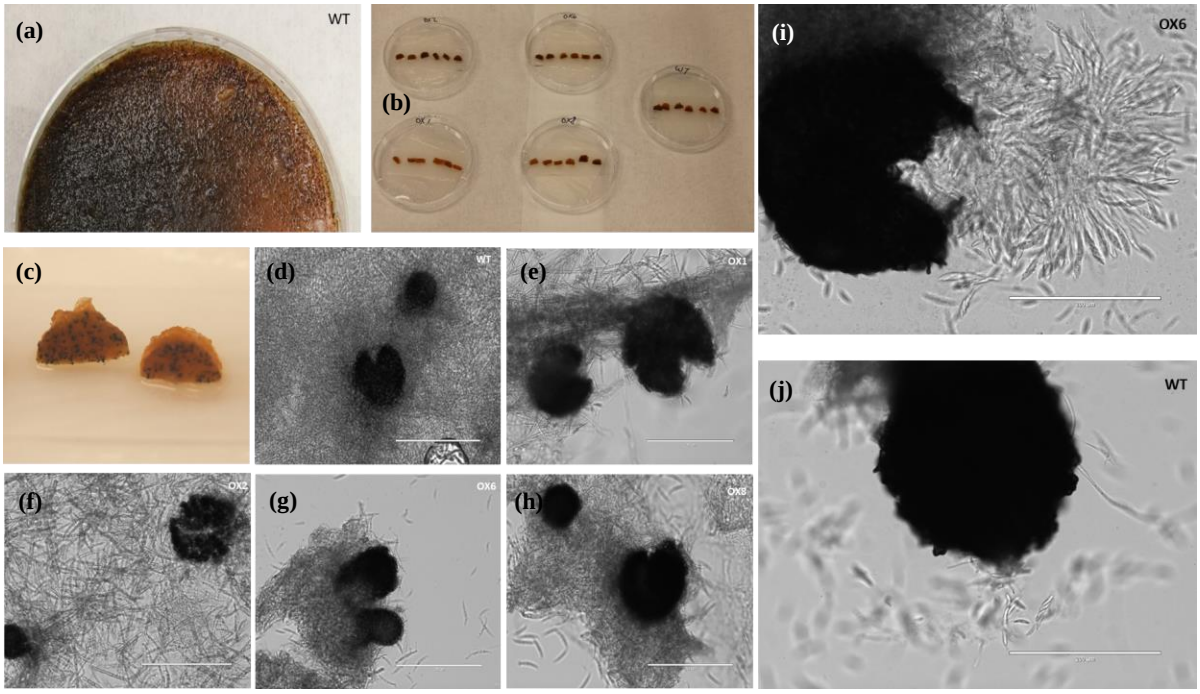

Figure 2.7. Perithecia and ascospores released from *F. graminearum MGV1_OX* and WT strains. Bars represent 200 µm. **(a)** A WT plate with black perithecia structures. **(b)** Plates with wet filter paper and a slide with agar plugs containing perithecia. **(c)** A closer view of agar discs containing perithecia. (**d-j)** Perithecia observed under the microscope for WT, *MGV1_OX1*, *MGV1_OX2*, *MGV1_OX6* and *MGV1_OX8*. **(i-j)** Higher magnification of ascospore release from perithecia (*MGV1_OX6* and WT).

2.3.3 The overexpression of *MGV1* does not increase the virulence in wheat or *B. distachyon*

In order to determine whether the overexpression of *MGV1* will affect the virulence in wheat heads, two cultivars were inoculated with the *MGV1_OX* transformants. The Canadian cultivars Roblin (susceptible to FHB) and Penhold (moderately resistant to FHB) were both point inoculated with macroconidia of *MGV1_OX* strains and WT. The number of infected spikelets in each spike was counted after 7, 12 and 18 dpi. There was no difference in the infection rate caused by *MGV1_OX* transformants compared to the WT in either of the cultivars tested (Figures 2.8 and 2.9). Interestingly, Penhold was as susceptible as Roblin to these strains; however, the

variance among the plants was higher in the former. In general, the disease spread at the same rate in all the strains tested in the same cultivar (Figures 2.8 and 2.9).

In Roblin, at 7 dpi the average number of infected spikelets per spike was close to four, while in Penhold this value was less than three. At 12 and 18 dpi, a similar disease pattern was observed for both cultivars, but at 18 dpi, even though around 100 % of spikelets were showing disease symptoms, there were more infected spikelets in Penhold than in Roblin since the former contains fewer spikelets than the latter (Figures 2.8 and 2.9).

A similar experiment was repeated where *Δmgv1* was included to corroborate that the deletion of the gene does not allow the spread of the disease through the inoculated spikelet (Chapter 3, Figures 3.6 and 3.7). After 7, 12 and 18 dpi, the disease was not observed in more than the inoculated spikelets (Figures 3.6 and 3.7).

B. distachyon, a model plant for cereals, was also inoculated with two of the *MGV1_OX* transformants. The number of infected spikelets per spike were not statistically different among all tested strains after 3, and 5 dpi (Figure 2.10).

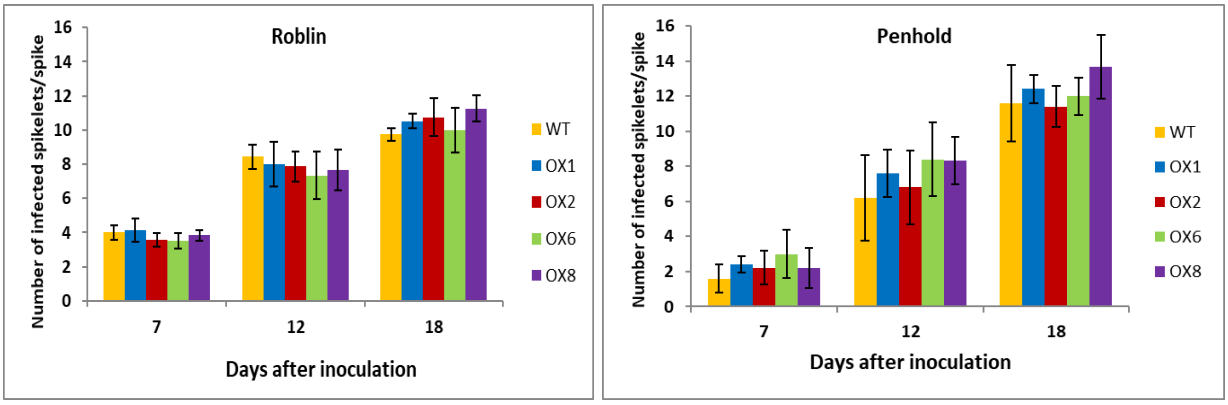

Figure 2.8. *F. graminearum* virulence in wheat spikes. Number of infected spikelets/spike after 7, 12 and 18 dpi in the susceptible cultivar "Roblin" and the moderately resistant cultivar "Penhold". Bars represent the average of one repetition which consisted of five plants/strain, analyzed for differences in virulence through one-way ANOVA, followed by Tukey's HSD test ($\alpha = 0.05$). Error bars represent the standard deviation. The experiment was repeated twice more with similar results.

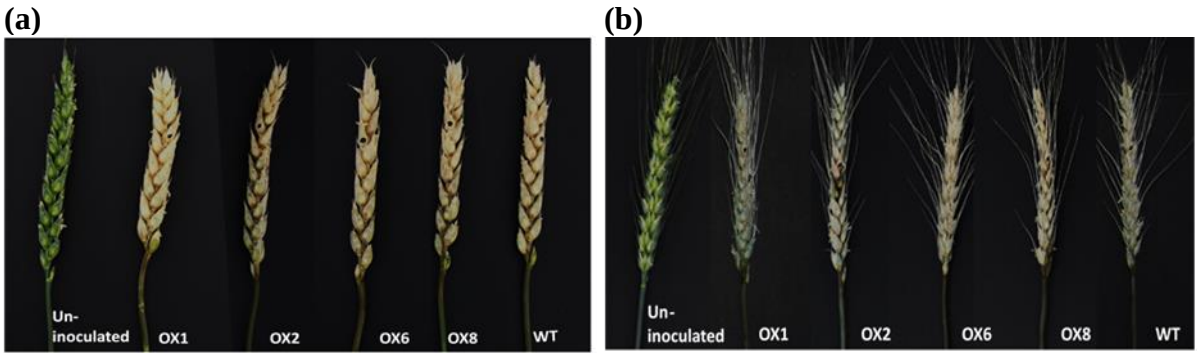

Figure 2.9. Spikes of the susceptible wheat cultivar Roblin **(a)** and the moderately resistant wheat cultivar Penhold **(b)** at 18 dpi. The black dot in the 5th-7th spikelet from the top represents the point where 1 x 10^4 spores in a 10 µL volume were inoculated.

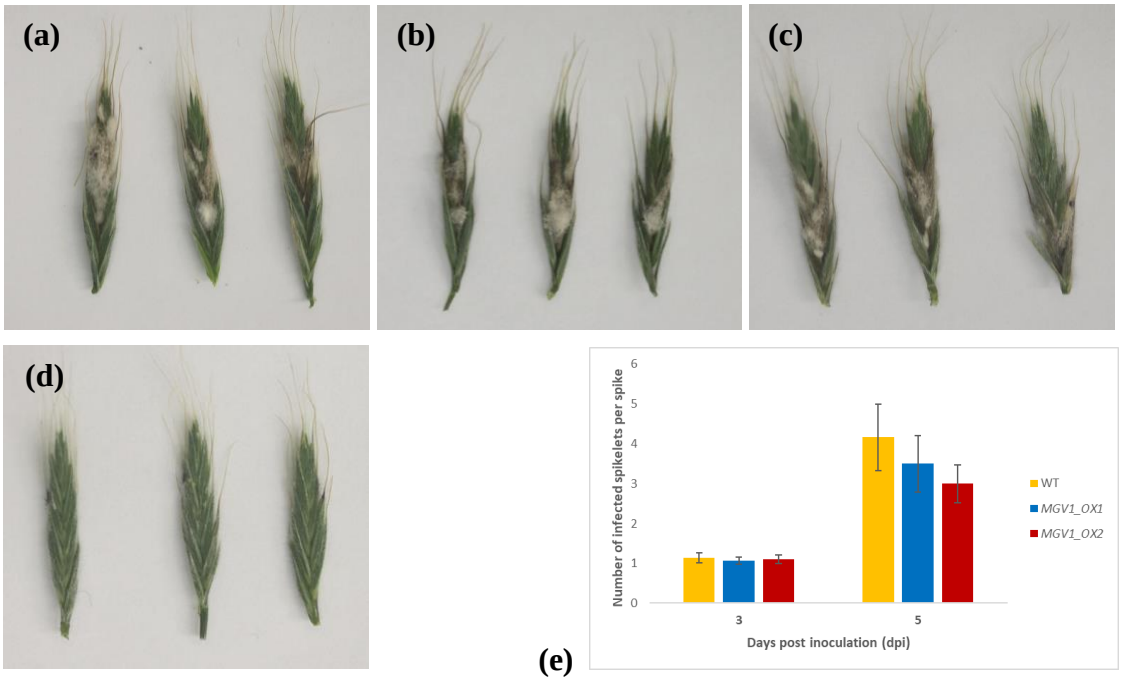

Figure 2.10. *B. distachyon* spikes were point inoculated at the fifth spikelet from the top, with 3 µL of macroconidial suspension (1 x 10^5 spores mL^{-1}) of **(a)** WT, **(b)** *MGV1_OX1*, **(c)** *MGV1_OX2*. **(d)** Spikelets were inoculated with 3 µL of autoclaved distilled water (control). **(e)** Number of infected spikelets in each spike was counted at 3 and 5 dpi. Mean values of 30 plants are showed, and bars represent confidence levels for α = 0.05, n=30. No statistical differences were observed among treatments. Pictures were taken at 6 dpi.

2.3.4 The role of Mgv1 in secondary metabolite production

Metabolomic profiling was carried out to study the outcome of *MGV1* deletion or overexpression in secondary metabolite production. This analysis was performed by Dr. Rajagopal Subramaniam and Dr. Kristina Shostak, collaborators at AAFC-Ottawa lab. The results have been already published (Shostak, 2020) but specific aspects of interest will be highlighted here in this thesis.

The data regarding metabolite accumulation by each *F. graminearum* strain was used to perform a principal component analysis (PCA) at 12 days after inoculation (endpoint of the time course experiment) and under DON-condition 3. The results showed that WT, *MGV1_OX1* and *MGV1_OX6* were more similar among them than *Δmgv1* (Figure 2.11). The main differences among the samples were attributed to the differences between strains, which explained a variation about 48 % in PC1. Therefore, the deletion of *MGV1* had a stronger impact on secondary metabolite production than overexpression of the gene.

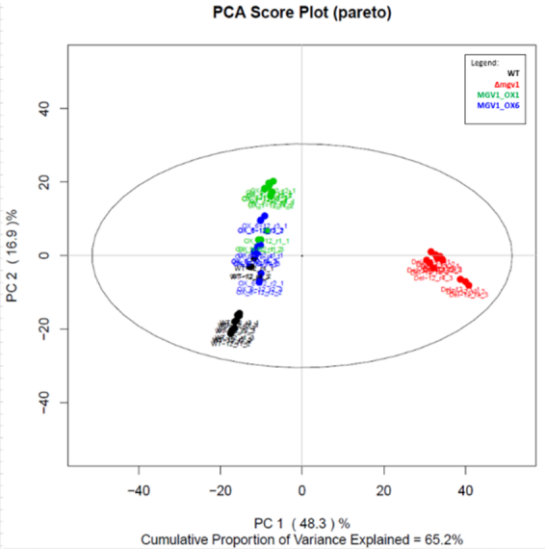

Figure 2.11. Principal component analysis of metabolite accumulation data from samples collected 12 dpi. WT (black), *MGV1_OX1* (green), *MGV1_OX6* (blue) and *Δmgv1* (red).

After 12 days, the deletion of *MGV1* affected 818 different features (ionized molecule or fragment of a molecule) from which 33 corresponded to known metabolites, including gramillin, fusarins, fusaoctaxin (and related compounds), sambucinol, and some trichothecene intermediates. From those 818, 223 where also shared with *MGV1_OX1* and *MGV1_OX6*, and just 3 of the shared ones were representations of gramillins A and B, leaving 220 unidentified. The *MGV1_OX* transformants, also shared 42 features of the total 602 and 293 from *MGV1_OX1* and *MGV1_OX6*, respectively. In the case of *MGV1_OX6*, only 5 of the metabolites detected were known, including gramillins, fusarielin, and shearinine (Figure 2.12).

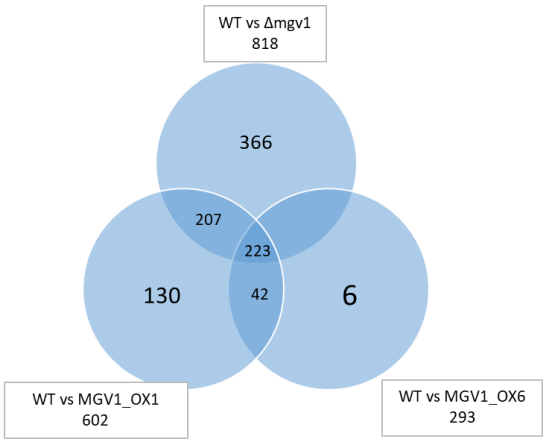

Figure 2.12. Venn diagram of differentially produced secondary metabolites by *F. graminearum Δmgv1* mutant, and the *MGV1_OX1* and *MGV1_OX6* transformants, compared to WT at 12 dpi.

2.3.4.1 Trichothecenes

The secondary metabolite DON is considered a virulence factor used by *F. graminearum* during the spread of the disease within wheat heads. It was previously suggested that Mgv1 might be involved in the regulation of DON production since its deletion reduced the accumulation of this metabolite (Hou *et al*., 2002). The question arose whether a higher abundance of this protein could affect DON production. Thus, the accumulation of 15-ADON, a precursor of DON, was

measured in axenic cultures under DON-inducing condition # 2. Interestingly, the overexpression of *MGV1* did result in increased accumulation of this mycotoxin; however, the amount produced by *Δmgv1* was similar to that of the WT (Figure 2.13).

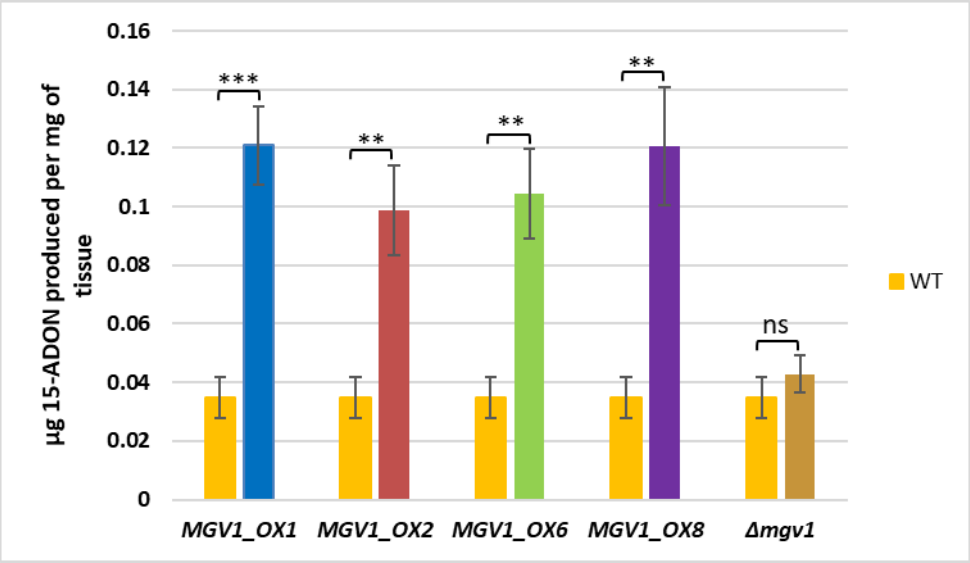

Figure 2.13. 15-ADON accumulation under axenic conditions in *F. graminearum MGV1_OX* transformants, *Δmgv1* and WT strains. Bars represent mean of four values, analyzed by Student t-test. Error bars represent the standard deviation. Asterisks indicate a statistically significant difference with ** $p \leq 0.01$ and *** $p \leq 0.001$, while ns stands for no statistical differences.

In PDA, the relative expression of *TRI5*, the enzyme that catalyzes the first step in DON biosynthesis, was not significantly different in the transformants compared to WT (Figure 2.14). Similarly, the global transcription factor, *TRI6*, that regulates *TRI* gene expression was not differentially expressed in the *MGV1_OX* transformants, with the exception of *MGV1_OX2*, which showed a slight increase in relative expression (Figure 2.14).

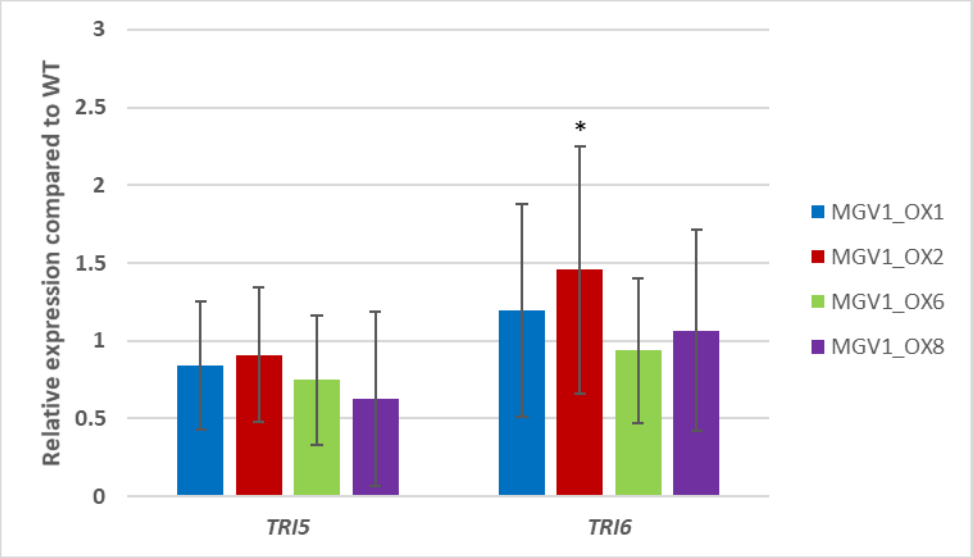

Figure 2.14. Relative *TRI5* and *TRI6* gene expression in the *MGV1_OX* transformants compared to WT. Mycelia were collected from PDA plates five days after inoculation. Relative expression was calculated using REST© software, that uses the pair wise fixed reallocation randomisation test © for comparing the expression ratios of the transcripts. The asterisk represents statistical differences at $p \leq 0.05$ (*). Bars represent the standard errors of three biological replicates and three technical replicates (n=9). CT-values were normalized with the housekeeping gene *β-TUBULIN*.

The transcriptomic analysis performed on samples collected from DON-inducing condition #1, showed that the *TRI5* and *TRI6* genes were downregulated in *Δmgv1* mutant, but in *MGV1_OX6* the regulation was similar to WT (Table 2.4). These results from the RNA-seq analysis were confirmed by RT-qPCR (Figure 2.15), and it supported what was previously observed in Figure 2.14 (without DON-induction). Interestingly, *MGV1* overexpression did lead to an increase in 15-ADON production under DON-inducing condition #2 (Figure 2.13).

Table 2.4. Fold-change of the *TRI* gene cluster transcription, as assessed by RNA-seq in *Δmgv1, MGV1_OX1* and *MGV1_OX6* compared to WT. Samples were collected under DON-inducing condition #1. Empty cells indicate no change compared to WT.

Cluster ID	Gene	Description	Fold-change		
			***Δmgv1* vs WT**	***MGV1_OX1* vs WT**	***MGV1_OX6* vs WT**
C03|23 (Trichothecenes)	FGSG_00071	cytochrome P450 monooxygenase (TRI1)	-5		
	FGSG_03529	glycosyl hydrolase family 17	-30		
	FGSG_03531	monooxygenase	-235		
	FGSG_03532	trichothecene C-15 esterase (TRI8)	-7		
	FGSG_03533	3-acetyltrichothecene4-O-acetyl transferase	-4		
	FGSG_03534	15-O-acetyl transferase	-8		
	FGSG_03535	trichodiene oxygenase	-5		
	FGSG_03537	trichodiene synthase (TRI5)	-7		
	FGSG_03538	Regulatory			
	FGSG_03539	AF359360_10 (TRI9)	-8		
	FGSG_03540	isotrichodermin C-15 hydroxylase	-4		
	FGSG_03541	trichothecene efflux pump	-3		
	FGSG_03542	cytochrome P450 (TRI13)	-4		
	FGSG_03543	trichothecene biosynthesis gene(TRI14)	-5		
	FGSG_16251	Regulatory	-5		

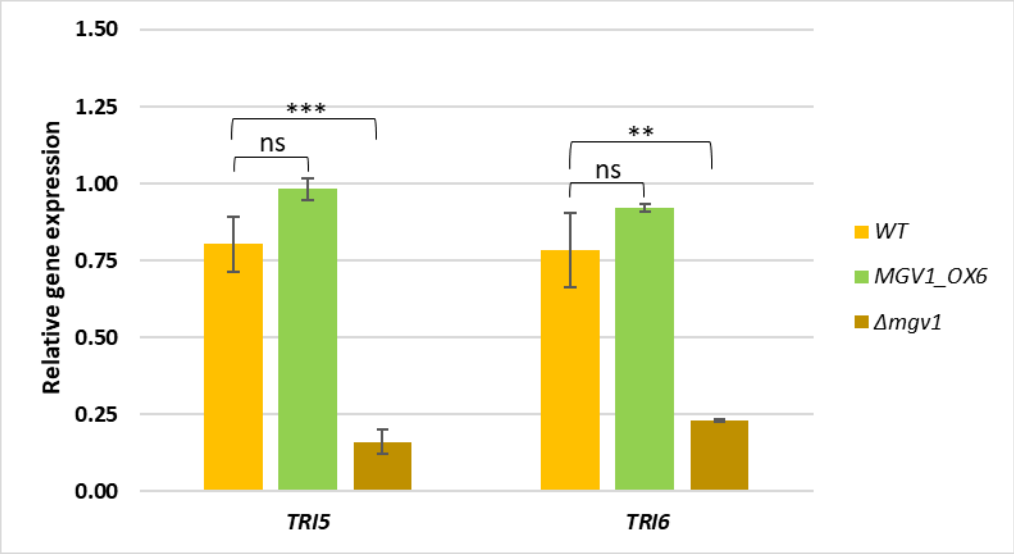

Figure 2.15. Relative *TRI5* and *TRI6* gene expression in WT, *MGV1_OX6* and *Δmgv1* strains. Mycelia were collected under DON-inducing condition #1 for RNA-seq and RT-qPCR analyses. Bars represent mean of the values, analyzed by Student t-test. Error bars represent the standard errors of three biological replicates and three technical replicates (n=9), with ** $p \leq 0.01$, *** $p \leq 0.001$, while ns stands for no statistical differences. CT-values were normalized with the housekeeping gene *EF-1α*.

Metabolomic profiling showed a high impact of *MGV1* deletion on trichothecenes production and accumulation, in particular at 9 dpi. From a total of 12 features, 11 were increased in *Δmgv1* compared to WT, with 15-ADON highly produced at 9 dpi (Table 2.5). The overexpression of *MGV1* did not affect the amount of the trichothecenes compared to WT. The data suggests a negative regulation of trichothecene production by Mgv1 under these conditions (DON-induction condition #3), which is the opposite of what was observed for *TRI5* and *TRI6* expression under DON-inducing conditions #1 (Figure 2.15).

Table 2.5. Differentially produced and accumulated secondary metabolites (DON and its derivatives) in *Δmgv1* and *MGV1_OX* transformants compared to WT at 3, 6, 9 and 12 dpi in DON-induction media. (+) symbol indicates the amount of the metabolite detected in the mutant or the transformant is higher than in the WT, while (-) symbol indicates the amount in the mutant or transformant is lower compared to the WT. Empty cells indicate no change compared to WT. SMC: secondary metabolites cluster. RT: retention time.

SMC ID	Feature ID	RT	*Δmgv1 vs* WT				*MGV1_OX1 vs* WT				*MGV1_OX6 vs* WT			
			3	6	9	12	3	6	9	12	3	6	9	12
CO3/23 Trichothecene)	4-deoxynivalenol (DON)	3.53_279.1216			+									
	15-ADON	3.53_321.1322			+									
		3.53_339.1427			+									
	DON-related	3.99_414.1928			+									
		4_235.1684			+	-								
		4.3_251.1633		-		-								
		4.36_235.1684			+									
		4.39_275.1609		+	+	+								
		4.4_251.1633			+									
		4.4_398.1966		+	+	+								
		4.7_396.1793	-		+	+								
		4.93_235.1684			+	+								

Despite the results of the metabolomics study, where more secondary metabolites associated with the CO3/23 (Trichothecene) metabolite cluster were produced in *Δmgv1* than in the WT at 9 dpi, the transcriptomic analysis performed on *Δmgv1*, where samples were collected under DON-inducing condition #1, showed downregulation of 14 genes in the trichothecene biosynthetic pathway (Table 2.4), suggesting a positive regulation of those genes by Mgv1. There was no

difference in gene expression when *MGV1* was constitutively overexpressed compared to the WT. This might suggest that *mgv1* deletion does regulate the trichothecene secondary metabolic cluster (SMC) and trichothecene production levels, but its overexpression does not affect the *TRI* gene cluster.

2.3.4.2 Non-ribosomal peptides (NRPs)

The secondary metabolites and non-ribosomal peptides gramillins (A and B), which are considered virulence factors of *F. graminearum* towards maize (Bahadoor *et al*., 2018), were positively regulated by Mgv1 under DON-inducing condition #3, since the deletion of *MGV1* negatively affected its production at 6, 9 and 12 dpi (Table 2.6). However, the results of the RNA-seq analysis, where mycelium was collected after a shorter time than then metabolomic analysis under DON-inducing condition #1, showed that neither the deletion nor the overexpression changed its expression compared to WT (Table 2.7).

Table 2.6. Differentially produced and accumulated secondary metabolites in *Δmgv1* mutant and *MGV1_OX* transformants compared to WT at 3, 6, 9 and 12 dpi in DON-induction media. (+) symbol indicates the amount of the metabolite detected in the mutant or the transformant is higher than in the WT, while (-) symbol indicates the amount in the mutant or transformant is lower compared to the WT. Empty cells indicate no change compared to WT. SMC: secondary metabolites cluster. RT: retention time.

SMC ID	Feature ID	RT	*Δmgv1 vs* WT				*MGV1_OX1 vs* WT				*MGV1_OX6 vs* WT			
			3	6	9	12	3	6	9	12	3	6	9	12
C02	Gramillin A	4.19_869.3477		-	-	-								
		4.2_847.3672		-	-	-								
		4.39_829.3573			-	-								
	Gramillin B	4.22_861.3817		-		-								
		4.42_843.3714		-	-									
C21	Fusarinine	3.1_243.1331		-	+								+	

Table 2.7. Fold-change of the gramillin and triacetylfusarinine gene cluster transcription, as assessed by RNA-seq in *Δmgv1, MGV1_OX1* and *MGV1_OX6* compared to WT. Samples were collected under DON-inducing condition #1. Empty cells indicate no change compared to WT.

Cluster ID	Gene	Description	Fold-change		
			***Δmgv1* vs WT**	***MGV1_OX 1* vs WT**	***MGV1_OX6* vs WT**
C02 Gramillins	FGSG_00036	fatty acid synthase alpha partial			
	FGSG_00039	Hypothetical protein			
	FGSG_00043	thioredoxin reductase			
	FGSG_00044	hydrolase or acyl transferase of alpha beta super family			
	FGSG_00045	Alpha beta hydrolase fMIPS_-1			
	FGSG_00046	hypothetical protein			
	FGSG_00047	hypothetical protein			
	FGSG_00048	Oxoglutarate iron-dependent oxygenase			
	FGSG_00049	branched-chain-amino-acidamino transferase			
	FGSG_11653	unnamed protein product			
	FGSG_11656	fatty acid synthase beta subunit			
	FGSG_11657	Nitrogencatabolic enzyme regulatory			
	FGSG_11658	Myc-typebasic helix-loop-helix bHLH domain			
	FGSG_15673	Non-ribosomal peptide synthetase			
	FGSG_15680	Cytochrome E-group I			
C21 Triacetylf usarinine	FGSG_03744	siderophore iron transporter mirB	2		
	FGSG_03745	related to aerobactin siderophore biosynthesis iucB			
	FGSG_03747	nonribosomal peptide synthetase			
	FGSG_16211	enoyl-hydratase			
	FGSG_16212	ferri-bacillibactin esterase			

Fusarinines are also NRPs, and are considered hydroxamate-type siderophores composed of 2 or 3 fusarinine subunits (Holinsworth and Martin, 2009). Fusarinine production was less in *Δmgv1* than in WT at 6 dpi, but by 9 dpi opposite pattern was observed (Table 2.6). The increased fusarinine in *Δmgv1* compared to WT at 9 dpi was in accordance with the upregulation of FGSG_03744, a siderophore iron transporter mirB associated with this pathway, and whose expression was upregulated in *Δmgv1* under DON-induction media (Table 2.7). Interestingly, at 9 dpi the transformant *MGV1_OX6* also produced more fusarinine than the WT (Table 2.6).

2.3.4.3 Fusarin and Aurofusarin

The production of the polyketide mycotoxins, fusarins, seemed to be negatively regulated by *MGV1* (Table 2.8). *MGV1* deletion caused a billion-fold increase of Fusarin A accumulation at 6, 9 and 12 dpi compared to WT. The overexpression of *MGV1* did not change the Fusarin A

production in the transformants compared to WT. Fusarin C/D/B were less produced at 3 dpi in the *Δmgv1* mutant compared to WT but the pattern changed, and it was more abundant at 9 and 12 dpi, similar to what was observed for Fusarin A. The transcriptomic analysis showed up-regulation in 9 of the 10 genes associated with the C42 fusarins cluster in *Δmgv1* (Table 2.9), in accordance with the metabolomics results for 6, 9 and 12 dpi, even though the conditions of the media were different. The overexpression of *MGV1* reduced Fusarin C/D/B production compared to the WT at 3 and 6 dpi, and except for 1 feature in *MGV1_OX1* that was 14 billion-fold less than the WT, the level of the other features were around 10-fold diminished. Contrary to this reduction in Fusarin C/D/B production, the RNA-seq analysis showed up-regulation in 7 and 9 genes of the C42 fusarin cluster in *MGV1_OX1* and *MGV1_OX6*, respectively, compared to WT, suggesting that the regulation changed when conditions changed as well.

Table 2.8. Differentially produced and accumulated secondary metabolites in *Δmgv1* mutant and *MGV1_OX* transformants compared to WT at 3, 6, 9 and 12 dpi in DON-inducing condition #3. (+) symbol indicates the amount of the metabolite detected in the mutant or the transformant is higher than in the WT, while (-) symbol indicates the amount in the mutant or transformant is lower compared to the WT. Empty cells indicate no change compared to WT. SMC: secondary metabolites cluster. RT: retention time.

SMC ID	Feature ID	RT	*Δmgv1 vs* WT				*MGV1_OX1 vs* WT				*MGV1_OX6 vs* WT			
			3	6	9	12	3	6	9	12	3	6	9	12
C42	Fusarin A	4.88_398.1953		+	+	+								
		4.93_438.1878		+	+	+								
	Fusarin C/D/B	4.61_432.2001	-		+	+	-	-			-	-		
C13	Aurofusarin	4.9_571.0851		+		+								

Table 2.9. Fold-change of the fusarin and aurofusarin gene cluster transcription, as assessed by RNA-seq in *Δmgv1, MGV1_OX1* and *MGV1_OX6* compared to WT,. Samples were collected under DON-inducing condition #1. Empty cells indicate no change compared to WT.

Cluster ID	Gene	Description	Fold-change		
			***Δmgv1* vs WT**	***MGV1_OX1* vs WT**	***MGV1_OX6* vs WT**
C42 Fusarins	FGSG_07795	hypothetical protein	-4		
	FGSG_07798	polyketide synthase	13	5	8
	FGSG_07801	fusarinC cluster-oxido reductase	5	3	5
	FGSG_07802	fusarinC cluster-transporter	4	2	3
	FGSG_13222	alpha beta hydrolase	7	3	4
	FGSG_13223	fusarinC cluster-translationElongation factor	4	1.8	2
	FGSG_16898	fusarinC cluster-peptidase	3	1.9	3
	FGSG_16899	fusarinC cluster-oxido reductase	14	4	5
	FGSG_16900	fusarinC cluster-cytochrome P450	10	4	7
	FGSG_16901	fusarinC cluster-methyl transferase	9	4	7
C13 Aurofusarin	FGSG_02320	transcription factor (AURR1)	4		
	FGSG_02321	6-hydroxy-d-nicotine oxidase (AUR0)	4		
	FGSG_02322	major facilitator super family transporter			
	FGSG_02323	fungalspecific transcription factor domain-containing (AURR2)	1.6		
	FGSG_02324	polyketide synthase (PKS12)	69	4	3
	FGSG_02325	conidial pigment polyketide synthase partial	55	3	
	FGSG_02326	sterigmatocystin 8-o-methyl transferase (AURJ)	98	5	3
	FGSG_02327	dimethylaniline monooxygenase 3 (AURF)	82	5	3
	FGSG_02328	conidial pigment biosynthesis oxidasearb2 brown2 (GIP1)	74	4	
	FGSG_02329	fasciclin domain family	83	4	2
	FGSG_02330	L-ascorbate oxidase	2		-3

Aurofusarin is a fungal polyketides red pigment, and as secondary metabolite, its biosynthetic pathway genes are usually found in clusters. *AURR1* encodes a TF necessary for the full expression of several genes in the aurofusarin cluster, such as *AURR2* (transcription factor), *AURJ* (O-methyltransferase), *GIP1* (a putative laccase) and *PKS12* (polyketide synthase). Under DON-inducing condition #3, aurofusarin was inferred to be negatively regulated by *MGV1* since its deletion increased the production of the metabolite (Table 2.8). These results were in accordance with the expression of the genes in the biosynthetic pathway measured during the RNA-seq analyses (Table 2.9), and with the RT-qPCR that was performed to confirm the transcriptomic results (Figure 2.16). Even though *MGV1* deletion caused a strong increase in the transcript levels of the genes, *MGV1* overexpression also increased the expression of some genes

in the biosynthetic pathway but at a modest level (Table 2.9). In general, the results suggest that aurofusarin is transcriptionally regulated by Mgv1.

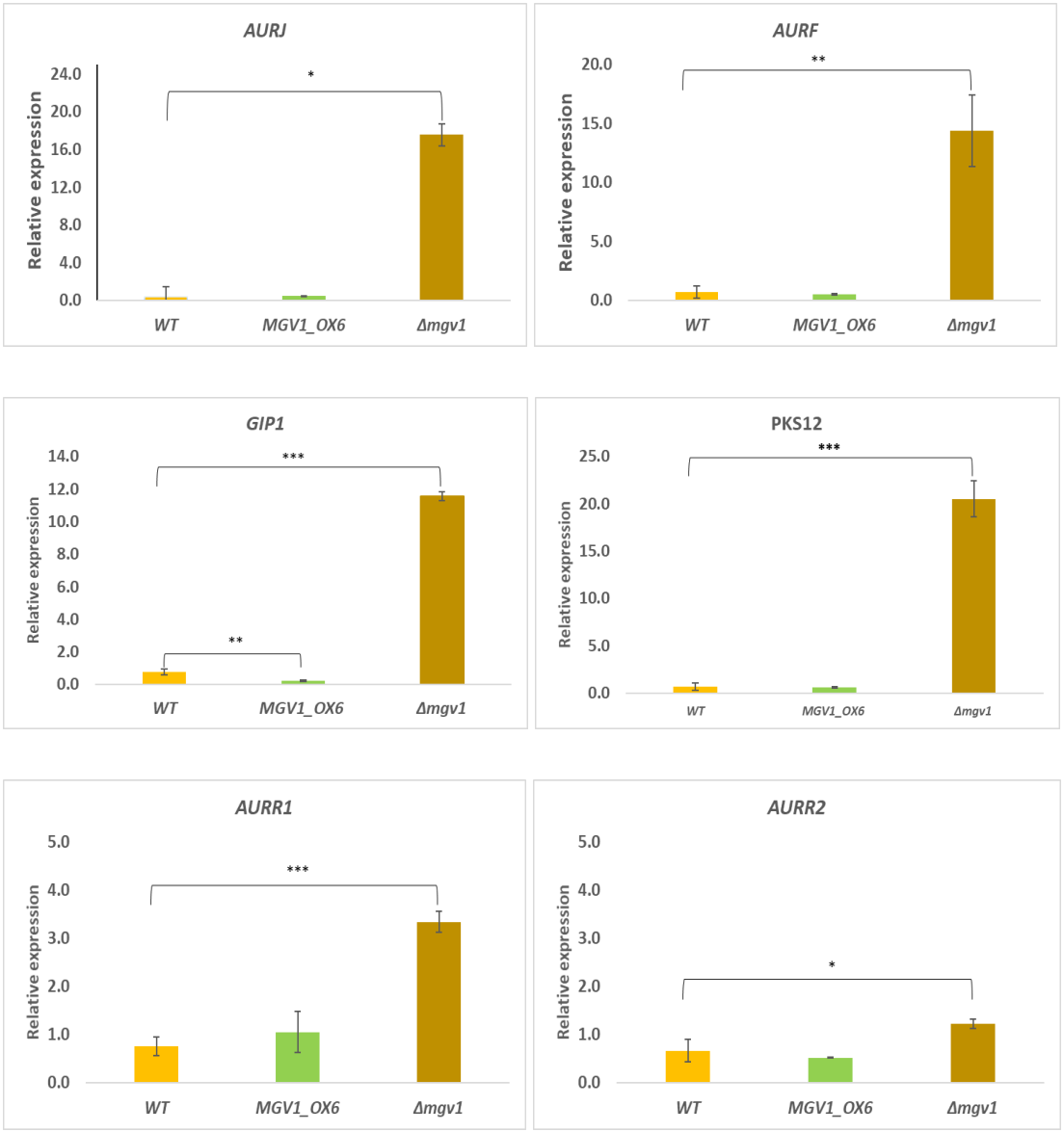

Figure 2.16. Relative expression of genes in the aurofusarin biosynthetic pathway. Mycelia were collected under DON-inducing condition #1 for RNA-seq, RT-qPCR and Western blot analyses. Bars represent mean of the values, analyzed by Student t-test. Error bars represent the standard errors of three biological replicates and three technical replicates (n=9), with * $p \leq 0.05$, ** $p \leq 0.01$, *** $p \leq 0.001$. CT-values were normalized with the housekeeping gene *EF-1α*.

Analysis of the expression of genes in the aurofusarin biosynthetic pathway from samples collected from PDA, revealed no change or downregulation in the *MGV1_OX* transformants compared to WT (Figure 2.17). Some values were highly variable, which may be a result of fast transcript turnover that might occur in TFs and in some secondary metabolites.

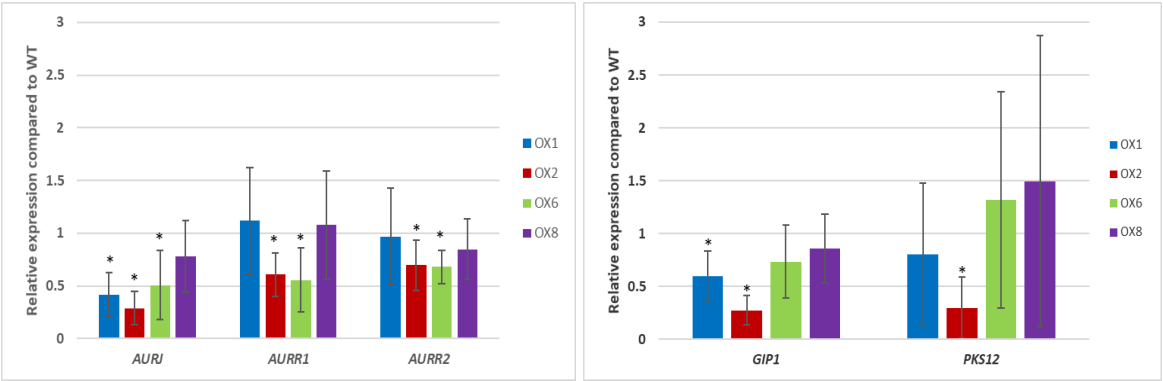

Figure 2.17. Relative expression of genes from the aurofusarin biosynthetic pathway in the *MGV1_OX* transformants compared to WT. Mycelia were collected from PDA plates five days after inoculation. Relative expression compared to WT was calculated using REST© software, that uses the pair wise fixed reallocation randomisation test © for comparing the expression ratios of the transcripts. The asterisk represents statistical differences at $p \leq 0.05$ (*). Bars represent the standard errors of three biological replicates and three technical replicates (n=9). CT-values were normalized with the housekeeping gene *β-TUBULIN*.

Under DON-inducing condition #3, samples were taken to analyse the metabolomic profile of the strains, but also to check the protein levels of the MAPKs, in order to compare the effect of the activation of Mgv1. More intense phosphorylated bands corresponding to Mgv1 were observed in *MGV1_OX6* compared to WT, which could simply be a result of an increased abundance of the Mgv1 protein itself in *MGV1_OX6* (Figure 2.18). The abundance of Gpmk1, phosphorylated and unphosphorylated, was similar among all the strains. In addition, Hog1 accumulation was higher in *Δmgv1* than in the other tested strains, which could also explain its apparently increased phosphorylation.

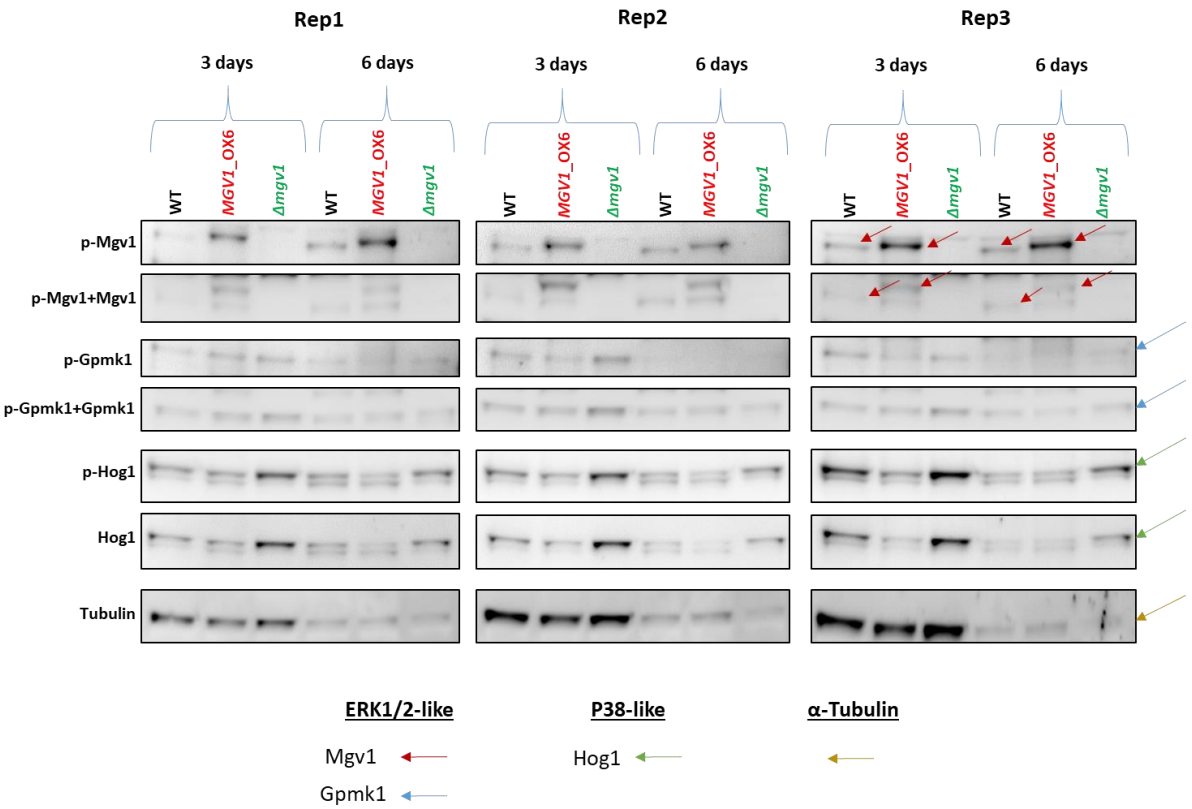

Figure 2.18. Western blotting of protein extracted from WT, *MGV1_OX6* and Δ*mgv1* strains. Mycelia were collected under DON-inducing condition #3 for metabolomics and Western blot analyses (3 and 6 days). The antibody anti-Phospho-p44/42 MAPK (ERK1/2) (Thr202/Tyr204) from Cell Signal, recognizes phosphorylated forms of ERK1/2-like proteins, such as p-Mgv1 and p-Gpmk1. The antibody anti-M5670 from Sigma, recognizes phosphorylated and unphosphorylated forms of ERK1/2-like proteins, such as Mgv1 and Gpmk1. Mgv1 size is estimated as 46.9 kDa in the WT, and about 47.8 kDa in *MGV1_OX6* due to the N-6xHis-tag, while Gpmk1 is around 41.2 kDa. The antibody anti-Phospho-P38, from Cell Signal, recognizes only the phosphorylated form of P38 (Hog1) while anti-P38 recognizes only the unphosphorylated P38 (41.1 kDa).

2.3.5 Effect of overexpressing or deleting *MGV1* on the *F. graminearum* transcriptome

Transcriptomic analysis of *Δmgv1, MGV1_OX1* and *MGV1_OX6* strains *vs* WT revealed that 1495, 419 and 730 genes, respectively, were differentially expressed compared to WT (Figure 2.19). From those genes, 134, 55 and 77 were from SMC in *Δmgv1, MGV1_OX1* and *MGV1_OX6*, respectively. Some of the results are presented in a previous section.

The analysis showed that the three strains shared 160 genes differentially expressed compared with the wild-type, with 28 belonging to the SMCs, including 7 from the C42 cluster producing fusarins; four from the C13 cluster producing aurofusarin; and one (NPS5) from the fusaoctaxin-producing cluster C64.

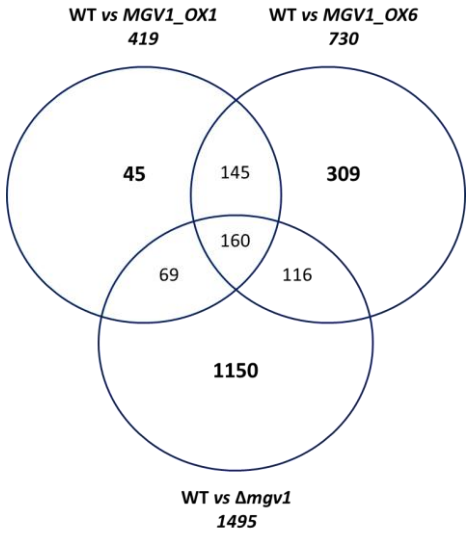

Figure 2.19. Venn diagram of differentially expressed genes in *Δmgv1, MGV1_OX1* and *MGV1_OX6* strains compared to WT.

A functional category analysis (FungiFun2) of the 160 genes differentially expressed in all three pairwise comparisons was performed, and the following four categories were enriched: C-compound and carbohydrate metabolism, metabolism of polyketides, toxins, and photoperception and response (Table 2.10). In general, Mgv1 regulates several cell processes associated with primary and secondary metabolism, cellular transport, cellular defense and virulence, and cell type differentiation, among others. As a conclusion regarding the effect of *MGV1* deletion or overexpression of genes involved in secondary metabolite production, a comparison between transcriptomic and metabolomic analyses was summarized in Table 2.11.

Table 2.10. Categories enriched in the RNA-seq analysis for genes differentially expressed in *Δmgv1, MGV1_OX1* and *MGV1_OX6* strains compared to WT.

Description	Main category
C-compound and carbohydrate metabolism	Metabolism
Metabolism of polyketides	Metabolism
Toxins	Cell rescue, defense and virulence
Photoperception and response	Interaction with the environment

Table 2.11. Summary of transcriptomic and metabolomic profiles of *Δmgv1, MGV1_OX1* and *MGV1_OX6* strains compared to WT, related to secondary metabolite biosynthesis and accumulation. Positive and negative symbols represent at least a two-fold change towards more and less, respectively, gene expression or metabolite accumulation. NP, and NDE stands for not produced, and for not differentially expressed, respectively. The asterisk indicates that the number depends on the cultural conditions used during the experiments.

		METABOLOMIC			TRANSCRIPTOMIC		
Metabolite	**# of DEGs**	***Δmgv1* vs WT**	***MGV1_OX1 vs* WT**	***MGV1_OX6 vs* WT**	***Δmgv1* vs WT**	***MGV1_OX1 vs* WT**	***MGV1_OX6 vs* WT**
Trichothecenes	14	-	NP	NP	+4/-2	NDE	NDE
Gramillins	0	NP	NP	NP	-	NDE	NDE
Zearalenone	0	NP	NP	NP	+	NDE	NDE
Fusaoctaxin	3-7*	-	+	+	+	+	NDE
Fusarins	7-10*	+	+	+	+	NDE	NDE

Samples collected under the same conditions of the transcriptomic analysis were used for Western blotting. Three biological replications of each strain were analyzed in the same blot (Figure 2.20). *MGV1_OX6* strains showed higher levels of phosphorylation compared to WT, which was expected since the strain has a higher abundance of Mgv1 protein; however, the ratio phosphorylated-Mgv1/total (phospho and unphosphorylated) Mgv1 was not increased. No phosphorylation was observed for Gpmk1, and total Gpmk1 abundance was similar among all the strains. In general, the abundance of unphosphorylated Hog1 and phosphorylated Hog1 (p-Hog1)

did not change; however, a slight increase in Hog1 and p-Hog1 was noticed in *Δmgv1* in replications 1 and 2.

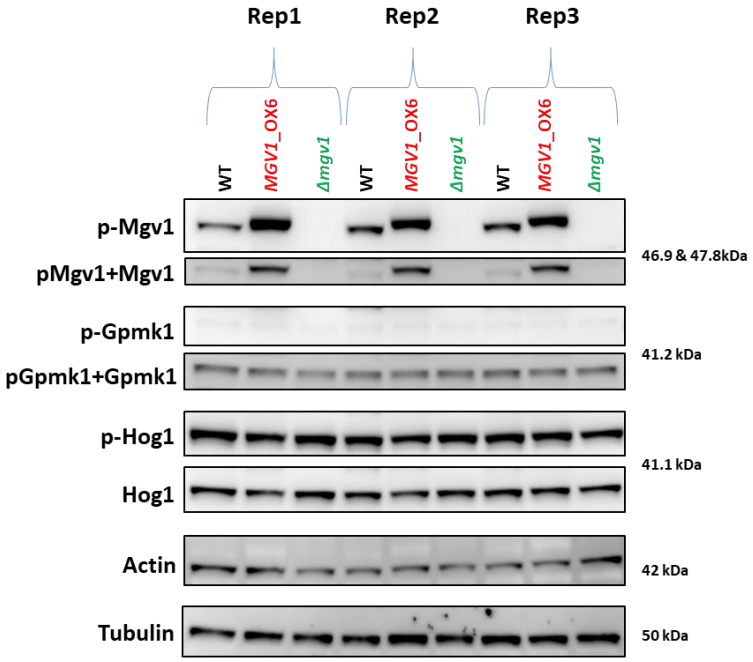

Figure 2.20. Western blotting of WT, *MGV1_OX6* and *Δmgv1* collected under DON-inducing condition #1 for RNA-seq, RT-qPCR and Western blot analyses. The antibody anti-Phospho-p44/42 MAPK (ERK1/2) (Thr202/Tyr204) from Cell Signal, recognizes phosphorylated forms of ERK1/2-like proteins, such as p-Mgv1 and p-Gpmk1. The antibody anti-M5670 from Sigma, recognizes phosphorylated and unphosphorylated forms of ERK1/2-like proteins, such as Mgv1 and Gpmk1. Mgv1 size is estimated as 46.9 kDa in the WT, and about 47.8 kDa in *MGV1_OX6* due to the N-6xHis-tag, while Gpmk1 is around 41.2 kDa. The antibody anti-Phospho-P38, from Cell Signal, recognizes only the phosphorylated form of P38 (Hog1) while anti-P38 recognizes only the unphosphorylated P38 (41.1 kDa).

2.3.6 Effect of *MGV1* overexpression on the cell wall integrity (CWI) pathway

In order to determine if the overexpression of *MGV1* has an impact on the expression of genes associated with cell wall formation that may confer extra resistance to cell wall stress agents, the transcript levels of some genes, such as the *CHITIN SYNTHASES*, were measured after mycelial growth was collected from PDA plates. The relative expression of *CHITIN SYNTHASE 5* (*CHS5*) in the *MGV1_OX* strains was similar to WT with a small but significant

increase in *MGV1_OX1*. For *CHITIN SYNTHASE* 6 (*CHS6*), *MGV1_OX1*, *MGV1_OX2* and *MGV1_OX6* again showed small but significant increases when compared to WT, but in *MGV1_OX8* the value was similar to the parental strain (Figure 2.21).

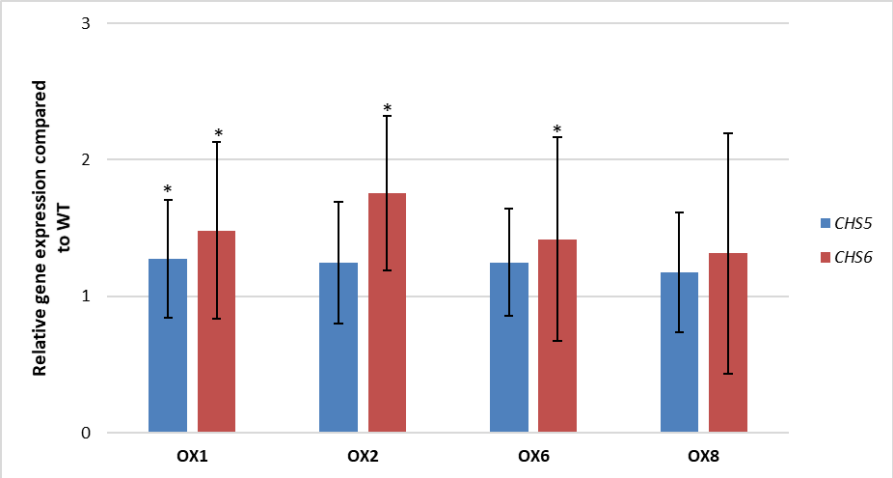

Figure 2.21. Relative expression of *CHS5* (FGSG_01964) and *CHS6* (FGSG_15914) in the *MGV1_OX* transformant *vs* WT strains. Mycelia were collected from PDA plates five days after inoculation. Relative expression was calculated using REST© software that uses the pair wise fixed reallocation randomisation test © for comparing the expression ratios of the transcripts. The asterisk represents statistical differences at $p \leq 0.05$ (*). Bars represent the standard errors of three biological replicates and three technical replicates (n=9). CT-values were normalized with the housekeeping gene *β-TUBULIN*.

2.3.6.1 *MGV1* overexpression does not confer resistance against cell wall and osmotic stress agents

Cell wall stressing agents, such as CFW, CR and SDS affected *F. graminearum* mycelial growth in different ways. The transformants and the WT did not show a difference in the germination and subsequently colony formation on YPD media supplemented with the stressor compounds (Figure 2.22). The results showed that there are no differences in their susceptibility to these chemicals, and the overexpression of *MGV1* does not confer extra resistance to the cell wall of the germ tube or the hyphae.

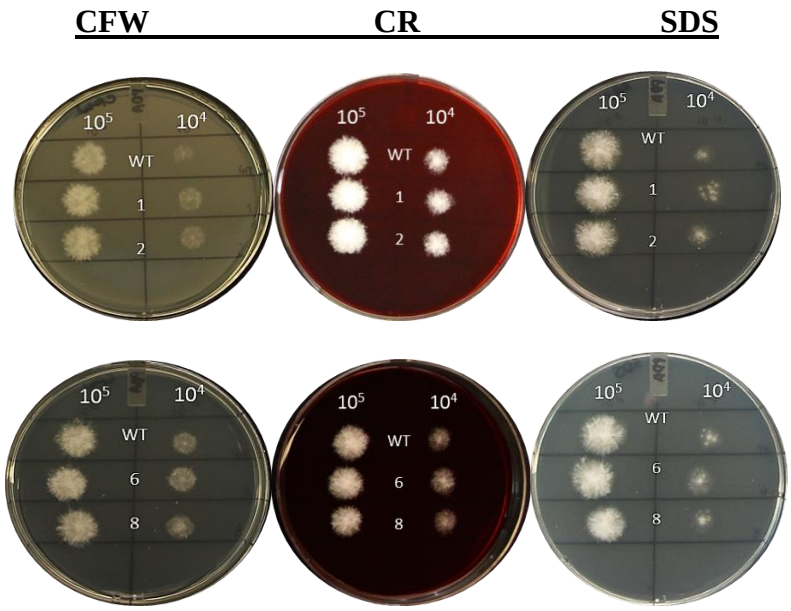

Figure 2.22. Effect of cell wall stress and osmotic stress compounds on spores germination on YPD media after 2 days post inoculation with 5 µL suspension of 1 x 10^5 and 1 x 10^4 spores.

The experiment was repeated this time with a macroconidia solution pipetted onto the center of a PDA plate, which prolonged the assay and enabled a longer observation time to determine whether an effect of the stress agents in the strains might be observed over a long period. The colony diameter was measured five days after inoculation, and no significant differences were found between the WT and the transformants. While the diameter of the colonies on PDA was similar to those on PDA+SDS, the radial growth of the transformants on PDA+CR and PDA+NaCl was slightly reduced in all of the strains evaluated. Interestingly, CFW induced faster mycelial growth in all five strains (Figure 2.23). Each of the colonies grown on PDA supplemented with or without CR, CFW and SDS were bushy, whereas those grown in the osmotic stress treatment (supplemented with NaCl) showed less dense colonies maybe due to fewer hyphae ramification.

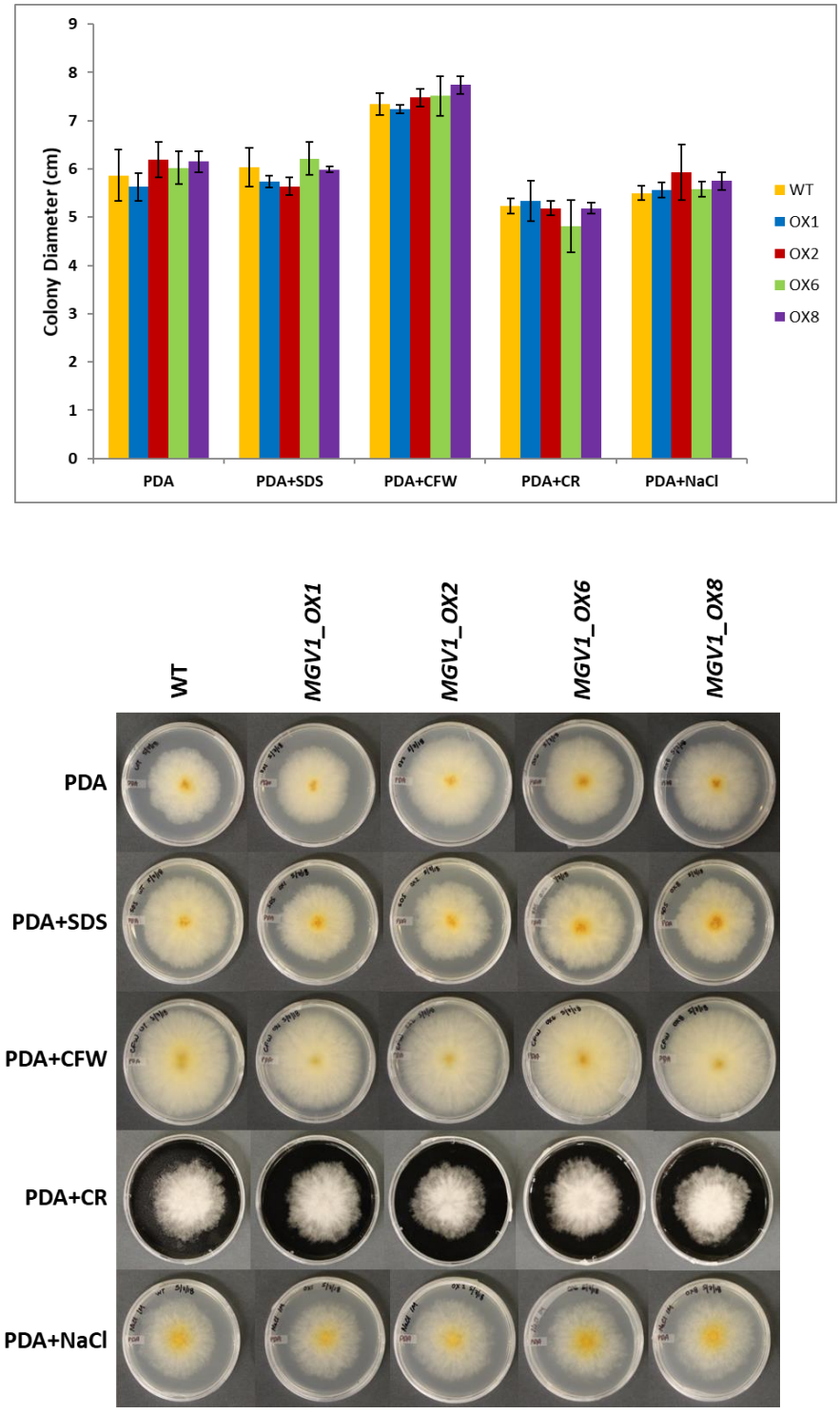

Figure 2.23. Effect of cell wall and osmotic stress agents on mycelial growth. **(a)** Colony diameter on PDA media five days post inoculation. Mean values do not differ at a confidence levels of 95 %. **(b)** Colonies of the *F. graminearum MGV1_OX* transformants and the WT at five days post inoculation.

The experiment was repeated using a mycelial plug at the centre of PDA plates instead of spores, and the *Δmg*v1 strain was included as an additional control. The deletion of *MGV1* negatively affected the mycelial growth on PDA Petri plates, while *MGV1*_OX mutants grew similar to WT.

The percentage of mycelial growth inhibition caused by the presence of the cell wall and osmotic stress agents is shown in Figure 2.24. In general, the radial growth of the WT and the *MGV1_OX* transformants were similarly affected among treatments, without increasing resistance in the *MGV1* overexpressing strains compared to WT (Figure 2.24). Interestingly, when NaCl was incorporated into the media, *Δmgv1* showed more resistance to the stressor than the transformants and, in general, those were slightly more resistant than the WT (Figure 2.24 A). By contrast, and as shown in the previous assay, CFW seemed to enhance mycelial growth in all the strains (WT, *MGV1_OX* and *Δmgv1*) in a similar manner (Figure 2.24 B). As expected, the presence of SDS or CR negatively affected mycelial growth; and a more robust effect was observed in *Δmgv1* compared with WT for CR treatment. In addition, no increased resistance was found when *MGV1* was overexpressed (Figures 2.24 C and 2.24 D).

(a)

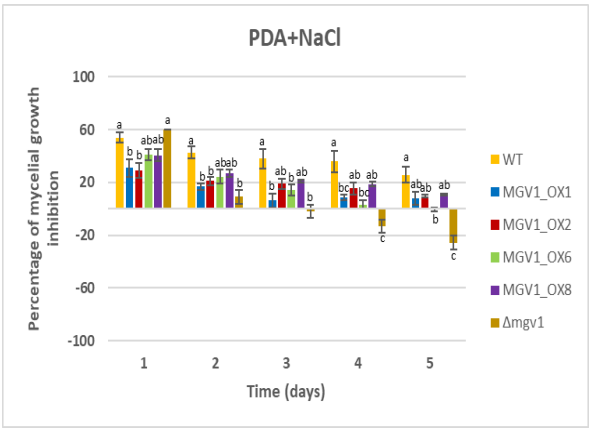
PDA+NaCl
Percentage of mycelial growth inhibition
100
60
20
-20
-60
-100
1
2
3
4
5
Time (days)
WT
MGV1_OX1
MGV1_OX2
MGV1_OX6
MGV1_OX8
Δmgv1

(b)

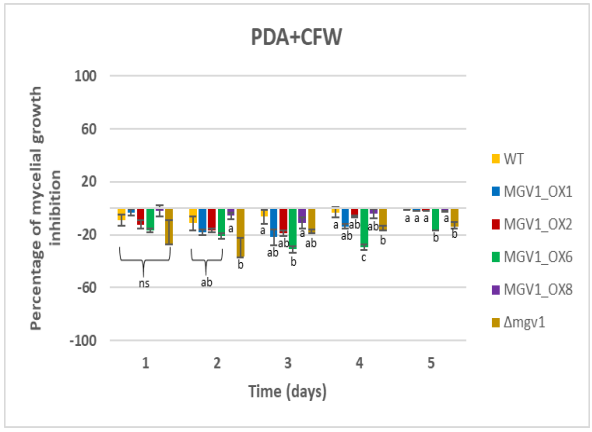
PDA+CFW
Percentage of mycelial growth inhibition
100
60
20
-20
-60
-100
1
2
3
4
5
Time (days)
WT
MGV1_OX1
MGV1_OX2
MGV1_OX6
MGV1_OX8
Δmgv1

(c)

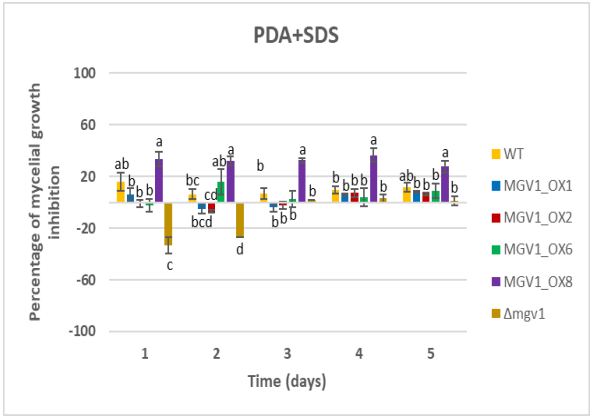
PDA+SDS
Percentage of mycelial growth inhibition
100
60
20
-20
-60
-100
1
2
3
4
5
Time (days)
WT
MGV1_OX1
MGV1_OX2
MGV1_OX6
MGV1_OX8
Δmgv1

(d)

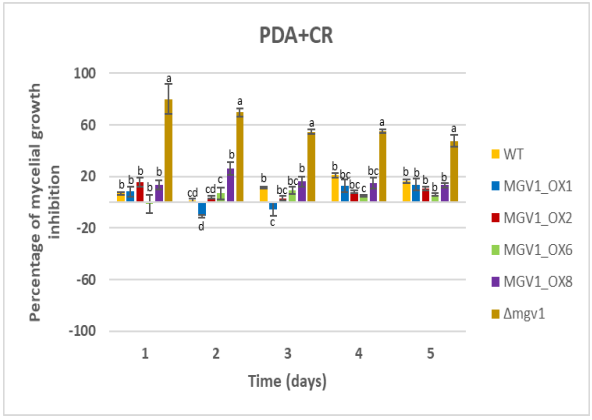
PDA+CR
Percentage of mycelial growth inhibition
100
60
20
-20
-60
-100
1
2
3
4
5
Time (days)
WT
MGV1_OX1
MGV1_OX2
MGV1_OX6
MGV1_OX8
Δmgv1

(e)

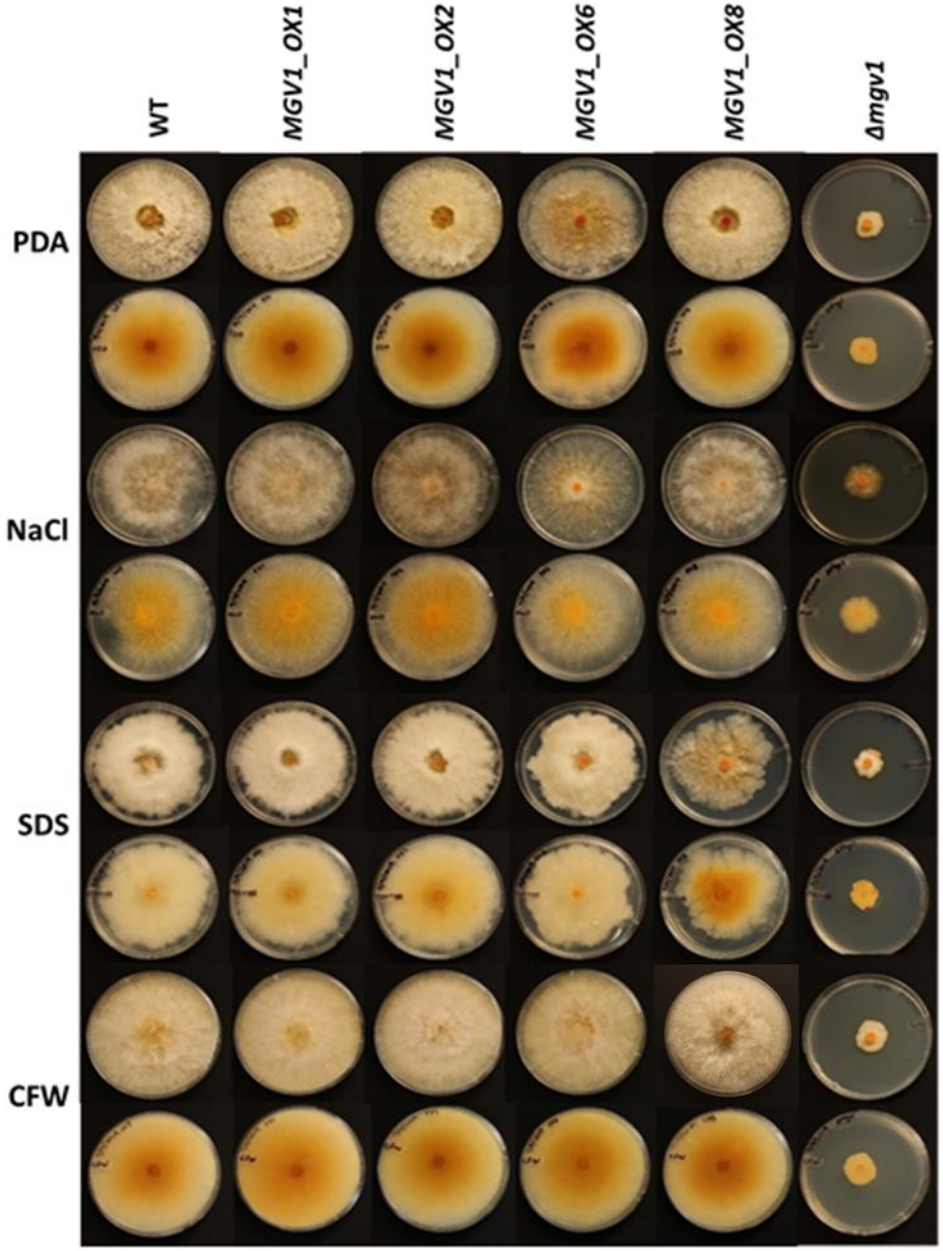

Figure 2.24. *F. graminearum* WT, *MGV1_OX* transformants and *Δmgv1* colonies grown on PDA supplemented with different cell wall stress agents. **(a-d)** Percentage of mycelial growth inhibition was calculated for each strain as a ratio of the difference between the diameter of the colony on PDA and the diameter on PDA supplemented with an stressor compound, divided by the colony diameter on PDA. Mean comparisons were performed for each day, using one-way ANOVA. Bars represent the standard deviation. Similar letters indicate no statistical differences among treatments for $p \leq 0.05$. **(e)** Colonies of the *F. graminearum MGV1_OX* transformants, *Δmgv1* mutant, and the WT at six days post inoculation.

2.3.6.2 Activation of the CWI pathway in presence of CR

In different fungal species, the CWI pathway is activated in the presence of cell wall stress agents, such as CR. Thus, the addition of CR to PDB medium inoculated with macroconidial suspensions of different *F. graminearum* strains should induce phosphorylation, and therefore activation, of Mgv1 protein. In the absence of CR treatments, the intensity of the p-Mgv1 band (47.8 kDa) was more substantial in all the *MGV1_OX* transformants compared to WT (Figure 2.25); however, band intensity varied among the *MGV1_OX* transformants, where *MGV1_OX6* appears to have the highest accumulation of phosphorylated Mgv1. In the presence of CR, Mgv1 phosphorylation seems to have increased in the WT; however, in the *MGV1_OX* transformants the band intensity did not change (Figure 2.25).

There was no band corresponding to a phosphorylated form of the MAPK Gpmk1 (41.2 kDa) in any of the lanes representing the different strains after the membrane was exposed to the anti-phospho-ERK1/2 antibody. However, a band representing total (phospho and unphosphorylated) Gpmk1 showed that this MAPK was not affected among the tested strains (Figure 2.25). The MAPK Hog1 (41.1 kDa) was barely detected in the blots using the antibodies anti-p-P38 and anti-P38, and only for *Δmgv1* a very faint band was detected, with a slightly more intensity in *Δmgv1*-CR (Figure 2.25).

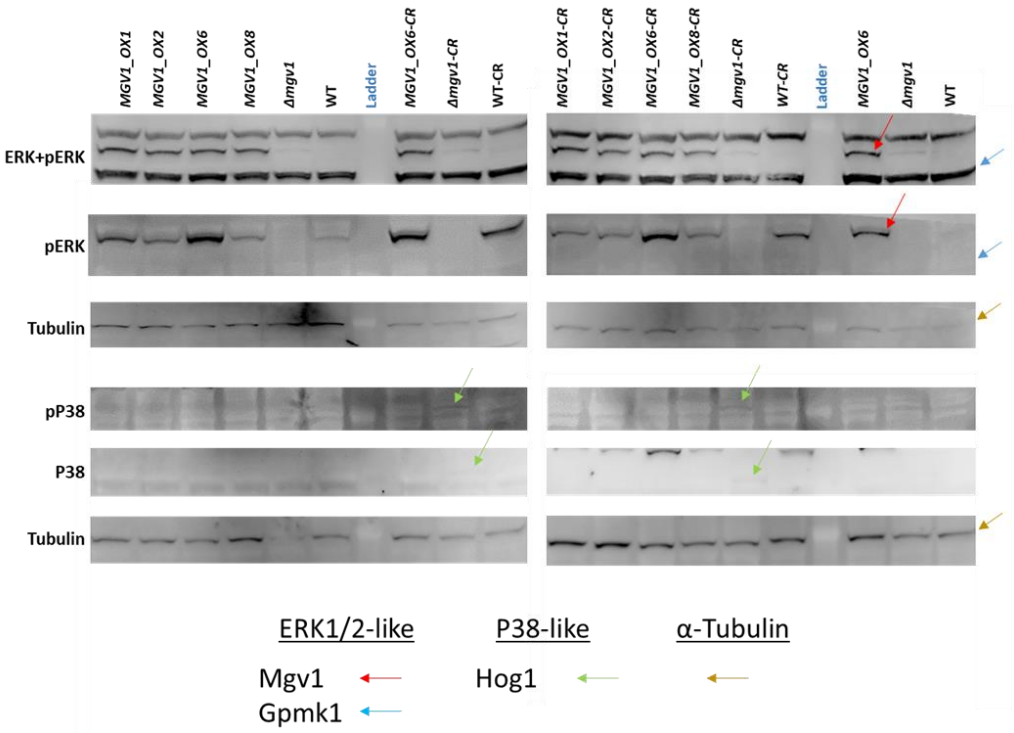

Figure 2.25. Western blotting of WT, *MGV1_OX* transformants and *Δmgv1* strains of *F. graminearum.* Mycelia were collected after growth on PDB for 40 h and challenged with 100 µg mL^{-1} of CR for 45 min. The antibody anti-Phospho-p44/42 MAPK (ERK1/2) (Thr202/Tyr204) from Cell Signal, recognizes phosphorylated forms of ERK1/2-like proteins, such as p-Mgv1 and p-Gpmk1. The antibody anti-M5670 from Sigma, recognizes phosphorylated and unphosphorylated forms of ERK1/2-like proteins, such as Mgv1 and Gpmk1. Mgv1 size is estimated as 46.9 kDa in the WT, and about 47.8 kDa in *MGV1_OX6* due to the N-6xHis-tag, while Gpmk1 is around 41.2 kDa. The antibody anti-Phospho-P38, from Cell Signal, recognizes only the phosphorylated form of P38 (Hog1) while anti-P38 recognizes only the unphosphorylated P38 (41.1 kDa).

To evaluate the effect of longer exposure times to CR and different CR concentrations, an initial screen with the WT, *MGV1_OX6* and *Δmgv1* strains was assessed. One of three replications is presented in Figure 2.26, where a robust presence of total Mgv1 was observed in the *MGV1_OX6* lanes compared to WT (red arrow in the upper panels). Gpmk1, another ERK1/2-like protein is recognized by the same antibody at 41.2 kDa. After CR treatment, the intensity of the band of Gpmk1 seemed to be very similar between WT and *MGV1_OX6.* When comparing the Gpmk1 band of *Δmgv1* with the WT, there seems to be less protein abundance in

the former, and when taking into consideration the actin and tubulin bands, this difference is more pronounced. These results suggest that the deletion of *MGV1* might affect the abundance of Gpmk1.

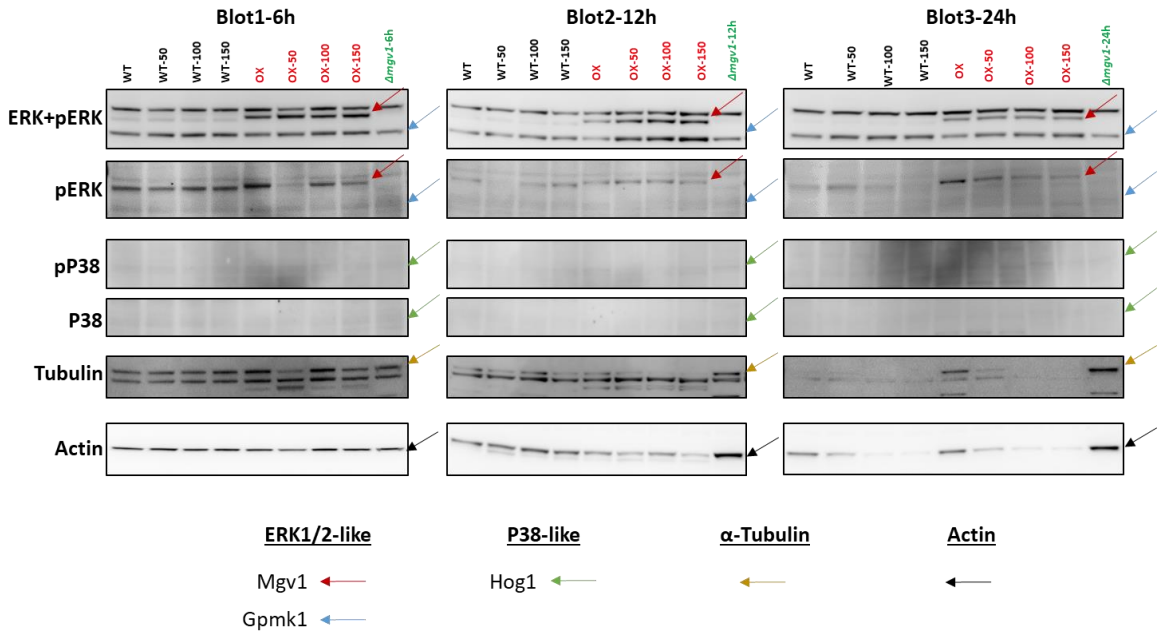

Figure 2.26. Western blotting of WT, *MGV1_OX6* and *Δmgv1 strains.* Mycelia were collected after grown on PDB for 40 h and challenged with 50, 100 and 150 µg mL^{-1} of CR. The antibody anti-Phospho-p44/42 MAPK (ERK1/2) (Thr202/Tyr204) from Cell Signal, recognizes phosphorylated forms of ERK1/2-like proteins, such as p-Mgv1 and p-Gpmk1. The antibody anti-M5670 from Sigma, recognizes ERK1/2-like proteins (such as Mgv1 and Gpmk1) regardless of phosphorylation status. Mgv1 size is estimated as 46.9 kDa in the WT, and about 47.8 kDa in *MGV1_OX6* due to the N-6xHis-tag, while Gpmk1 is around 41.2 kDa. The antibody anti-Phospho-P38, from Cell Signal, recognizes only the phosphorylated form of P38 (Hog1) while anti-P38 recognizes only the unphosphorylated P38 (41.1 kDa). Each blot represents different time of exposure to CR: 6, 12 and 24 h.

Phosphorylation of the ERK-like protein Mgv1 is observed for *MGV1_OX* and the WT after 6 h (red arrow, 2nd row-panels), but this effect decreased at 12 and 24 h, and the bands became less intense on WT than on *MGV1_OX6* (Figure 2.26). Phosphorylation of Gpmk1 (blue arrow, 2nd row-panels) are almost undetected in all cases (Figure 2.26).

The phosphorylated and unphosphorylated forms of Hog1 (recognized with the antibodies anti-pP38 and anti-P38, respectively) were undetected in all cases (Figure 2.26). Interestingly, while the total protein was observed to be uniformly loaded on the blot (Figure 2.26), there was an apparent decrease in the intensity of the tubulin and actin bands after 12 and 24 h (Figure 2.26A).

To understand the effect of CR on the CWI pathway in the WT strain, three biological replications of CR-treated cultures were processed for Western blot analysis. Each of the three replications was analyzed on a separate blot, and the second replication is presented in Figure 2.27. The strains *Δmgv1* and *MGV1_OX6* were included in the blot as controls. No significant differences were observed on total Mgv1 (Figure 2.27, red arrow in the top panel) among WT with or without CR treatment for 6, 12 and 24 h. Mgv1 phosphorylated band (Figure 2.27, red arrow in the second panel from top to bottom) was also similar among treatments with slight variations among replicates. Even though the total amount of protein detected in the blot after the transfer was similar among the lanes (Figure 2.27B), the abundance of tubulin was not uniform, which could be caused by depletion of nutrients after 64 h of incubation (40 h of spores on PDB + 24 h of treatment). For this reason, and since the total protein shown on the blot (Figure 2.26) appears to be uniform in abundance among all lanes, the analysis was carried out without using tubulin as a control.

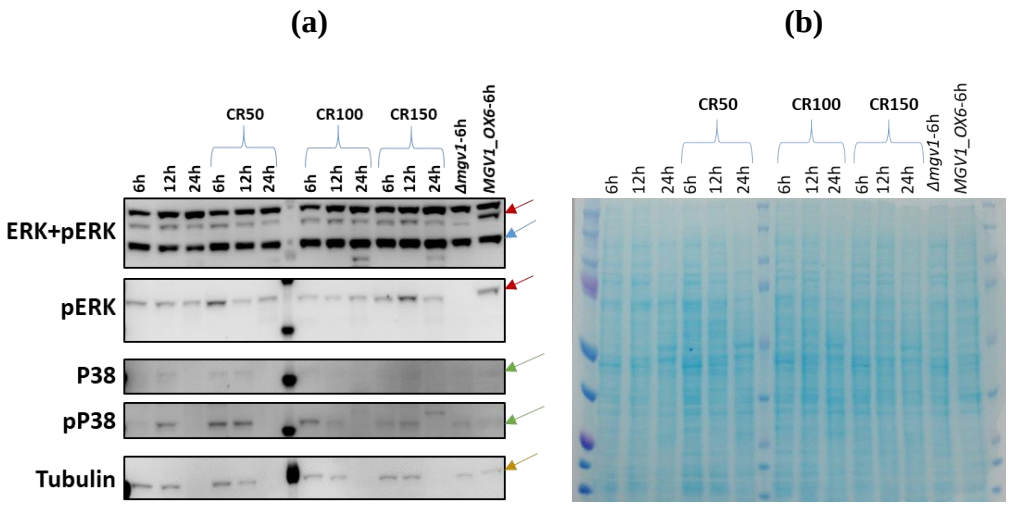

Figure 2.27. (a) Western blotting of WT strain. Mycelia were collected after growth on PDB for 40 h and challenged with 50, 100 and 150 µg mL^{-1} of CR. *Δmgv1* and *MGV1_OX6* were used as controls. The antibody anti-Phospho-p44/42 MAPK (ERK1/2) (Thr202/Tyr204) from Cell Signal, recognizes phosphorylated forms of ERK1/2-like proteins, such as p-Mgv1 and p-Gpmk1. The antibody anti-M5670 from Sigma, recognizes phosphorylated and unphosphorylated forms of ERK1/2-like proteins, such as Mgv1 and Gpmk1. Mgv1 (red arrow) size is estimated as 46.9 kDa in the WT, and about 47.8 kDa in *MGV1_OX6* due to the N-6xHis-tag, while Gpmk1 (blue arrow) is around 41.2 kDa. The antibody anti-Phospho-P38, from Cell Signal, recognizes only the phosphorylated form of P38 (Hog1) while anti-P38 recognizes only the unphosphorylated P38 (41.1 kDa). **(b)** Total proteins were detected with Pierce^{TM} reversible protein stain kit for PVDF membranes.

Total Gpmk1 (Figure 2.27, blue arrow on top panel) was uniform among treatments and the phosphorylated form of Gpmk1 was not detected (Figure 2.27, blue arrow on 2nd panel). The abundance of Hog1 (detected by anti-P38 antibody) was similar among all the treatments; however, this protein appears to be more phosphorylated after treatments with 50 µg mL^{-1} of CR in the first 6 and 12 h of exposure (Figure 2.27, 3rd and 4th panel from top).

To determine how the presence of CR affected fungal gene expression, samples were collected for real-time PCR analysis at 6, 12 and 24 h following a 100 µg mL^{-1} CR treatment. The *MGV1* gene was upregulated following 6 and 12 exposure times compared with untreated WT (Figure 2.28 A). It should be noted that the upregulation did not reach a two-fold difference.

Nevertheless, 6 and 24 h of exposure were enough to increase the expression of *RLM1*, the known downstream target of Mgv1 (Figure 2.28 B). The upregulation of *RLM1* might have triggered the observed upregulation of *CHS1A* and *CHS5* (Figures 2.28 C and D), genes that encode for *CHITIN SYNTHASES*, enzymes involved in the formation of chitin in the cell wall.

The transcript levels of the other MAPKs, *GPMK1* and *HOG1* were also analysed and they appeared to be very similar to WT (Figure 2.28 E & F), in correspondence with what was observed for protein accumulation (Figure 2.27 A). By contrast, the expression of *KIN4*, a kinase that putatively interacts with Mgv1, showed an increase over the time course of CR exposure (Figure 2.28 E).

After 6 h of exposure to CR 100 μg mL^{-1}, different strains showed that several genes associated with the CWI pathway were differentially expressed compared to the same strain without CR (Figures 2.29 and 2.30). The presence of the cell wall stress agent induced upregulation of *MGV1* and its downstream functional component, *RLM1*, in the WT and the *MGV1_OX6* strains. Interestingly, *RLM1* was also upregulated in *Δmgv1*-CR compared to *Δmgv1*, but the fold-change was smaller than in the other cases. In addition to *RLM1*, the Mgv1 interacting partner *KIN4* was also upregulated in all strains under these conditions.

When *MGV1_OX6* was treated with CR, *CHS1A*, *CHS1B*, *CHS5*, *CHS6* and *FKS1* were upregulated, while for *CHS3* and *CHS4* there was no difference compared to the untreated strain (Figure 2.30). In the WT strain, the CR treatment induced a higher expression in *CHS1A*, *CHS5*, *CHS6* and *FKS1*, while the other analysed genes were similarly expressed to the non-CR sample. Unexpectedly, *Δmgv1*-CR showed upregulation of *CHS1A* and *CHS3*, no differences in *CHS4*, *CHS5* and *CHS6*, and downregulation in *CHS1B* and *FKS1*, compared to *Δmgv1* sample (Figure 2.30).

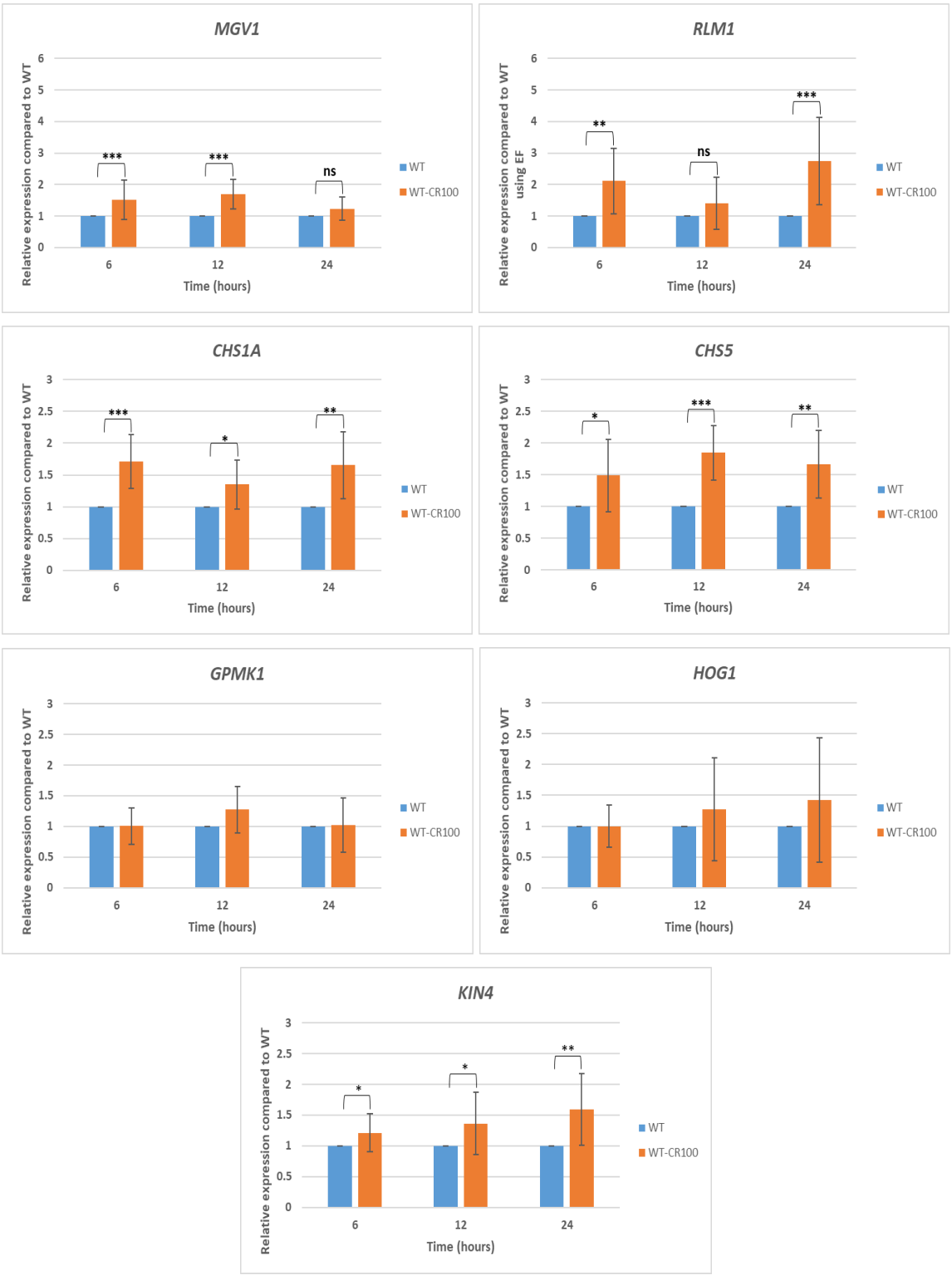
MGV1
Relative expression compared to WT
Time (hours)
6
12
24
***
***
ns
WT
WT-CR100
RLM1
Relative expression compared to WT using EF
**
ns
***
CHS1A
*
**
CHS5
GPMK1
HOG1
KIN4

Figure 2.28. Relative expression of genes in the WT strain treated with CR (orange bars) compared to the WT untreated (control- blue bars). Genes represented were: the three MAPKs genes (*MGV1*, *GPMK1* and *HOG1*), the transcription factor *RLM1* (downstream of Mgv1), *CHITIN SYNTHASES* (*CHS5* and *CHS6*), and a putative Mgv1-interacting protein, *KIN4*. Mycelia were collected after grown on PDB for 40 h and challenged with 100 µg mL^{-1} of CR during 6, 12 and 24 h. Relative expression was calculated using REST© software that uses the pair wise fixed reallocation randomisation test © for comparing the expression ratios of the transcripts. Asterisks represent statistical differences at $p \leq 0.05$ (*), $p \leq 0.01$ (**), and $p \leq 0.001$ (***), while ns stands for no statistical differences. Bars represent the standard errors of three biological replicates and three technical replicates (n=9). CT-values were normalized with the housekeeping gene *EF-1α*.

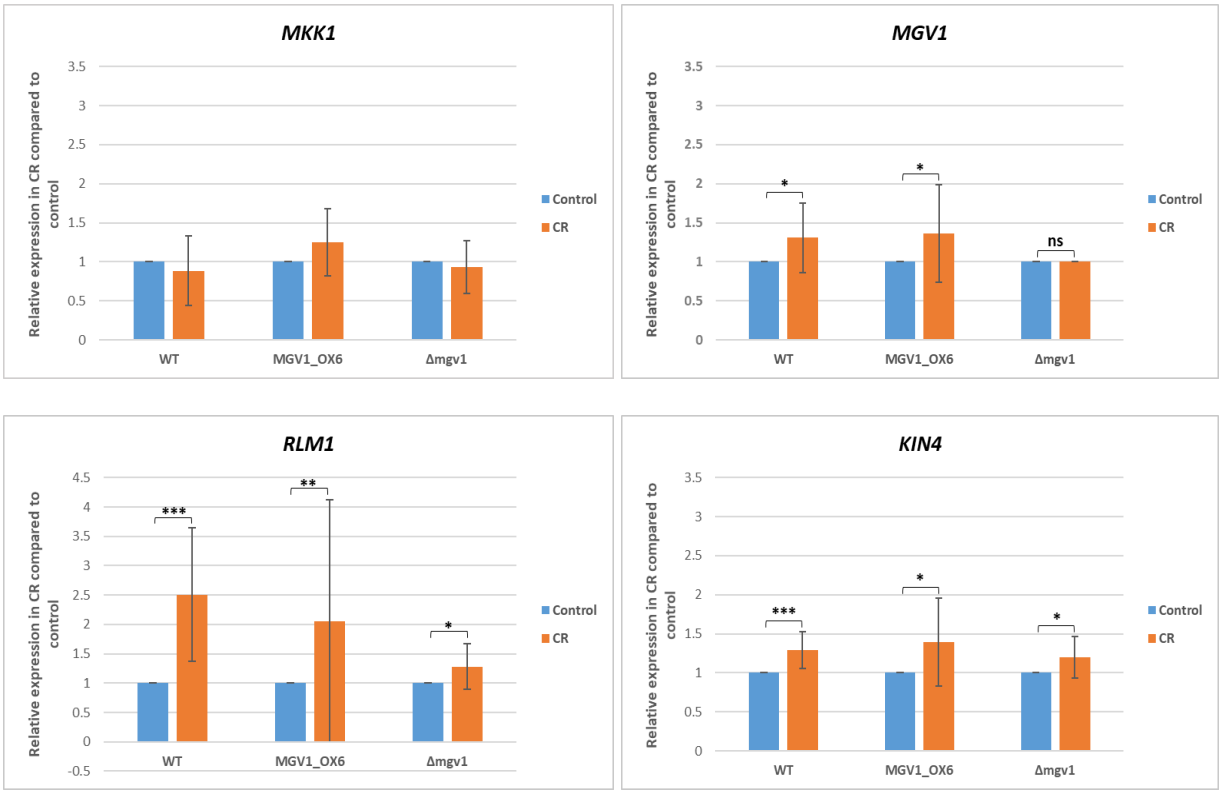

Figure 2.29. Relative expression of genes of, or associated with, the CWI pathway, in the strains treated with CR (orange bars) compared to the same untreated strain (control- blue bars). Mycelia were collected after growth on PDB for 40 h and challenged with 100 µg mL^{-1} of CR during 6 h. Relative expression was calculated using REST© software that uses the pair wise fixed reallocation randomisation test © for comparing the expression ratios of the transcripts. Asterisks represent statistical differences at $p \leq 0.05$ (*), $p \leq 0.01$ (**), and $p \leq 0.001$ (***), while ns stands for no statistical differences. Bars represent the standard errors of three biological replicates and three technical replicates (n=9). CT-values were normalized with the housekeeping gene *EF-1α*.

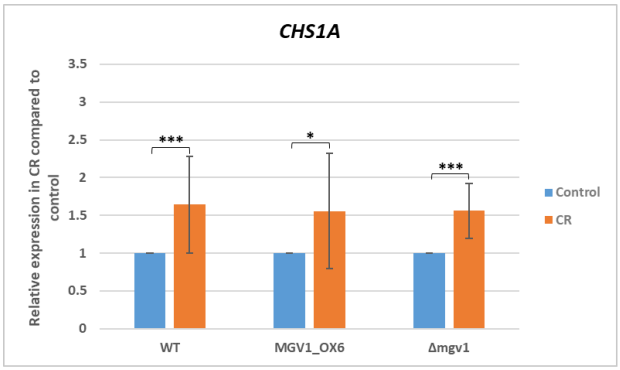
CHS1A
Relative expression in CR compared to control
3.5
3
2.5
2
1.5
1
0.5
0
***
*
***
WT
MGV1_OX6
Δmgv1
Control
CR

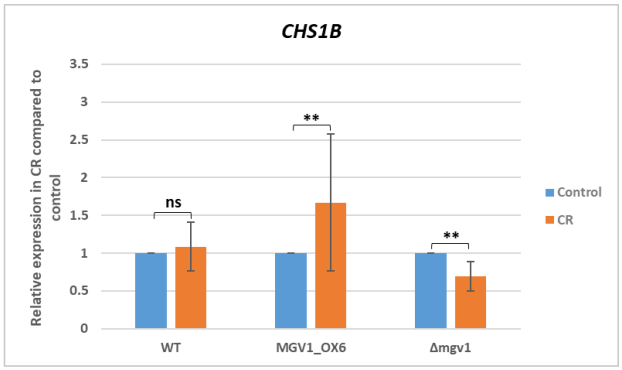
CHS1B
Relative expression in CR compared to control
3.5
3
2.5
2
1.5
1
0.5
0
ns
**
**
WT
MGV1_OX6
Δmgv1
Control
CR

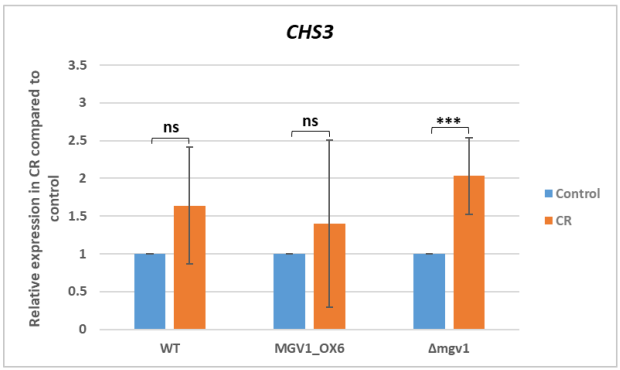
CHS3
Relative expression in CR compared to control
3.5
3
2.5
2
1.5
1
0.5
0
ns
ns
***
WT
MGV1_OX6
Δmgv1
Control
CR

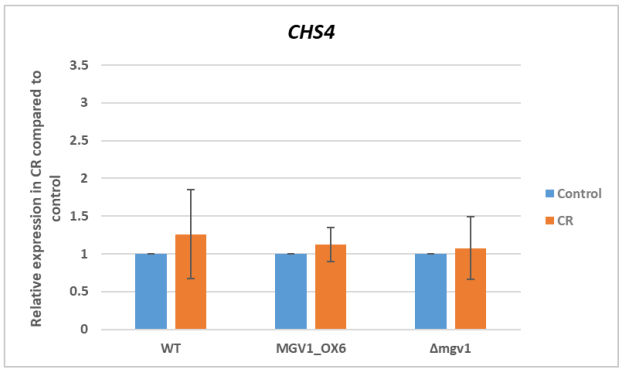
CHS4
Relative expression in CR compared to control
3.5
3
2.5
2
1.5
1
0.5
0
WT
MGV1_OX6
Δmgv1
Control
CR

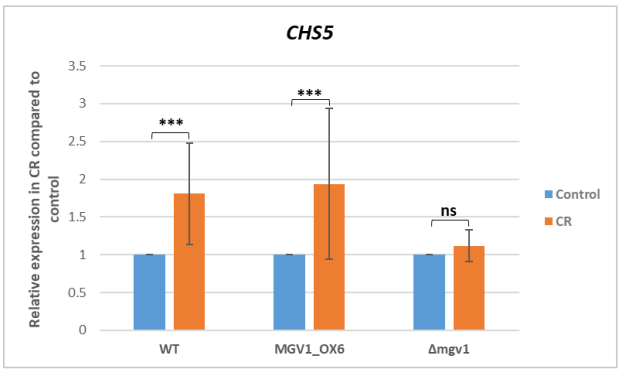
CHS5
Relative expression in CR compared to control
3.5
3
2.5
2
1.5
1
0.5
0
***
***
ns
WT
MGV1_OX6
Δmgv1
Control
CR

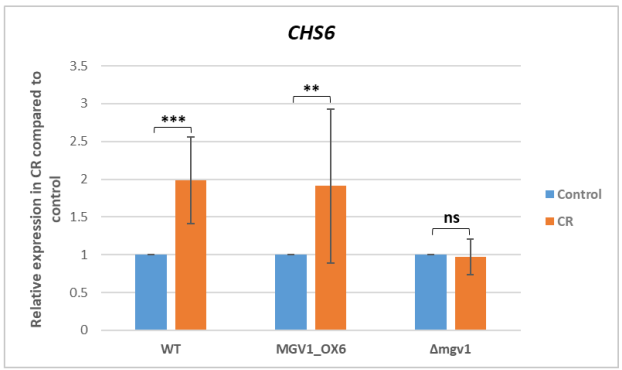
CHS6
Relative expression in CR compared to control
3.5
3
2.5
2
1.5
1
0.5
0
***
**
ns
WT
MGV1_OX6
Δmgv1
Control
CR

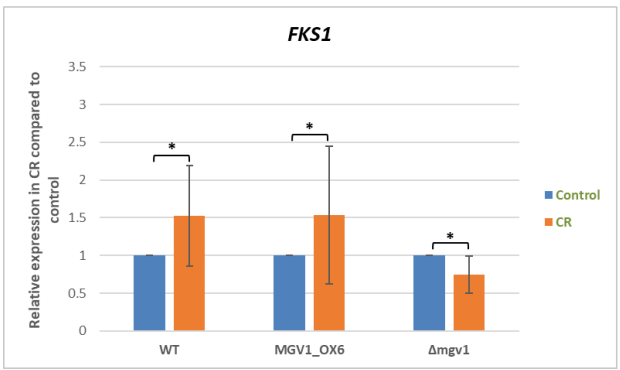
FKS1
Relative expression in CR compared to control
3.5
3
2.5
2
1.5
1
0.5
0
*
*
*
WT
MGV1_OX6
Δmgv1
Control
CR

Figure 2.30. Relative expression of *CHITIN SYNTHASES* (*CHS*) and the putative *FKS1* (*β-GLUCAN SYNTHASE*) genes associated with the CWI pathway in the strains treated with CR (orange bars) compared to the same untreated strain (control- blue bars). Mycelia were collected after growth on PDB for 40 h and challenged with 100 µg mL^{-1} of CR during 6 h. Relative expression was calculated using REST© software that uses the pair wise fixed reallocation randomisation test © for comparing the expression ratios of the transcripts. Asterisks represent statistical differences at $p \leq 0.05$ (*), $p \leq 0.01$ (**), and $p \leq 0.001$ (***), while ns stands for no statistical differences.. Bars represent the standard errors of three biological replicates and three technical replicates (n=9). CT-values were normalized with the housekeeping gene *EF-1α*.

2.3.7 Effect of CR treatment on expression of MAPKs

HOG1 expression did not change in WT and *MGV1_OX6* while treated with CR, compared to the untreated strains; however, after *Δmgv1* was challenged with the stress agent, *HOG1* was upregulated. As it has been previously shown, *GPMK1* expression was not affected by CR treatments (Figure 2.31).

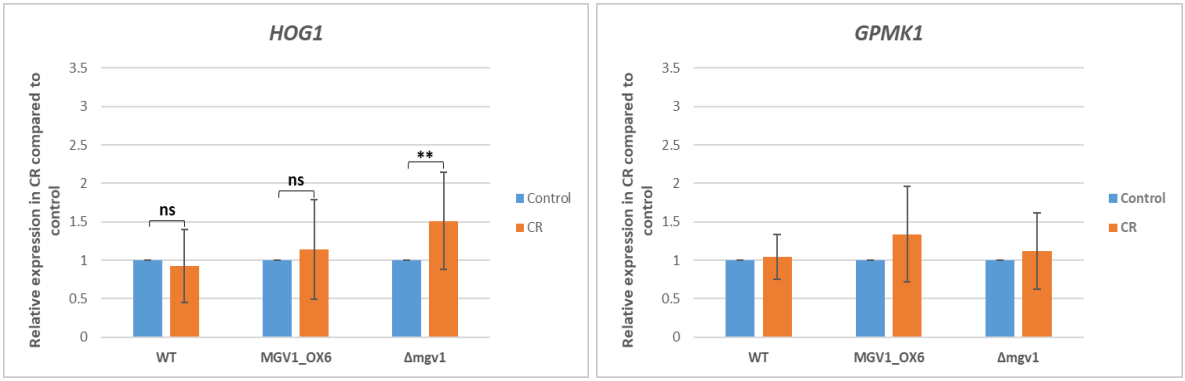

Figure 2.31. Relative expression of the MAPKs *HOG1* and *GPMK1* in the treated strains with CR (orange bars) compared to the same untreated strain (control- blue bars). Mycelia were collected after growth on PDB for 40 h and challenged with 100 µg mL^{-1} of CR during 6 h. Relative expression was calculated using REST© software that uses the pair wise fixed reallocation randomisation test © for comparing the expression ratios of the transcripts. Asterisks represent statistical differences at $p \leq 0.05$ (*), $p \leq 0.01$ (**), and $p \leq 0.001$ (***), while ns stands for no statistical differences. Bars represent the standard errors of three biological replicates and three technical replicates (n=9). CT-values were normalized with the housekeeping gene *EF-1α*.

2.3.8 CR affects the relative expression of genes in the biosynthetic pathway of aurofusarin

To evaluate how CR might affect the production of secondary metabolites, a preliminary study analyzing the relative expression of the genes in the aurofusarin biosynthetic pathway was conducted (Figure 2.32).

The abundance of *AURR1* transcripts, a transcription factor, in the WT strain was low at 6 and 12 h of CR exposure and no difference was observed after 24 h, compared to the untreated WT. Another transcription factor, *AURR2*, was also downregulated but only after 6 h of exposure, whereas at 12 and 24 h, the relative expression was similar to the untreated control. In contrast, expression of the *AUR* pathway genes, polyketide synthase (*PKS12*) and laccase (*GIP1*), remained low over the 24 h period (Figure 2.32).

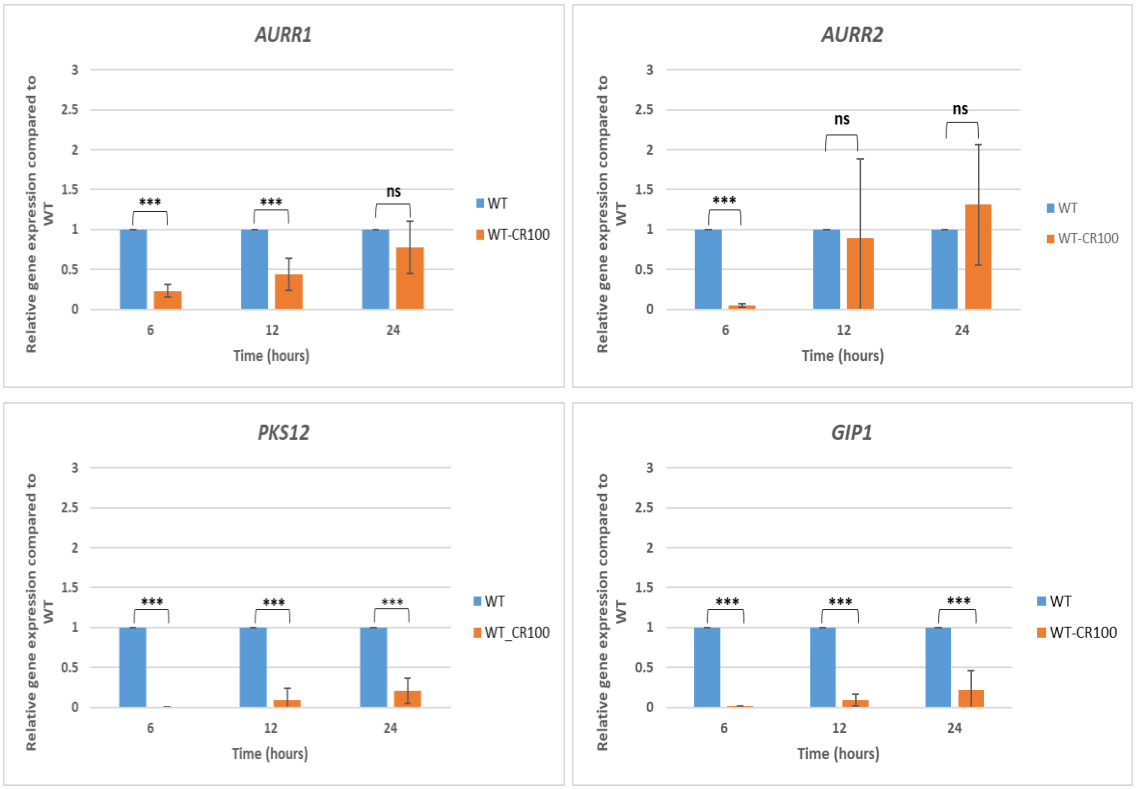

Figure 2.32. Relative expression of genes from the aurofusarin biosynthetic pathway in the WT strain treated with CR (orange bars) compared to the WT untreated (control- blue bars). Mycelia were collected after grown on PDB for 40 h and challenged with 100 µg mL^{-1} of CR during 6, 12 and 24 h. Relative expression was calculated using REST© software that uses the pair wise fixed reallocation randomisation test © for comparing the expression ratios of the transcripts. Asterisks represent statistical differences at $p \leq 0.05$ (*), $p \leq 0.01$ (**), and $p \leq 0.001$ (***), while ns stands for no statistical differences. Bars represent the standard errors of three biological replicates and three technical replicates (n=9). CT-values were normalized with the housekeeping gene: *EF-1α*.

2.4 Discussion

2.4.1 *MGV1* overexpression does not affect mycelial growth and macroconidia germination

The MAPK cascade known as the cell wall integrity pathway is involved in several cellular processes beyond cell wall formation or cell wall integrity; it plays a significant role in the resistance to heat and other stresses affecting the structure of the cell wall, as observed in *S. cerevisiae* (Lee *et al*., 1993; Kamada *et al*., 1995; Watanabe *et al*., 1997; Levin, 2011). In filamentous fungi, such as *F. graminearum*, it has been shown that Mgv1 (the homolog of Slt2) is essential for female fertility, heterokaryon formation, plant infection, and it is involved in other processes such as mycelial growth on solid media and chemotropic sensing (Hou *et al*., 2002; Sridhar *et al*., 2020). The results presented in this thesis confirm that the deletion of *MGV1* causes a strong phenotype in *F. graminearum* mycelial growth on solid media (Figure 2.24), and therefore, one might expect that *MGV1* overexpression could cause some opposite effect. Interestingly, the mycelial growth rate was not increased in any of the four *MGV1* overexpressing transformants generated (Figure 2.24). In addition, the perithecia structures in *MGV1_OX* transformants resembled those present in the WT parental strain, and when broken, they were able to release asci and ascospores, as observed in the WT (Figure 2.7). Furthermore, the number

of germinated macroconidia from 3 to 8 h in *MGV1_OX* transformants was also similar to WT (Figure 2.6).

2.4.2 *MGV1* overexpression does not enhance *F. graminearum* virulence but increases 15-ADON production in axenic cultures.

In several microorganisms, the MAPK in the CWI pathway has been identified as involved in virulence (Hou *et al*., 2002; Mehrabi *et al*., 2006; Luo *et al*., 2012; Li *et al*., 2014; Onyilo *et al*., 2018). In *Pseudocercospora fijiensis*, the causal agent of black Sigatoka disease in *Mussa* spp., the deletion of *SLT2* caused a decrease in banana plant leaf infection (Onyilo *et al*., 2018), while in *Mycosphaerella graminicola* this protein was necessary for invasive growth, but was not essential for penetration in wheat leaves, which led the authors to consider it a pathogenicity factor for this fugal pathogen (Mehrabi *et al*., 2006). In *F. graminearum*, a previous study showed that the deletion of *MGV1* created a less virulent strain in wheat heads than the WT, and this fact could be associated with reduced growth on solid media or due to a reduced DON accumulation quantified in the spikes (Hou *et al*., 2002). The anticipated negative impact of *MGV1* deletion on mycelial growth (Figure 2.23) and pathogenicity towards wheat (information in the next chapter) was observed. Unexpectedly, it was found that the *Δmgv1* mutant could produce the same amount of 15-ADON in axenic cultures as the WT (Figure 2.11). Therefore, it could be hypothesized that the low mycotoxin production found in wheat spikes by other authors (Hou *et al*., 2002) might be associated with fewer mycelia present in the plant due to the low mycelial growth on solid surfaces, rather than a trichothecene production inhibition.

When *MGV1* was overexpressed, 15-ADON production in axenic cultures was increased (Figure 2.11). One might expect that this strain would have had the capacity to produce higher amounts of DON, and since this mycotoxin is considered a virulence factor, it could increase its

virulence. However, the number of diseased spikelets in wheat and *B. distachyon* was similar among the *MGV1_OX* strains and the WT (Figures 2.8, 2.9 and 2.10). In conclusion, *MGV1* overexpression showed similar macroconidia germination levels and growth rate as the WT, and did not confer higher virulence to *F. graminearum*, even though *MGV1_OX* strains have the potential to produce more 15-ADON compared to WT. Thus, *MGV1* overexpression did not induce the formation of a more aggressive strain towards wheat and *B. distachyon* spikes.

2.4.3 Effect of Mgv1 in biosynthetic pathways of secondary metabolites

Mgv1 has been previously associated with the regulation of trichothecenes (Hou *et al*., 2002; Rampitsch *et al*., 2011; Yun *et al*., 2014) and other secondary metabolite pathways, such as aurofusarin (Yun *et al*., 2014) and butenolide (Rampitsch *et al*., 2011). Metabolomics and transcriptomic analyses of samples collected under DON-inducing conditions were performed to determine whether *MGV1* overexpression affects secondary metabolite accumulation and the expression of genes associated with their biosynthesis and regulation. An *MGV1* deletion mutant was also included as a control. The results suggest a complex regulation of secondary metabolite production where diverse factors, such as the environment or post-translational modifications in other proteins, might be involved. The outcomes of the RNA-seq analysis are schematized in Figure 2.33.

The metabolomic and transcriptomic analyses showed a high impact of *MGV1* deletion on trichothecene levels and in the expression of genes associated with their biosynthesis and regulation (Tables 2.3 and 2.4). The transcriptomic results were confirmed through RT-qPCR (Figure 2.13). However, while both studies (transcriptomic and metabolomic) were performed under DON-inducing conditions, different methodologies and harvest times may have contributed to the different results observed.

(a)

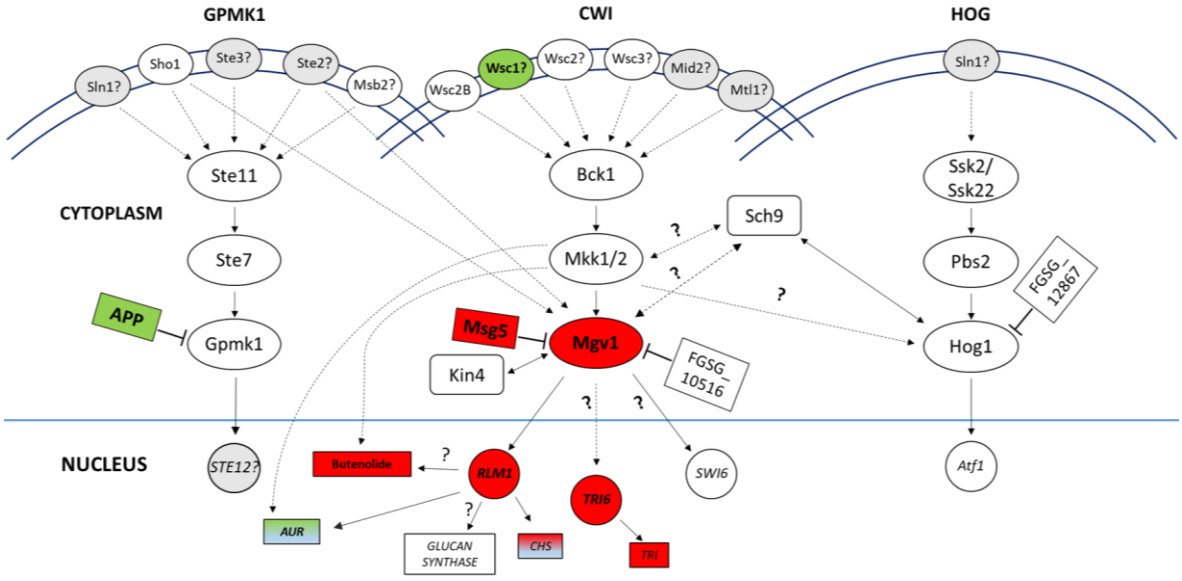
GPMK1
CWI
HOG
Sho1
Ste3?
Ste2?
Sln1?
Msb2?
Wsc1?
Wsc2?
Wsc3?
Mid2?
Wsc2B
Mtl1?
Sln1?
Ste11
Bck1
Ssk2/
Ssk22
CYTOPLASM
Sch9
Ste7
Mkk1/2
Pbs2
FGSG_
12867
APP
Gpmk1
Msg5
Mgv1
Hog1
Kin4
FGSG_
10516
NUCLEUS
STE12?
Butenolide
RLM1
SWI6
Atf1
TRI6
AUR
GLUCAN
SYNTHASE
CHS
TRI

(b)

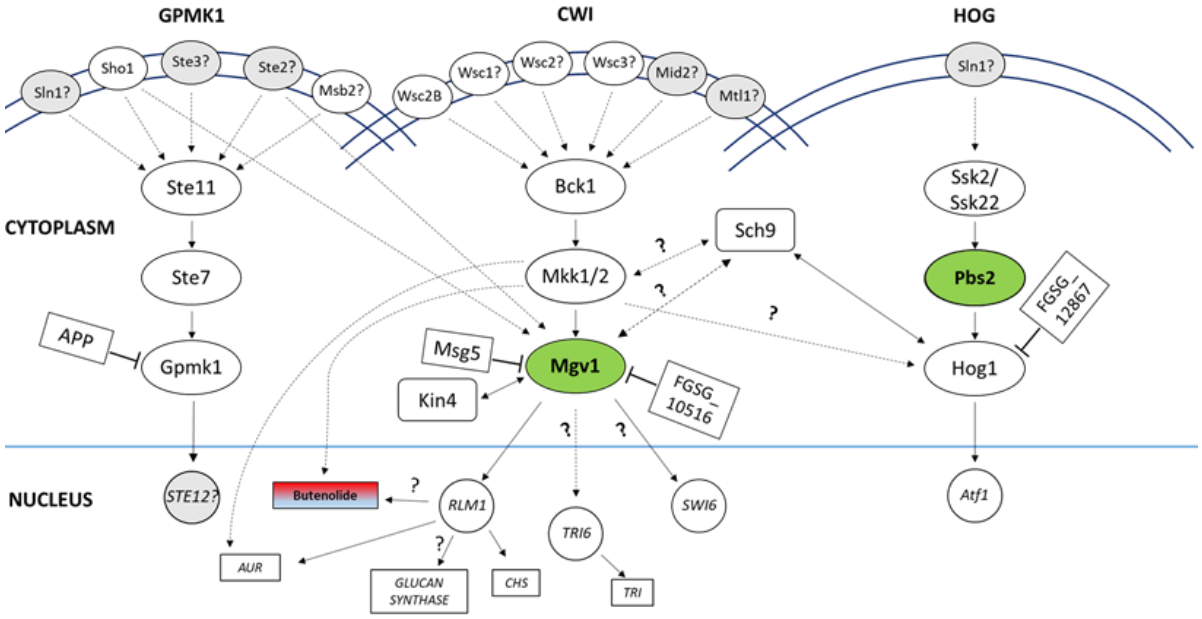
GPMK1
CWI
HOG
Sho1
Ste3?
Ste2?
Sln1?
Msb2?
Wsc1?
Wsc2?
Wsc3?
Mid2?
Wsc2B
Mtl1?
Sln1?
Ste11
Bck1
Ssk2/
Ssk22
CYTOPLASM
Sch9
Ste7
Mkk1/2
Pbs2
FGSG_
12867
APP
Gpmk1
Msg5
Mgv1
Hog1
Kin4
FGSG_
10516
NUCLEUS
STE12?
Butenolide
RLM1
SWI6
Atf1
TRI6
AUR
GLUCAN
SYNTHASE
CHS
TRI

Figure 2.33. Representation of the three MAPK pathways in *F. graminearum*: GPMK1 (*Gibberella* pathogenicity MAPK1), CWI (cell wall integrity) and HOG (high osmolarity glycerol), and how the deletion **(a)** or overexpression **(b)** of *MGV1* affected their components and some interacting elements (e.g. phosphatases, kinases, transcription factors, and genes involved in cell wall formation, or associated with secondary metabolite biosynthesis). The question marks (with arrows) represent a possible interaction between the elements, and in the case of receptors it represent a possible interaction, but not yet demonstrated. The discontinuous arrow represent that more elements might be between the two related components. Green colour represents genes that are upregulated, while red colour represents those downregulated. A combination of blue and green colours represent that some genes in the pathway were upregulated or not differentially expressed. A combination of red and blue colours represent that some genes were downregulated or not differentially expressed. Gray colour represents genes that were not included in the analysis. The schemes were made from the RNA-seq data.

The RNA-seq analysis showed that trichothecenes might be positively regulated by Mgv1, since *MGV1* deletion caused downregulation of the *TRI* gene cluster (24 h in NPN media, Table 2.4). Interestingly, after 48 h in NPN media, 15-ADON accumulation was similar in *Δmgv1* and WT, and it was more abundant in the *MGV1_OX* strains (Figure 2.13). The metabolomic analysis performed after several days in NPN media, revealed that similar amounts of trichothecenes were accumulated in *MGV1_OX* strains and the WT, but the amounts in *Δmgv1* were significantly higher at 6 and 9 days (Table 2.5). These results suggest that *MGV1* deletion might cause a delay in trichothecene accumulation rather than a complete inhibition of this metabolite, and that when the gene is overexpressed, trichothecene production might start earlier than in the WT.

Among the genes used to confirm the RNA-seq analysis by RT-qPCR were *TRI5* and *TRI6*. *TRI5*, is the gene encoding for trichodiene synthase, the first enzyme in DON production, while *TRI6*, is considered a global transcription regulator (Seong *et al*., 2009; Nasmith *et al*., 2011). *TRI5* and *TRI6* appear to be positively regulated by Mgv1 since *MGV1* deletion caused a strong decrease in the transcript levels of both genes (Figure 2.13), but interestingly, this effect was not observed in 15-ADON accumulation that was similar to WT (Figure 2.11), which leads to a

question about the presence of other significant elements that can interfere in the pathway. Their expression values were also analysed from mycelia that grew for five days on PDA plates to know if under non-DON-inducing conditions these genes might also be regulated by *MGV1*. Thus, *TRI5* and TRI6 were not differentially expressed when *MGV1* was overexpressed. At the time that this experiment was carried out, I did not have access to the *Δmgv1* mutant, so it cannot be discussed the effect of this MAPK deletion in *TRI5* and *TRI6* expression.

Gramillins (A and B) are NRPs that have been recently identified as the products of the *NRPS8* gene cluster (Bahadoor *et al*., 2018). *GRA1* is the biosynthetic gene that has gramillin A and B as the bicyclic polypeptide products, while *GRA2* is the transcription factor that regulates its biosynthesis. Gramillins are produced *in planta* and are considered virulence factors of *F. graminearum* towards maize infection, but not for wheat (Bahadoor *et al*., 2018). The same authors also showed that *NRPS8* can be co-induced with the *TRI* gene cluster. In this thesis, under DON-inducing condition #3, gramillins seemed to be positively regulated by Mgv1 after 6, 9 and 12 dpi (Table 2.5) since *MGV1* deletion decreased gramillin A and gramillin B production. However, according to the RNA-seq results, the expression of genes involved in the biosynthetic pathway was not affected by *MGV1* overexpression or deletion (Table 2.6). These apparently contradictory results could be related to the time points when the samples were collected, which differed for the metabolomic and transcriptomic assays.

Bahadoor *et al*. (2018) showed a dynamic of *GRA1* gene expression and metabolite (gramillins A and B) accumulation, where at the fourth day of *F. graminearum* being growing in second stage medium, these compounds reached a peak in abundance. However, *GRA1*expression was declining (compared to day 1 and 3) and continued to decline until 6 days, the final sampling date. As these authors showed how gene expression and metabolite accumulation could be

different at the same time point, the results presented in this thesis might be a reflection of the same phenomenon. It may be that the collection time used for RNA-seq analysis was too soon to observe a change in the expression of genes associated with these metabolites. However, after several days of exposure to second stage media, those genes might be differentially expressed, which lead to a difference in metabolite accumulation after 6 days in the WT *vs* the *Δmgv1* strain.

Aurofusarin is a naphthoquinone homodimer, a polyketide produced by *Fusarium* species, including *F. graminearum*. The *PKS12* cluster that regulates the biosynthesis of this pigment was first identified in the early 2000s, and it is under the control of the transcription factor *AURR1* (Kim *et al*., 2005a; Malz *et al*., 2005). The gene cluster includes transcription factors (*AURR1, AURR2*), laccases (*GIP1* and *AURL2*), a rubrofusarin pump (*AURT*), and enzymes, such as a monooxygenase (*AURF*), an oxidoreductase (*AURO*), an O-methyl-transferase (*AURJ*), and a polyketide synthase (*PKS12*) (Kim *et al*., 2005a; Malz *et al*., 2005; Frandsen *et al*., 2006; Frandsen *et al*., 2011). Yun *et al*. (2014) suggested that the CWI pathway might regulate the *PKS12* gene cluster through the MAPKK, Mkk1. The authors noticed less pigmentation in the *Δmkk1* mutant when compared to the WT strain, and they observed downregulation of the *AURJ, AURF* and *AURO* genes. Our results show that under DON-inducing media (condition #1), Mgv1 negatively regulates the *PKS12* cluster, since *MGV1* deletion caused an upregulation of *AURR1, AURR2, AURJ, AURF, GIP1* and *PKS12* genes (Table 2.9 and Figure 2.16) and more aurofusarin is produced at 6 and 12 days than in the WT (Table 2.8). However, *MGV1* overexpression did not cause an increase in the metabolite production (Table 2.8) even when the RNA-seq analysis showed upregulation of most of the genes compared to WT, but this fold-change was less than 15-times compared to the *Δmgv1*-WT ratio (Table 2.9). The difference observed in gene expression and metabolite production could be associated with the collection point since the

RNA-seq analysis was performed in samples that were under DON-inducing condition #1 for a shorter time than the conditions used for the metabolomic assay (DON-inducing condition #3). When samples were collected from *MGV1_OX* transformants that grew on PDA without any condition for supporting DON production, *AURR1*, *AURR2*, *AURJ* and *GIP1* were similarly or less expressed than the WT (Figure 2.32), suggesting that if DON conditions are not present, these genes will not be differentially expressed towards aurofusarin production.

2.4.4 Effect of Congo red in the CWI pathway and its downstream components

In *F. graminearum*, the core of the CWI pathway is composed of the three proteins Bck1, Mkk1 and Mgv1. It is known that the deletion of Mkk1 increases the susceptibility to cell wall stress agents, such as CR or CFW (Yun *et al*., 2014), therefore, it was a question if the overexpression of one of the core components, such as Mgv1, could increase the resistance to these compounds over the WT strain. In general, it was observed that cell wall or membrane stress agents, such as CR or SDS, negatively affected mycelial growth, but there was no difference in the percentage of mycelial growth inhibition between *MGV1_OX* transformants and the WT (Figures 2.22, 2.23 and 2.24). Therefore, the overexpression of *MGV1* did not confer extra resistance to these compounds. On the other hand, *MGV1* deletion did make a more susceptible strain towards CR, but not for SDS (Figures 2.23 and 2.24). Unexpectedly, 200 µg mL^{-1} of CFW enhanced the growth of all the colonies (Figures 2.23 and 2.24).

The stress agent CR seemed to activate the CWI pathway, as supported by the presence of a more intense band corresponding to the phosphorylated Mgv1 protein in the WT strain treated with CR than in untreated WT (Figure 2.25). However, this band did not change in intensity in samples from *MGV1_OX* transformants, whether they were treated with CR or not, and this could be related to the fact that these strains already had accumulated more Mgv1 protein than the WT,

prior to treatment, and the treatment (regarding concentration and time of exposure) might not be strong enough to induce more phosphorylation. Another explanation could be that the threshold of Mgv1 was already reached in *MGV1_OX* transformants without the necessity of a CWI activation treatment, hence no more phosphorylation could be accepted by Mgv1 proteins. A similar assay but with higher CR concentrations or time of exposure to CR, such as 500 μg mL^{-1} of CR for 2 h, could be recommended, as Yun *et al*. (2014) showed an increase in Mgv1 phosphorylation in *F. graminearum* with these conditions. However, higher culture volume would be recommended, since these CR conditions would likely lead to disaggregation of mycelia making it difficult to obtain the necessary amount of tissue for protein extraction.

After studying the effect of a short time exposure to CR (2 h), longer exposures (6, 12, 24 h), various CR concentrations (0, 50, 100, 150 μg mL^{-1}), and larger working volumes were also tested. After 6 h of exposure to CR, higher phosphorylation levels of Mgv1 were observed compared to 12 and 24 h, but if analyzing actin and tubulin as a loading control, there was a lower amount of these proteins as well at 12 and 24 h (Figure 2.26). Nevertheless, a uniform load of proteins was observed among all the treatments (Supplementary Figure 2.2), suggesting that actin and tubulin are not good markers for longer hours of exposure to CR since this compound may affect these housekeeping proteins. The bands corresponding to the two other MAPKs, Gpmk1 and Hog1, did not change in the presence of CR: total Gpmk1 band (phosphorylated and unphosphorylated) was observed and seemed to be invariable regarding the CR treatment or time of exposure, while phosphorylated Gpmk1, total Hog1 and phosphorylated Hog1 were not detected in any treatment.

When focusing on how different CR concentrations and CR time of exposure could affect the activation of the CWI pathway in the WT strain, a clear pattern was not found (Figure 2.27).

Since previous assays in this chapter were performed with 100 μg mL^{-1} of CR, an initial screening was carried out to investigate how this CR concentration affected expression of key genes at different time points. The relative expression of the MAPKs genes, *GPMK1* and *HOG1* were not different compared to the untreated WT strain, but the other tested genes (*MGV1*, *RLM1*, *CHS1A*, *CHS5*, and *KIN4*) were upregulated after 6 h of CR treatment, offering further evidence that this compound activates the CWI pathway.

The genes *RLM1*, *CHS1A*, *CHS5* and *KIN4* were analysed after the CR treatments because all of them have been identified as part of the CWI cascade or as interacting partners of at least one of its components. In *S. cerevisiae*, Rlm1 is a downstream component of Slt2, the homolog of Mgv1 (Watanabe *et al*., 1995). In *F. graminearum*, it was also proposed to be the functional downstream of Mgv1 after some experiments confirmed its involvement in the CWI pathway, and a yeast-two-hybrid assay showed an interaction between Mgv1 and Rlm1 (Yun *et al*., 2014). *RLM1* was not differentially expressed after 12 h but was upregulated at 6 and 24 h. Interestingly, *MGV1* was upregulated after 6 and 12 h, but there was no change in its expression after 24 h. These apparently contradictory results could be explained because the relative gene expression values measured at a particular moment are the consequences of the previous activation of its functional upstream component. Therefore, the upregulation of *RLM1* at 24 h might not be the result of the CR effect over *MGV1* at 24 h, but the activation of Mgv1 at a previous moment. For a better understanding of Rlm1 activation by Mgv1, a dynamic curve of gene expression from samples collected at shorter periods could be carried out. As MAPKs work as ON/OFF switches, and can be activated by CR treatments, expression of *RLM1* and *MGV1* might change from different regulation levels. Nevertheless, these results illustrate how these genes are regulated in a particular time after a specific stress that activates the CWI pathway.

In addition to the expected *RLM1* upregulation, other genes also involved in this cascade were likewise upregulated after 6, 12 and 24 h of CR treatment, such as the genes of the *CHITIN SYNTHASES* (*CHS*) family. *CHSs* have been previously shown to be downregulated when *MKK1* (Mgv1 upstream) or *RLM1* (Mgv1 downstream) were deleted in *F. graminearum* (Yun *et al*., 2014). These authors also showed that CR upregulated *CHS1A* and *CHS5* (among other *CHS* member tested) gene expression in *F. graminearum* when in contact with 500 µg mL^{-1} of CR, but they do not specify if the exposure time was 2 or 4 h, which were the times used in the experiments. In this thesis results, 45 min of exposure to 100 µg mL^{-1} of CR was enough to increase the expression of these genes. Apart from Mkk1 and Rlm1 (upstream and downstream functional elements of Mgv1), the kinase Kin4, a component of the spindle position checkpoint that prevents the exit from mitosis when the nuclei are mispositioned (D'Aquino *et al*., 2005), has been identified as another interacting partner of Mgv1 (Wang *et al*., 2011). Not much information is available regarding the interaction of these two proteins in *F. graminearum*, and our results showed that the CR treatment induced upregulation of this gene after 6, 12 and 24 h of exposure to this cell wall stress agent. For other genes outside of the CWI pathway, such as the MAPKs Gpmk1 and Hog1, a CR treatment of 100 µg mL^{-1} for 6, 12 and 24 h did not change their expression while the WT strain was exposed to (Figure 2.28), which confirms the results observed in the WBs (Figure 2.26 and 2.27).

The analysis of how different strains with mutations in the CWI cascade can respond to 100 µg mL^{-1} of CR after 6 h of exposure to this cell wall stress agent, showed interesting results. Unexpectedly, *RLM1* and *KIN4* were upregulated, not only in the WT and the *MGV1_OX6*, strains but also in the *Δmgv1* mutant. We could assume that another MAPK may overlap with some Mgv1 functions that were lost in *Δmgv1*, and as *GPMK1* did not change its expression

(Figure 2.31), it could be hypothesized that Hog1 might recover part of those lost functions when *MGV1* was deleted. As Figure 2.31 shows, *HOG1* was upregulated under these CR conditions, and taking into account that *Δmgv1* mutant was more resistant than the other strains to the effects of 1 M NaCl (Figure 2.24), these results confirm previous studies that showed crosstalk between the CWI and the HOG pathway in *F. graminearum* (Zheng *et al*., 2012; Yun *et al*., 2014).

The *CHITIN SYNTHASE* (*CHS*) gene family and the *β-GLUCAN SYNTHASE* (*FKS1*) are a group of genes encoding enzymes involved in the cell wall formation (Kong *et al*., 2012; Orlean, 2012; Liu *et al*., 2017). In *S. cerevisiae*, the main components of the cell wall are glucans (β-1, 3 and β-1, 6 linked), mannoproteins and chitin (reviewed in (Orlean, 2012)). Chitin is a polysaccharide of β-1, 4 N-acetyl-glucosamine that contributes to a small percentage of the dry weight in the yeast cell wall while is a major component in filamentous fungi (reviewed in (Orlean, 2012)). Therefore, it is not surprising that there are up to three *CHS* genes in *S. cerevisiae* while in filamentous fungi there are at least seven classes that are involved in different processes (Kong *et al*., 2012; Orlean, 2012; Liu *et al*., 2017). Our results show that in the presence of CR, most of the *CHS* gene family were upregulated or not differentially expressed compared to the untreated samples (Figure 2.30). These results differ from previous studies wherein CR presence, all *CHS* except for *CHS1B* and *CHS4*, were upregulated in the WT compared to the non-treated WT (Yun *et al*., 2014). However, the CR concentration and time of exposure were different from our treatment. *CHS1A* was upregulated in all CR treatments, while *CHS5* and *CHS6* were only upregulated in the WT and the *MGV1_OX6* strains but no differentially expressed in *Δmgv1* (Figure 2.30). According to Kong *et al*. (2012), *CHS1* and *CHS6* are among the *CHSs* that play a significant role in *M. oryzae* pathogenesis, where *CHS1* is involved in conidiation and appressoria formation, while *CHS6* in conidiation and filamentous

growth. Regarding *CHS5*, it has been shown that class V of *CHS* plays a key role in filamentous fungi morphogenesis, pathogenicity, and tolerance to heat stress in the Fungi subdivision Pezizomycotina (Liu *et al*., 2017). In addition, it has overlapping functions with *CHS6*, regarding to vegetative and invasive hyphae, and they share a similar expression pattern, maybe because they are located next to each other in the *F. graminearum* genome with less than 3000 bp separating their open reading frame (Kong *et al*., 2012). Since the deletion of *MGV1* negatively affected mycelial growth of *F. graminearum*, but not the expression of other *CHS*, such as *CHS1A* and *CHS3*, in presence of a cell wall stressor (CR), maybe Mgv1 regulation of these family of genes does not involve the whole family but include *CHS5* and *CHS6*.

β-glucans can represent 30-60 % of dry weight in *S. cerevisiae*. In this microorganism, the *β*-1,3 glucan synthase multi-enzyme complex (GS) is formed by three main components: Fks1 and Fks2 and Rho-GTPase (Douglas *et al*., 1994; Inoue *et al*., 1995; Mazur *et al*., 1995; Qadota *et al*., 1996). Fks1 and Fks2 are enzymes that catalyze the synthesis β-1,3 glucan (Douglas *et al*., 1994; Inoue *et al*., 1995; Mazur *et al*., 1995), while Rho1-GTPase is a regulatory subunit of the GS complex, and also activates Pkc1, the upstream functional component of the MAPKKK in the CWI pathway, Bck1 (Qadota *et al*., 1996). In filamentous fungi, the GS complex is formed by only two components since only one Fks protein has been identified (Riquelme, 2013; Garcia-Rubio *et al*., 2020). Our results show that in the presence of CR, a putative *FKS1* was upregulated in the WT and the *MGV1_OX* strains, but it was negatively regulated in the *Δmgv1* mutant, suggesting a possible regulatory role or feedback by Mgv1 over the GS complex, maybe involving another component of the CWI pathway.

Members of the CWI pathway, such as Rlm1 and Mkk1, also seem to regulate the expression of genes involved in the synthesis of the secondary metabolite aurofusarin (Yun *et al*., 2014).

Therefore, it was expected that the presence of a cell wall stress agent, such as CR, would somehow affect the regulation of these genes. Indeed, *AURR1*, *PKS12*, and *GIP1* were downregulated in the WT strain treated with CR, compared to the same untreated strain. Interestingly, these results are the opposite observed after samples were collected for RNA-seq analysis (Figure 2.16), where most of the genes were upregulated in the *Δmgv1* mutant, suggesting a negative regulation by *MGV1*. Therefore, if *MGV1* is not active (as in *Δmgv1* mutant), those genes are upregulated, but when *MGV1* or the pathway is activated, the genes are not differentially expressed or downregulated. Even though there is still no clear path between Mgv1 and the aurofusarin pathway, these results provide an insight into the regulation of this secondary metabolite by the CWI cascade.

In conclusion, *MGV1* overexpression does not increase mycelial growth, macroconidia germination or virulence, but it does increase 15-ADON production. RNA-seq and metabolomic analyses showed that *MGV1* overexpression caused a significant change in some gene expression and metabolite accumulation; however, this change was not as significant as when *MGV1* was deleted. In addition, *MGV1_OX* transformants were not more resistant than a WT strain to the cell wall or membrane stress agents, nor to osmotic stress. Therefore, *MGV1* overexpression will induce changes in metabolite production and gene expression, but will not confer extra powers to *F. graminearum* regarding mycelial growth, conidia germination, virulence, or resistance to different stresses.

Chapter 3. Overexpression of the *MITOGEN-ACTIVATED PROTEIN KINASE KINASE, MKK1*, and its putative phosphomimic (*MKK1*^{197E,203E}) in *F. graminearum*

3.1 Introduction

Protein phosphorylation is one of the most important post-translational modifications that occur in the cell. This process is carried out by protein kinases, enzymes that transfer the γ-phosphate from an ATP molecule onto specific serine, threonine or tyrosine residues of the target protein. This modification typically leads to a conformational change in the target protein that may alter, for example, its activity or localization.

A typical protein kinase core posses two lobes (N-term (smaller) and C-term (larger)) that are connected by a region in the middle of the protein that binds ATP, as it is represented in Figure 3.1 (Pucheta-Martínez *et al*., 2016; Modi and Dunbrack, 2019). In addition to the ATP-binding domain, kinases possess a substrate domain where they can accommodate and phosphorylate their target protein. Many of these require a cofactor, such as Mg^{2+}, to induce a fully active conformation (Pucheta-Martínez *et al*., 2016).

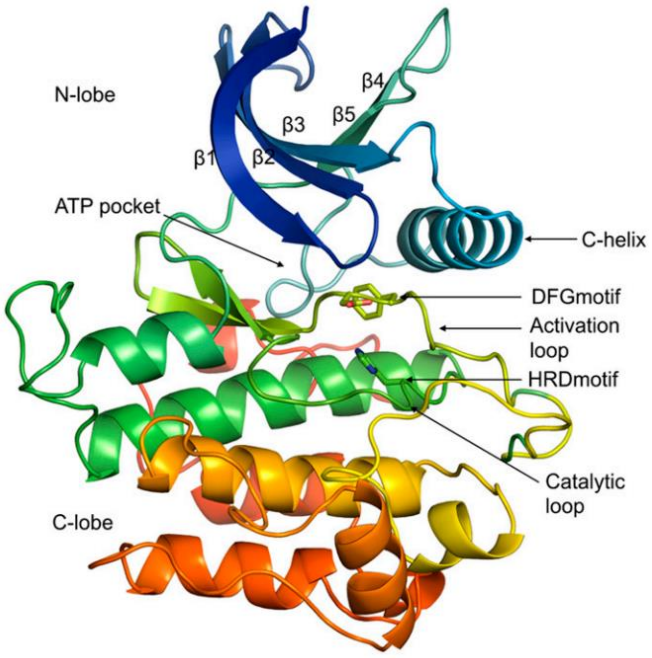

Figure 3.1. Diagram of a typical protein kinase where the main structures are represented: two lobes (N and C), the ATP pocket, the activation loop, and the catalytic loop. This figure was taken from Modi and Dunbrack (2019).

Kinases regulate multiple processes in the cell through phosphorylation, and they themselves are also regulated by phosphorylation in the activation loop domain. The activation loop is around 20-30 residues that starts with a conserved DFG motif and finishes with an APE motif (reviewed in (Lai and Pelech, 2016; Modi and Dunbrack, 2019)). This activation loop forms a cleft where the substrate binds to active kinases and interacts with the protein kinase HRD domain. Conformational changes of the activation loop, due to the phosphorylation of targeted residues, stimulates the proper orientation of the substrate domain and stabilizes the protein for catalysis (reviewed in (Lai and Pelech, 2016)). In this way, phosphorylation of the activation loop controls catalytic activity of the kinase because when the T-loop becomes phosphorylated, the

phosphotransferase activity of the kinase is stimulated (reviewed in (Lai and Pelech, 2016; Modi and Dunbrack, 2019)).

The active site of kinases has important structural variations which have been shown in numerous crystal structures. A nomenclature has been recently established for these different structures, based first on the location of the DFG-Phe side chain, and then, in the orientation of the activation loop (Modi and Dunbrack, 2019). Multiple inactive conformations are shown in inactive kinases because they do not possess the conformation that is necessary for the catalytic activity, and, for instance, the activation loop is collapsed in the surface of the kinase protein and blocks the substrate binding region (Modi and Dunbrack, 2019).

One of the proteins considered a paradigm for regulation of protein kinases in signalling cascades is the human MAPK ERK1 (Lai and Pelech, 2016). The MAPK modules are formed by a MAPKKK that is activated in response to a stimulus and phosphorylates a MAPKK on Ser and/or Thr residues in the activation loop, and in turn, the MAPKK will be activated and can phosphorylate a MAPK in the TXY motif of the activation loop. ERK1 has a TEY motif with Thr202 and Tyr204 as phosphorylation sites. Three other flanking phosphorylation sites (Thr198, Thr207 and Tyr210) have been identified in ERK1 where Thr207 and Tyr210, highly conserved phosphosites in eukaryotic kinases, negatively regulates the catalytic activity of ERK1. Y210F mutant inhibited the recognition of ERK1 by MEK1 (MAPKK) and the subsequent phosphorylation of Thr202 and Tyr204 *in vitro*, while autophosphorylation of Thr207 diminished the stability and catalytic activity of ERK1. Lai and Pelech (2016) suggested that phosphorylation of the flanking sites in ERK1, after its activation by MEK1, leads to kinase inhibition, and these phosphosites could be acting as a mechanism for tight regulation of the kinase protein. Therefore,

they hypothesized that hyperphosphorylation of the T-loop can be a mechanism for downregulation of protein kinases after their activation by its upstream component in the cascade.

A path to study the role of the phosphosites in the activation loop of kinases could be through phosphomimetics created by site-directed mutagenesis. Phosphomimetics can be constructed by switching Ser, Thr or Tyr residues, the three phosphorylatable amino acids, for glutamic or aspartic acid which have a similar structure to a phosphorylated Ser, Thr or Tyr. Therefore, the kinase will be considered phosphorylated and will be activated, if that is what the phosphorylation provokes in the protein, since sometimes phosphorylation can lead to deactivation. In human ERK1, the Ser, Thr and Tyr residues corresponding to a phosphosite were switched for glutamic acid, and the protein's function was mimicked 70, 77.6 and 55.6 % of the time, respectively. However, aspartic acid seemed to be a better mimetic because the protein's function was mimicked in 89.8, 85 and 83.3 % when this amino acid substituted a Ser, Thr or Tyr, respectively (Lai and Pelech, 2016).

In *F. graminearum*, one of the causal agents of FHB disease in cereal crops, there are two MAPKs considered ERK-like proteins, which possesses a TEY motif in their activation loops: Mgv1 and Gpmk1. The third MAPK in this fungus is Hog1, a p38-like with a TGY motif. Mgv1 is the MAPK of the cell wall integrity (CWI) pathway, where only one downstream target of Mgv1 has been identified in *F. graminearum*, the transcription factor Rlm1 (Yun *et al*., 2014), but other targets are expected to be found as well.

The *F. graminearum* CWI cascade is formed by the MAPKKK Bck1 (Bypass of C kinase), the MAPKK Mkk1, and the MAPK Mgv1 (Hou *et al*., 2002; Wang *et al*., 2011; Yun *et al*., 2014). The *MKK1* gene (FGSG_07295) has 53 % identity with the *MKK1/2* of *S. cerevisiae,* and its deletion was shown to cause inhibition of Mgv1 phosphorylation, consistent with the behavior of

an upstream component of Mgv1 (Yun *et al*., 2014). The same study also showed a decrease in phosphorylation levels of the MAPK protein for the HOG pathway, Fgr-Hog1, suggesting that there is cross-talk between the two cascades.

Mkk1 seems to play a critical role in the CWI pathway, and is associated with mycelial growth, conidiation and perithecia formation in filamentous fungi (Wang *et al*., 2011; Yun *et al*., 2014; Yin *et al*., 2018b). In the fungus *B. cinerea*, the deletion of *MKK1* caused a more significant reduction in growth and conidiation than what was observed following the deletion of the other core components, Bck1 and Bmp3 (Bci-Slt2). In addition, the disruption of *MKK1* triggered changes in *B. cinerea* hyphae, characterized by a thickened septa, and in some cases a larger central pore (Yin *et al*., 2018b).

Consistent with other fungal species, the *F. graminearum MKK1* gene has also been shown to play a role in the CWI pathway. Yun *et al*. (2014) showed that *CHITIN SYNTHASE* genes were down-regulated when *MKK1* was deleted. Furthermore, the *Δmkk1* mutant displayed slower hyphal growth, and cell wall weakness was inferred through observation of peripheral tips autolysis. The mutant also showed higher sensitivity to cell wall and osmotic stressors, such as Congo red (CR), calcofluor white (CFW), NaCl and sorbitol, compared with the WT strain. The authors also found that Mkk1 plays a significant role in the production of the pigment aurofusarin, having observed that the *Δmkk1* mutant had less pigmentation and lower expression of some aurofusarin biosynthesis genes.

In the CWI pathway of *F. graminearum*, only one component downstream of Mgv1 has been identified to date, namely Rlm1 (Yun *et al*., 2014); however, MAPKs are known to have multiple targets. Phosphomimetics could be used as a tool to characterize MAPK pathways. For example, generating a constitutively active phosphomimetic of Mkk1 that can continuously phosphorylate

Mgv1 could enable the identification of downstream elements in this pathway. The phopshomimic of Mgv1 *per se* could be difficult to obtain, since the Mgv1 activation loop is formed by TEY residues, where the chemical structure of Tyr might not be compatible with Asp and Glu, in the same way that Ser and Thr are, respectively. For this reason, **I hypothesize that transgenic expression of phosphomimetics in the activation loop of Mkk1 will enable phosphorylation of Mgv1. This could then be used in future studies to screen Mgv1 candidate targets, such as those previously identified by Rampitsch *et al*. (2010).** Therefore, **the overarching goal of this chapter was to generate and characterize a *F. graminearum* mutant overexpressing a putative constitutively active (CA) form of *MKK1* (*MKK1*^{197E,203E}*_OX*).**

3.2 Materials and methods

3.2.1 *F. graminearum* strains, growth conditions and spore production

All *F. graminearum* strains, including the WT (GZ3639) and the mutants or transformants generated in the previous or present chapter, were grown and spores produced as described in section 2.2.1.

3.2.2 Identification of a possible Mkk1 activation loop sequence and its modification

The encoded protein sequence of *MKK1* (FGSG_07295) was obtained from NCBI database. A sequence alignment was performed with Clustal Omega, which allowed identification of possible activation loop sequences using other *MKK1* homologous from different fungal species (Supplementary Figure 3.1). A neighbour-joining tree without distance corrections is shown in Supplementary Figure 3.2.

A fragment of the *MKK1* sequence was modified in the putative activation loop (Thr-X_5-Thr) so that it would encode a constitutively active form: the codon encoding the two threonine residues in the motif $_{197}$**T**KGEAN**T**$_{203}$ (encoding sequence $_{1413}$**ACC** AAG GGC GAG GCC AAT **ACC** $_{1433}$**)** were modified to encode glutamic acid $_{197}$**E**KGEAN**E**$_{203}$ (encoding sequence $_{1413}$**GAA** AAG GGC GAG GCC AAT **GAA**$_{1433}$). The position of the putative activation loop, flanked by DFG and APE motifs, is shown in Figure 3.2. A fragment containing this modification in the sequence was synthesized into a pUC57 vector by Genscript. In addition, a 6x-His-Tag was appended to the N-terminus of the *MKK1* gene using adaptor primers (as described in section 2.2.2) for further protein purification steps.

MERDGSLQGLEAFDKLTIEKARTLDVDDLDEEGWRIASLEKRIVEIGNLGEGAGGAVTRCKLKGGNTVFA
LKVITTNPDPDVKKQILRELGFNKECASDHICKYYGAFVDPSTATISIAMEFCEGGSLDSIYKEVKRLGGRTG
EKVLGKIAEGVLGGLTYLHTRRIIHRDIKPSNILLCRDGAVKLCDFGVSGDFGTKGEANTFIGTSYYMAPERI
TGQSYTITSDVWSTGVTLLEVAQHRFPFPADGTEMQPRANLIDLLTYIVRQDVPKLKDEPDMDVYWSNN
FKYFIECCLEKQPNRRASPWKMMEHPWMVEMRSKRVNMVKYLSYVWGWGDQPKDS

Figure 3.2. Amino acid sequence of Mkk1 in *F. graminearum*. The activation loop domain contains three main motifs, starting with a conserved DFG motif (blue font), followed by two phosphosites (highlighted in gray) separated by five amino acids (Thr-X_5-Thr), and finishes with a conserved APE motif (red font). Other putative phosphosites (Thr-X_5-Thr) are highlighted in gray and underlined, but these are not flanked with DFG and APE sequences.

3.2.3 Generation of *F. graminearum* transformants overexpressing either *MKK1* (*MKK1_OX*) or its putative constitutively active form (*MKK1*^{197E,203E}*_OX*)

Two different sets of transformants/mutants overexpressing *MKK1* were generated, as described in section 2.2.2 and Figure 2.1. One construct was designed to overexpress *MKK1* (*MKK1_OX*), while the other one (*MKK1*^{197E,203E}*_OX*) contains the two TΔE mutations in the putative activation loop of *MKK1*, as described in section 3.2.2. Primers used to amplify the

upstream region of *MKK1* and the starting region of *MKK1* (P1-P2, P5-P8) are listed in Table 3.1.

Table 3.1. Primers used to generate *F. graminearum* transformants, and for qRT-PCR analysis. Adaptor sequence (for the transformation) font colour is orange, while 6xHis-tag is in purple.

Name/position	Accession #	Primer name	F/R	Sequence
Upstream of *MKK1*	FGSG_07295	P1 P2	F R	5' TCG TTG TGT CTT TTA TCC AAC T -3' 5' AGA AAC GCC ACC TTC ACT T -3'
MKK1	FGSG_07295	P3	F	5' ATG **CAC CAT CAC CAT CAC CAT** GAG CGT GAC GGA AG -3'
		P4	R	5' CTA AGA GTC CTT GGG CTG G -3'
Upstream of *MKK1* + adaptors	FGSG_07295	P5 P6	F R	5' **GGT CTT AA/ideoxyU/** TCG TTG TGT CTT TTA -3' 5' **GGC ATT AA/ideoxyU/** AGA AAC GCC ACC TTC -3'
***MKK1*+ adaptors +NHis**	FGSG_07295	P7 P8	F R	5' **GGA CTT AA/ideoxyU/** ATG **CAC CAT CAC CAT CAC CAT** GAG CGT GAC GGA AG -3' 5' **GGG TTT AA/ideoxyU/** CTA AGA GTC CTT GGG CTG G -3'
Upstream of *MKK1* (RF2b)	FGSG_07295	P9	F	AAC TCC CTC GAT CTC AGT GC -3'
HU2E cassette (RF2)		P10	R	TCTCCTTGCATGCACCATTCCTTG
HU2E cassette (RF3)		P11	F	TTGCGTCAGTCCAACATTTGTTGCCA
***MKK1*- RF3b**	FGSG_07295	P12	R	ACGTCAGGATCTGGATTCGT
HPH		P13 P14	F R	AGCTGCGCCGATGGTTTCTACAA GCGCGTCTGCTGCTCCATACAA
β-TUBULIN	FGSG_09530	P15 P16	F R	GTTCTGGACGTTGCGCATCTG TGATGGCCGCTTCTGACTTCC
EF-1α	FGSG_08811	P17 P18	F R	CCTCGCTACTATGTCACCGT CAAGGGTGTAGGCAAGGAGA
MGV1	FGSG_10313	P19 P20	F R	ATGGAGTGTGATTTGGCTGC TGGATGTACTTGAGACCGCA
ACTIN	FGSG_07335	P21 P22	F R	ATCCACGTCACCACTTTCAA TGCTTGGAGATCCACATTTG
KIN4	FGSG_11812	P25 P26	F R	GTTCGAAGTTGCTCGACACA TCGGGAGAAACACCTGAATC
TRI5	FGSG_03537	P27 P28	F R	TGTCACCTGCCATGAGATCA TCCGAGAAGACAGCAACCAT
TRI6	FGSG_03536	P29 P30	F R	GGCATTACCGGCAACACTTCAA CATGTTATCCACCCTGCTAAAGACC
CHS 5	FGSG_01964	P31 P32	F R	ACGGTCTGCAAGCCATTATC TAAAGAGGCAGACCGAAGGA
CHS 6	FGSG_15914	P33 P34	F R	CGTGCTGAAGATGGATGTGT TTGTAAATGGATGCGGGAAT

PKS12	FGSG_02324	P35 P36	F R	ACGATGGAGCAGACGGATAC CCCAGAATGACACCGAGAAT
MKK1	FGSG_07295	P37 P38	F R	CTTTGCGATTTCGGTGTCTC ACGACTGGCCTGTAATACGC

Positive colonies that grew on PDA medium containing 150 µg mL^{-1} hygromycin were screened by PCR, using primers P9-P14 (Table 3.1 and Supplementary Figure 3.3) as described in section 2.2.2. The correct integration of the cassette was verified by a combination of PCRs (primer information in Table 3.1) and sequence analysis of the amplicons (primer's information in Table 3.2 and Supplementary Figure 3.3). Primers P9 and P44 located upstream and downstream of the homologous recombination sites and were thus not part of the insertion cassette. P9 and P10 were used to confirm the insertion (*MKK1* upstream region) in the right place. Correct integration of the construct was also verified by a combination of PCRs, using primers P39-P46 (as represented in Supplementary Figure 3.3), and sequence analysis of the amplicons. Sequencing was carried out by the Genome Québec service lab (Montréal, Québec, Canada). New colonies were named *MKK1*^{197E,203E}*_OX* or *MKK1_OX*, depending on the inserted modification.

Table 3.2. Primers used for amplifying the whole *MKK1* gene, part of its upstream and downstream sequence to corroborate the sequence after USER-cloning.

Name	Primer Number	Sequence	Tm (°C)	Size (bp)
Pgpda/MKk1_F1	P39	CCATCCTTCCCATCCCTTAT	53.8	528
***MKK1*_R1**	P40	CCGTAGATGGGTCCACAAAT	54.6	
***MKK1*_F2**	P41	AGATTTATGCGCAGGCAGTT	55.1	510
***MKK1*_R2**	P42	GACCAGACATCCGAGGTGAT	56.3	
MKK1_SeqF3	P43	AGGACGAGCCTGATATGGAC	56.1	442
***MKK1*_SeqR3**	P44	TATGAGAAACAGCGGTCACG	54.9	
***MKK1*_Seq4F**	P45	TCGGTGTCTCGGGTGACTTT	58.4	456
***MKK1*_Seq4R**	P46	ACCATGTTAACGCGCTTGCT	58	

3.2.4 *MKK1* copy number and confirmation of *MKK1* overexpression

To determine the copy number of *MKK1* in *MKK1_OX* and *MKK1*^{197E,203E}*_OX*, a qPCR was carried out as described in section 2.2.3, with primers P15-P38 (Table 3.1) and a standard curve was used to normalize the abundance of *MKK1* gene *vs* the housekeeping genes (*TUBULIN* and *EF*) in each strain. Names and accession numbers of genes used in this chapter are listed in Supplementary Table 3.1.

RT-qPCR was used to determine whether the *MKK1* gene was overexpressed in *MKK1*^{197E,203E}*_OX* and *MKK1_OX* as described in section 2.4, using the primers in Table 3.1. *MGV1_OX6* (generated in Chapter 2) and Δ*mgv1* (received from Dr. Gopal Subramaniam from AAFC-Ottawa) were included for comparison. RNA extraction, cDNA synthesis and RT-qPCR was performed as described in section 2.2.4, with annealing temperatures outlined in the primer table (Table 2.2).

3.2.5 Immunodetection of MAPKs

Total protein was extracted from the mycelium of *MKK1*^{197E,203E}*_OX*, *MKK1_OX*, *MGV1_OX6*, Δ*mgv1* and the WT progenitor strain grown in PDB, as described in section 2.2.5. Immunoblotting analysis was performed with the same antibodies (Table 2.3) and buffers as in section 2.2.5.

3.2.6 Wheat disease assay

FHB assays were carried out in Roblin (susceptible to FHB) and Penhold (moderately resistant to FHB) wheat Canadian cultivars, as previously described in section 2.2.7. *Δmgv1* and *MGV1_OX1* were included in the assay, in addition to *MKK1*^{197E,203E}*_OX*, *MKK1_OX* and the WT, in order to compare with the results of the previous chapter. The experiment was repeated

three times over the course of four weeks. Mean values of five plants per inoculum were calculated for each repetition using one-way ANOVA, followed by Tukey's HSD test ($\alpha = 0.05$).

3.2.7 15-acetylated DON (15-ADON) accumulation in axenic cultures

DON accumulation and metabolomic analysis of the *MKK1*^{197E,203E}*_OX*, *MKK1_OX*, *MGV1_OX1*, *Δmgv1* and the WT strains, were carried out at AAFC-Ottawa by Drs. Kristina Shostak and Gopal Subramaniam, as described in the PhD dissertation Shostak (2020). The methods are briefly described in section 2.2.10.

3.2.8 Effect of cell wall stress and osmotic stress agents on mycelial growth and MAPK pathway activation

To determine whether the overexpression of *MKK1* or the putative phosphomimic (*MKK1*^{197E,203E}*_OX*) could improve the resistance of the strains to cell wall stress agents, a plug of 7-mm diameter of mycelia obtained from the border of a four-day old colony was used to inoculate PDA plates amended with 0.01 % sodium dodecyl sulfate (SDS), 200 µg mL^{-1} calcofluor white (CFW) or 500 µg mL^{-1} Congo red (CR). To determine whether there is an effect caused by the overexpression of *MKK1* or *MKK1*^{197E,203E} on the HOG pathway, the osmotic stress agent NaCl (1 M) was also included as a treatment. Three plates per treatment were incubated at 27°C and the mycelial diameter was measured every 48 h until nine days post inoculation. Pictures were taken 6 days after inoculation. Percentage of mycelial growth inhibition for each strain was calculated as: ((C-T)/C) x 100, where C is the diameter of the colony in PDA medium (control) and T represents the diameter on PDA supplemented with the stress agent. For each assay, data were analysed using a one-way ANOVA, followed by Tukey's HSD test ($\alpha = 0.05$).

3.2.9 MAPK pathway activation with Congo red

Eight 50 mL-conical tubes containing 20 mL of potato dextrose broth (PDB) were inoculated with 2 x10^5 spores of *MKK1*^{197E,203E}*_OX*, *MKK1_OX*, *MGV1_OX6* or WT, and 16 tubes with *Δmgv1* (due to its slow growth). After 40-42 h of incubation at 180 rpm and 27°C, 80 µL of CR solution at 25 mg mL^{-1} were added to half of the tubes, for a final concentration of 100 µg mL^{-1} of CR, and 80 µL of autoclaved Optima water was added to the other half (control). Samples were returned to the shaking incubator for 45 min. Mycelium was collected in autoclaved paper towel (described in section 2.2.1) after filtration from the media, and was washed with 100 mL of autoclaved Nanopure water. The washed mycelium was frozen in liquid Nitrogen and stored at -80°C until the tissue was ground for protein analysis, as described in section 2.2.5. The experiment was replicated three times.

3.2.10 Differential expression of genes associated with the CWI pathway

RT-qPCR was used to compare the expression of specific genes among *MKK1_OX* and the WT progenitor strain. Erlenmeyer flasks (250-mL) with 100 mL PDB were inoculated with 10^5 spores of *F. graminearum* WT, *MKK1_OX*, *MKK1*^{197E,203E}*_OX*, *MGV1_OX* or *Δmgv1* strains. The flasks were kept at 27°C, shaking at 180 rpm and mycelia were collected 40 h after incubation. A pool of three flasks per treatment per strain was considered one replication. The experiment was replicated three times. Mycelium was collected in autoclaved paper towel (described in section 2.1) after filtration from the media, and was washed with 100 mL of autoclaved Nano pure water. Mycelium was transferred to liquid nitrogen and stored at -80°C until the tissue was ground for total RNA extraction, as outlined in section 2.2.4. RT-qPCR was performed as described in section 2.2.4 with the primers that are listed in Table 3.1 and the reverse transcriptase SuperScript® IV RT.

3.3 Results

3.3.1 Generation of transformants *in locus* overexpressing *MKK1*^{197E,203E} *or MKK1*

The transformation of *F. graminearum* with the *MKK1*^{197E,203E}*_OX* and *MKK1_OX* cassettes yielded ten colonies in total (only two of them with the *MKK1*^{197E,203E}*_OX* cassette) resistant to hygromycin. For the purpose of this study two colonies from each group were selected (Figure 3.3). Colonies were named based on the construction they carried: *MKK1_OX4*, *MKK1_OX5*, *MKK1*^{197E,203E}*_OX9* and *MKK1*^{197E,203E}*_OX10*. Sequence analyses of the amplicons obtained with the primer sets P39-P46 (Supplementary Figure 3.4) confirmed that the entire cassette, without unwanted mutations, was correctly incorporated into the genomes of each of the transformant strains at the desired location. Further to this, qPCR confirmed that only a single copy of the *MKK1* or the *MKK1*^{197E,203E} gene is present in each of the transformants (Figure 3.4).

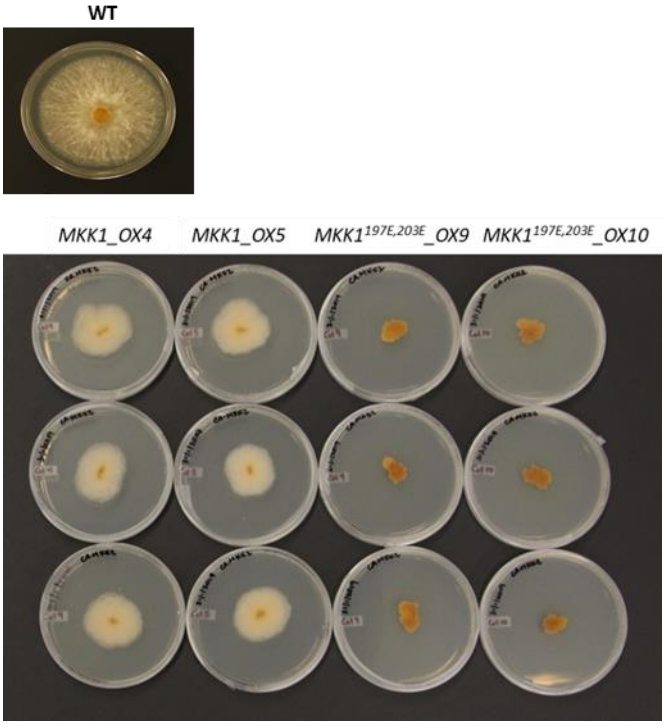

Figure 3.3. Colonies obtained after USER-cloning transformation for generating *MKK1_OX* and *MKK1*^{197E,203E}*_OX* mutants, four days after inoculation on PDA media. The WT strain was also grown for four days on PDA medium, and is shown for comparison.

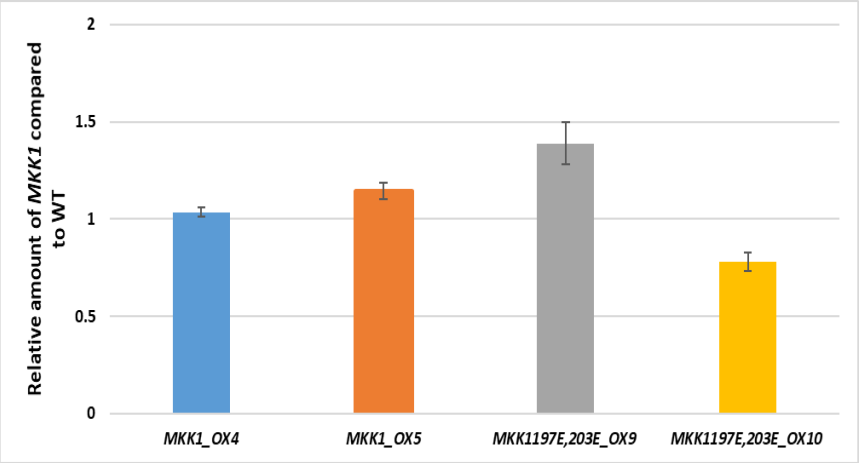

Figure 3.4. Copy number of *MKK1*. Values of the *MKK1*^{197E,203E}*_OX* and *MKK1_OX* transformants were normalized against its housekeeping genes *EF-1α* and *β-TUBULIN*, and with WT, using REST© software, $p \leq 0.05$. Bars represent the standard errors. No statistical differences were observed for each strain compared to WT.

3.3.2 Confirmation of *MKK1* overexpression by RT-qPCR

The overexpression of *MKK1* was confirmed using RT-qPCR (Figure 3.5). In all the *MKK1*^{197E,203E}*_OX* and the *MKK1_OX* transformants the expression was at least 12-fold higher than the WT. As expected, *MKK1* transcript levels in the strain *MGV1_OX6* were similar to the WT. Interestingly, *MKK1* expression was downregulated in *Δmgv1*.

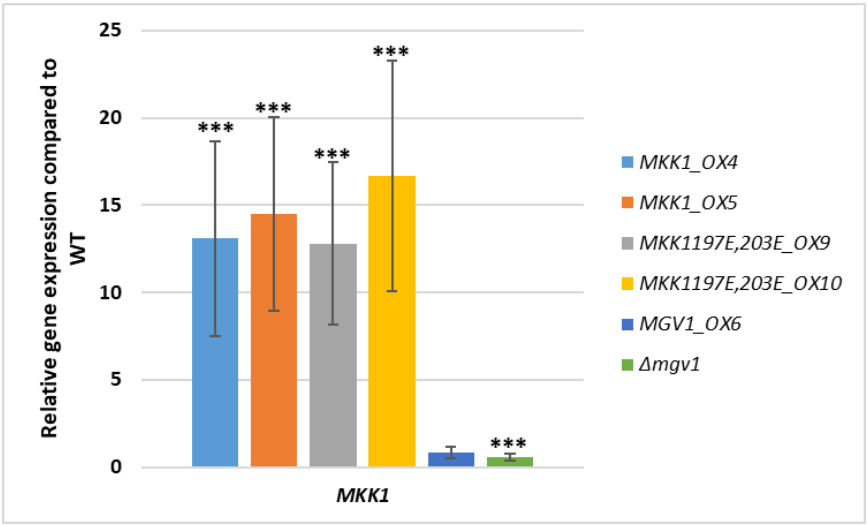

Figure 3.5. Relative expression of *MKK1* in the transformants *MKK1*^{197E,203E}*_OX*, *MKK1_OX*, *MGV1_OX* and *Δmgv1*, compared to WT. Mycelia were extracted from PDB 40 h after inoculation. Relative expression was calculated using REST© software that uses the pair wise fixed reallocation randomisation test © for comparing the expression ratios of the transcripts. Asterisks represent statistically differences at $p \leq 0.05$ (*), $p \leq 0.01$ (**), and $p \leq 0.001$ (***). Bars represent the standard errors of three biological replicates and three technical replicates (n=9). CT-values were normalized with the housekeeping gene *β-TUBULIN*..

3.3.3 Effect of the overexpression of the putative phosphomimic (*MKK1*^{197E,203E}*_OX*) and *MKK1* on MAPKs and *KIN4* expression in *F. graminearum*

To understand the effect that this putative phosphomimic would have on the expression of Mgv1, Gpmk1 and Hog1 (MAPKs of the CWI, the pathogenesis and the HOG pathways, respectively), RT-qPCRs were performed. In addition, the expression of the kinase *KIN4*, a putative Mgv1-interacting partner, was also evaluated.

The relative expression of *MGV1* was similar to WT or sometimes slightly downregulated when *MKK1* was overexpressed, whether or not the activation loop was modified. *MGV1_OX6* and *Δmgv1* were used as controls, corroborating the up- or downregulation of *MGV1*, respectively (Figure 3.6). *GPMK1* showed a similar pattern to *MGV1* for *MKK1*^{197E,203E}*_OX* and *MKK1_OX* mutants. *GPMK1* transcript levels did not change when *MGV1* was overexpressed, but *GPMK1* was downregulated when *MGV1* was deleted (Figure 3.6). In addition, the only change observed in *HOG1* expression across the mutants was its downregulation in *Δmgv1*. The expression of *KIN4*, a kinase that putatively interacts with Mgv1, was only upregulated in the *MGV1_OX* strain, while in the other cases the *KIN4* transcript accumulation was similar to WT or slightly reduced, with a stronger effect when *MGV1* was deleted (Figure 3.6).

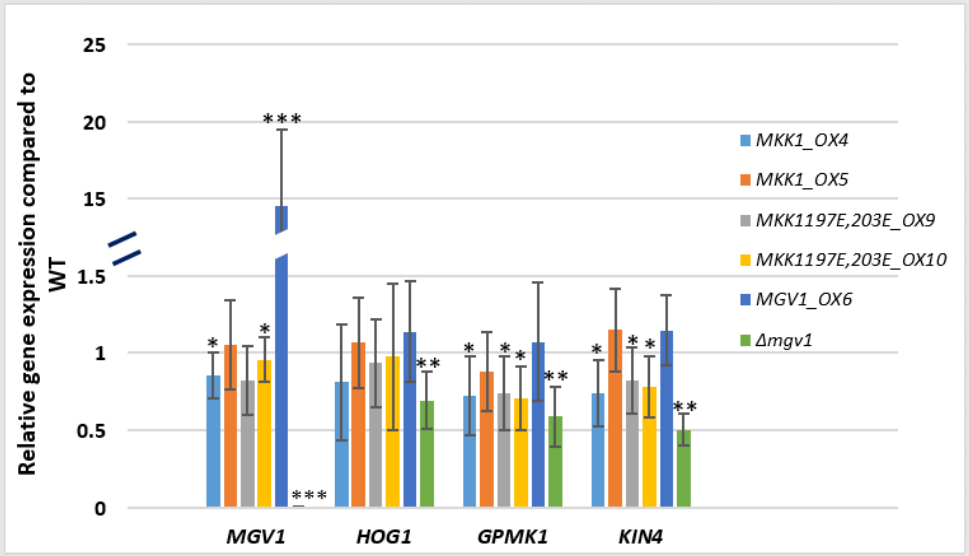

Figure 3.6. Relative expression of *MAPK*s in the transformants *MKK1*^{197E,203E}*_OX*, *MKK1_OX*, *MGV1_OX* and *Δmgv1*, compared to WT. Mycelia were extracted from PDB 40 h after inoculation. Relative expression was calculated using REST© software that uses the pair wise fixed reallocation randomisation test © for comparing the expression ratios of the transcripts. Asterisks represent statistical differences at $p \leq 0.05$ (*), $p \leq 0.01$ (**), and $p \leq 0.001$ (***). Bars represent the standard errors of three biological replicates and three technical replicates (n = 9). CT-values were normalized with the housekeeping gene *β-TUBULIN*.

3.3.4 Overexpression of *MKK1* (*MKK1_OX*) and its putative phosphomimic (*MKK1*^{197E,203E}*_OX*) affects *F. graminearum* virulence on wheat heads

The effect of overexpressing *MKK1* (or its putative phosphomimic) on virulence was evaluated through point inoculation of wheat heads of two Canadian cultivars (Figures 3.7 and 3.8). In Roblin, a susceptible wheat cultivar, the number of diseased spikelets when inoculated with *MKK1_OX* was only around 30 % compared with the WT, while in plants inoculated with *MKK1*^{197E,203E}*_OX* it was less than 7 %, a similar effect to that observed with the *Δmgv1* mutant (Figures 3.7 A and 3.8 A). *MGV1_OX1* was used as a control from a previous experiment (section 2.7), and consistent with previous results the disease symptoms did not differ from the WT (Figures 3.7 A and 3.8 A). In Penhold, a moderately resistant wheat cultivar, the inoculation

of *MKK1*^{197E,203E}*_OX* and *MKK1_OX* strains caused a similar result to what was observed for Roblin, with *MKK1_OX* strains causing less disease than the WT, but *MKK1*^{197E,203E}*_OX* causing even less than *MKK1_OX*. In addition, *Δmgv1* caused only rare cases of necrotic lesion in the inoculated spikelet. These results showed that overexpression of *MKK1* or *MKK1*^{197E,203E} negatively affects *F. graminearum* virulence in wheat heads, and that *MKK1*^{197E,203E}*_OX* has a similar effect on wheat disease as the deletion of *MGV1* (Figures 3.7 B and 3.8 B).

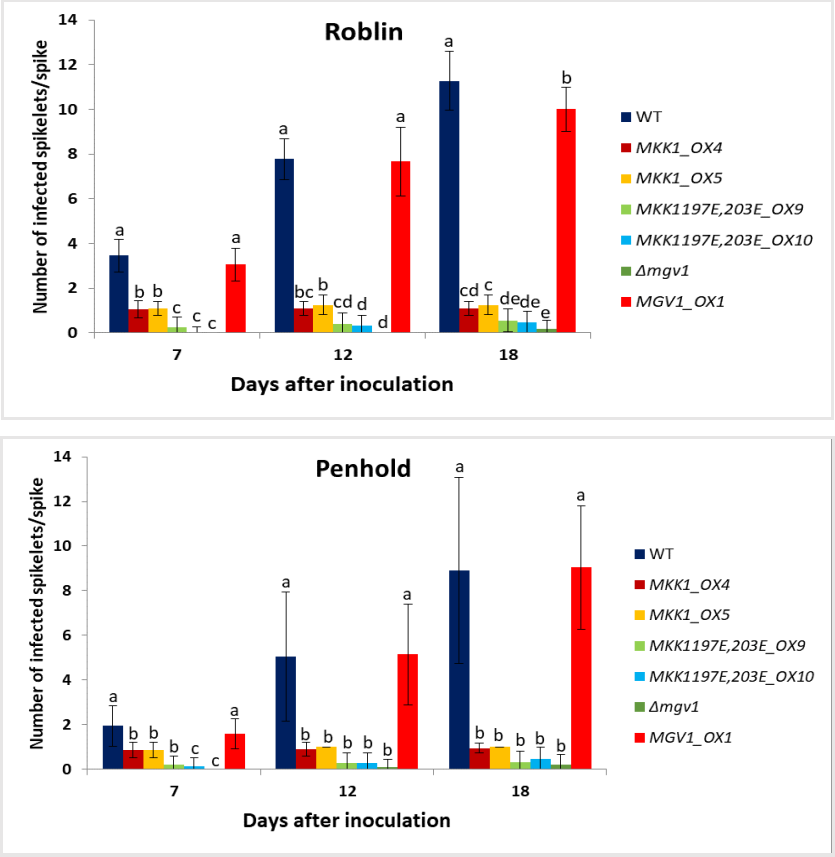

Figure 3.7. *F. graminearum* virulence in wheat spikes. Number of infected spikelets/spike after 7, 12 and 18 dpi in the susceptible cultivar Roblin and the moderately resistant cultivar Penhold. Bars represent the average of one repetition consisting of five plants/strain analyzed for differences in virulence through one-way ANOVA, followed by Tukey's HSD test ($\alpha = 0.05$). Same letters indicate not a statistically significant difference at the 5 % level. The experiment was repeated two more times over the course of four weeks, with similar results.

Figure 3.8. Spikes of the susceptible wheat cultivar Roblin **(a)** and the moderately resistant wheat cultivar Penhold **(b)** at 18 dpi. The black dot in the 5th-7th spikelet (from top) represents the point where 10^4 spores in a 10 µL volume were inoculated.

3.3.5 Effect on 15-ADON accumulation

DON production is often used as a measure of a strain virulence, since this secondary metabolite produced by *F. graminearum* is considered a virulence factor that facilitates the pathogen spread through the host tissue. To determine if the reduced virulence observed in *MKK1_OX* and *MKK1*^{197E,203E}*_OX* might be also influenced by the production of this mycotoxin, 15-ADON accumulation was measured in axenic cultures (Figure 3.9).

The overexpression of *MKK1* increased 15-ADON accumulation; however, overexpression of *MKK1*^{197E,203E}*_OX* did not affect the production of the mycotoxin and the abundance was similar to WT (Figure 3.9).

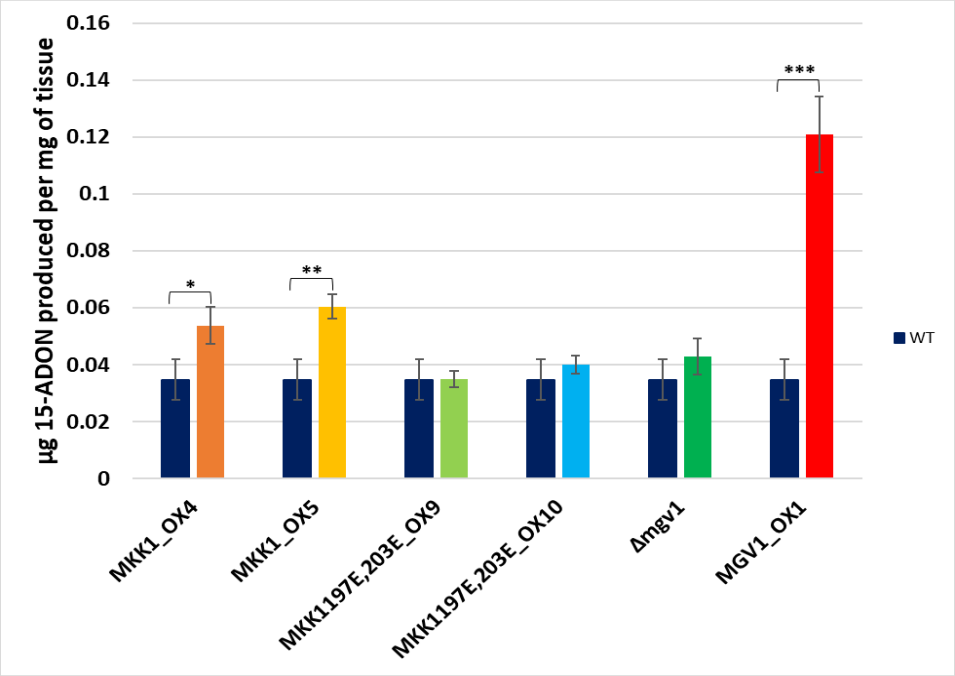

Figure 3.9. 15-ADON accumulation under axenic conditions (DON-induction media) in *F. graminearum* strains overexpressing *MKK1 (MKK1_OX)* or its putative active form *(MKK1^{197E,203E}_OX)*, overexpressing *MGV1* (*MGV1_OX1*) or without *MGV1* (*Δmgv1)*, compared to WT. Bars represent the mean of four measures analysed by Student's t-Test. Asterisks indicate statistically significant differences compared with the WT for $p \leq 0.05$ (*), $p \leq 0.01$ (**), and $p \leq 0.001$ (***).. Note: this experiment was carried out together with that presented in section 2.2.3.

3.3.6 Effect on genes associated with DON production and regulation

The first step in the DON biosynthetic pathway is regulated by the enzyme trichodiene synthase (Tri5). *TRI5* expression in mycelia produced from spores growing on PDB for 40 h was downregulated in all strains tested compared to WT (Figure 3.10). The overexpression of *MKK1*, and its putatively active form, as well as the overexpression of *MGV1* or its deletion, negatively affected the transcript levels of *TRI5* (Figure 3.10). A similar pattern was observed for the transcription factor Tri6 which regulates the trichothecene biosynthetic pathway.

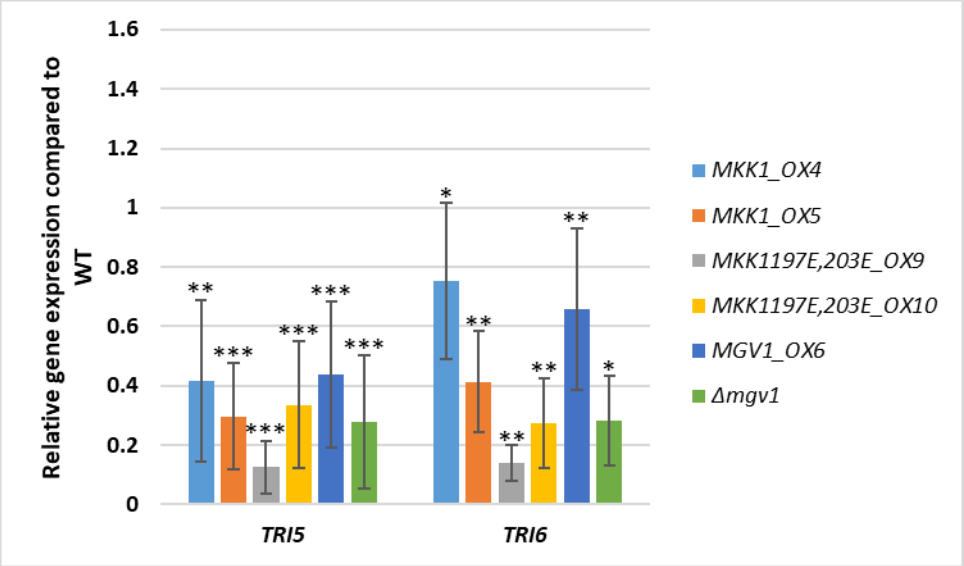

Figure 3.10. Relative *TRI5* and *TRI6* expression in the *MKK1_OX*, *MKK1*^{197E,203E}*_OX*, *MGV1_OX6* and *Δmgv1* transformants compared to WT. Mycelia were extracted from PDB 40 h after inoculation. Relative expression was calculated using REST© software that uses the pair wise fixed reallocation randomisation test © for comparing the expression ratios of the transcripts. Asterisks represent statistical differences at $p \leq 0.05$ (*), $p \leq 0.01$ (**), and $p \leq 0.001$ (***). Bars represent the standard errors of three biological replicates and three technical replicates (n=9). CT-values were normalized with the housekeeping gene *β-TUBULIN*.

3.3.7 Effect of overexpression of *MKK1* and *MKK1*^{197E,203E}*_OX* in the CWI pathway

The CWI pathway components regulate the response to certain stresses or processes in the cell that involves the formation or reinforcement of the cell wall. *CHITIN SYNTHASES* (*CHS*) form a family of genes that regulates the biosynthesis, transport and deposition of chitin in the cell wall. *CHS5* and *CHS6* expression showed a similar pattern and were downregulated in *MKK1_OX*, *MKK1*^{197E,203E}*_OX* and *Δmgv1* compared to WT (Figure 3.11). When *MGV1* was overexpressed, *CHS5* transcript levels were no statistically different from the WT, but for *CHS6* a slight increase was detected, suggesting that Mgv1 positively regulates *CHS5* and *CHS6* expression (Figure 3.11).

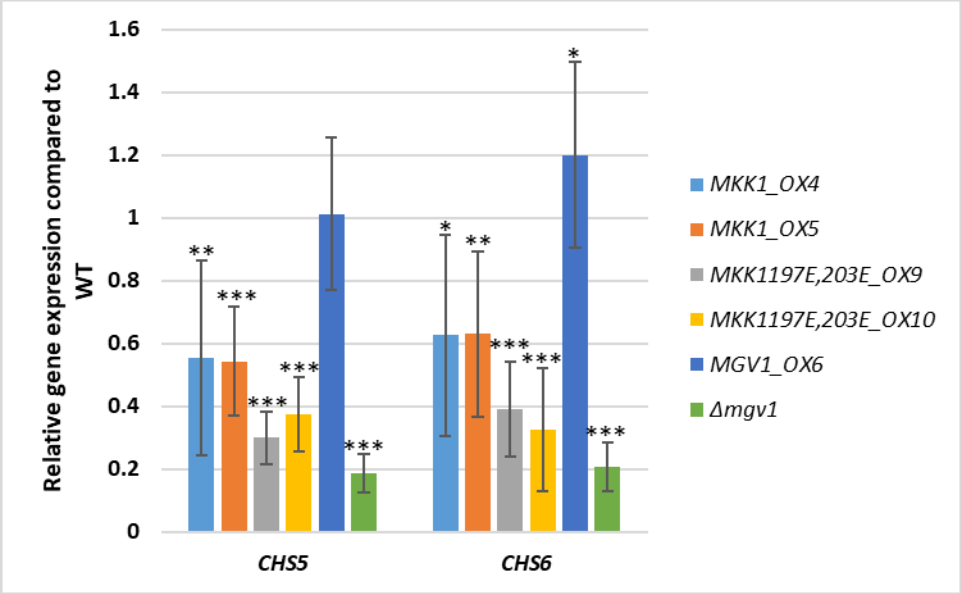

Figure 3.11. Relative expression of *CHS5* and *CHS6*, genes of the *CHITIN SYNTHASE* family in the *MKK1_OX*, *MKK1*^{197E,203E}*_OX*, *MGV1_OX6* and *Δmgv1* transformants compared to WT. Mycelia were extracted from PDB 40 h after inoculation. Relative expression was calculated using REST© software that uses the pair wise fixed reallocation randomisation test © for comparing the expression ratios of the transcripts. Asterisks represent statistical differences at $p \leq 0.05$ (*), $p \leq 0.01$ (**), and $p \leq 0.001$ (***). Bars represent the standard errors of three biological replicates and three technical replicates (n=9). CT-values were normalized with the housekeeping gene *β-TUBULIN*.

Secondary metabolite production, such as the pigment aurofusarin, is also associated with the proteins that function in the CWI pathway. Several genes are involved in the biosynthetic pathway of aurofusarin and are grouped together in one cluster. *MKK1* overexpression negatively affected the expression of some of those genes, such as *PKS12*, a PKS responsible for the first step in the aurofusarin biosynthesis pathway, and the multicopper oxidase *GIP1* (putative laccase); however, in *MKK1*^{197E,203E}*_OX* these genes were similarly regulated compared to WT (Figure 3.12). The overexpression of *MGV1* or its deletion (*Δmgv1*) did not affect *GIP1* expression but *PKS12* was upregulated in *MGV1_OX* transformant, while it was not affected in *Δmgv1* (Figure 3.12).

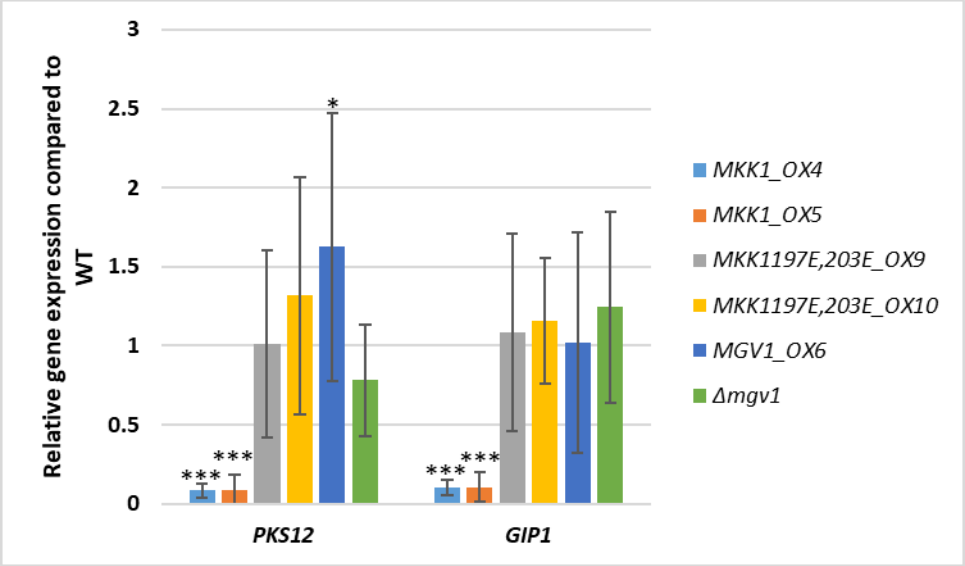

Figure 3.12. Relative expression of genes involved in the pathway of the pigment aurofusarin (*PKS12* and *GIP1*) in the *MKK1_OX*, *MKK1*^{197E,203E}*_OX*, *MGV1_OX6* and *Δmgv1* transformants compared to WT. Mycelia were extracted from PDB 40 h after inoculation. Relative expression was calculated using REST© software that uses the pair wise fixed reallocation randomisation test © for comparing the expression ratios of the transcripts. Asterisks represent statistical differences at $p \leq 0.05$ (*), $p \leq 0.01$ (**), and $p \leq 0.001$ (***). Bars represent the standard errors of three biological replicates and three technical replicates (n=9). CT-values were normalized with the housekeeping gene *β-TUBULIN*.

3.3.8 Mycelial growth response to cell wall stress and osmotic stress agents

Mycelial growth in *MKK1_OX* transformants and *MKK1*^{197E,203E}*_OX* mutants was affected, compared to WT, with a stronger effect in the putative phosphomimic (Figure 3.13). Mycelial growth inhibition for each strain was calculated as a ratio of the difference between the growth on PDA and the growth of the same strain on PDA supplemented with stress agents. At seven days after inoculation, the colony diameter of the WT and *MGV1_OX6* reached the edge of the plate in all treatments, and that is why the percentage of growth inhibition for those strains was zero at 7 and 9 days post inoculation.

A similar percentage of growth inhibition was observed in WT, *MGV1_OX6* and *MKK1_OX* transformants when the osmotic stressor, NaCl (1 M), was added to the culture media (Figure 3.13). This value diminished over time because the strains were compared to its control (growth on PDA media without NaCl), and the control reached the maximum growth, defined as the size of the plate, at different time points. The WT and the *MGV1_OX6* strains grew faster than *Δmgv1*, therefore this percentage was reduced earlier for them. Interestingly, *MKK1*^{197E,203E}*_OX* and *Δmgv1* were not only resistant to 1 M NaCl, but their growth was enhanced by more than 200 % and 80 %, respectively, at both 7 and 9 days post inoculation.

The presence of cell membrane stress agents (SDS) or cell wall stress agents (CFW, BPB or CR) affected the radial growth of the transformants/mutants in different ways (Figure 3.13). SDS slightly affected the WT (around 16 % inhibition) but it had a stronger effect on *MKK1_OX* (up to 38 % of growth inhibition in *MKK1_OX5*); however it does not seem to negatively affect *MKK1*^{197E,203E}*_OX* mutants, nor *Δmgv1*. Instead, SDS enhanced *MKK1*^{197E,203E}*_OX9* and *MKK1*^{197E,203E}*_OX10* growth, with stronger effect on *MKK1*^{197E,203E}*_OX9,* which doubled its colony diameter compared to PDA at 7 days on solid culture media (Figure 3.13). Surprisingly, CFW, in general, did not affect mycelial growth, but enhanced it in all the strains, having a stronger effect on *MKK1*^{197E,203E}*_OX* mutants (around 65 % in *MKK1*^{197E,203E}*_OX10*) by 7 days after growing on culture medium (Figure 3.13). The pH indicator BPB also negatively affected mycelial growth of the strains, with a stronger effect on *MKK1_OX*, *MKK1*^{197E,203E}*_OX* and *Δmgv1*. The CR treatment inhibited the mycelial growth of all strains tested, with WT and *MGV1_OX6* as the most resistant ones (Figure 3.13). Unexpectedly, *MKK1*^{197E,203E}*_OX* were found to be the most susceptible mutants compared with the WT, followed by *MKK1_OX* and *Δmgv1*. Interestingly, a strong black halo was observed around *Δmgv1* (data not shown),

suggesting that under these conditions, this mutant might secrete some compounds into the media.

(a)

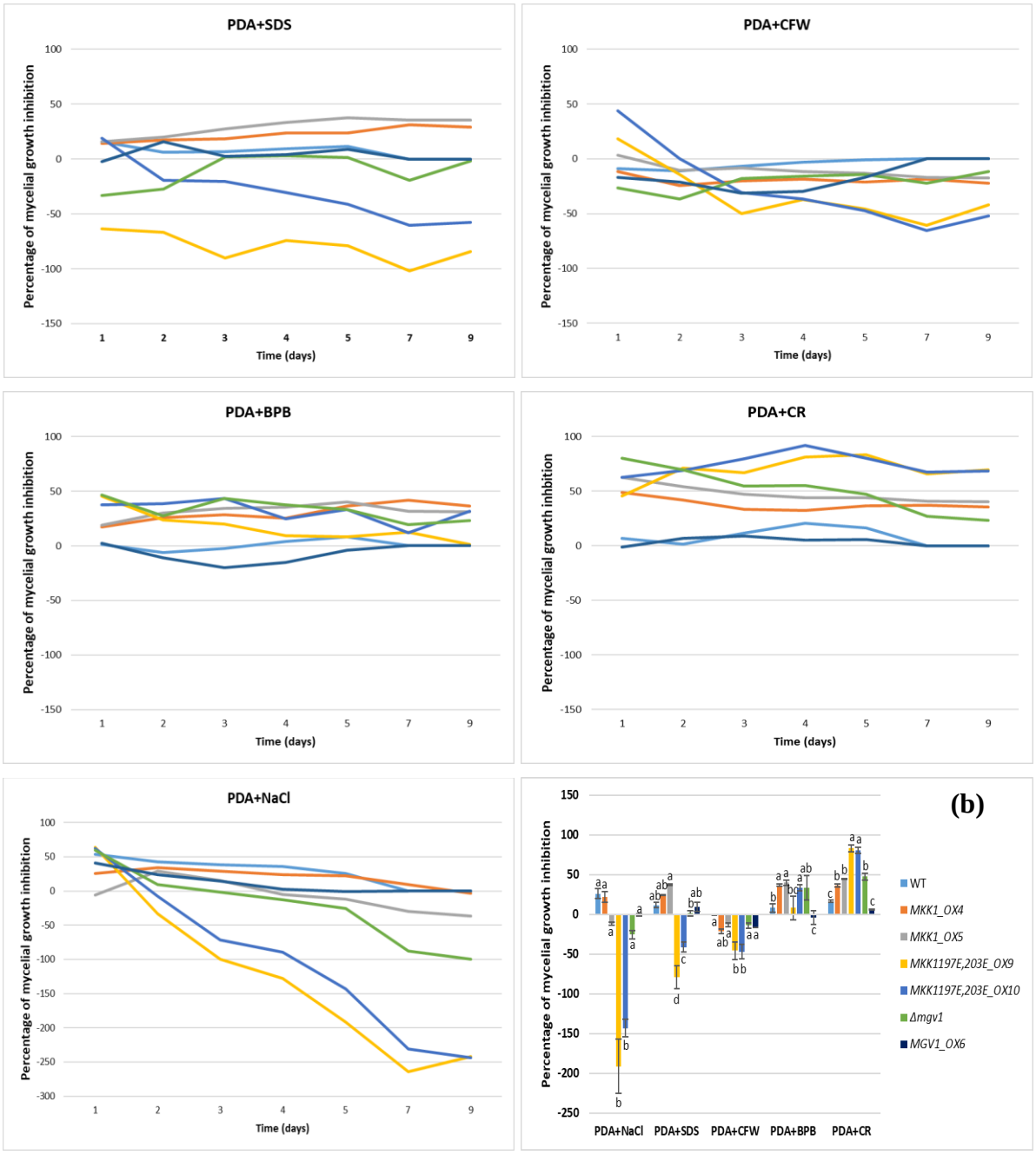

(c)

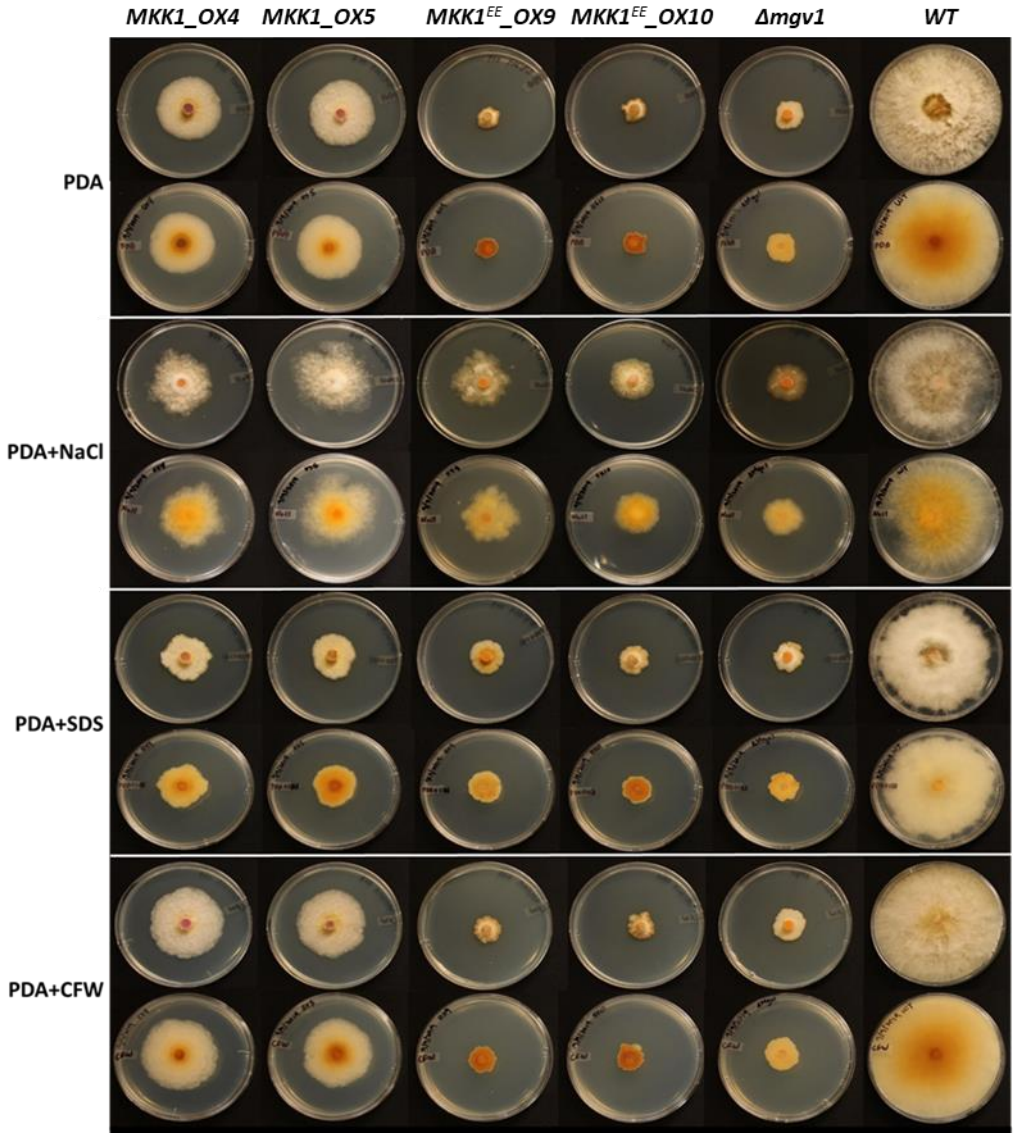

Figure 3.13. Mycelial growth of *F. graminearum* mutants, and a WT strain, growing on PDA supplemented with cell wall stress agents (SDS**,** CFW, BPB, CR) or an osmotic stressor (1 M-NaCl). **(a)** Line charts show the percentage of mycelial growth inhibition over a course of 9 days. **(b)** Data at five days after inoculation was analyzed through one-way ANOVA, followed by Tukey's HSD test ($\alpha = 0.05$). Bars represent the mean of the percentage of inhibition, calculated from three plates per strain per treatment. Error bars correspond the standard error of three values. Different letters represent statistically significant values for $p \leq 0.05$, for each stress treatment. (**c)** Top and bottom of colonies six days after inoculation.

3.3.9 Effect of the cell wall stress compound, CR, in MAPK proteins activation

In the putative phosphomimic, *MKK1*^{197E,203E}*_OX*, it is anticipated that Mgv1 will be constitutively activated. Interestingly, it was shown that Mgv1 was phosphorylated in the WT but not in either of the *MKK1* overexpression strains *MKK1*^{197E,203E}*_OX* and *MKK1_OX* (Figure 3.14). The abundance of the total (phosphorylated and unphosphorylated) Mgv1 was similar among *MKK1_OX*, *MKK1*^{197E,203E}*_OX* and WT strains. The phosphorylated and total (phosphorylated and unphosphorylated) Gpmk1, another Erk1/2-like protein, was similar among all the strains tested Unexpectedly, in *MKK1*^{197E,203E}*_OX* the band representing the total Hog1, the MAPK in the HOG pathway, was very intense, as well as in its phosphorylated form.

(a) **(b)**

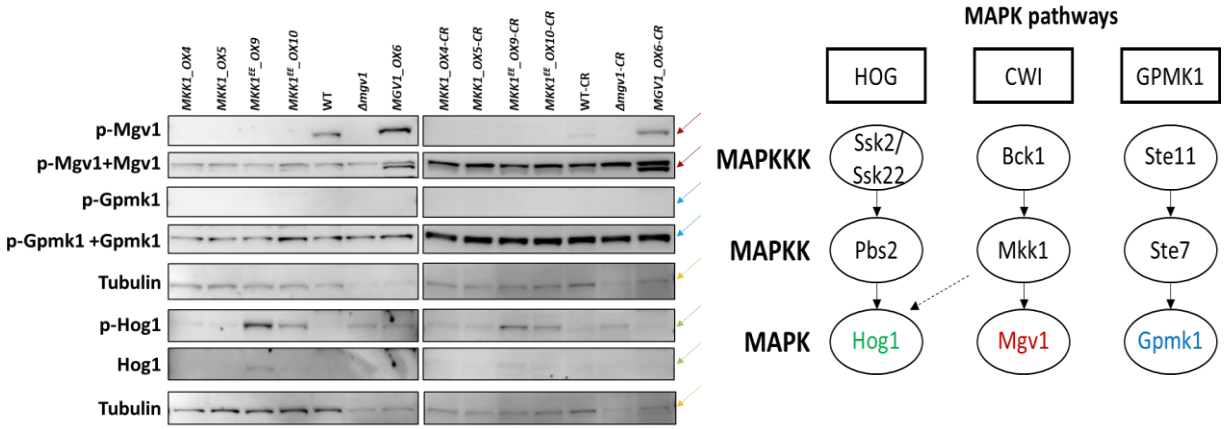

Figure 3.14. (a) Western blot of samples grown in PDB with or without 45 min CR (100 µg mL^{-1}) treatments, and an schematic representation of the three MAPK pathways. The antibody anti-phospho-ERK1/2 (9101S) from Cell Signal recognizes p-Mgv1 and p-Gpmk1. The antibody anti-M5670 from Sigma, recognizes phosphorylated and unphosphorylated forms of ERK1/2-like proteins, such as Mgv1 and Gpmk1. Mgv1 size is estimated as 46.9 kDa in the WT, and about 47.8 kDa in *MGV1_OX6* due to the N-6xHis-tag, while Gpmk1 is around 41.2 kDa. The antibody anti-phospho-P38 recognizes only the phosphorylated form of P38 (p-Hog1) while anti-P38 only recognizes the unphosphorylated P38 (Hog1) of approximately 41.1 kDa. **(b)** Schematization of the three MAPK pathways, with the red, green and blue colours matching the arrows in the panel **(a)** with the MAPK of each cascade.

3.4 Discussion

Protein kinases have evolved to be dynamic switches (Taylor *et al*., 2021) that transduce signals in the cell after they become phosphorylated by a kinase or dephosphorylated by a phosphatase. Through phosphorylation in Ser, Thr or Tyr residues localized in the domain known as the activation loop, kinases undergo a conformational change that will make the protein active or inactive. Once they become active, they will transfer a phosphate group to another protein (substrate) while the target is bound in the kinase catalytic loop.

To identify whether the phosphorylation of a particular Ser, Thr or Tyr residue plays a significant role in the activity of a protein, a phosphomimetic approach could be used (Fujikawa *et al*., 2009; Guerra-Castellano *et al*., 2016; Lai and Pelech, 2016; Somale *et al*., 2020; Yin *et al*., 2020). This is performed by the substitution of an amino acid that can be phosphorylated, by another amino acid that possesses a similar structure to the one substituted in its phosphorylated form. Therefore, Glu and Asp are often used to mimic the structure of the phosphorylated Ser, Thr or Tyr (Fujikawa *et al*., 2009; Lai and Pelech, 2016; Yin *et al*., 2020). However, this approach will not always be successful since the interaction of the new amino acid with its surroundings might not have the same impact in the conformational structure as different bonds will be established, and therefore the activity of the protein might be compromised (Somale *et al*., 2020).

In this work, mutants overexpressing a putative MAPKK phosphomimic (*MKK1*^{197E,203E}*_OX*) were generated. Thus, the effect of the constitutive activation of Mkk1 could be studied. Mkk1 is considered the MAPKK in the CWI pathway (Yun *et al*., 2014), and it was expected that its downstream components, such as Mgv1, were phosphorylated after the modification in the activation loop. As a control for the gene overexpression, *MKK1_OX*

transformants were also generated. Unexpectedly, no phosphorylation was observed in Mgv1 when *MKK1* or *MKK1*^{197E,203E} were overexpressed, even when an activator of the CWI pathway, namely CR, was used. Interestingly, an increase in the amount and phosphorylation of Hog1 was detected.

Even though constitutive overexpression of *MKK1* does not mean that the Mkk1 or the CWI pathway is active, a change in this protein abundance can affect different processes in the cell. In this work, it was observed that the overexpression of *MKK1* or *MKK1*^{197E,203E} strongly affected processes previously associated with the CWI pathway (i.e. mycelial growth and virulence), and the effect was similar to that provoked by the deletion of *MGV1* or *MKK1* genes (Hou *et al*., 2002; Yun *et al*., 2014). The reduced ability to cause disease in wheat heads was observed even though the production of 15-ADON (a precursor of the virulence factor DON) in axenic cultures was not affected in any of the *MKK1*^{197E,203E}*_OX* or *MKK1_OX* strains. In fact, in culture media these strains produced equal or higher quantities of 15-ADON, respectively, compared to the WT (Figure 3.9).

The detection of 15-ADON in axenic cultures is an approach frequently used to determine the ability of a strain to produce DON (Rampitsch *et al*., 2011), since 15-ADON is deacetylated *in planta* (McCormick, 2009). Therefore, considering the role of DON as a virulence factor (Proctor *et al*., 1995a; Harris *et al*., 1999; Ilgen *et al*., 2008), one might expect to find a higher virulence in those strains with higher 15-ADON production values, which was not the case in this study, and in fact, was the opposite. However, DON is not the only factor that can affect virulence, and other elements, such as the retarded mycelial growth observed in the *MKK1_OX* and *MKK1*^{197E,203E}*_OX* strains (Figure 3.13), might interfere with their ability to cause disease. As less mycelia are produced, less DON is present in wheat heads. In addition, as a result of the

slow growth (observed on solid media), the host will have a longer period to induce its defenses against these mutants than if the infection was caused by the WT strain, which could lead to the observed difference among the strains regarding diseased spikelets. Moreover, it is necessary to clarify that the 15-ADON accumulation assays were performed under DON-inducing conditions and it was not estimated from the plant *per se*. Nevertheless, it was important to know that the strains have the ability to produce similar (*MKK1*^{197E,203E}*_OX*) or more (*MKK1_OX*) amount of 15-ADON than the WT (Figure 3.9).

The results observed in this thesis showed that the DON biosynthetic pathway is not truncated or affected even though *TRI5* and *TRI6* genes were downregulated (Figure 3.10) when the mutants were grown in PDB. However, the expression of *TRI5* and *TRI6* might be different under DON-inducing conditions, when trichothecenes are usually produced. *TRI5* is a gene that encodes for the enzyme trichodiene synthase, the first step in DON biosynthetic pathway, and its frequently used as a marker for estimating the effect of a mutation in the trichothecenes biosynthetic pathway (Proctor *et al*., 1995a; Harris *et al*., 1999; Desjardins *et al*., 2000; Kumaraswamy *et al*., 2012). *TRI6* is a transcription factor that plays a significant role regulating *TRI* gene expression and therefore it is also frequently analysed when studying the role of genes in trichothecene production; however, it has also been found to regulate other processes in the cell and it is now considered a global transcription regulator (Proctor *et al*., 1995b; Seong *et al*., 2009; Nasmith *et al*., 2011; Subramaniam *et al*., 2015; Cong *et al*., 2016).

Interestingly, genes associated with other secondary metabolite biosynthetic pathways, such as aurofusarin, a pigment in *F. graminearum*, were downregulated in *MKK1_OX* but not in the putative phosphomimic. *PKS12*, a polyketide synthase, is a regulator of the aurofusarin genes, while *GIP1*, a putative laccase, is also associated with the pathway (Kim *et al*., 2005a; Frandsen

et al., 2006). It has been previously shown that genes associated with the pathway, such as *AURF*, *AURJ* and *AUR0* were downregulated when *MKK1* was deleted (Yun *et al*., 2014). Recently, the significance of this compound moved beyond to the study of its presence in the fungus, and it has been studied as a natural source of pigment for an increasing demanding industry of naturally-produced colorants (Westphal *et al*., 2018a).

Other genes that have been previously associated with the CWI pathway are the *CHITIN SYNTHASES* (*CHS*), which are involved in the synthesis of the cell wall (Jung and Levin, 1999; Levin, 2011). *CHS* is a gene family in which the number of members vary significantly among the Fungi kingdom: while in yeast there are one to three *CHS* genes that have been identified, in filamentous fungi there are around seven classes (Liu *et al*., 2017). Their evolution is correlated to fungal morphogenesis process, and they have been involved in the fungal adaptation to ecological niches (Liu *et al*., 2017) In *M. oryzae*, *CHS5* and *CHS6* are more similar to each other than the other *CHS* genes, and they seem to play a significant role in vegetative growth and during the infection of rice leaves, since they were highly expressed compared to the other *CHS* genes (Kong *et al*., 2012). In PDB media, the *F. graminearum* transcript levels of *CHS5* and *CHS6* were lower compared to the WT, and again, *MKK1*^{197E,203E}*_OX*, was the most affected (Figure 3.11). Similar results were observed in *F. graminearum* and in *B. cinerea* when *MKK1* was deleted (Yun *et al*., 2014; Yin *et al*., 2018b). These results suggest that the overexpression of *MKK1* or its putative phosphomimic may cause a similar negative effect in *CHS* expression as the deletion of *MKK1*.

The putative phosphomimic (*MKK1*^{197E,203E}*_OX*) was predicted to increase the phosphorylation of Mgv1, and therefore the activation of the CWI pathway with its corresponded downstream targets (included the *CHS* genes). However, this modification did not show the

expected results in the cascade. Apparently, the CWI pathway was truncated in the *MKK1_OX* and *MKK1*^{197E,203E}*_OX* strains, since reduced phosphorylation in Mgv1 and lower resistance to CR, compared to WT, were observed. These results were unexpected due to the significant role of Mkk1 in the CWI pathway in resistance to cell wall stressors (Yun *et al*., 2014; Yin *et al*., 2018b).

Several possible explanations as to why Mgv1 showed reduced or no phosphorylation in the *MKK1_OX* and *MKK1*^{197E,203E}*_OX* strains compared to the WT, or why the unexpected phenotypes observed in these strains were stronger in *MKK1*^{197E,203E}*_OX* compared with *MKK1_OX* are described below. Briefly, these are (1) the presence of the N-terminal His-tag on *MKK1* and *MKK1*^{197E,203E} in the expression strains may interfere with the protein's function; (2) increasing the ratio of Mkk1:Mgv1 may result in hyperphosphorylation of Mgv1 that is then silenced by the fungus as a regulatory mechanism; (3) the putative activation loop in *MKK1*^{197E,203E} was incorrectly assigned; (4) the substitutions T197E and T203E would be better suited as an T197D and T203D; (5) the overexpression of *MKK1*^{197E,203E} could negatively affect a pathway associated with nutrient intake, as the strains did not growth well on PDA.

The simplest possibility listed explaining the lack of phosphorylation of Mgv1 in *MKK1_OX* or *MKK1*^{197E,203E}*_OX*, is that the addition of the N-His-tag compromised Mkk1 activity. While a 6-His addition is a small change at the N-terminus and is less likely to interfere with activity, it is not impossible that these changes could affect the tertiary structure and interfere with domains that regulate the activity of the MAPKK, such as the catalytic loop, or the ATP binding motif. In any case, this would not explain the differences in phenotype and in protein activity observed between the two sets of strains.

The second explanation offered here proposes that the overexpression of *MKK1* might trigger the silencing of the pathway as a mechanism to prevent a possible over-phosphorylation of its downstream targets. It has been suggested that hyperphosphorylation of proteins can change the equilibrium of certain processes in the cell, and therefore it is detected as a problem that should be quickly removed (Lai and Pelech, 2016). In particular, it has been observed that the phosphorylation of certain amino acids in the human ERK1, in flanking sites (Thr207 and Tyr210) to the well-known Thr202 and Tyr204 phosphosites, negatively regulates the phosphotransferase activity of this protein. The human ERK1 contains a Thr207 residue that is autophosphorylated while the Tyr210 is phosphorylated by MEK1 (upstream MAPK component in the pathway). Apparently, those flanking phosphosites will slowly start its phosphorylation after ERK1 is activated by MEK1, and this flanking phosphorylation might trigger the inhibition of the ERK1 kinase activity. Lai and Pelech (2016) suggested that hyperphosphorylated forms of kinases might have higher rates of degradation or dephosphorylation *in vivo,* as a regulatory mechanism. Since I did not detect phosphorylation of Mgv1 in the *MKK1_OX* or *MKK1*^{197E,203E}_OX transformants, it could be considered that this pathway was silenced in order to prevent hyperphosphorylation. Nevertheless, this alone would not explain the differences in phenotype observed between the *MKK1_OX* and *MKK1*^{197E,203E}_OX strains.

The third explanation assumes that the modified residues in *MKK1*^{197E,203E}*_OX* are not the correct phosphosite in the activation loop. In this scenario, an argument could be made that it would not have caused significant phenotypic change in the mutants if it is not the activation loop; however, kinases posses several regulatory domains that are key for a proper activity, including negative regulation by phosphorylation (Khan et al., 2013). Additionally, point mutations at some amino acids not involved in activity may cause structural changes resulting in

interference with protein-protein interaction or activity. In any case, we have good reason to believe that the activation domain was correctly assigned. If we dissect the sequences found between the DFG and APE domains, where the activation loop is found within proteins kinases, there are five Ser or Thr residues present (Figure 3.2), and among these there is one Thr-X_5-Thr and one Thr-X_3-Thr sequence (Figure 3.2 and Supplementary Figure 3.1). While in principle, we might select either of these two sequences as the activation loop, the Thr-X_5-Thr seemed the more likely based on alignment with MKK1 homologues in other species. Furthermore, the Thr-X_3-Thr region aligns with the Shaggy-like domain described in (Khan *et al*., 2013). In their work, Khan *et al*. (2013) investigated the interaction of *Arabidopsis thaliana* Bin2 (brassinosteroid-insensitive 2), a homolog of Gsk3 (Glycogen kinase synthase 3)/Shaggy-like kinase, with the MAPKK's, Mkk4 and Mkk5. Phosphorylation of Mkk4 by Bin2 strongly reduced Mkk4 activity towards its substrate, Mpk6. Two important phosphosites were identified, namely Ser230 and Thr234, that formed a classical Gsk3 phosphorylation domain: (Ser/Thr)-XXX-(Ser/Thr). It was suggested that Thr234 played a more significant role than the other residue since it is a highly conserved amino acid in MAPKKs, its phosphorylation by Bin2 made Mkk4 inactive, and its substitution completely abolished Mkk4 phosphorylation by Bin2. It should be noted that Ser230 is the second phosphosite in the Mkk4 activation loop: TMDPCNSSVGT, where the key residues of the activation loop are highlighted and those of the Gsk3 phosphorylation domain are underlined. The authors suggested that the phosphorylation of Thr234 by Bin2 may hinder the phosphorylation site of the activation loop that should be phosphorylated by YDA (the MAPKKK in the cascade YDA-MKK4/5-MPK3/6). Since the sequence from *F. graminearum* MKK1 chosen for this thesis is TKGEANTFIGTSYYMAPE, where the substitutions were made to the highlighted Thr residues, it is possible that underlined Thr and the second highlighted Thr

could form a Shaggy-like domain which would inhibit MKK1 activation. Thus, while I am confident in the selection of Thr197 and Thr203 as the activation loop residues, further studies to test other potential phosphosites might prove otherwise.

Another consideration regarding to the strong phenotype associated with *MKK1*^{197E,203E}*_OX*, could be related to the choice of substitution within the proposed activation loop (TKGEANT), where a Thr-Asp substitution might be more suitable for a phosphomimetic. There is a chance that the Thr-Glu substitution that was made in the Mkk1 activation loop resulted in the silencing of the CWI cascade, as it could affected the establishment of bonds with the right amino acids in the same protein or with other Mkk1 interacting partners. I selected the Thr-Glu substitution since this is considered to be more conservative change based on the side chain structures (Dissmeyer and Schnittger, 2011; Levy et al., 2019). However, these substitutions do not always work because, for example, the introduction of a negative charge might have a different impact in the protein behaviour, since it does not match the charge in the Ser or Thr amino acids when they are phosphorylated, as discussed by Dephoure et al. (2013). According to Somale *et al*. (2020), the substitution of the Ser or Thr residues in the hydrophobic loop of RSK (p90 ribosomal S6 kinase) with Asp or Glu leads to a constitutive activation of the protein, whereas phosphomimetics in the activation loop failed to form the necessary bonds to reorient the α C-helix and therefore failed to activate the protein. The authors made this observation in RSK, a kinase of the AGC protein kinase family that is regulated by two phosphorylation events that occur in the activation loop and in the hydrophobic motif. Although the activation of the MAPKs is different to RSK, since MAPKs become active after they are phosphorylated in the activation loop, the results of Somale *et al*. (2020) open a question about the efficiency of phosphomimetic studies, and how this approach will not always be effective or suitable. However, in

Magnaporthe grisea, which has an activation loop that aligns with the Mkk1 used in our studies (Supplementary Figure 3.1), a Mkk1 phosphomimic was successful generated by the substitution of the Thr residues in the activation loop to Asp, which led to a constitutive phosphorylation of Mps1, the MAPK in the cascade (Fujikawa *et al*., 2009). Therefore, it might be that Asp would have been a more suitable substitution than Glu in the *F. graminearum* Mkk1, and is perhaps an avenue for future directions of this work .

Finally, after observing that *MKK1*^{197E,203E}*_OX* strains grew very slowly on PDA, a possible lethality caused by this transformation was discussed during the thesis defense. However, when the strains grew on agar supplemented with carrot juice (200 mL of carrot juice *per* L of culture media), the *MKK1*^{197E,203E}*_OX* strains grew faster than on PDA, and reached the edge of the plate in less than two weeks (data not shown). That said, based on preliminary observations, while *MKK1*^{197E,203E}*_OX* strains grow faster on carrot agar than on PDA, it still grows slower than the WT strain. These observations might suggest a nutrient intake problem, as the carrot media could offer different nutrients, including sterols (Decloedt et al., 2017) that might not be present in the semisynthetic PDA medium that was used in most of the experiments. Liu et al. (2019) suggested that the transcription factor SR control sterol production in *F. graminearum*, and it is regulated by Hog1 and possibly by other kinases. Therefore, the near lethal effect observed on PDA media caused by overexpressing *MKK1*^{197E,203E} could be associated with a deficiency in nutrients. As only two colonies were obtained in this transformation (USER cloning) process, it might be considered that these two strains survived as a result of a random mutation which could have occurred during transformation, perhaps in the *MGV1* gene. To determine whether this is the case, PCR amplification and subsequent sequencing of *MGV1* from the *MKK1*^{197E,203E} overexpression strain may provide some insights. Moreover, the sequencing of the whole

MKK1^{197E,203E} genome would provide more in depth information regarding possible mutations in other genes that might explain the strong phenotype observed in these strains.

It has previously been shown that there is crosstalk among the CWI, the GPMK1 and the HOG pathways in *F. graminearum* (Zheng *et al*., 2012; Yun *et al*., 2014). The deletion of any of the core components of the HOG cascade in this pathogen, while in presence of the osmotic stressor agent, NaCl (0.7 M), enhanced the phosphorylation of the Mgv1 and the Gpmk1 MAPKs (Zheng *et al*., 2012). However, when the deleted element was from the CWI pathway, as it happens in the *Δmkk2* mutant, the phosphorylation of Hog1 was reduced in presence of the cell wall stressor CR, which is considered an activator of the CWI pathway (Yun *et al*., 2014). In our results, it was observed that the deletion of *MGV1* increased resistance to 1 M NaCl (Figure 3.13 A and B), and more intense bands corresponding to the phosphorylated and unphosphorylated forms of Hog1, compared to the WT, were also observed (Figure 3.14). These results suggest that when the CWI pathway is truncated by the deletion of the MAPK in the cascade, the HOG cascade might become more active than usual.

In this thesis, it was also observed that the HOG cascade was activated in *MKK1*^{197E,203E}*_OX*, since these strains showed a higher abundance (and phosphorylation) of Hog1, and also grew faster in 1 M NaCl than the WT and the other tested strains (Figure 3.13 A and B). These data support the hypothesis about the cross-talk between the HOG and the CWI pathways (Figure 3.15) that might involve Mkk2 as a key component (Yun *et al*., 2014).

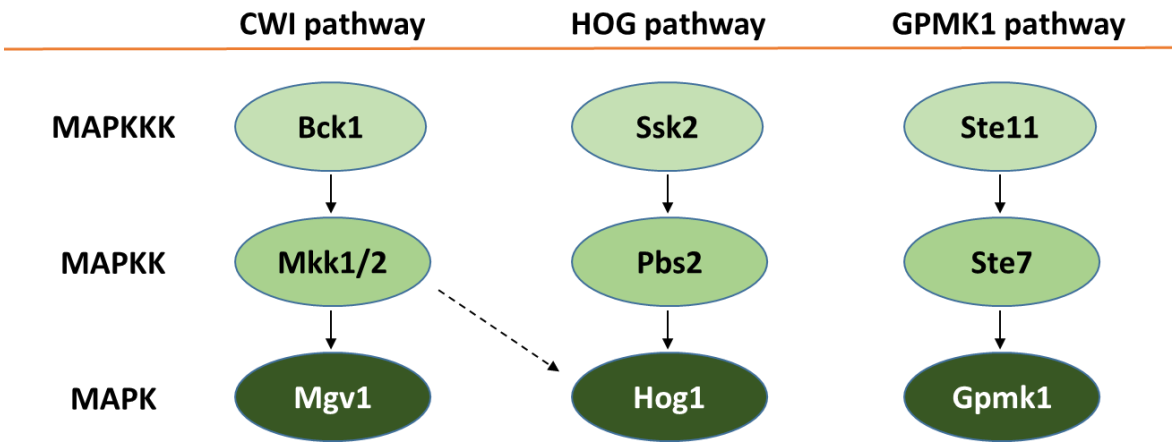

Figure 3.15. The three MAPK pathways (CWI, HOG and GPMK1) in *F. graminearum*. A continuous line points to the known target while the dashed line shows the putative target.

The nature of the HOG and CWI cascade interaction remains unknown, and some hypotheses to explain this interaction will be presented within this discussion. For instance, Mkk1 might posses another regulating domain, in addition to the known activation loop, to regulate other downstream components, as has been recently shown in *M. oryzae* (Yin *et al.*, 2020). In this pathogen, the causal agent of rice blast fungus, the Ser115 plays a significant role in Mkk1 activation, and its substitution for Asp activates the CWI pathway as well as the autophagy mechanism (Yin *et al.*, 2020). This site does not align with FGSG_07295 (*MKK1*) in *F. graminearum* (Supplementary Figure 3.5). Nevertheless, there is a possibility that a similar site also exists in this fungal pathogen, in which case the substitutions in the *MKK1*^{197E,203E}*_OX* activation loop might inactive Mkk1 towards Mgv1, while enabling activation of another phosphosite, perhaps orthologous to Ser115 in *M. oryzae* (Supplementary Figure 3.5), which might have a preference for Hog1. Therefore, one might consider the possibility that the modified phosphosites (in *MKK1*^{197E,203E}*_OX*) affected substrate-specificity, such that Mkk1 preferentially interacted with elements of the HOG pathway. Furthermore, additional components may control

the pathways. For example, Yun *et al*. (2014) proposed a model for the interaction of both cascades through a type 2C protein phosphatase (FgPtc3) or other unknown phosphatases that might negatively regulate both CWI and HOG MAPK cascades.

A simpler explanation of our unexpected results could be that FGSG_07295, previously reported as an element upstream of Mgv1 and Hog1, might be the MAPKK in the HOG pathway, instead of the CWI pathway, even when it can regulate the phosphorylation of the MAPK proteins in both cascades and affect processes associated to the CWI (Yun *et al*., 2014). This would explain the higher phosphorylation levels of Hog1 in *MKK1*^{197E,203E}*_OX* (Figure 3.14), the improved resistance to osmotic stress (1 M NaCl), and the high susceptibility to CR, a cell wall stress agent (Figure 3.13). However, the alignment and phylogenetic tree (Supplementary Figures 3.1 and 3.2) of other Mkk1 sequences showed that FGSG_07295 is closer to Mkk1 than Pbs2 (MAPKK in HOG pathway) or Ste7 (MAPKK in Gpmk1 pathway).

Last, but not least, as Hog1 is a different MAPK type (p38, while Mgv1 is ERK-like) it might not be phosphorylated by Mkk1, and the similarities observed between the *MKK1*^{EE}*_OX* and the *Δmgv1* strains could be a result of some compensatory role in response to the lack of Mgv1 phosphorylation. Nevertheless, further studies will be necessary for a better understanding of the MAPK pathways and their crosstalk in *F. graminearum*.

In conclusion, the overexpression of *MKK1* negatively affected mycelial growth on solid media, and virulence; however it did not affect 15-ADON production in axenic cultures. In addition, the CWI pathway was compromised, since Mgv1 showed less phosphorylation than the WT, and in presence of a cell wall stressor, such as CR, the percentage of mycelial growth inhibition was higher than in the control. Moreover, the substitution of two Thr residues with Glu in the Mkk1 putative activation loop, used as a path to generate a phosphomimic, did not increase

the phosphorylation of Mgv1, previously identified as Mkk1 downstream target; however, it did increase the abundance and phosphorylation of Hog1, the MAPK in the HOG pathway. Based on these results, we could hypothesize that *i)* MKK1 (FGSG_07295) is not the upstream element in the CWI cascade in *F. graminearum* but it is the MAPKK in the HOG pathway; *ii)* there is more than one phosphosite in Mkk1 that can activate this MAPK to target Mgv1 or Hog1; *iii)* if the phosphosites in the T-X_5-T activation loop in Mkk1 are changed to E, the protein will not be able to phosphorylate Mgv1 but it will instead increase the abundance and phosphorylation of Hog1. The results presented support previous research that showed the cross-talk between the CWI and the HOG cascades, while at the same time open new questions regarding the role of Mkk1 (and its activation loop) as a significant element in the interaction of both MAPK modules.

Chapter 4. Transcriptomic profile of *MKK1_OX* and *MKK1^{197E,203E}_OX* strains

4.1 Introduction

MAPK pathways are signalling cascades in eukaryotes that regulate the response of the cell upon particular stress or during a developmental process. Once the receptors detect a stimulus, the signal is transduced through several components, including a set of three proteins (MAPKKKs, MAPKKs and MAPKs) that are phosphorylated in a sequential manner. As result, several elements are activated, and a response to the signal received is on its way.

Three MAPK cascades are present in *F. graminearum*, one of the causal agents of FHB disease in cereal crops: the cell wall integrity (CWI) pathway, the high osmolarity glycerol (HOG) pathway and the *Gibberella* pathogenicity MAPK 1 (Gpmk1) pathway. The CWI pathway is composed of a MAPKKK (Bck1), a MAPKK (Mkk1) and a MAPK (Mgv1), and it is mainly activated for cell wall formation and maintenance upon an environmental stress is detected, or as part of a developmental process.

The MAPK Mgv1 interacts with Rlm1, a transcription factor that regulates the expression of genes that are mostly associated with cell wall formation, such as *CHITINASES* and *GLUCANASES,* but also with secondary metabolites such as aurofusarin (Yun *et al*., 2014). In addition, Mgv1 appears to be involved in the regulation of secondary metabolites, such as trichothecenes and butenolide (Hou *et al*., 2002; Rampitsch *et al*., 2011; Shostak, 2020), and it has been hypothesized that this regulation is carried out through the transcription factor *TRI6* (Shostak, 2020).

The MAPKK *MKK1* plays a significant role in the CWI cascade, and it regulates the expression of several genes in the cell after particular stress conditions, such as heat or cell wall stressing agents are detected (Irie *et al*., 1993; Yun *et al*., 2014; Yin *et al*., 2018b). Mkk1 is

involved not just in the CWI, but also in the HOG cascade, a hypothesis established after less phosphorylation was reported in Hog1 (the MAPK in the HOG pathway) in a *Δmkk1* mutant compared to a WT strain (Yun *et al*., 2014). In addition, this MAPKK is involved in the regulation of the pigment aurofusarin, and the deletion of *MKK1* resulted in reduced colony pigmentation and downregulation of some of its biosynthetic gene cluster (Yun *et al*., 2014). According to Shostak (2020) and to the 2nd Chapter of this thesis, Mgv1 is thought to regulate the expression of some secondary metabolite gene clusters, primarily through *TRI6*; however, other components of the CWI pathway, such as Mkk1, might be involved as well.

In the previous chapter, the overexpression of *MKK1*^{197E,203E}*_OX*, a putative Mkk1 phosphomimic, was generated to understand the effect of continuous Mgv1 phosphorylation in *F. graminearum*. As a control, a transformant overexpressing *MKK1* was included in the analysis to differentiate which changes might be due to the modifications of two amino acids in the Mkk1 activation loop, and which to the overexpression of the MAPKK. Contrary to what was expected, there was less phosphorylation of Mgv1 in the mutants than in the WT, and variations in morphology, physiology (wheat infection and 15-ADON production) and biochemistry were observed, which raises the question about which genes might be regulated by Mkk1.

The objective of this chapter is to study the transcriptomic profile of *MKK1*^{197E,203E}*_OX* and *MKK1_OX* to understand the impact of this MAPKK on the CWI cascade among other cellular pathways with an emphasis on secondary metabolites.

4.2 Materials and methods

4.2.1 *F. graminearum* strains, growth conditions and spore production

F. graminearum strains used in this chapter are: the WT (GZ3639), the mutants/transformants generated in the previous chapters (*MGV1_OXs*, *MKK1_OXs* and *MKK1*^{197E,203E}*_OXs*), and the *Δmgv1* mutant (received from Dr. Rajagopal Subramaniam from AAFC-Ottawa, and previously generated by Rampitsch *et al*. (2011)). Growth conditions and spore production were performed as described in Chapter 2 (section 2.2.1).

Twenty millilitres of potato dextrose broth (PDB) in 50-mL conical tubes were inoculated with 2 x 10^4 spores of *MKK1_OX*, *MKK1*^{197E,203E}*_OX* transformants or WT, and incubated with gentle agitation (180 rpm) for 40 h at 27°C. Mycelium was collected from a pool of eight 50 mL-Falcon tubes for each strain in autoclaved paper towel (described in section 2.1) and the filtride (mycelium) was washed with 100 mL of autoclaved Nano pure water. The mycelium was gently dried with autoclaved lab towel (Wypall*60, 35401-02), wrapped with aluminium foil, and quickly frozen in liquid nitrogen. The samples were stored at -80°C until the tissue was ground for total RNA extraction. The experiment was replicated three times.

4.2.2 RNA extraction and sequencing

Total RNA was extracted using the RNeasy® Plant Mini Kit (QIAGEN,74904), with an on-column DNase digest using RNase-free DNase I (QIAGEN, 79254). RNA concentration and purity were measured using Qubit® RNA BR assay kit (ThermoFisher, Q10210) and Agilent RNA 6000 Nano Kit with the Agilent 2100 Bioanalyzer, respectively. RNA (3.3 µg) was further treated with DNase I, RNase-free (ThermoFisher, EN0521) to eliminate residual DNA contamination. A PCR was performed using the cleaned RNA as a template, to verify the absence of contaminating DNA. RNA quality was observed by agarose gel electrophoresis prior to

sending the samples for RNA-sequencing through Genome Québec using Illumina NovaSeq 6000 S4 PE150 - 70M reads.

4.2.3 RNA-seq and differential expression analyses

RNA-Seq analysis was performed with the nf-core/rnaseq worfklow v1.4.2 (https://doi.org/10.5281/zenodo.3503887), using Nextflow v20.01.0. Briefly, raw reads were trimmed with cutadapt and Trim Galore v0.6.4. The trimmed reads were aligned to *F. graminearum* PH-1, assembly ASM24013v3 (NCBI assembly accession number GCF_000240135.3) using the STAR aligner (vSTAR_2.6.1d). Quality of RNA-Seq data was assessed with RSeQC v3.0.1, and Preseq v2.0.3 was used to estimate the complexity of the libraries. Qualimap v.2.2.2-dev was used for calculating read alignment assignment, transcript coverage, read genomic origin, junction analysis and 3'-5' bias. FPKM metrics for genes and transcripts as well as the transcript features were generated with StringTie v2.0. t plots the duplication rate against expression (RPKM) for every gene.

Differential expression analysis was performed in R (version 3.5) with the edgeR package. Fold-changes to achieve a statistical power of 0.8 were calculated with the RNASeqPower package, and the power provided by specific thresholds was also calculated. Data from transformants *MKK1_OX4* and *MKK1_OX5* was combined for the analysis of *MKK1_OXs vs* WT, as well as data from *MKK1*^{197E,203E}*_OX9* and *MKK1*^{197E,203E}*_OX10* was pooled together for comparing *MKK1*^{197E,203E}*_OXs vs* WT. In addition, *MKK1_OXs* was compared to *MKK1*^{197E,203E}*_OXs*.

FungiFun (https://elbe.hki-jena.de/fungifun/) webpage was used for establishing the functional categories (FunCat) for the differentially expressed genes, but using a more restringing condition, as it was similarly established in the Mgv1 analyis performed in Chapter 2: $\log_2$FC ≥

0.99 (upregulation) or $log_2FC \leq 0.99$ (downregulation). A large number of uncharacterized proteins were identified in the FungiFun database and so the annotation was supplement with information available from NCBI, Fusarium comparative genomics platform (FCGP) and UniProtKB databases. Graphs of significantly enriched categories were generated using the FungiFun website, and Venn diagrams were created using the webpage **https://bioinfogp.cnb.csic.es/tools/venny/.**

4.3 Results

4.3.1 Effect of *MKK1* overexpression in *F. graminearum*

The RNA-seq analysis showed that *MKK1* regulates several genes in *F. graminearum*. Pairwise comparison of *MKK1_OX* transformants with the WT showed that a power analysis at a 0.8 cut-off was suitable for analysing the data (Figure 4.1). From the power analysis it was established that genes with a $Log_2FC = 0.55$, which is 1.47 fold-change, and with a False Discovery Rate (FDR) smaller than 0.05 were chosen for the volcano plot and for further analysis.

The volcano map shows which genes were upregulated or downregulated when *MKK1* was overexpressed, and at which level (Figure 4.2). Genes on top of the volcano graph represent those with the lowest p-values, therefore, their difference was highly significant compared to the WT. As expected, FGSG_07295 (*MKK1*) was highly significant and expressed, but there were also two unidentified genes in the same category (green dots in Figure 4.2): FGSG_03518 (conserved hypothetical protein) and FGSG_03586 (hypothetical protein). Most of the differentially expressed genes (DEGs) were associated with "metabolism" and "cell rescue, defense and virulence" main functional categories.

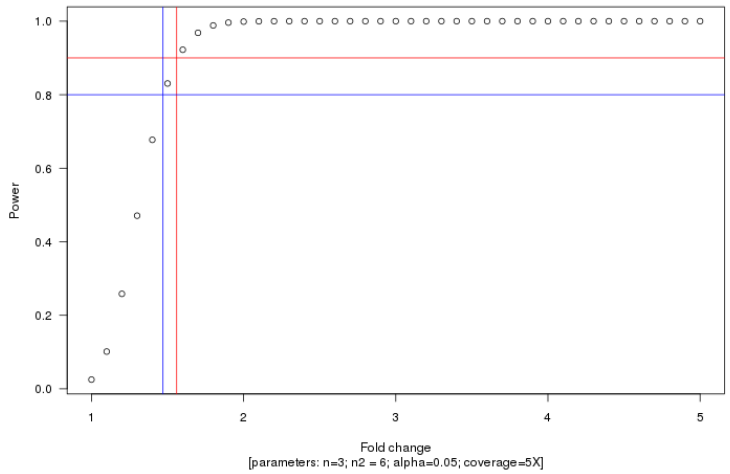

Figure 4.1. Power analysis of the comparison of *MKK1_OX* (a pool of *MKK1_OX*9 and *MKK1_OX10*) *vs* WT.

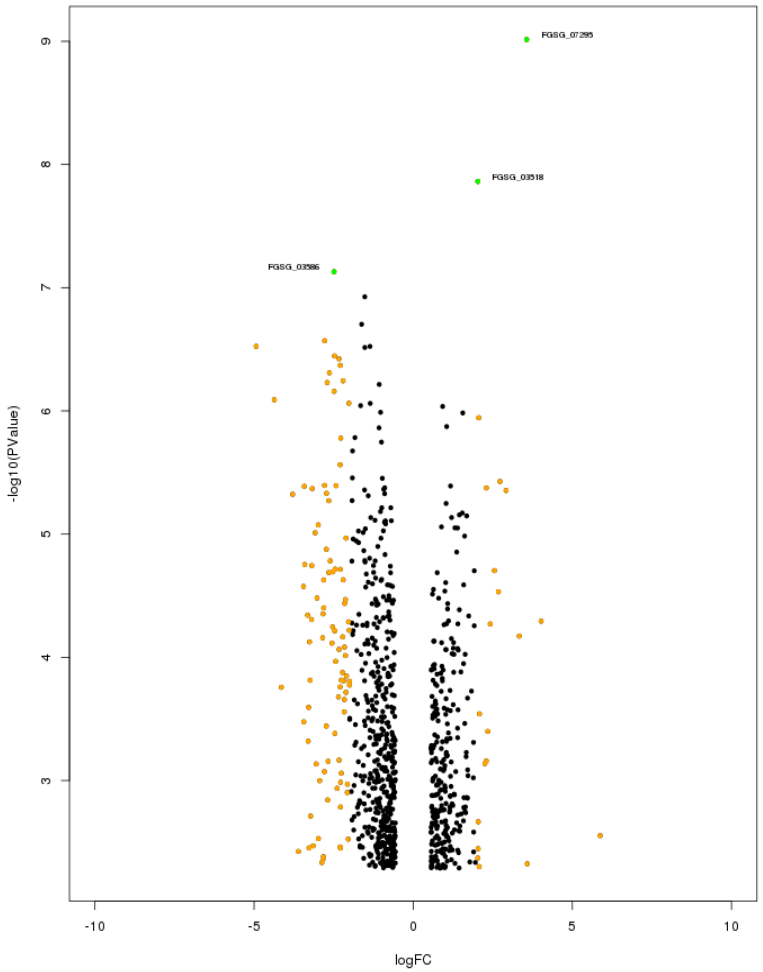

Figure 4.2. Volcano plot showing the negative logarithm of the p-value (Y axis) *vs* Log_2FC (X axis) when comparing *MKK1_OX* transformants (a pool of *MKK1_OX4* and *MKK1_OX5*) *vs* WT. Dots represent genes that were significantly expressed: FDR < 0.05, and $Log_2FC > 0.55$ (1.47 fold-change), which were the parameters established after the power analysis at 0.8 was performed.

Legend:

Dot colour	**Log_2FC**	**–log (P-value)**
Orange	> 2	≤ 8
Black	$0.55 \leq Log_2FC \leq 2$	≤ 8
Red	$0.55 \leq Log_2FC \leq 2$	> 8
Green	> 2	> 8

A total of 838 genes (548 downregulated and 290 upregulated) were annotated as differentially expressed in *MKK1_OX* transformants (Supplementary Table 4.1 shows a list of the top 15 upregulated and top 15 downregulated genes). From those genes, 461 (314 downregulated and 147 upregulated) reached a Log_2FC value lower than -0.99 or higher than 0.99, which is a two-fold change, and were used for FunCat analysis (Supplementary Table 4.2 shows a list of the top 15 upregulated and top 15 downregulated genes). Thirty-four percent (155 genes) of the 461 differentially expressed genes were found annotated in the database used by FungiFun2 for FunCat analysis, but only 71 were significant, according to the overrepresentation analysis (ORA) performed by the software (Figure 4.3A). Genes were distributed in 224 groups, and from those, only five enriched categories or FunCat descriptions were significant: “C-compound and carbohydrate metabolism”, “secondary metabolism”, “polysaccharide metabolism”, “toxins” and “metabolism of alkaloids” (Figures 4.3 B and C, and Table 4.1). Ninety-eight genes were distributed into those five descriptions, and most of them were in the “C-compound and carbohydrate metabolism”, which represented 4.4 % of the total genes (1018) previously annotated in this group (Table 4.1). The category that had the highest percentage of its annotated

genes differentially expressed in *MKK1_OX* transformants was the "metabolism of alkaloids" with 16 %, followed by "toxins", but those only represented 1.5 % and 1.5 % of the 461 DEGs, respectively (Table 4.1).

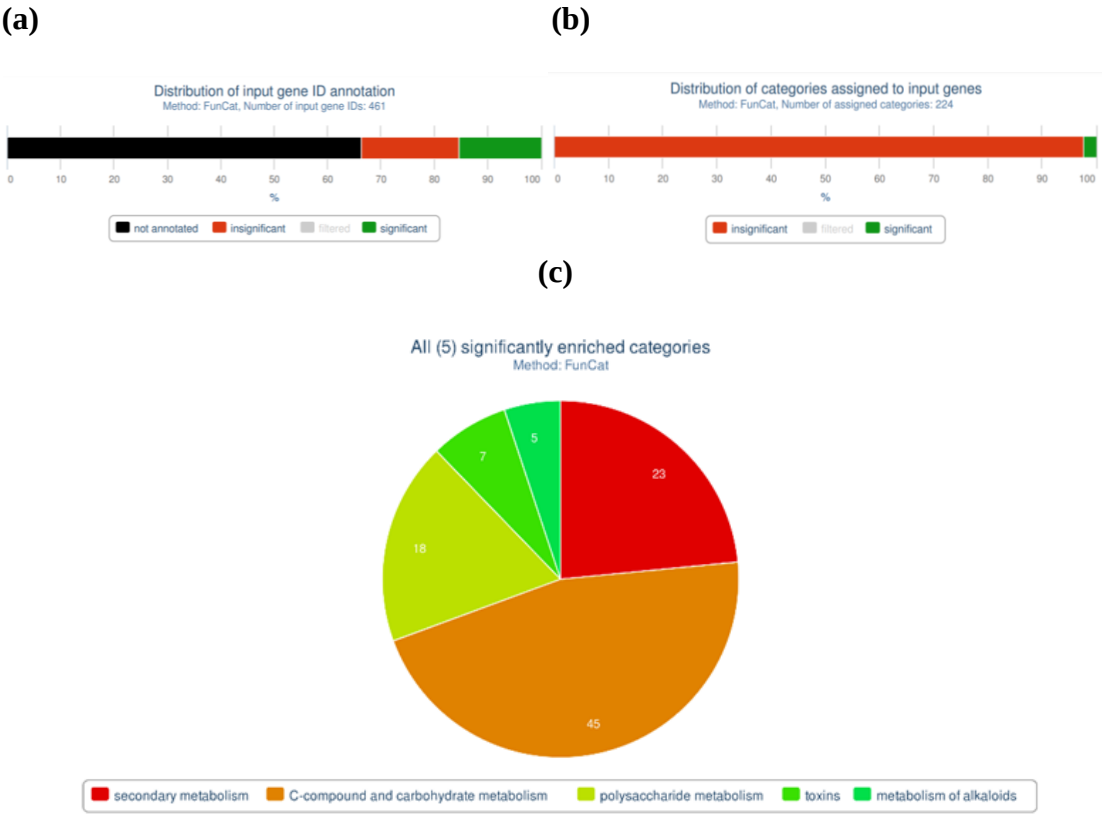

Figure 4.3. (a) Distribution of annotated genes from the 461 that were differentially expressed. **(b)** Distribution of categories associated with 461 genes that were differentially expressed in *MKK1_OX*. **(c)** Pie chart of the five significantly enriched categories.

Table 4.1. Genes that were differentially expressed in *MKK1_OX* transformants are classified into two main categories. FunCat analysis shows how many of the 461 DEGs belong to each category (# genes / input) and how many genes are per category. The green colours represent the higher values in the column, and the gradient changes until red tones, which represent the lowest values.

FunCat ID	FunCat description	FunCat main category	# genes/ category	% genes/ category	# genes/ input	% genes/ input
1.2	secondary metabolism	Metabolism	23 / 284	8.1	23 / 461	5.0
1.05	C-compound and carbohydrate metabolism	Metabolism	45 / 1018	4.4	45 / 461	9.8
01.05.03	polysaccharide metabolism	Metabolism	18 / 280	6.4	18 / 461	3.9
32.05.05.01	toxins	Cell rescue, defense and virulence	7 / 62	11.3	7 / 461	1.5
01.20.17.09	metabolism of alkaloids	Metabolism	5 / 31	16.1	5 / 461	1.1

In the main category “Cell rescue, defense and virulence” the “toxins” description comprised genes from different toxin pathways that were downregulated. Two genes were associated with the aurofusarin metabolite (FGSG_02324 and FGSG_02326), while two others belonged to the cytochrome P450 family (FGSG 02367 and FGSG_03542). The gene FGSG_03542 is also known as *TRI13*, and it is part of the trichothecene gene cluster (Sieber *et al*., 2014; Shostak, 2020). Genes FGSG_04694 and FGSG_08795 are described as hypothetical proteins similar to *PKS*, known as *PKS1* and *PKS7*, respectively (Sieber *et al*., 2014), while FGSG_10990 encodes for the octapeptide fusaoctaxin A (Westphal *et al*., 2019), also known as *NRPS9* (Sieber *et al*., 2014). An overview of the expression of some secondary metabolite gene cluster is showed in Supplementary Table 4.3.

FGSG_02324 is a non-reducing polyketide synthase known as *PKS12* that belongs to the PKS26 class (Connolly *et al*., 2013), therefore it is referred as *PKS12* or *PKS26* (https://www.uniprot.org/uniprot/I1RF58) (Sieber *et al*., 2014; Shostak, 2020). However, *PKS12* has also been assigned to FG_12040 where it was described as part of the aurofusarin cluster (Frandsen *et al*., 2006). In any case, the PKS in the aurofusarin pathway condenses one acetyl-CoA and six malonyl-CoA to form the cyclic heptaketide YWA1. This compound (that is later converted into nor-rubrofusarin by the dehydratase AurZ) is a yellow pigment and is considered the first intermediate in the aurofusarin biosynthetic pathway (Frandsen *et al*., 2011).

Another gene in the aurofusarin cluster that was highly downregulated was *AURJ*, an O-methyltransferase that converts nor-rubrofusarin into rubrofusarin. Surprisingly, the FunCat analysis did not include any other genes involved in the aurofusarin biosynthetic cluster; however, *AURF*, *GIP1* and *AURS* were also highly downregulated. These genes form part of an extracellular enzymatic complex involved in the conversion of rubrofusarin into aurofusarin, after

rubrofusarin in pumped out of the cell by AurT (Frandsen *et al*., 2011). Therefore, the biosynthesis of aurofusarin seemed to be negatively affected by *MKK1* overexpression (Supplementary Table 4.3 A).

The butenolide cluster contains eight genes, from which three (FGSG_08079, FGSG_08081 and FGSG_08083) were upregulated in *MKK1_OX* transformants (Supplementary Table 4.3 B). The gene FGSG_08081 is in the "secondary metabolism" description, while FGSG_08083 is in "C-compound and carbohydrate metabolism" both from the "Metabolism" main category. FGSG_08079 is also upregulated, but it did not make the list in the FunCat analysis. These results suggest that *MKK1* might positively regulates the biosynthesis of butenolide.

In the "polysaccharide metabolism" description, at least eight genes encoding proteins with a glycosyl hydrolase domain were differentially expressed. One of them is an exo-1,4-*β*-D-glucosaminidase (FGSG_02314), a secreted protein involved in the hydrolysis of chitosan or its oligosaccharides that was upregulated. Three genes had chitin-binding or chitin deacetylase domains, one with similarities to class V chitinase (FGSG_02354) was also upregulated, while the other two were downregulated. Two genes associated with the CWI pathway were downregulated: FGSG_11097 (has a WSC domain) and FGSG_09980 (Supplementary Table 4.4). FGSG_09980 is the 1,3-β-glucanosyltransferase gel1 precursor, involved in the cell wall glucan formation. This gene was included in the description "polysaccharide metabolism", but also in the "C-compound and carbohydrate metabolism".

When *MKK1* was overexpressed, 548 genes were downregulated with log_2FC values ranging from -0.556 to -4.934. After a new cut-off at a $Log_2FC = -0.99$, 314 genes with smaller values were selected for FunCat analysis. Seventeen percent of the 314 genes were significant, according to the ORA (over-representation analysis) performed by the software, even though 33

% of the total genes (314) were already annotated (Figure 4.4 A). The downregulated genes were distributed among 172 categories (Figure 4.4 B), but only four categories were significant: "secondary metabolism", "polysaccharide metabolism", "toxins" and "C-compound and carbohydrate metabolism" (Figure 4.4 C). The category most represented was "C-compound and carbohydrate metabolism" with 10 % of the total genes, but only 3.1 % of the total amount of genes (1018) involved in that FunCat description (Table 4.2). The category that had the highest percentage of its annotated genes was "toxins" with 11.3 %, which represented 2.2 % of all downregulated genes. This category was also represented when all DEGs in *MKK1_OX* transformants were analyzed (Table 4.1), and all those identified genes were also downregulated.

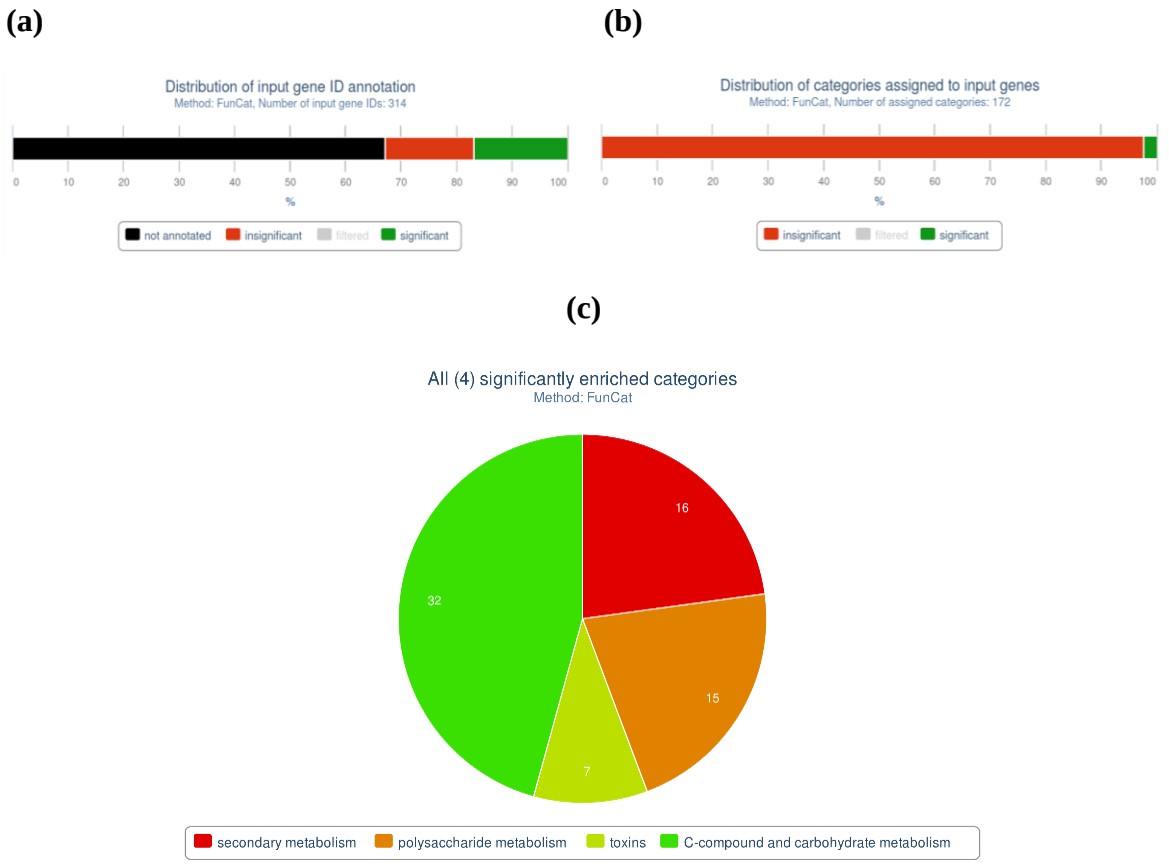

Figure 4.4. (a) Distribution of annotated genes from the 314 that were downregulated. **(b)** Distribution of categories associated with 314 genes that were downregulated when *MKK1* was overexpressed. **(c)** Pie chart of the four significantly enriched categories.

Table 3.2. Genes that were downregulated when *MKK1* was overexpressed are classified into four FunCat descriptions. FunCat analysis shows how many of the 314 downregulated genes belong to each four categories (# genes / input) and how many genes are per category. The green colours represent the higher values in the column, and the gradient changes until red tones, which represent the lowest values.

FunCat ID	FunCat description	FunCat main category	# genes/ category	% genes/ category	# genes/ input	% genes/ input
1.2	secondary metabolism	Metabolism	16 / 284	5.6	16 / 314	5.1
01.05.03	polysaccharide metabolism	Metabolism	15 / 280	5.4	15 / 314	4.8
32.05.05.01	toxins	Cell rescue, defense and virulence	7 / 62	11.3	7 / 314	2.2
1.05	C-compound and carbohydrate metabolism	Metabolism	32 / 1018	3.1	32 / 314	10.2

Among the genes that were differentially expressed, 290 were upregulated with Log_2FC values that varied from 0.5565 to 5.875. A new cut-off at $Log_2FC > 0.99$ allowed a selection of 147 of those genes for FunCat analysis. From those 147 genes, 52 were annotated (35 %), and only five genes were significant (Figure 4.5 A). The "pyridoxal phosphate binding" category was the only one significant from 123 enriched categories (Figure 4.5 B) and had five genes annotated in it, representing 3.4 % of total genes upregulated, and 8 % of total genes identified in the database that corresponds to this group (Table 4.3). Among these five genes, there is FGSG_03888, which has the highest Log_2FC value (5.875) in the analysis (Supplementary Tables 4.1 and 4.2).

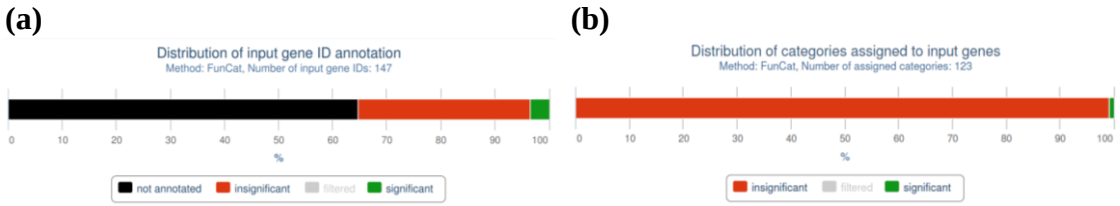

Figure 4.5. (a) Distribution of annotated genes from the 147 that were upregulated. **(b)** Distribution of categories associated with 147 genes that were upregulated when *MKK1* was overexpressed.

Table 4.3. Genes that were upregulated when *MKK1* was overexpressed are classified into one main category. FunCat analysis shows how many of the 147 upregulated genes belong to each main category.

FunCat ID	FunCat description	FunCat main category	# genes/ category	% genes/ category	# genes/ input	% genes/ input
16.21.17	pyridoxal phosphate binding	Protein with binding function or cofactor requirement (structural or analytic)	5 / 63	7.9	5 / 147	3.4

4.3.2 Effect of the overexpression of the putative phosphomimic *MKK1*^{197E,203E}_in *F. graminearum*

The overexpression of a putative phosphomimic *MKK1* (*MKK1*^{197E,203E}) induced a change in the transcriptomic profile of *F. graminearum*, and there were more DEGs than in the comparison *MKK1_OX vs* WT. A power analysis at a 0.8 cut-off was chosen for the present study. A volcano plot showed that 26 genes had a high significance (green dots), with 6 of them upregulated while 20 were downregulated (Figure 4.6). A total of 2,890 genes were differentially regulated, and from those, 1,700 were downregulated while 1,190 were upregulated (Supplementary Table 4.5 shows a list of the top 15 upregulated and top 15 downregulated genes). After analysing the Log_2FC values in the 2,890 genes, genes with a $Log_2FC < -0.99$ or $Log_2FC > 0.99$ were selected, resulting in 1,192 downregulated and 681 upregulated, respectively, for a total of 1,873 genes (Supplementary Table 4.6 shows a list of the top 15 upregulated and top 15 downregulated genes). Most of the genes were associated with metabolism, cell rescue, defense and virulence functions, similar to what was observed in *MKK1* overexpression.

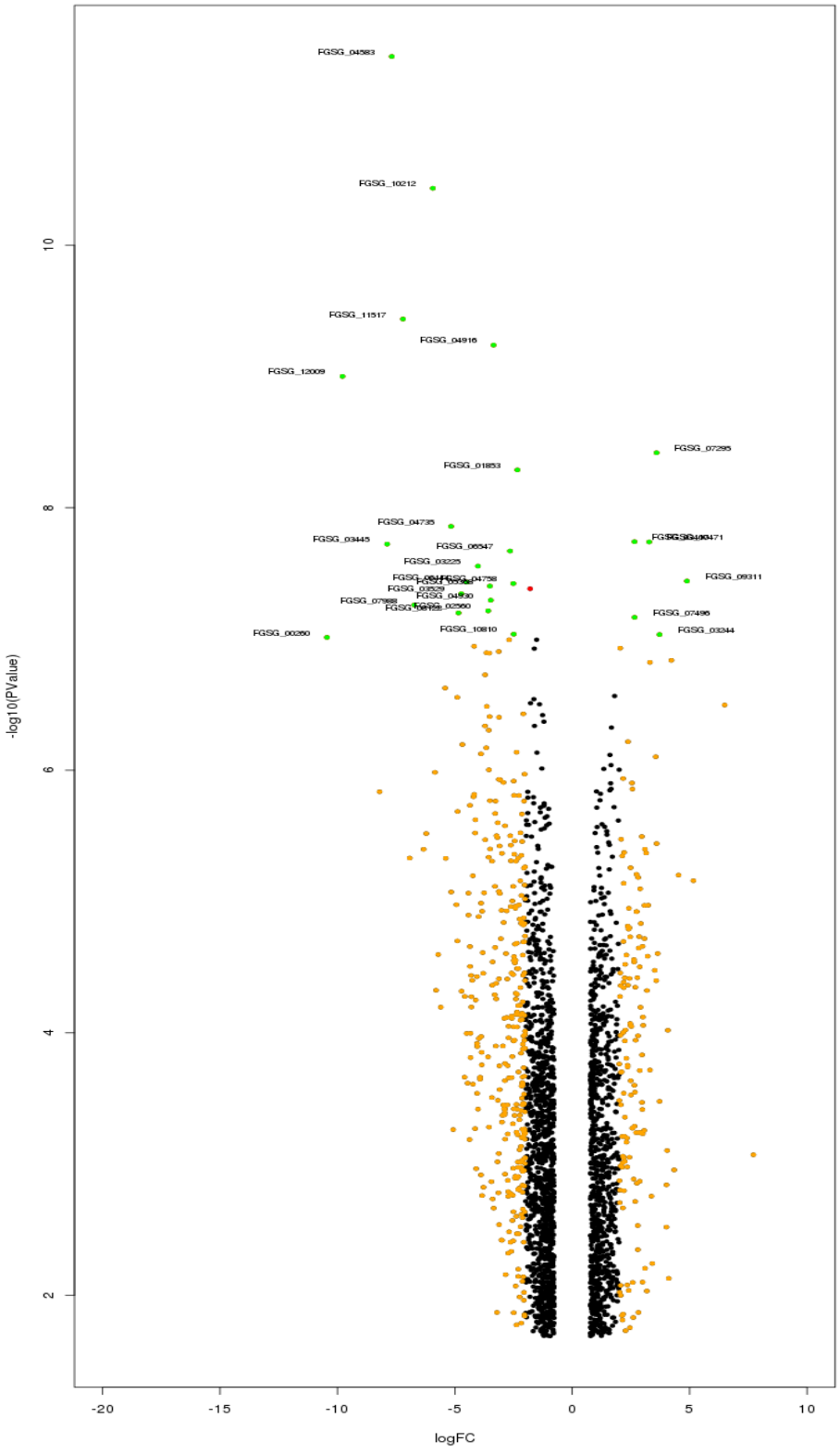
FGSG_04583
FGSG_10212
FGSG_11517
FGSG_04916
FGSG_12009
FGSG_07295
FGSG_01853
FGSG_04735
FGSG_03445
FGSG_06547
FGSG_03225
FGSG_09311
FGSG_07496
FGSG_03244
FGSG_00260
FGSG_10810
-log10(PValue)
logFC
10
8
6
4
2
-20
-15
-10
-5
0
5
10

Figure 4.6. A volcano plot shows the negative logarithm of the p-value (Y axis) *vs* Log_2FC (X axis) when comparing gene expression in *MKK1*^{197E,203E}*_OXs* (a pool of *MKK1*^{197E,203E}*_OX9* and *MKK1*^{197E,203E}*_OX10*) *vs* WT. Dots represent genes that were significantly expressed: FDR < 0.05, and $Log_2FC > 0.669$ (1.59 fold-change), which were the parameters established after the power analysis at 0.8 was performed.

Legend:

Dot colour	**Log_2FC**	**–log (P-value)**
Orange	> 2	≤ 8
Black	$0.55 \leq Log_2FC \leq 2$	≤ 8
Red	$0.55 \leq Log_2FC \leq 2$	> 8
Green	> 2	> 8

The top three most significant DEGs were also downregulated. Among those genes, there was one uncharacterized protein (FGSG_04583), a secreted protein associated with virulence (FGSG_10212) that encodes for a cerato-platanin, and a tyrosinase with a Cu-binding domain (FGSG_11517). In the top three most significant genes that were upregulated there was the expected *MKK1* (FGSG_07295), and two uncharacterized hypothetical proteins (FGSG_03407 and FGSG_10471). FGSG_03407 contains a fungal STAND N-terminal Goodbye domain, while FGSG_10471 is protein found in the nucleus that contains a SNF2 family N-terminal domain and a Zinc finger, C3HC4 type domain.

From the 1,873 DEGs, 680 were already annotated, which represented 36 % of the total (Figure 4.7 A). Regarding the categories of aggrupation, nine were significant from a list of 431 assigned (Figures 4.7 B and C), and 405 genes were distributed among those nine groups (Table 4.4). The category with the highest number of genes (158) was the "C-compound and carbohydrate metabolism", which represented 8.4 % of the 1,873 DEGs and 15.5 % of the genes in that category. The second-largest group was "secondary metabolism", representing 2.9 % of the total genes but 19 % of the genes in that category. The third position was tied between the "nitrogen, sulfur and selenium metabolism" and the "polysaccharide metabolism", with 2.6 % of

the 1,873 DEGs, but with 22.3 % and 17.1 %, respectively, of the genes previously annotated in their categories.

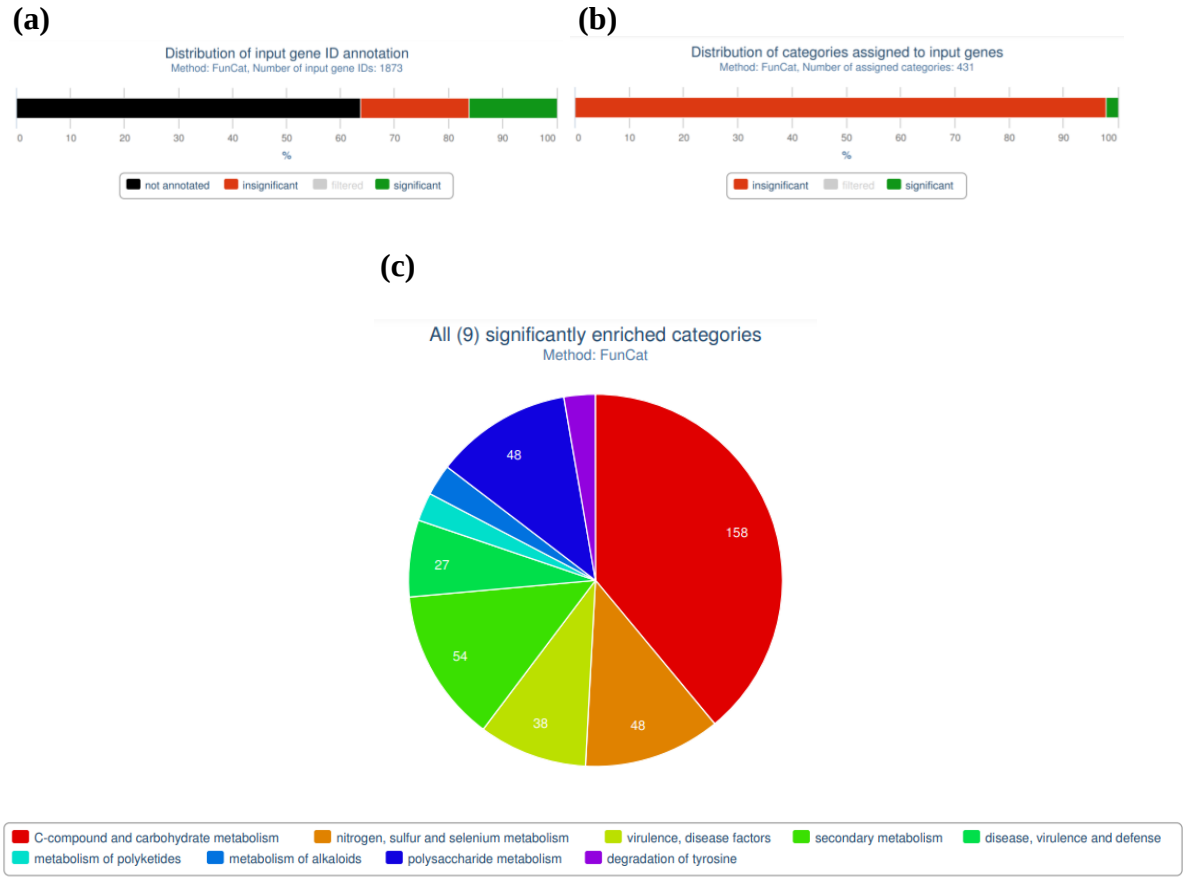

Figure 4.7. (a) Distribution of annotated genes from the 1,873 that were differentially expressed. **(b)** Distribution of categories associated with 1,873 genes that were differentially expressed when *MKK1*^{197E,203E}*_OX* was overexpressed. **(c)** Pie chart of the nine significantly enriched categories.

Table 4.4. Genes that were differentially expressed when *MKK1*^{197E,203E} was overexpressed are classified into nine main categories. FunCat analysis shows how many of the 1,873 DEGs belong to each category (# genes / input) and how many genes are per category. The green colours represent the higher values in the column, and the gradient changes until red tones, which represent the lowest values.

FunCat ID	FunCat description	FunCat main category	# genes/ category	% genes/ category	# genes/ input	% genes/ input
1.05	C-compound and carbohydrate metabolism	Metabolism	158 / 1018	15.5	158 / 1873	8.4
1.02	nitrogen, sulfur and selenium metabolism	Metabolism	48 / 215	22.3	48 / 1873	2.6
32.05.05	virulence, disease factors	Cell rescue, defense and virulence	38 / 173	22.0	38 / 1873	2.0
1.2	secondary metabolism	Metabolism	54 / 284	19.0	54 / 1873	2.9
32.05	disease, virulence and defense	Cell rescue, defense and virulence	27 / 125	21.6	27 / 1873	1.4
01.20.05.11	metabolism of polyketides	Metabolism	10 / 26	38.5	10 / 1873	0.5
01.20.17.09	metabolism of alkaloids	Metabolism	11 / 31	35.5	11 / 1873	0.6
01.05.03	polysaccharide metabolism	Metabolism	48 / 280	17.1	48 / 1873	2.6
01.01.09.05.02	degradation of tyrosine	Metabolism	11 / 33	33.3	11 / 1873	0.6

The FunCat description "metabolism of polyketides" had the highest percentage (38.5 %) of its genes differentially expressed compared to the other eight categories in *MKK1*^{197E,203E}*_OXs* (Table 4.4). The DEGs encoded for proteins containing domains associated with three main groups: *PKS*, *NRPS* and *GATase1* (or DJ-1_PfpI). The *PKS* represents the group with the highest amount of genes (six from a total of ten), and all were downregulated (Supplementary Table 4.3 F). In the *NRPS*, FGSG_03245 (*NRPS11*, according to Sieber *et al*. (2014)) was upregulated, while FGSG_13153 (*NRPS13*- related to *NRPS* according to (Sieber *et al*., 2014)) was downregulated (Supplementary Table 4.3 E). Last, the proteins with GATase1 domain, FGSG_03354 and FGSG_08979, were down and upregulated, respectively.

The FunCat description with the second-highest representation of its genes in *MKK1*^{197E,203E}*_OX* transformants is "Metabolism of alkaloids" with 35.5 % (Table 4.4). All those 11 genes, contain at least a FAD-binding domain (except for FGSG_01285, an aminotransferase), and while six of them were downregulated, five were upregulated. In addition, the gene FGSG_10998, a hypothetical protein with FAD/FMN-containing dehydrogenase, is considered a chitooligosaccharide oxidase according to UniProtKB, and was the most downregulated gene in the 'metabolism of alkaloid" description.

The “degradation of tyrosine” forms the third-highest group regarding the percentage of representation, since it has a 33.3 % of its genes differentially expressed in *MKK1*^{197E,203E}*_OX* (Table 4.4). Six of the 11 DEGs contain a Tyrosinase-Cooper-binding domain, and were divided into two groups: three characterized and three uncharacterized proteins. The characterized proteins were identified as Tyrosinase_Cu-bd domain-containing proteins, and were downregulated, while the uncharacterized proteins possessed two Tyrosine-Cooper-binding domains, and two of them (FGSG_05628 and FGSG_11528) were upregulated. Three of the 11 DEGs were involved in the tyrosine metabolic process but also in the L-Phe degradation pathway (FGSG_02347, FGSG_06001 and FGSG_08358), and all were upregulated.

The FunCat descriptions “virulence, disease factors” and “disease, virulence and defense” were also highly represented with 22 % of its genes in each case (Table 4.4). From 48 genes between both categories, 17 genes were shared. Most of the genes were uncharacterized proteins, but among those that are characterized there was FGSG_02155, a hypothetical protein with a CFEM (common in fungal extracellular membrane) domain that was upregulated. Two other hypothetical proteins with CFEM domains were also differentially expressed, but where not included in the list of the FunCat descriptions: FGSG_00588 and FGSG_02077 that were downregulated and upregulated, respectively. In “virulence, disease factors”, FGSG_00126, a hypothetical protein with a Glycosyl transferase family 90 domain, had the highest expression level, while the lowest expressed was FGSG_08208 (*PKS6*). In “disease, virulence and defense” the most strongly upregulated gene was the *NRPS11*, while the most downregulated was the cerato-platanin FGSG_10212.

The CWI pathway components include the three main proteins of the core (MAPKKK-MAPKK-MAPK): Bck1 (FGSG_06326), Mkk1 (FGSG_07295) and Mgv1(FGSG_10313), and

the transcription factor, Rlm1. Only *RLM1* (FGSG_09339) was differentially expressed, and interestingly, it was downregulated. Rlm1 regulates the expression of genes associated with the cell wall, such as chitinases (*CHS*) and glucan synthases. However, the only differentially expressed gene from the *CHS* family, *CHS5* (FGSG_01964), was downregulated, while the expression of the putative *FKS1* (a subunit of the 1,3-*β*-D-glucan synthase), did not change in *MKK1*^{197E,203E}*_OXs* compared to WT (Supplementary Table 4.4).

Expression of the core proteins from the other two MAPK cascades formed by Ste11 (FGSG_05484), Ste7 (FGSG_09903) and Gpmk1 (FGSG_06385) for the virulence pathway, and with Ssk2/Ssk22 (FGSG_00408), Pbs2 (FGSG_08691) and Hog1(FGSG_09612) for the HOG pathway, were unaffected by *MKK1*^{197E,203E} overexpression. Interestingly, the phosphatase *MSG5* (FGSG_06977), which is thought to dephosphorylates Mgv1 (Yu *et al*., 2014), was downregulated in *MKK1*^{197E,203E}*_OXs* (Supplementary Table 4.4).

Regarding secondary metabolites, an overview of the expression of some gene clusters is listed on Supplementary Table 4.3. The eight genes of the butenolide cluster (FGSG_08077-FGSG_08084) were upregulated in *MKK1*^{197E,203E}*_OXs* (Supplementary Table 4.3 B). However, they were all distributed in different FunCat descriptions, such as “N, sulfur, and selenium metabolism” (FGSG_08078 and FGSG_08079), “secondary metabolism” (FGSG_08080) and “C-compound and metabolism” (FGSG_08083). Four other genes were not included in the list, but were also upregulated.

Another secondary metabolite that has some of its biosynthetic genes differentially expressed was the aurofusarin, but with only two of them (*AURR2* and *AURT*), and they were upregulated Supplementary Table 4.3 A. *AURR2* is a transcription factor, while AurT is a major facilitator pump involved in the transport of rubrofusarin across the plasma membrane.

In the trichothecene gene cluster only *TRI13* was differentially expressed with a $Log_2FC < -0.99$; however, even though other genes, such as *TRI8* (FGSG_03532) and *TRI9* (FGSG_03539), did not reach that value, they could be considered downregulated if less stringent conditions, such as $Log_2FC < -0.9$ (1.86-fold change) were selected (Supplementary Table 4.3 D).

When $MKK1^{197E,203E}$ was overexpressed, around 1,700 genes were downregulated, but 1,192 genes had a $Log_2FC \leq -0.991$. From those 1,192 genes, 385 (32.3 %) were annotated, but only 15.2 % were significant (Figure 4.8 A). The genes were then distributed into 332 categories with only nine significant (Figures 4.9 B and C). "C-compounds and carbohydrate metabolism" was the category with the highest number of downregulated genes from the 1,192 analyzed, which represented 9.2 % of the genes assigned to that FunCat description (Table 4.5). This group was followed by the "polysaccharide metabolism" and "secondary metabolism", representing around 12 % of the annotated genes in each group (Table 4.5). The most represented category was the "sulfate assimilation" since 45.5 % of its genes were downregulated, followed by "metabolism of polyketides" with 31 % of its genes identified in this analysis (Table 4.5).

(a) **(b)**

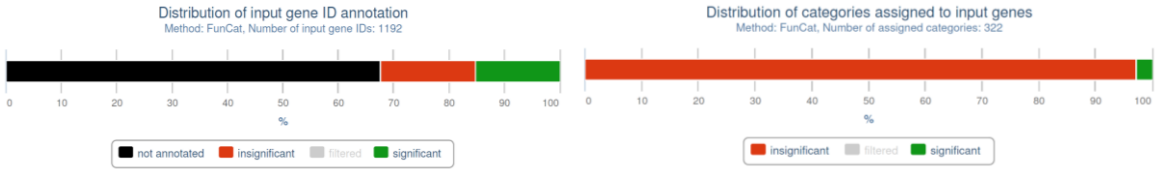

(c)

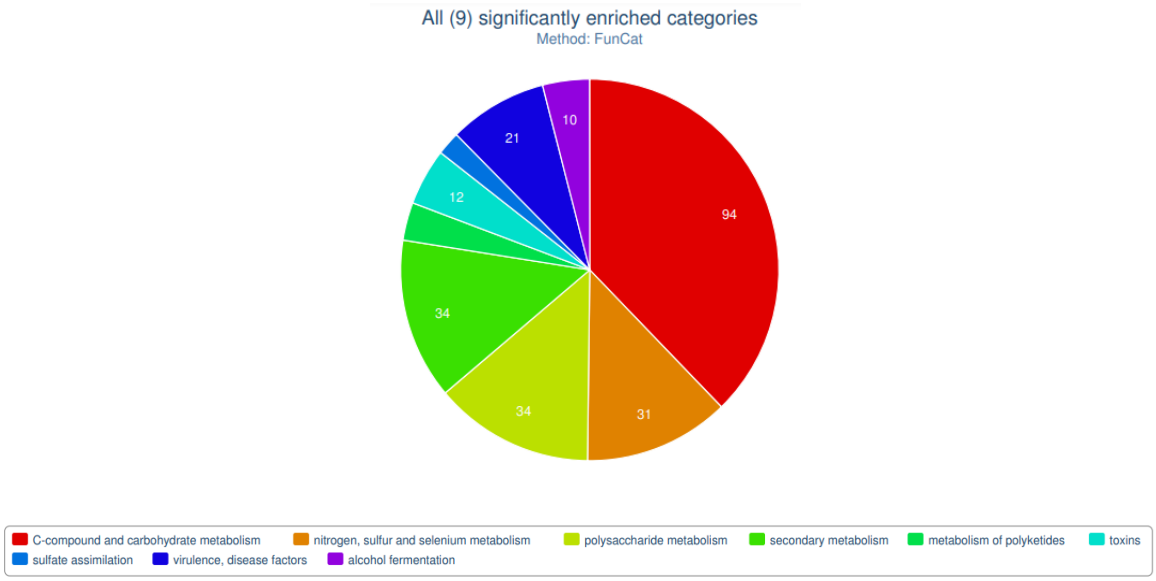

Figure 4.8. (a) Distribution of annotated genes from the 1192 that were downregulated. **(b)** Distribution of categories associated with 1192 genes that were downregulated when *MKK1*^{197E,203E}*_OX* was overexpressed. **(c)** Pie chart of the nine significantly enriched categories.

Table 4.5. Genes that were downregulated when *MKK1*^{197E,203E} was overexpressed are classified into nine main categories. FunCat analysis shows how many of the 1,192 genes that were downregulated belong to each category. The green colours represent the higher values in the column, and the gradient changes until red tones, which represent the lowest values.

FunCat ID	FunCat description	FunCat main category	# genes/ category	% genes/ category	# genes/ input	% genes/ input
1.05	C-compound and carbohydrate metabolism	Metabolism	94 / 1018	9.2	94 / 1192	7.9
1.02	nitrogen, sulfur and selenium metabolism	Metabolism	31 / 215	14.4	31 / 1192	2.6
01.05.03	polysaccharide metabolism	Metabolism	34 / 280	12.1	34 / 1192	2.9
1.2	secondary metabolism	Metabolism	34 / 284	12.0	34 / 1192	2.9
01.20.05.11	metabolism of polyketides	Metabolism	8 / 26	30.8	8 / 1192	0.7
32.05.05.01	toxins	Cell rescue, defense and virulence	12 / 62	19.4	12 / 1192	1.0
01.02.03.01	sulfate assimilation	Metabolism	5 / 11	45.5	5 / 1192	0.4
32.05.05	virulence, disease factors	Cell rescue, defense and virulence	21 / 173	12.1	21 / 1192	1.8
02.16.01	alcohol fermentation	Energy	10 / 56	17.9	10 / 1192	0.8

The overexpression of the putative phosphomimic led to the upregulation of 1,190 genes with Log_2FC varying from 0.66909 to 7.7143. After a cut-off at a Log_2FC = 0.993, 681 genes with higher Log_2FC values were selected for FunCat analysis, and from those, only 295 genes were annotated (Figure 4.9 A). All genes were distributed into 330 categories, but only three were significant: "rRNA processing", "ribosome biogenesis" and "metabolism of tyrosine" (Figures 4.9 B and C). The "rRNA processing" category groups 28 of the identified genes, which represents 15 % of the annotated genes in this category (Table 4.6). The "ribosome biogenesis" group contains 24 genes, equivalent to 12.8 % of the annotated genes in the category, while in the "metabolism of tyrosine", there were eight genes grouped, but it represented 20 % of the genes in that category (Table 4.6). Interestingly, the categories that were significantly upregulated by the overexpression of *MKK1*^{197E,203E} were not included in the overall categories when all DEGs were analyzed in the *MKK1*^{197E,203E}*_OX* transformants *vs* WT (Table 4.4).

(a) **(b)**

(c)

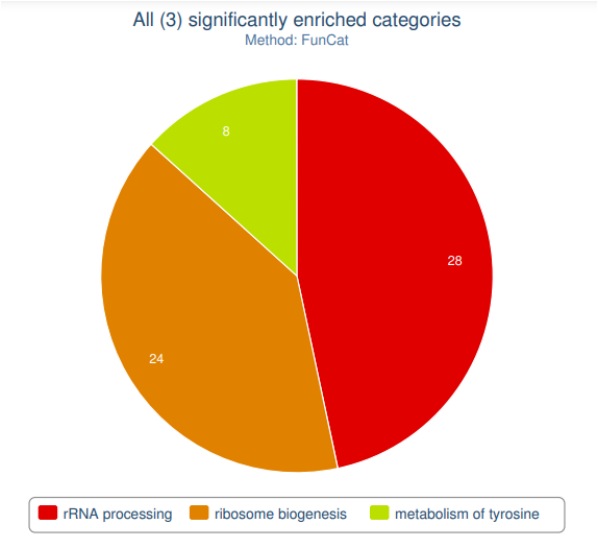

Figure 4.9. (a) Distribution of annotated genes from the 681 that were upregulated. **(b)** Distribution of categories associated with 681 genes that were upregulated when *MKK1*^{197E,203E}*_OX* was overexpressed. **(c)** Pie chart of the three significantly enriched categories.

Table 4.6. Genes that were upregulated when *MKK1*^{197E,203E}*_OX* was overexpressed are classified into three main categories. FunCat analysis shows how many of the 681 genes that were upregulated belong to each category. The green colours represent the higher values in the column, and the gradient changes until red tones, which represent the lowest values.

FunCat ID	FunCat description	FunCat main category	# genes / category	% genes/ category	# genes / input	% genes/ input
11.04.01	rRNA processing	Transcription	28 / 187	15.0	28 / 681	4.1
12.01	ribosome biogenesis	Protein synthesis	24 / 187	12.8	24 / 681	3.5
01.01.09.05	metabolism of tyrosine	Metabolism	8 / 40	20.0	8 / 681	1.2

4.3.3 Effect of the overexpression of *MKK1 vs* the overexpression of the putative phosphomimic *MKK1*^{197E,203E} in *F. graminearum*

The comparison of the *MKK1_OX* and *MKK1*^{197E,203E}*_OX* transcriptomic profile showed the significant impact caused by the modification of the amino acids in the Mkk1 activation loop. The data of two strains overexpressing *MKK1* (*MKK1_OX4* and *MKK1_OX5*) was compared to the two strains overexpressing *MKK1*^{197E,203E} (*MKK1*^{197E,203E}*_OX9* and *MKK1*^{197E,203E}*_OX10*). As a result of the power analysis, a 0.8 value was chosen for the study. The comparison between *MKK1_OXs* and *MKK1*^{197E,203E}*_OXs* showed that a total of 1,891 DEGs with 675 downregulated and 1,216 upregulated (Supplementary Table 4.7 shows a list of the top 15 upregulated and top 15 downregulated genes). From those, 19 genes had a highly significant value, with four of them downregulated, while 15 were upregulated in *MKK1_OX* (Figure 4.10). From the 1,891 DEGs, those with a two-fold change value were selected to perform the next analysis. Thus, a new list with 288 genes that were downregulated, while 566 were upregulated, was generated for the FunCat analysis (Supplementary Table 4.8 shows a list of the top 15 upregulated and top 15 downregulated genes).

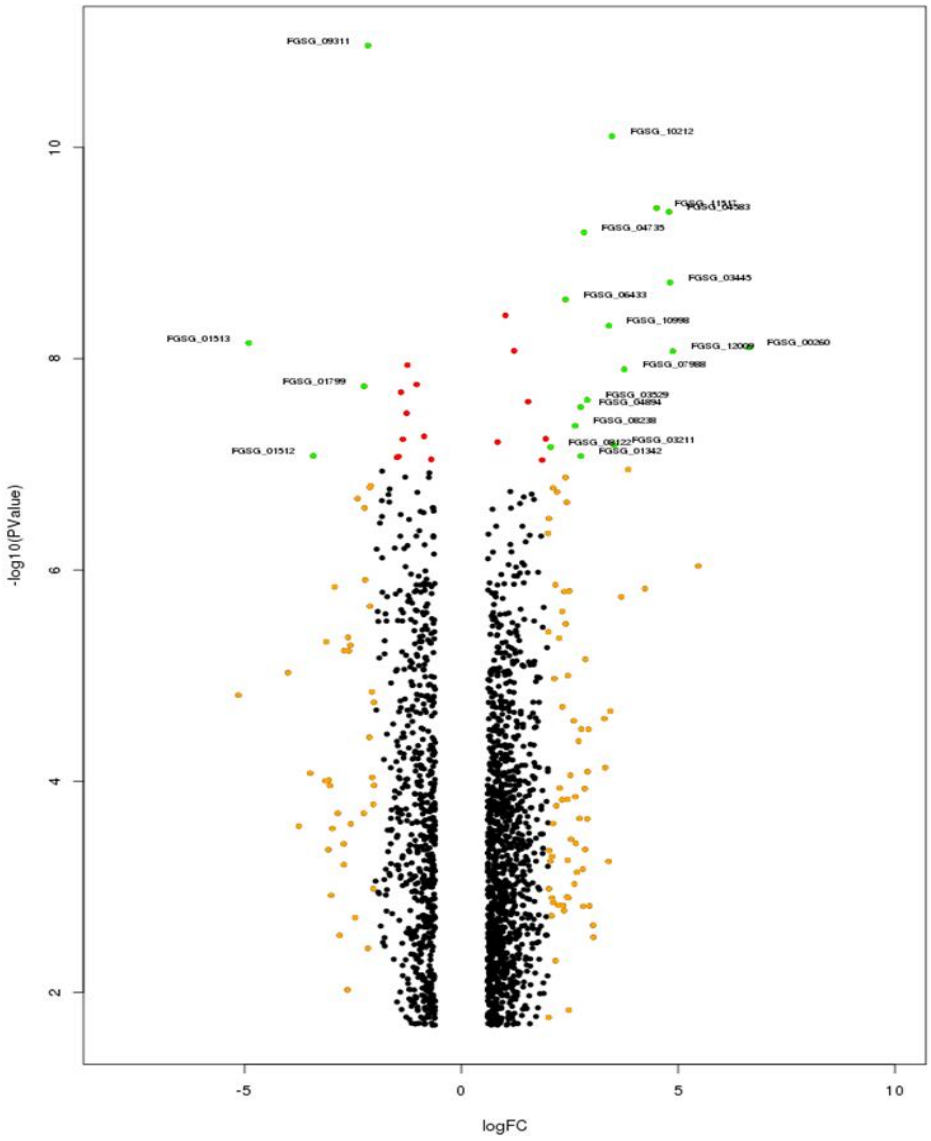

Figure 4.10. A volcano plot shows the negative logarithm of the p-value (Y axis) *vs* Log_2FC (X axis) when comparing *MKK1_OXs* (a pool of *MKK1_OX4* and *MKK1_OX5*) *vs* *MKK1*^{197E,203E}*_OXs* (a pool of *MKK1*^{197E,203E}*_OX9* and *MKK1*^{197E,203E}*_OX10)*. Dots represent genes that were significantly expressed: FDR < 0.05, and $Log_2FC > 0.6$ (1.52 fold-change), which were the parameters established after the power analysis at 0.8 was performed.

Legend:

Dot colour	**Log_2FC**	**–log (P-value)**
Orange	> 2	≤ 8
Black	$0.55 \leq Log_2FC \leq 2$	≤ 8
Red	$0.55 \leq Log_2FC \leq 2$	> 8
Green	> 2	> 8

From the 854 genes that were differentially expressed in *MKK1_OXs vs MKK1*^{197E,203E}*_OXs*, 34.9 % were annotated and 22.72 % were significant (Figure 4.11 A). The genes were distributed into 313 categories with 21 FunCat descriptions (Figures 4.11 B and C, Table 4.7). The 21 groups were also classified into four main categories: “metabolism”, “protein with binding function or cofactor requirement (structural or analytical)”, “cell rescue, defense and virulence”, and “cellular transport, transport facilitation and transport routes” (Table 4.7). The “C-compound and carbohydrate metabolism”, which belongs to the “metabolism” main category, was the group (among the 21) with the highest number of genes: 9.4 % of the total DEGs (854), but this was the second-lowest represented category since it only had 7.9 % of the genes previously annotated for this group. The category that had the highest number of its genes differentially expressed (40 %) was “metabolism of peptide-antibiotics” followed by “non-ribosomal peptide synthesis” with 25 %, both of them from the “metabolism” mains group, and then “toxins” (from “cell rescue, defense and virulence”) with 23 %.

(a) **(b)**

(c)

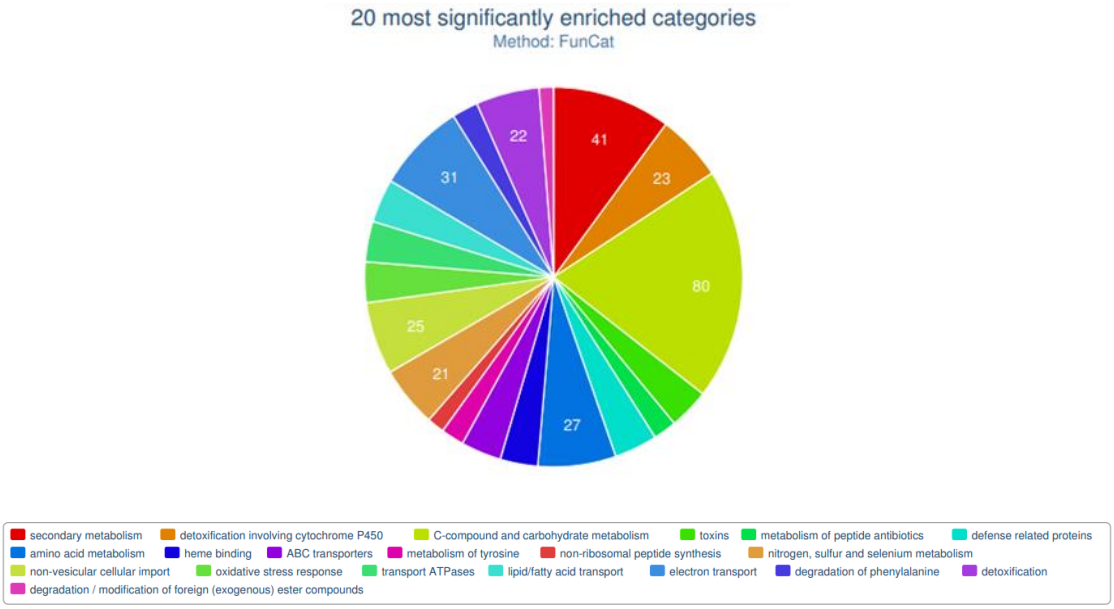

Figure 4.11. (a) Distribution of annotated genes from the 854 that were differentially expressed in *MKK1_OX* compared to *MKK1*^{197E,203E}*_OX*. **(b)** Distribution of categories associated with 854 genes that were differentially expressed in *MKK1_OX* compared to *MKK1*^{197E,203E}*_OX*. **(c)** Pie chart of the 20 most significantly enriched categories.

Table 4.7. Genes that were differentially expressed when *MKK1_OX* was compared to *MKK1*^{197E,203E}*_OX* are classified into four main categories. FunCat analysis shows how many of the 854 genes that were up or downregulated belong to each category. The green colours represent the higher values in the column, and the gradient changes until red tones, which represent the lowest values.

FunCat ID	FunCat description	FunCat main category	# genes/ category	% genes/ category	# genes/ input	% genes/ input
1.2	secondary metabolism	Metabolism	41 / 284	14.4	41 / 854	4.8
32.07.01	detoxification involving cytochrome P450	Cell rescue, defense and virulence	23 / 111	20.7	23 / 854	2.7
1.05	C-compound and carbohydrate metabolism	Metabolism	80 / 1018	7.9	80 / 854	9.4
32.05.05.01	toxins	Cell rescue, defense and virulence	14 / 62	22.6	14 / 854	1.6
01.20.37.03	metabolism of peptide antibiotics	Metabolism	8 / 20	40.0	8 / 854	0.9
32.05.03	defense related proteins	Cell rescue, defense and virulence	15 / 92	16.3	15 / 854	1.8
1.01	amino acid metabolism	Metabolism	27 / 248	10.9	27 / 854	3.2
16.21.01	heme binding	Protein with binding function or cofactor requirement (structural or analytic)	13 / 91	14.3	13 / 854	1.5
20.03.25	ABC transporters	Cellular transport, transport facilitation ar	14 / 106	13.2	14 / 854	1.6
01.01.09.05	metabolism of tyrosine	Metabolism	8 / 40	20.0	8 / 854	0.9
01.20.36	non-ribosomal peptide synthesis	Metabolism	6 / 24	25.0	6 / 854	0.7
1.02	nitrogen, sulfur and selenium metabolism	Metabolism	21 / 215	9.8	21 / 854	2.5
20.09.18.07	non-vesicular cellular import	Cellular transport, transport facilitation and transport routes	25 / 278	9.0	25 / 854	2.9
32.01.01	oxidative stress response	Cell rescue, defense and virulence	14 / 122	11.5	14 / 854	1.6
20.03.22	transport ATPases	Cellular transport, transport facilitation and transport routes	14 / 123	11.4	14 / 854	1.6
20.01.13	lipid/fatty acid transport	Cellular transport, transport facilitation and transport routes	15 / 141	10.6	15 / 854	1.8
20.01.15	electron transport	Cellular transport, transport facilitation and transport routes	31 / 398	7.8	31 / 854	3.6
01.01.09.04.02	degradation of phenylalanine	Metabolism	9 / 64	14.1	9 / 854	1.1
32.07	detoxification	Cell rescue, defense and virulence	22 / 258	8.5	22 / 854	2.6
32.10.09	degradation / modification of foreign (exogenous) ester compounds	Cell rescue, defense and virulence	5 / 23	21.7	5 / 854	0.6
01.01.09.05.02	degradation of tyrosine	Metabolism	6 / 33	18.2	6 / 854	0.7

In “metabolism of peptide antibiotics” there were eight DEGs from the 20 genes that belong to this FunCat description. All of them have been annotated as *NRPS,* or proteins that contains NRPS domains, in some of the different databases used in this study (NCBI, FCGP or UniProtKB) or in publications (Sieber *et al*., 2014). Among the five of these DEGs that were upregulated, the strongest upregulation was in *NRPS7* (FGSG_08209), which mediates the biosynthesis of the lipopeptide and secondary metabolite fusaristatin A. Another upregulated gene involved in this pathway is FGSG_08207, a Cytocrhome P450 monoxoygenase, which was not included in this Funcat description, but in the “heme binding group”.

A higher number of DEGs were found in *MKK1*^{197E,203E}*_OX* than in *MKK1_OX*, and from those, 415 were shared by both strains (Figure 4.12 A). Genes that were downregulated are showed in Figure 4.12 B, while upregulated genes is presented in Figure 4.12 C. In both strains, the number of downregulated genes is bigger than the upregulated ones. In general, *MKK1* regulates several genes in the cell, and the putative phosphomimic *MKK1*^{197E,203E}*_OX* generates a more significant change in gene expression.

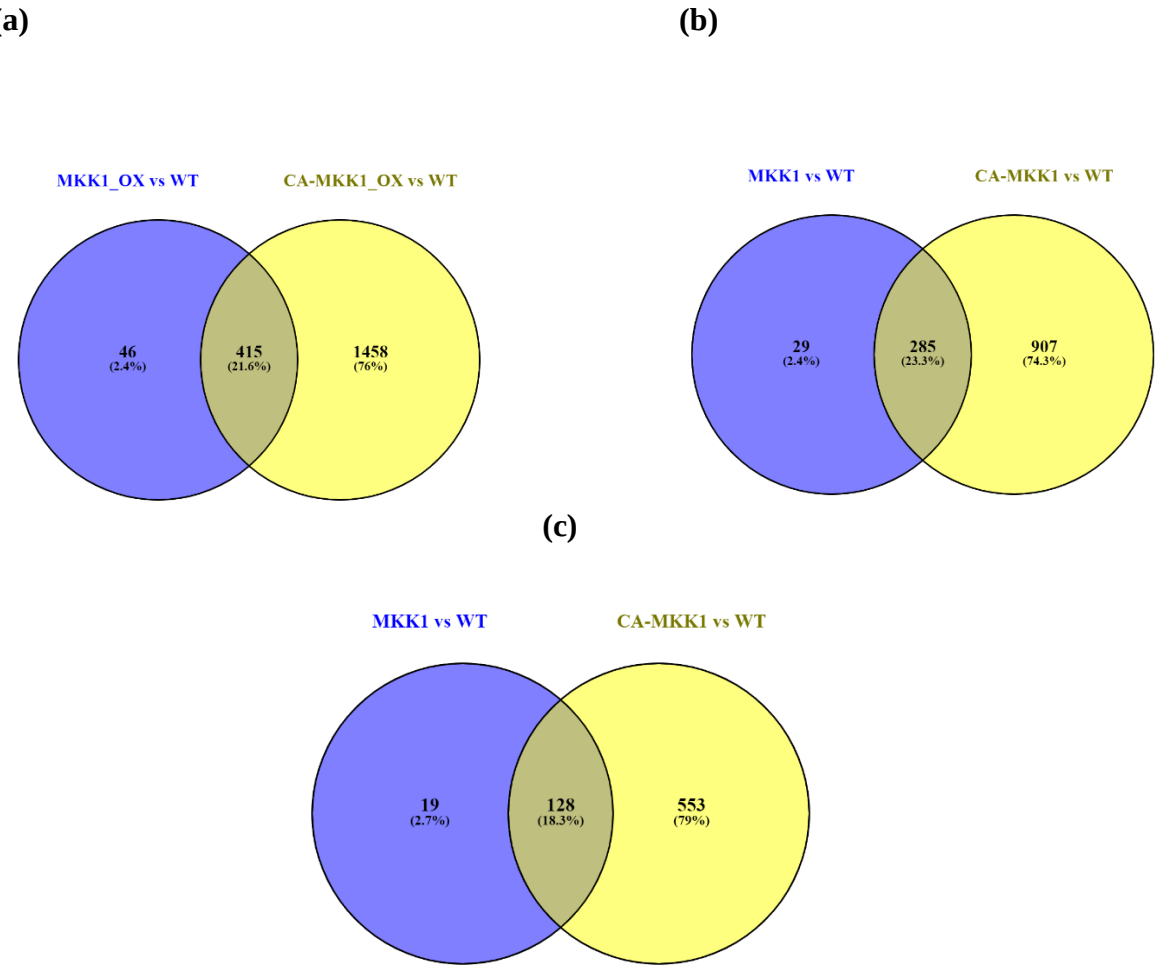

Figure 4.12. Venn diagram for genes differentially expressed in *MKK1_OXs* and *MKK1*^{197E,203E}*_OXs*. **(a)** Total DEGs **(b)** Downregulated genes **(c)** Upregulated genes.

From 288 downregulated genes with a $Log_2FC < -0.99$, a total of 120 genes (41.7 %) were already annotated, and only 65 genes (22.6 % from the total) were significant, according to ORA (Figure 4.13 A). A total of 214 enriched categories were assigned to the genes, but only 12 were significant, which were grouped in two main categories: “metabolism”, and “cell rescue, defense and virulence” (Figures 4.13 B and C, Table 4.8). The highest amount of genes that were differentially downregulated (11.5 %) corresponded to the “C-compound and carbohydrate metabolism” category, but it was also the group with the lowest number of its genes represented (3.2 %). The category that had the highest percentage of representation was “degradation of isoleucine” (three genes), followed by “degradation of valine” (three genes), but those genes were the same in both categories. The next category was “degradation/modification of foreign (exogenous) ester compounds” followed by “detoxification by degradation” where, again, four genes were shared between these two groups.

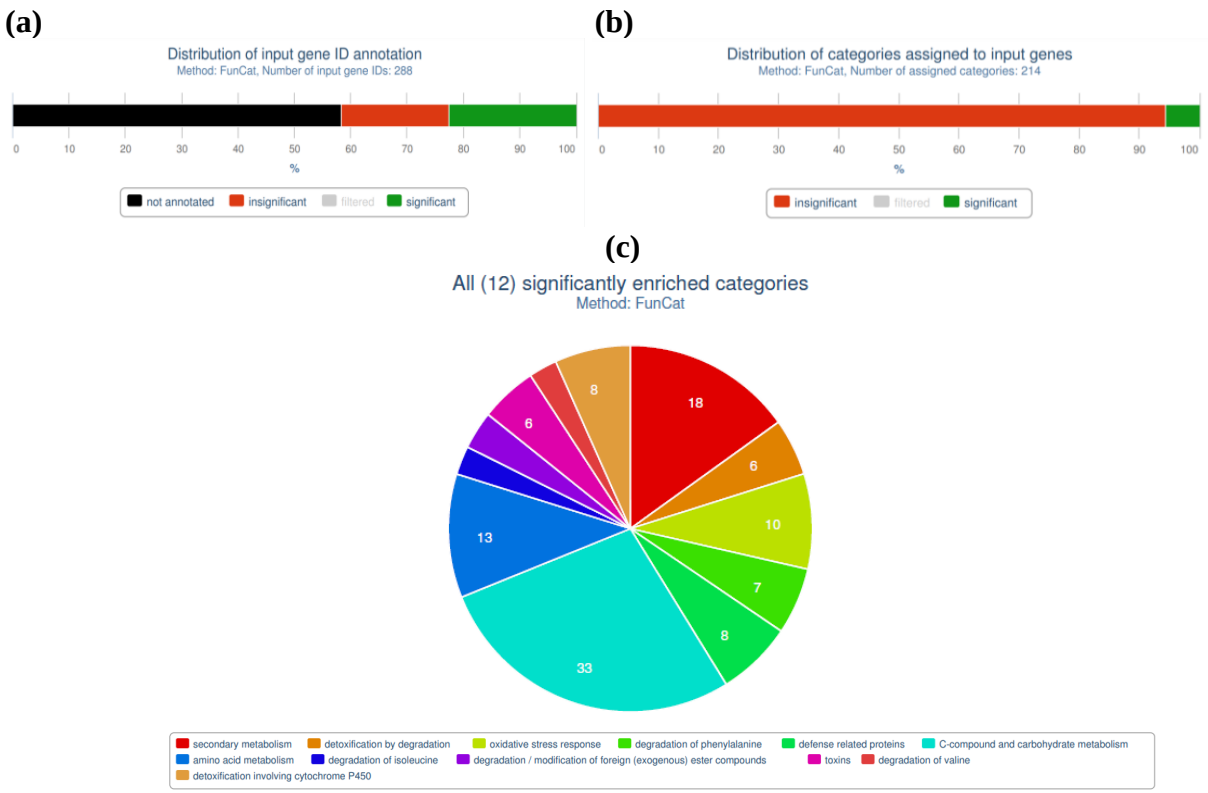

Figure 4.13. (a) Distribution of annotated genes from the 288 that were downregulated in *MKK1_OX* when compared to *MKK1*^{197E,203E}*_OX*. **(b)** Distribution of categories associated with 288 genes that were downregulated in *MKK1_OX* when compared to *MKK1*^{197E,203E}*_OX*. **(c)** Pie chart of the 12 most significantly enriched categories.

Table 4.8. Genes that were downregulated when *MKK1_OX* was compared to *MKK1*^{197E,203E}*_OX* are classified into two main categories: metabolism, and cell rescue, defense and virulence. FunCat analysis shows how many of the 288 genes that were downregulated belong to each category. The green colours represent the higher values in the column, and the gradient changes until red tones, which represent the lowest values.

FunCat ID	FunCat description	FunCat main category	# genes/ category	% genes/ category	# genes/ input	% genes/ input
1.2	secondary metabolism	Metabolism	18 / 284	6.3	18 / 288	6.3
32.07.09	detoxification by degradation	Cell rescue, defense and virulence	6 / 38	15.8	6 / 288	2.1
32.01.01	oxidative stress response	Cell rescue, defense and virulence	10 / 122	8.2	10 / 288	3.5
01.01.09.04.02	degradation of phenylalanine	Metabolism	7 / 64	10.9	7 / 288	2.4
32.05.03	defense related proteins	Cell rescue, defense and virulence	8 / 92	8.7	8 / 288	2.8
1.05	C-compound and carbohydrate metabolism	Metabolism	33 / 1018	3.2	33 / 288	11.5
1.01	amino acid metabolism	Metabolism	13 / 248	5.2	13 / 288	4.5
01.01.11.02.02	degradation of isoleucine	Metabolism	3 / 10	30	3 / 288	1.04
32.10.09	degradation / modification of foreign (exogenous) ester compounds	Cell rescue, defense and virulence	4 / 23	17.4	4 / 288	1.4
32.05.05.01	toxins	Cell rescue, defense and virulence	6 / 62	9.7	6 / 288	2.1
01.01.11.03.02	degradation of valine	Metabolism	3 / 11	27.3	3 / 288	1.04
32.07.01	detoxification involving cytochrome P450	Cell rescue, defense and virulence	8 / 111	7.2	8 / 288	2.8

From 1,216 genes that were upregulated, 566 had a $Log_2FC > 0.99$ that varied from 0.995 to 6.635, and were analyzed with FunCat. The analyses revealed that 178 genes were annotated, and the genes were distributed among 229 categories, but only eight were significant. Those FunCat descriptions were grouped into: “metabolism”, “cell rescue, defense and virulence”, “protein with binding function or cofactor requirement (structural or analytical)” and “cellular transport, transport facilitation and transport routes” (Figures 4.14 B and C, Table 4.9).

Most of the genes (79) corresponded to the “metabolism” main category, and from those, 47 were linked to the “C-compound and carbohydrate metabolism” group, representing 4.6 % of the genes in this class. When comparing *MKK1* vs *MKK1*^{197E,203E}*_OX*, only five genes were upregulated in the “metabolism of peptide antibiotics”, but this was the most represented category with 25 % of its genes. The “metabolism of secondary products derived from L-phenylalanine and L-tyrosine” was the second-most represented group with only four genes equivalent to 23.5 % of the genes in its group. The third-most represented group was “detoxification involving Cytochrome P450” (13.5 % of the genes in this group) which belonged to the main category “cell rescue, defense and virulence” that also has the group “toxins” with 13 % of its genes.

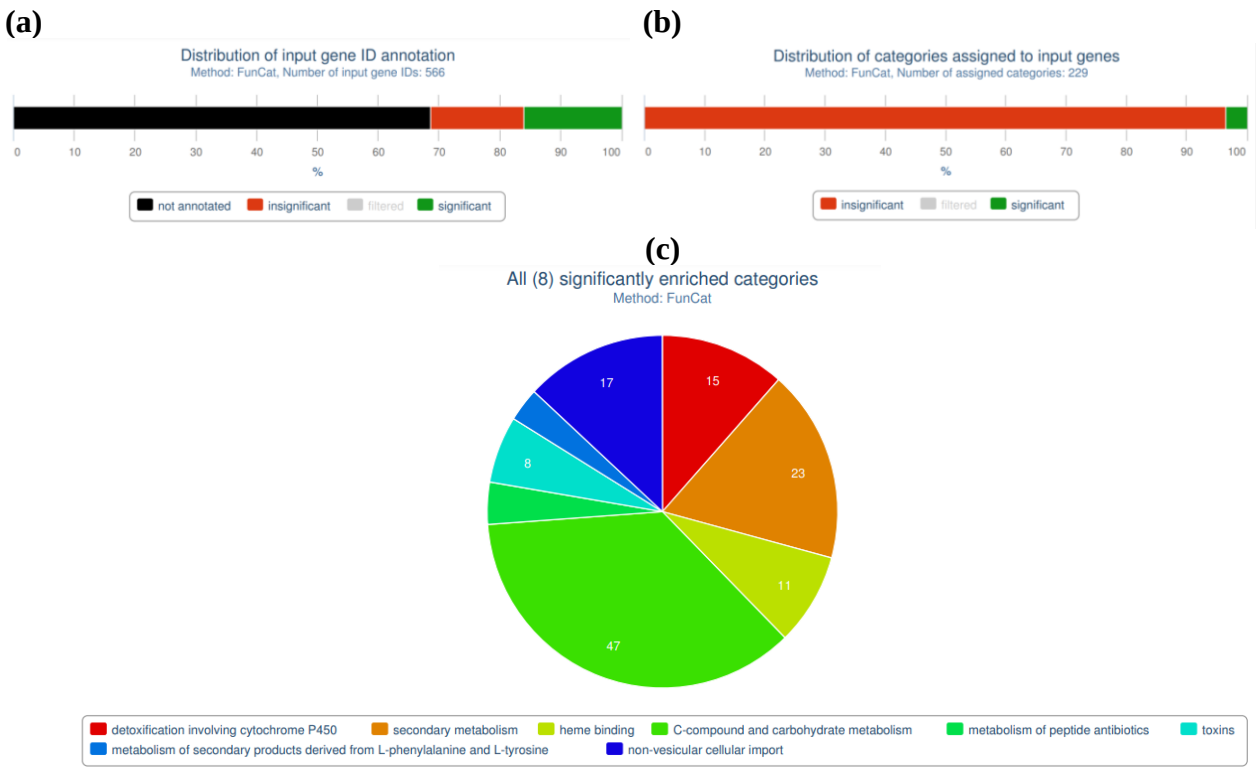

Figure 4.14. (a) Distribution of annotated genes from the 566 that were upregulated in *MKK1_OX* when compared to *MKK1*^{197E,203E}*_OX*. **(b)** Distribution of categories associated with 566 genes that were upregulated in *MKK1_OX* when compared to *MKK1*^{197E,203E}*_OX*. **(c)** Pie chart of the 8 most significantly enriched categories.

Table 4.9. Genes that were upregulated when *MKK1_OX* was compared to *MKK1*^{197E,203E}*_OX* are classified into four main categories. FunCat analysis shows how many of the 566 genes that were upregulated belong to each category. The green colours represent the higher values in the column, and the gradient changes until red tones, which represent the lowest values.

FunCat ID	FunCat description	FunCat main category	# genes/ category	% genes/ category	# genes/ input	% genes/ input
32.07.01	detoxification involving cytochrome P450	Cell rescue, defense and virulence	15 / 111	13.5	15 / 566	2.7
1.2	secondary metabolism	Metabolism	23 / 284	8.1	23 / 566	4
16.21.01	heme binding	Protein with binding function or cofactor requirement (structural or analytic)	11 / 91	12.1	11 / 566	1.9
1.05	C-compound and carbohydrate metabolism	Metabolism	47 / 1018	4.6	47 / 566	8.3
01.20.37.03	metabolism of peptide antibiotics	Metabolism	5 / 20	25	5 / 566	0.9
32.05.05.01	toxins	Cell rescue, defense and virulence	8 / 62	12.9	8 / 566	1.4
01.20.35	metabolism of secondary products derived from L-phenylalanine and L-tyrosine	Metabolism	4 / 17	23.5	4 / 566	0.7
20.09.18.07	non-vesicular cellular import	Cellular transport, transport facilitation and transport routes	17 / 278	6.1	17 / 566	3

4.4 Discussion

The study of the transcriptomic profile of *MKK1_OX* and *MKK1*^{197E,203E}*_OX* strains revealed that two main FunCat categories were enriched in both sets of strains: "Metabolism" and "Cell rescue, defense and virulence" (Table 4.10). *MKK1*^{197E,203E}*_OXs* and *MKK1_OXs* shared four FunCat descriptions, which also belonged to the metabolism category. For the purpose of this discussion, I will focus on whether MAPK and secondary metabolite pathways were affected by the overexpression of *MKK1* or its putative *MKK1* phosphomimic (Supplementary Tables 4.7 and 4.8), but, interestingly, many genes belonging to other pathways are differentially expressed, and could be the target of further discussion.

Table 4.10. Main categories and FunCat descriptions enriched in the RNA-seq analysis performed in *MKK1_OX* and *MKK1*^{197E,203E} *_OX* strains compared to WT. "X" indicates that category or FunCat description is present in the overexpressing strains.

MKK1_OX	***MKK1*^{197E,203E}*_OX***	**FunCat description**	**Main category**
X	X	C-compound and carbohydrate metabolism	Metabolism
X	X	Secondary metabolism	Metabolism
X	X	Polysaccharide metabolism	Metabolism
X	X	Metabolism of alkaloids	Metabolism
	X	Nitrogen, sulfur and selenium metabolism	Metabolism
	X	Metabolism of polyketides	Metabolism
	X	Degradation of tysorine	Metabolism
X		Toxins	Cell rescue, defense and virulence
	X	Virulence, disease factors	Cell rescue, defense and virulence
	X	Disease, virulence and defnse	Cell rescue, defense and virulence

4.4.1 Effect of *MKK1* or *MKK1*^{197E,203E} overexpression on the MAPK pathways

The CWI pathway has a core of three proteins, that in *F. graminearum* is formed by Bck1 (MAPKKK), Mkk1 (MAPKK), and Mgv1 (MAPK). The overexpression of *MKK1* or a putative phosphomimic (*MKK1*^{197E,203E}) did not change the expression levels of any of the two other main components of the pathway. In addition, it did not alter the expression of *KIN4*, a kinase that putatively interacts with Mgv1 (Wang *et al*., 2011), nor the regulation of the transcription cofactor *SWI6* (FGSG_04220). Swi6 is a downstream target of Slt2 (Mgv1 orthologue) in *S. cerevisiae*, but it has not been identified as an Mgv1 downstream in *F. graminearum*. This transcription co-factor in *F. graminearum* is a hybrid between the Swi4 and Swi6 TFs of *S. cerevisiae*, and it was suggested that the complexes (Sbf and Mbf) that form both TFs with Mbp1 (a DNA-binding protein), are both carried out by the Swi6 and Mbp1 in *F. graminearum* (Liu *et al*., 2013). An overview of how the overexpression of *MKK1* or *MKK1*^{197E,203E} affected the expression of these and other cellular components is represented in Figure 4.15 and Supplementary Table 4.4.

(a)

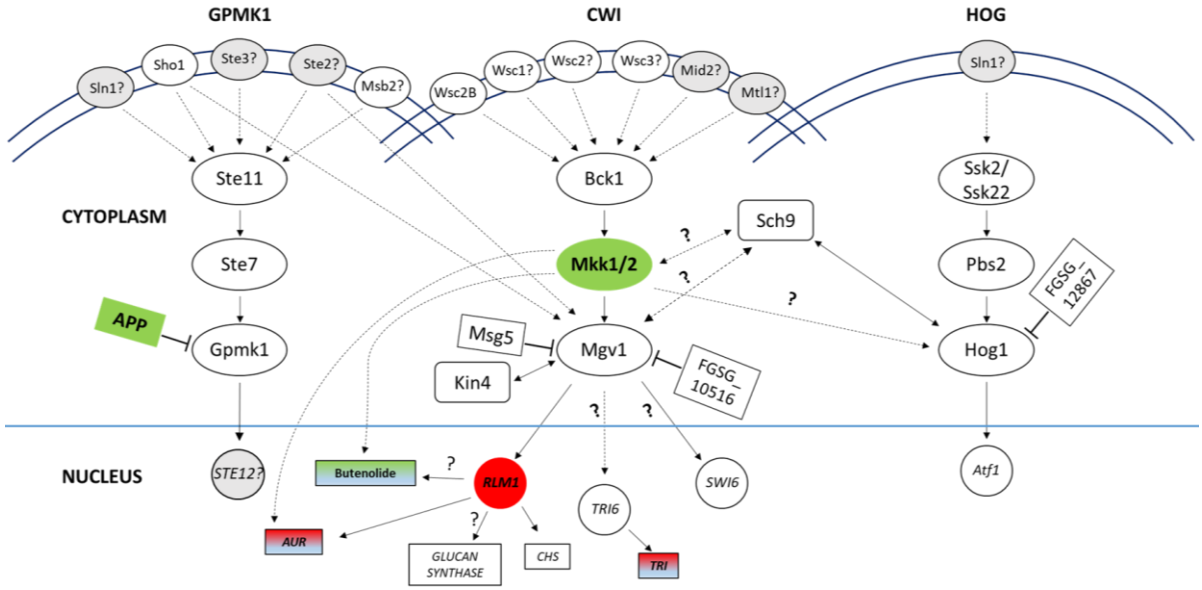
GPMK1
CWI
HOG
Sho1
Ste3?
Ste2?
Msb2?
Sln1?
Wsc1?
Wsc2?
Wsc3?
Wsc2B
Mid2?
Mtl1?
Sln1?
Ste11
Bck1
Ssk2/
Ssk22
CYTOPLASM
Sch9
Ste7
Mkk1/2
Pbs2
FGSG_
12867
App
Gpmk1
Msg5
Mgv1
Hog1
Kin4
FGSG_
10516
NUCLEUS
STE12?
Butenolide
RLM1
SWI6
Atf1
TRI6
AUR
GLUCAN
SYNTHASE
CHS
TRI

(b)

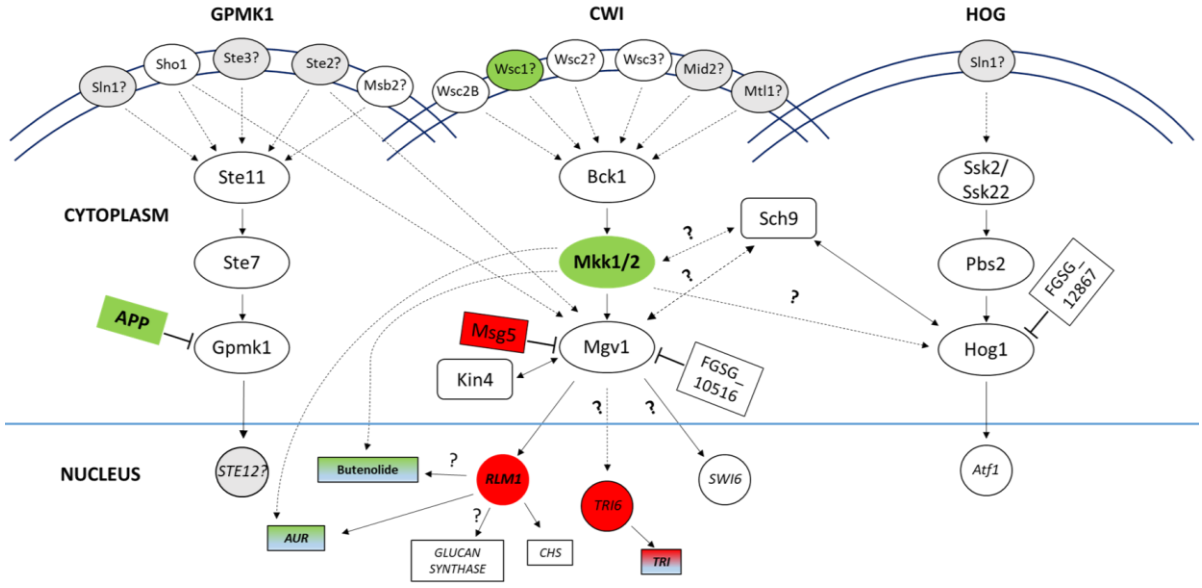
GPMK1
CWI
HOG
Sho1
Ste3?
Ste2?
Msb2?
Sln1?
Wsc1?
Wsc2?
Wsc3?
Wsc2B
Mid2?
Mtl1?
Sln1?
Ste11
Bck1
Ssk2/
Ssk22
CYTOPLASM
Sch9
Ste7
Mkk1/2
Pbs2
FGSG_
12867
App
Gpmk1
Msg5
Mgv1
Hog1
Kin4
FGSG_
10516
NUCLEUS
STE12?
Butenolide
RLM1
SWI6
Atf1
TRI6
AUR
GLUCAN
SYNTHASE
CHS
TRI

Figure 4.15. Representation of the three MAPK pathways in *F. graminearum*: GPMK1 (*Gibberella* pathogenicity MAPK1), CWI (cell wall integrity) and HOG (high osmolarity glycerol), and how the overexpression of *MKK1* **(a)** or *MKK1*^{197E,203E} **(b)** affected their components and some interacting elements (e.g. phosphatases, kinases, transcription factors, and genes involved in cell wall formation, or associated with secondary metabolite biosynthesis). The question marks (with arrows) represent a possible interaction between the elements, and in the case of receptors it represent a possible interaction, but not yet demonstrated. The discontinuous arrow represent that more elements might be between the two related components. Green colour represents genes that are upregulated, while red colour represents those downregulated. A combination of blue and green colours represent that some genes in the pathway were upregulated or not differentially expressed. A combination of red and blue colours represent that some genes were downregulated or not differentially expressed. Gray colour represents genes that were not included in the analysis. The schemes were made from the RNA-seq data.

The overexpression of *MKK1* does not mean that Mkk1 is a more active protein, therefore no additional phosphorylation of Mgv1 is necessarily expected, and indeed, was not observed (Figure 3.13), even though the tyrosine phosphatase *MSG5* (FGSG_06977) that negatively regulates Mgv1 (Yu *et al*., 2014) was downregulated in *MKK1*^{197E,203E}*_OXs*. Nevertheless, it is possible that a change in the stoichiometry of the core cascade components would alter the pathway somehow. Interestingly, the overexpression of *MKK1* and its putative phosphomimic did cause downregulation of the Mgv1 downstream target, the transcription factor *RLM1* (FGSG_09339), with a lower expression in *MKK1*^{197E,203E}*_OX* mutants.

It has been shown that Rlm1 is involved in the regulation of at least 25 genes associated with cell wall formation in *S. cerevisiae* (Jung and Levin, 1999), including the family of chitin synthases (*CHS*) and *β*-glucan synthase genes. These enzymes play a significant role in the formation of two of the major components of this structure: chitin and glucans. However, in the *CHS* family (*CHS1A, 1B, 3, 4, 5, 6* and *7*) and other chitin synthase-related proteins (FGSG_02729, FGSG_07937, FGSG_08673 and FGSG_16005), only *CHS5* (FGSG_01964) was differentially expressed in *MKK1_OXs* or *MKK1*^{197E,203E}*_OXs*, being downregulated in both cases (Supplementary Table 4.4). Chs5 is an enzyme localized in the cell membrane that transfers the

sugar from UDP-GlcNAc to the growing chitin (N-acetyl-*β*-D-glucosamine) polymer. Another downregulated gene in *MKK1*^{197E,203E}*_OXs* was a chitooligosaccharide oxidase (FGSG_10998) which oxidizes N-acetyl-D-glucosamine.

On the other hand, the 1,3-*β*-D-glucan-UDP glucosyltransferase, putative *FKS1* (FGSG_07946), which is involved in the synthesis of the 1,3-*β*-D-glucan, was neither differentially expressed in any of the *MKK1_OXs* or *MKK1*^{197E,203E}*_OXs.* Another protein involved in the cell wall formation, FGSG_09980, a *β*-1,3- glucanosyltransferase gel 1 precursor, was downregulated. This protein is involved in the elongation of the *β*-1,3-glucan chain in the cell wall since it splits a *β*-glucan chain and transfers the new generated reducing end to a non-reducing end. Possibly the downregulation of some of these genes involved in the cell wall formation was one of the causes for what the *MKK1_OXs* and *MKK1*^{197E,203E}*_OXs* colonies were smaller than the WT strain while growing on PDA, and for what they were more susceptible to a cell wall stress agent, such as CR (Figure 3.12).

In filamentous fungi, such as *B. cinerea*, the kinase Rim15 is considered another downstream of Mkk1, and Rim15 interactions with the kinase Sch9 regulates the secondary metabolite oxalic acid biosynthesis (Yin *et al*., 2018b). There is no report regarding interactions of Mkk1 with Rim5 (FGSG_01312) or Mkk1 with Sch9 (FGSG_00472) in *F. graminearum*, and these genes were not differentially expressed in *MKK1*^{197E,203E}*_OXs* or *MKK1_OXs*.

Moving upstream of the core proteins in the CWI pathway, Pkc1 (FGSG_09660), a protein known to phosphorylate Bck1 upon a particular stress, was not differentially expressed. However, there were some differences in the expression of other upstream elements in the cascade. The family receptors Wsc (cell wall and stress response component) are considered the sensors in the *S. cerevisiae* CWI pathway (Gray *et al*., 1997; Verna *et al*., 1997; Lodder *et al*.,

1999), but in *F. graminearum*, only Sho1 and Wsc2B have been suggested as upstream of the Mgv1 cascade (Qin *et al*., 2015; Xu *et al*., 2019). In this thesis, it was found that Sho1, Wsc2, Wsc2B and Wsc3 were not differentially expressed. Only Wsc1 and the gene FGSG_11097, that encodes for a protein with a WSC domain, were upregulated and downregulated, respectively, in both sets of strains, with a stronger effect in *MKK1*^{197E,203E}*_OXs* (Supplementary Table 4.4).

MAPKs have cross-talk with other cascade components (Yun *et al*., 2014), therefore a change in one member of the cascade might alter other elements in different pathways. In *MKK1_OXs* or *MKK1*^{197E,203E}*_OXs*, no variation in the expression of the core components of the HOG (Ssk2/Ssk22-Pbs2-Hog1) nor of the GPMK1 (Ste11/ste7/Gpmk1) cascades were observed (Supplementary Table 4.4). Interestingly, the gene that encodes for the phosphatase APP (FGSG_03333) that negatively affects Gpmk1 phosphorylation (Yun *et al*., 2015) was upregulated in both strains, but no changes in Gpmk1 phosphorylation were observed in Figure 3.13. Other phosphatases, such as FGSG_12867 and FGSG_10516, that negatively regulate Hog1 and Mgv1 phosphorylation, respectively (Yun *et al*., 2015), were not differentially expressed compared to the WT. Interestingly, the gene that encodes the tyrosine phosphatase *MSG5* (FGSG_06977) that has been suggested to dephosphorylates Mgv1 (Yu *et al*., 2014), was downregulated in *MKK1*^{197E,203E}*_OX*s, but no change in Mgv1 phosphorylation was observed in Figure 3.13.

4.4.2 Effect of *MKK1* or *MKK1*^{197E,203E} overexpression on secondary metabolite production

Three significant metabolite groups can be found in *Fusarium* species: terpenoids, non-ribosomal peptides (NRP) and polyketides. Some examples in the terpenoid group include the sesquiterpenes DON and T2-toxin, while NRPs include enniatin, beauvericin, fusaoctaxin A and grammilin, and polyketides encompass zearalenone, Fusarin C, aurofusarin and orsellinic acid. In

F. graminearum 17 terpenoid synthases, 19 NRPS and 15 PKS have been identified, but only a few of these enzymes are associated with identified products or metabolites (Gaffoor *et al*., 2005; Hansen *et al*., 2012; Sieber *et al*., 2014). A list of PKS and NRPS obtained from Sieber *et al*. (2014) was used as a baseline for analyzing the regulation of the genes involved in these metabolite clusters. An overview of the expression of *NRPS, PKS* and some secondary metabolite gene clusters, is summarized in Supplementary Table 4.3.

It has been shown that the CWI pathway is involved in the regulation of secondary metabolite biosynthesis in *F. graminearum*, such as trichothecenes (i.e. DON), butenolide and aurofusarin (Hou *et al*., 2002; Rampitsch *et al*., 2010; Rampitsch *et al*., 2011; Yun *et al*., 2014). Part of this thesis (Chapter 2) was recently published by Shostak (2020), where it was found that Mgv1 might regulate some metabolite pathways, including the trichothecenes, through the transcription factor *TRI6*. In this biosynthetic pathway, *TRI6*, as well as most of the *TRI* genes, was not differentially expressed. The genes that were no differentially expressed were then downregulated. Therefore, under the conditions that the RNA-seq analysis was performed in this chapter, which was not a trichothecene-inducing environment, these strains will probably not produce more trichothecenes than the WT (Supplementary Table 4.3 D).

Butenolide (4-acetamido-4-hydroxy-2-butenoic acid gamma-lactone) is another secondary metabolite produced by *Fusarium* species, including *F. graminearum*. This metabolite is toxic to mammalians, where it has been associated with myocardial toxicity in rats, and with Keshan disease in humans (Liu *et al*., 2007; Wang *et al*., 2009). In addition, it can increase the toxicity of DON in human liver cells (HepG2) (Woelflingseder *et al*., 2018). However, it does not play a significant role in virulence in wheat plants, or at least the authors found that it is not involved in

the pathogen spread in wheat heads after they were point inoculated, but it is unknown if it could be involved in initial infection process (Harris *et al*., 2007).

The butenolide and the trichothecene biosynthesis clusters had a strong correlation in their expression patterns, and these pathways are usually induced under nutrient limitation conditions (Harris *et al*., 2007; Rampitsch *et al*., 2011; Sieber *et al*., 2014). In this thesis, the RNA-seq analysis was not carried out under these conditions, and these results should be considered in that context.

A few genes from the trichothecene biosynthetic pathway were downregulated in *MKK1*^{197E,203E}*_OX*, but all the eight genes in the butenolide pathway (FGSG_08077-FGSG_08084) were upregulated (Supplementary Table 4.3 B). In *MKK1_OX* some of the *TRI* genes were also downregulated, and three (from the eight) of the butenolide genes were upregulated. This is the first time it is reported that the expression of one of these two metabolic pathways is separated from the other one. In addition, a medium with nutrient limitation was not necessary for inducing the expression of these genes, which may also explain the downregulation of *TRI* genes. Interestingly, it appears that the butenolide could be produced by *F. graminearum* when *MKK1* is overexpressed, and even more could be obtained in *MKK1*^{197E,203E}*_OX*. However, an increase in gene expression does not always lead to a higher metabolite accumulation, and some post-transcriptional modifications may need to take place for increasing the metabolite production. For example, Rampitsch *et al*. (2011) showed that the expression of two regulatory genes in the *TRI* cluster did not change in a *Δmgv1* mutant compared to WT while growing under nutrient-limiting conditions, but the accumulation of DON was significantly lower compared to the WT. For a better understanding of the relationship between these pathways (CWI,

trichothecenes and butenolide), and whether nutrient limitations can enhance butenolide production in these strains, a metabolite profile in DON-induction media could be performed.

Shostak (2020) showed that most of the butenolide gene cluster seemed to be positively regulated by the transcription factor *TRI6* and by Mgv1, except for FGSG_08077, FGSG_08080 and FGSG_08081, which were not regulated by the MAPK. In accordance with those results, the genes FGSG_08079, FGSG_08083, as well as FGSG_08081 (which was not regulated by Mgv1), were upregulated in *MKK1_OX* transformants, confirming that the CWI pathway is involved in the regulation of this secondary metabolite. When the putative phosphomimic *MKK1*^{197E,203E} was overexpressed, all the genes in the butenolide cluster were upregulated, including the gene FGSG_08076, that according to Sieber *et al*. (2014), is also part of this cluster. However, the fact that *TRI6* is not differentially expressed, is not concordant with the hypothesis that Mgv1 and *TRI6* positively regulate the butenolide gene cluster. Nevertheless, this hypothesis refers to strains that grew in DON-inducing conditions, which is not the case in this chapter, and that could be what triggers the difference between both results.

Moreover, it was shown in the previous chapter that Mgv1 was less phosphorylated in *MKK1_OX* and in the putative phosphomimic *MKK1*^{197E,203E} compared to the WT, but a similar Mgv1 band was observed among all of the transformants (Figure 3.13). Yet, there was an increase in butenolide gene expression. These results might suggest that this metabolite gene cluster is not regulated through Mgv1 activation since no higher Mgv1 phosphorylation levels were observed but the opposite if compared to WT. In addition, most of the genes associated with the CWI pathway that are regulated by Mgv1 and/or its downstream, Rlm1, were not differentially expressed. Taking all this information into consideration, it could be hypothesized

that the CWI pathway regulates the butenolide gene cluster through Mkk1, Mgv1 or *TRI6*, with another possible intermediary.

From the 15 *PKS* identified in *F. graminearum* (Sieber *et al*., 2014) seven were differentially regulated in *MKK1_OX*s or *MKK1*^{197E,203E} *_OXs* strains, and all of them were downregulated (Supplementary Table 4.3 F). Both strains shared downregulation of *PKS1* and *PKS7*, associated with the clusters 31 and 44, respectively, which do not have a known product. Nevertheless, *PKS7* was recently found involved in perithecial development and hyphal growth (Kim *et al*., 2021). Other *PKS* that were downregulated only in *MKK1*^{197E,203E} *_OXs*, were *PKS10* (involved in the biosynthesis of Fusarin C), *PKS23*, *PKS24* (Fusarielin) and *PKS28* (orsellinic acid), which are part of the 42, 47, 60 and 18 gene clusters, respectively. In *MKK1_OX*s, in addition to the downregulated *PKS* that were shared by both strains, the other downregulated *PKS* was *PKS26* (FGSG_02324), also known as *PKS12*, which is involved in the aurofusarin pathway.

Aurofusarin is a red fungal pigment, a polyketide produced by some microorganisms, such as *F. graminearum* (Frandsen *et al*., 2006; Frandsen *et al*., 2011; Westphal *et al*., 2018a). Its biosynthetic cluster is composed of 10 genes (FGSG_02320-02329) plus a gene outside of the cluster, the laccase *AURL* (FGSG_02330), that is not necessary for aurofusarin production (Frandsen *et al*., 2006; Westphal *et al*., 2018a). Half of the aurofusarin biosynthetic gene cluster was downregulated in *MKK1_OX* transformants (Supplementary Table 4.3 A), suggesting that Mkk1 might negatively regulates this metabolite production.

The results obtained in the 2nd thesis chapter and by Shostak (2020) when *MGV1* was deleted, also suggested that the CWI pathway, in particular Mgv1, negatively regulates aurofusarin production. In a *Δmgv1* mutant was observed that the aurofusarin biosynthetic genes were upregulated, and the metabolite production was higher than the WT at 6 and 12 days after

growing in DON-inducing media (Tables 2.8 and 2.9). However, there was also some increase in the expression of some of the aurofusarin genes when *MGV1* was overexpressed (Table 2.9), but no differences were observed in this metabolite accumulation (Table 2.8) or in the colour of the colonies (Figure 2.24). Surprisingly, *Δmgv1* colony lacked the reddish colour in spite of upregulation of most of the aurofusarin genes (Figure 3.12), and in this mutant only *AURT*, a major facilitator superfamily transporter involved in pumping rubrofusarin (a precursor of aurofusarin) through the membrane, was not differentially expressed. AurT plays a significant role in the biosynthesis of this pigment because rubrofusarin needs to be pumped out through the membrane to be converted into aurofusarin by the complex Gip1-AurF-AurO-AurS *(Frandsen et al*., 2011). Therefore, maybe if *AURT* is not upregulated when the other biosynthetic genes are upregulated, there is no transport of the aurofusarin precursor through the membrane, and no more aurofusarin is produced by the mutant. Thus, the *Δmgv1* mutant colony lacks the red pigment. These results suggest that maybe some genes in the pathway might be regulated by other components.

In a previous study it was shown that the aurofusarin gene cluster was negatively affected by *TRI6*, and it has been proposed that Mgv1 regulation of this metabolite might be through this transcription factor (Shostak, 2020). However, other authors showed that some genes in the cluster (*AURJ*, *AURF* and *AURO*) were downregulated in *Δmkk1*, a mutant that also showed a less red-pigmented colony than the WT (Yun *et al*., 2014). This led to the suggestion that there was a positive regulation of the aurofusarin pathway by the CWI cascade, contrary to what we later observed. Surprisingly, the overexpression of the putative phosphomimic $MKK1^{197E,203E}$ did not affect the expression of most of the genes in the aurofusarin cluster, except for *AURT* and *AURR2*, that were upregulated. *AURR2* is a transcription factor, a possible co-regulator of

AURR1 (a TF and main regulator of the aurofusarin biosynthetic pathway), and it is known that *AURR2* deletion affects the ratio rubrofusarin/aurofusarin, by increasing rubrofusarin production. Interestingly, *AURR2* was also upregulated in *Δmgv1* (Chapter 2, and Shostak (2020)). However, *AURT* is not regulated by Mgv1 (Chapter 2, and Shostak (2020)). If taking into consideration that *Δmgv1* colony does not have the reddish colour as it is observed in the reverse of *MKK1*^{197E,203E}*_OX* colonies while growing on PDA (Figure 3.12), and that *AURT* was not differentially expressed in *Δmgv1*, but it was upregulated in *MKK1*^{197E,203E}*_OX*, it could be suggested that it might be a co-regulation of the biosynthesis pigment that includes Mgv1 but also Mkk1. For a more comprehensive result of how the CWI cascade might affect this pigment production, more assays involving metabolite accumulation that include a *Δmkk1* mutant and an *MKK1_OX* transformant are strongly recommended.

Six from the 19 NRPS identified were at least two-fold differentially expressed in *MKK1_OX* or *MKK1*^{197E,203E} *_OX* (Supplementary Table 4.3 E). In *MKK1*^{197E,203E} *_OX*, *NRPS6, NRPS7*, *NRPS13* and *NRPS15* were downregulated. In *MKK1_OX* transformants, *NRPS9*, which belongs to the fusaoctaxin A cluster was also downregulated. The only differentially expressed *NRPS* shared by both strains was *NRPS11*, that was upregulated with higher values in *MKK1*^{197E,203E} *_OX*. This gene encodes a hypothetical protein localized in the membrane, with a ferredoxin reductase (FNR) domain, an amino acid adenylation domain, and an AMP-binding domain, according to NCBI and UniProtKB database. The gene was included in the "disease, virulence and defense" Funcat description that belongs to the "cell rescue, defense and virulence" main category, as well as in the "metabolism of polyketides" from the main category "metabolism" in *MKK1*^{197E,203E} *_OX* vs WT analysis. However, its was not selected for the gene list of the most significant descriptions when *MKK1_OX* was compared to WT. There is no much

information regarding its cluster product but it was *in planta* detected after maize, barley and wheat were inoculated with *F. graminearum* (Harris *et al*., 2016).

In summary, the overexpression of *MKK1* or *MKK1*^{197E,203E} did not affect the expression of most of the genes involved in the CWI pathway nor did it affect expression of genes in the two other MAPK pathways. Therefore, the reduced mycelial growth phenotype observed in the previous chapter might be more associated with post-translational modifications, such as phosphorylation, than with the expression of genes associated with the cell wall formation. Moreover, the expression of secondary metabolite clusters did appear to be under the regulation of Mkk1, directly or indirectly. Nevertheless, additional work is needed to determine whether and how the metabolomic profiles are altered in *MKK1_OX* or *MKK1*^{197E,203E}*_OX*.

Chapter 5. Conclusions and future directions

The original goal of this thesis was to generate a *F. graminearum* strain able to produce high amounts of a phosphorylated Mgv1 protein that could be isolated and purified to screen candidate Mgv1 targets, identified by Rampitsch *et al*. (2010). For that purpose, I generated two main lines of transformants/mutants: *i*) a transformant overexpressing *MGV1 in locus*; *ii*) a putative constitutively active Mkk1 mutant which overexpress *MKK1*^{197E,203E} *in locus*. Unexpectedly, the *MKK1*^{197E,203E} modification did not increase Mgv1 phosphorylation. The observed changes redirected the objectives of this thesis towards the characterization of these strains in order to get a better understanding of how this modification in Mkk1 could trigger other responses.

5.1 Summary of findings

In this thesis, it was observed that transformants overexpressing *MGV1* produced more phosphorylated Mgv1 protein than the WT strain. This overexpression does not alter the phenotype (morphocultural pattern, conidia germination, or virulence towards wheat and *B. distachyon* plants) of *F. graminearum*, but it does provoke some biochemical changes (i.e. increase 15-ADON and other metabolite accumulation in axenic cultures).

Interestingly, the overexpression of *MKK1* negatively affected mycelial growth, with a stronger effect in the putative phosphomimic *MKK1*^{197E,203E}*_OX*. These strains had a similar growth rate to *Δmgv1* and *Δmkk1*, mutants that are less pathogenic, and with a suggested reduction in DON production in wheat heads (Hou *et al*., 2002; Yun *et al*., 2014). In addition, *MKK1_OX* and *MKK1*^{197E,203E}*_OX* strains produced more or similar amounts of 15-ADON in axenic cultures, respectively, compared to WT, but the disease that these strains provoked in wheat heads was diminished, and the disease caused by them was comparable to that caused by *Δmgv1*.

The overexpression of *MKK1*^{197E,203E} does not produce a phosphomimic. In fact, the overexpression of *MKK1* and *MKK1*^{197E,203E} reduced the phosphorylation of Mgv1, and increased the susceptibility to the cell wall stressor CR, an unexpected result for *MKK1*^{197E,203E}*_OX* that was more sensitive than any tested strain, including *Δmgv1*. Surprisingly, the overexpression of *MKK1*^{197E,203E} increased the abundance and phosphorylation of the MAPK, Hog1, and the resistance to osmotic stress. In addition, it seems that the mutants *MKK1*^{197E,203E}*_OX* and *Δmgv1* behave similarly regarding mycelial growth, 15-ADON production in axenic culture, virulence towards wheat heads, and resistance to CR and to osmotic stress. These findings suggest that the overexpression of *MKK1* with these amino acid changes in the activation loop might turn off the CWI pathway while turns on the HOG cascade.

Regarding secondary metabolites, it seems that Mkk1 and Mgv1 play a significant role in the regulation of different gene clusters, including trichothecenes, butenolide and aurofusarin. In particular, the effect of the overexpression of *MKK1* or *MKK1*^{197E,203E} towards the transcription of those genes was more significant than overexpressing *MGV1*.

5.2 Proposed future directions

MGV1_OX strains produce a high amount of phosphorylated Mgv1 protein, therefore it could be used for future assays to identify more Mgv1 targets. To date, only the transcription factor Rlm1 and the kinase Kin4 have been proposed as its downstream components in the CWI cascade (Wang *et al*., 2011; Yun *et al*., 2014), but as a MAPK, a myriad of targets is expected to be found. The phosphorylated form of Mgv1 could be purified (as a His-tag has been incorporated in the sequence) and used to screen some of its previously identified candidate targets (Rampitsch *et al.*, 2010) through kinase activity assays. In addition, the interaction between Mgv1 and its target could be validated, for example, through Yeast two-hybrid (Y2H) or

with Co-Immunoprecipitation (Co-IP) assays. Once the targets are identified, those that are transcription factors could be used in ChIP-seq (Chromatin immunoprecipitation) assay to identify which genes they regulate. Thus, more complete information regarding the components and the impact of the CWI pathway in *F. graminearum* will be obtained.

In my opinion, *Δmkk1* should be used as a control for the experiments involving *MKK1* mutants, as it will provide more complete information regarding the effect of this CWI component in its interaction with other proteins, and the effects on the cell. While writing this thesis, I have generated this mutant that shows slow mycelial growth on solid media (data not shown), similarly to the *Δmkk1* generated by Yun *et al*. (2014), and it should be included in the next assays with other *MKK1* mutants.

In this thesis and it previous report, it has been shown that the components of the CWI cascade regulate secondary metabolite production in fungal species (Rampitsch *et al*., 2011; Yun *et al*., 2014; Yin *et al*., 2018b; Shostak, 2020). However, fungal growth conditions have an impact in metabolite production. Therefore, in order to provide a deeper comprehension about the effect of Mkk1 in secondary metabolite production, more assays (such as RNA-seq analysis and metabolomics) could be performed under DON-inducing conditions, similarly to what was done for Mgv1. For example, one of the subjects to analyze will be if the observed difference between butenolide and trichothecene production (when non DON-inducing conditions were present) will be kept in a media that promotes metabolite production.

The nature of the interaction between HOG and CWI cascades is not completely known, hence, it will be interesting to study the cross-talk between both pathways. It was observed that the overexpression of *MKK1* or $MKK1^{197E,203E}$ (with a stronger effect in the latter) turned off the CWI cascade (i.e. increased the susceptibility to CR and decreased Mgv1 phosphorylation), but

increased the resistance to osmotic stress (i.e. higher abundance and phosphorylation of Hog1, and less affected mycelial growth in 1 M NaCl). These bring three main avenues for future directions:

1. Identify interacting partners of Mkk1. Since the Mkk1 protein in the *MKK1_OX* and the *MKK1*^{197E,203E}*_OX* strains possess a His-tag, this protein could be purified with Ni^{2+} or Co^{2+} columns, and the sample could be used in Western blotting with antibodies anti-p38 (Hog1) and anti-ERK (phosphorylated and unphosphorylated antibodies) for a quick check to identify which MAPK interacts with Mkk1. In addition, Mkk1 could be used in Co-IP and Y2H assays to validate its interaction with another protein.
2. There is the question of whether more elements could regulate the switch between these pathways, such as the kinase Rim15 or Sch9. In *B. cinerea*, the kinase Rim15 has been proposed as another Mkk1 downstream target (Yin *et al*., 2018b). Another kinase, Sch9, can also phosphorylate Rim15, and depending on which upstream element succeed in phosphorylating Rim15, the activity of this protein could be turned on or off in *B. cinerea* (Yin *et al*., 2018b). Extrapolating these results, one might consider that the *F. graminearum* Rim15 or Sch9 proteins could play a key role in the switch between pathways, since it is already known that Sch9 interacts with Hog1 in this pathogen (Gu *et al*., 2015). In addition, the deletion of Sch9 (FGSG_00472) affected DON accumulation, virulence and conidiation on wheat spikes and corn silks (Chen *et al.*, 2014), an effect also associated with the CWI pathway. In order to identify if Mkk1 interacts with Sch9 or Rim15, the same assays mentioned in the previous bullet point could be performed, but maybe antibodies anti-Sch9 and anti-Rim15 should be designed if they are not available.

3. The cross-talk between the HOG and the CWI cascades could also be studied through the components in the HOG pathway, such as Pbs2. It was shown that *PBS2* deletion inhibited Hog1 phosphorylation (Zheng *et al*., 2012), even when Mkk1 was present. Hence, in a *Δpbs2* the MAPK Mkk1 does not automatically phosphorylate Hog1, but the overexpression of $MKK1^{197E,203E}$ increased Hog1 abundance and phosphorylation. Therefore, a combination of assays with *Δmkk1 Δpbs2*, *MKK1_OX*, $MKK1^{197E,203E}$*_OX*, *PBS2_OX*, and double mutants generated with the combination of *Δpbs2 or Δmkk1* with $MKK1^{197E,203E}$*_OX* (or *MKK1_OX*) or *PBS2_OX*, could offer a more complete understanding of the cross-talk between the HOG and the CWI cascades. The double mutants could be generated using two different vectors or CRISPR/Cas system, and a His-Tag in the proteins will offer a suitable manner of purification.

As the original main goal of the thesis was to generate a mutant that enables constitutive activation of Mgv1, and that was not obtained in this thesis, another proposition is to generate an $MKK1^{197D,203D}$_OX mutant that will have Asp amino acids in lieu of the two Thr amino acids that are phosphorylated in the activation loop. A similar and successful change was accomplished in *M. grisea* (Fujikawa *et al*., 2009). If successfully obtained in *F. graminearum*, this will allow us to understand the changes in the cell that will be generated by continuous phosphorylation of Mgv1. In addition, Mgv1 could be purified in its phosphorylated form and could be used in kinase activity assays for screening its targets.

To continue with the studies using a modification in the activation loop, $MKK1^{197A,203A}$_OX, a null mutant with a change in the Thr amino acids for Ala (this will inhibit the phosphorylation of the MAPKK, therefore it will be inactive and unable to phosphorylate any other protein) will provide a more complete picture of how a non-active MAPKK can affect *F. graminearum* strain.

The mutants *Δmkk1*, *MKK1_OX*, *MKK1*^{197E,203E}*_OX*, *MKK1*^{197D,203D}*_OX* and *MKK1*^{197A,203A}*_OX* will contribute to understanding in which processes this cascade, and in particular Mkk1, is involved. Characterization of these strains regarding *i*) phenotype (morphology, formation of reproductive structures, and virulence), *ii*) transcriptomic, proteomic and metabolomic profiles, and *iii*) their response to different types of stresses that could trigger any of the three MAPK pathways (osmotic stress, cell wall damaging agents or chemotropic compounds) will provide more insight into the function of this MAPKK and the CWI cascade in general. In addition, the study of the phosphatome and kinome on these strains will be an interesting approach for a better understanding of the MAPK cascades and their interaction with phosphatases and other kinases.

In addition to the mutants with overexpression or deletion of *MGV1* (MAPK) and *MKK1* (MAPKK), the generation of mutants with deletion or overexpression of *BCK1* (the MAPKKK of the CWI pathway) could offer a more complete study of this cascade. I have initiated this process towards obtaining *Δbck1* and *BCK1_OX* for future studies. Moreover, a combination of mutants overexpressing and/or with deletion of these genes will help to understand the effect of each component in the regulation of processes associated with the pathway.

Bibliography

Alexander, N.J., McCormick, S.P., Larson, T.M., and Jurgenson, J.E. 2004. Expression of Tri15 in *Fusarium sporotrichioides*. Curr. Genet. 45:157-162.

Alisaac, E., Rathgeb, A., Karlovsky, P., and Mahlein, A.-K. 2021. Fusarium head blight: effect of infection timing on spread of *Fusarium graminearum* and spatial distribution of deoxynivalenol within wheat spikes. Microorganisms 9:79.

Alvarez-Buylla, E.R., Pelaz, S., Liljegren, S.J., Gold, S.E., Burgeff, C., Ditta, G.S., Ribas de Pouplana, L., Martínez-Castilla, L., and Yanofsky, M.F. 2000. An ancestral MADS-box gene duplication occurred before the divergence of plants and animals. Proc. Natl. Acad. Sci. U.S.A. 97:5328-5333.

Alvaro, C.G., and Thorner, J. 2016. Heterotrimeric G protein-coupled receptor signaling in yeast mating pheromone response. J. Biol. Chem. 291:7788-7795.

Bahadoor, A., Brauer, E.K., Bosnich, W., Schneiderman, D., Johnston, A., Aubin, Y., Blackwell, B., Melanson, J.E., and Harris, L.J. 2018. Gramillin A and B: Ccclic lipopeptides identified as the nonribosomal biosynthetic products of *Fusarium graminearum*. J. Am. Chem. Soc. 140:16783-16791.

Bai, G.H., Desjardins, A.E., and Plattner, R.D. 2002. Deoxynivalenol-nonproducing *Fusarium graminearum* causes initial infection, but does not cause disease spread in wheat spikes. Mycopathologia 153:91-98.

Beyer, M., Röding, S., Ludewig, A., and Verreet, J.-A. 2004. Germination and survival of *Fusarium graminearum* macroconidia as affected by environmental factors. J. Phytopathol. 152:92-97.

Boodley, J.W., and Sheldrake, R.J. 1972. Cornell pite-lite mixes for comercial plant growing. New York State College of Agriculture and Life Sciences, Cornell University, Ithaca, NY

Boulton, T., Yancopoulos, G., Gregory, J., Slaughter, C., Moomaw, C., Hsu, J., and Cobb, M. 1990. An insulin-stimulated protein kinase similar to yeast kinases involved in cell cycle control. Science 249:64-67.

Boulton, T.G., Gregory, J.S., and Cobb, M.H. 1991a. Purification and properties of extracellular signal-regulated kinase 1, an insulin-stimulated microtubule-associated protein 2 kinase. Biochemistry 30:278-286.

Boulton, T.G., Nye, S.H., Robbins, D.J., Ip, N.Y., Radzlejewska, E., Morgenbesser, S.D., DePinho, R.A., Panayotatos, N., Cobb, M.H., and Yancopoulos, G.D. 1991b. ERKs: A family of protein-serine/threonine kinases that are activated and tyrosine phosphorylated in response to insulin and NGF. Cell 65:663-675.

Brown, D.W., Dyer, R.B., McCormick, S.P., Kendra, D.F., and Plattner, R.D. 2004. Functional demarcation of the *Fusarium* core trichothecene gene cluster. Fungal Genet. Biol. 41:454-462.

Brown, D.W., Lee, S.-H., Kim, L.-H., Ryu, J.-G., Lee, S., Seo, Y., Kim, Y.H., Busman, M., Yun, S.-H., Proctor, R.H., and Lee, T. 2015. Identification of a 12-gene Fusaric Acid biosynthetic gene cluster in *Fusarium* species through comparative and functional genomics. Mol. Plant Microbe Interact. 28:319-332.

Burkholder, A.C., and Hartwell, L.H. 1985. The yeast alpha-factor receptor: structural properties deduced from the sequence of the STE2 gene. Nucleic Acids Res. 13:8463-8475.

Canadian Plant Disease Survey 2020 Volume 100: Disease Highlights 2019. 2020. Can. J. Plant Pathol. 42:1-175.

Chen, D., Wang, Y., Zhou, X., Wang, Y., and Xu, J.-R. 2014. The Sch9 kinase regulates conidium size, stress responses, and pathogenesis in *Fusarium graminearum*. PLoS One 9:e105811.

Chen, F., Zhang, J., Song, X., Yang, J., Li, H., Tang, H., and Liao, Y.-C. 2011. Combined metabonomic and quantitative Real-Time PCR analyses reveal systems metabolic changes of *Fusarium graminearum* induced by Tri5 gene deletion. J. Proteome Res. 10:2273-2285.

Chen, R.E., and Thorner, J. 2007. Function and regulation in MAPK signaling pathways: Lessons learned from the yeast *Saccharomyces cerevisiae*. BBA, Biochim. Biophys. Acta - Mol. Cell Res. 1773:1311-1340.

Cong, J., Chengkang, Z., Chunlan, W., Panpan, S., Rui, H., Huiquan, L., Chenfang, W., and Jin-Rong, X. 2016. *TRI6* and *TRI10* play different roles in the regulation of deoxynivalenol (DON) production by cAMP signalling in *Fusarium graminearum*. Environ. Microbiol. 18:3689-3701.

Connolly, L.R., Smith, K.M., and Freitag, M. 2013. The *Fusarium graminearum* histone H3 K27 methyltransferase KMT6 regulates development and expression of secondary metabolite gene clusters. PLoS Genet. 9:e1003916-e1003916.

Cristina, M.R., and Concepcion, H. 2016. The F-box protein Fbp1 functions in the invasive growth and cell wall integrity mitogen-activated protein kinase (MAPK) pathways in *Fusarium oxysporum*. Mol. Plant Pathol. 17:55-64.

Cundliffe, E., Cannon, M., and Davies, J. 1974. Mechanism of inhibition of eukaryotic protein synthesis by trichothecene fungal toxins. Proc. Natl. Acad. Sci. U.S.A. 71:30-34.

Cuzick, A., Urban, M., and Hammond-Kosack, K. 2008. *Fusarium graminearum* gene deletion mutants *map1* and *tri5* reveal similarities and differences in the pathogenicity

requirements to cause disease on *Arabidopsis* and wheat floral tissue. New Phytol. 177:990-1000.

D'Aquino, K.E., Monje-Casas, F., Paulson, J., Reiser, V., Charles, G.M., Lai, L., Shokat, K.M., and Amon, A. 2005. The protein kinase Kin4 inhibits exit from mitosis in response to spindle position defects. Mol. Cell 19:223-234.

Damveld, R.A., Arentshorst, M., Franken, A., VanKuyk, P.A., Klis, F.M., Van Den Hondel, C.A.M.J.J., and Ram, A.F.J. 2005. The *Aspergillus niger* MADS-box transcription factor RlmA is required for cell wall reinforcement in response to cell wall stress. Mol. Microbiol. 58:305-319.

David, S., Antonio, D.P., Elena, P.N., and David, T. 2017. Three *Fusarium oxysporum* mitogen-activated protein kinases (MAPKs) have distinct and complementary roles in stress adaptation and cross-kingdom pathogenicity. Mol. Plant Pathol. 18:912-924.

Davis, R.J. 1994. MAPKs: new JNK expands the group. Trends Biochem. Sci. 19:470-473.

de Groot, P.W., Ruiz, C., Vázquez de Aldana, C.R., Duenas, E., Cid, V.J., Del Rey, F., Rodríquez-Peña, J.M., Pérez, P., Andel, A., Caubín, J., Arroyo, J., García, J.C., Gil, C., Molina, M., García, L.J., Nombela, C., and Klis, F.M. 2001. A genomic approach for the identification and classification of genes involved in cell wall formation and its regulation in *Saccharomyces cerevisiae*. Comp. Funct. Genom. 2:124-142.

de Nadal, E., Casadomé, L., and Posas, F. 2003. Targeting the MEF2-like transcription factor Smp1 by the stress-activated Hog1 mitogen-activated protein kinase. Mol. Cell. Biol. 23:229-237.

Decloedt, A.I., Van Landschoot, A., Watson, H., Vanderputten, D., and Vanhaecke, L. 2017. Plant-Based Beverages as Good Sources of Free and Glycosidic Plant Sterols. Nutrients 10.

Del Ponte, E.M., Fernandes, J.M.C., and Bergstrom, G.C. 2007. Influence of growth stage on Fusarium head blight and deoxynivalenol production in wheat. J. Phytopathol. 155:577-581.

Dephoure, N., Gould, K.L., Gygi, S.P., and Kellogg, D.R. 2013. Mapping and analysis of phosphorylation sites: a quick guide for cell biologists 24:535-542.

Desjardins, A.E., Bai, G.-h., Plattner, R.D., and Proctor, R.H. 2000. Analysis of aberrant virulence of *Gibberella zeae* following transformation-mediated complementation of a trichothecene-deficient (Tri5) mutant. Microbiology 146:2059-2068.

Di Pietro, A., García-Maceira, F.I., Méglecz, E., and Roncero, M.I.G. 2001. A MAP kinase of the vascular wilt fungus *Fusarium oxysporum* is essential for root penetration and pathogenesis. Mol. Microbiol. 39:1140-1152.

Ding, Z., Xu, T., Zhu, W., Li, L., and Fu, Q. 2020. A MADS-box transcription factor FoRlm1 regulates aerial hyphal growth, oxidative stress, cell wall biosynthesis and virulence in *Fusarium oxysporum* f. sp. *cubense*. Fungal Biol. 124:183-193.

Ding, Z., Yang, L., Wang, G., Guo, L., Liu, L., Wang, J., and Huang, J. 2018. Fusaric acid is a virulence factor of *Fusarium oxysporum* f. sp. *cubense* on banana plantlets. Trop. Plant Pathol. 43:297-305.

Dissmeyer, N., and Schnittger, A. 2011. Use of Phospho-Site Substitutions to Analyze the Biological Relevance of Phosphorylation Events in Regulatory Networks. Pages 93-138 in: Plant Kinases: Methods and Protocols, N. Dissmeyer and A. Schnittger, eds. Humana Press, Totowa, NJ.

Dodou, E., and Treisman, R. 1997. The *Saccharomyces cerevisiae* MADS-box transcription factor Rlm1 is a target for the Mpk1 mitogen-activated protein kinase pathway. Mol. Cell. Biol. 17:1848-1859.

Dohlman, H.G., Thorner, J., Caron, M.G., and Lefkowitz, R.J. 1991. Model systems for the study of seven-transmembrane-segment receptors. Annu. Rev. Biochem. 60:653-688.

Doohan, F.M., Weston, G., Rezanoor, H.N., Parry, D.W., and Nicholson, P. 1999. Development and use of a Reverse Transcription-PCR assay to study expression of *TRI5* by *Fusarium* species *in vitro* and *in planta*. Appl. Environ. Microbiol. 65:3850-3854.

Douglas, C.M., Foor, F., Marrinan, J.A., Morin, N., Nielsen, J.B., Dahl, A.M., Mazur, P., Baginsky, W., Li, W., el-Sherbeini, M., and et al. 1994. The *Saccharomyces cerevisiae* FKS1 (ETG1) gene encodes an integral membrane protein which is a subunit of 1,3-beta-D-glucan synthase. Proc. Natl. Acad. Sci. U.S.A. 91:12907-12911.

Dweba, C.C., Figlan, S., Shimelis, H.A., Motaung, T.E., Sydenham, S., Mwadzingeni, L., and Tsilo, T.J. 2017. Fusarium head blight of wheat: Pathogenesis and control strategies. Crop Prot. 91:114-122.

Edite Bezerra da Rocha, M., Freire, F.d.C.O., Erlan Feitosa Maia, F., Izabel Florindo Guedes, M., and Rondina, D. 2014. Mycotoxins and their effects on human and animal health. Food Control 36:159-165.

El-Defrawy, M.M.H., and Hesham, A.E.-L. 2020. G-protein-coupled receptors in Fungi. Pages 37-126 in: Fungal Biotechnology and Bioengineering, A.E.-L. Hesham, R.S. Upadhyay, G.D. Sharma, C. Manoharachary, and V.K. Gupta, eds. Springer International Publishing, Cham.

Fleming, A. 1929. On the antibacterial action of cultures of a *Penicillium*, with special reference to their use in the isolation of *B. influenzæ*. Br. J. Exp. Pathol. 10:226-236.

Foroud, N.A., McCormick, S.P., MacMillan, T., Badea, A., Kendra, D.F., Ellis, B.E., and Eudes, F. 2012. Greenhouse studies reveal increased aggressiveness of emergent Canadian *Fusarium graminearum* chemotypes in wheat. Plant Dis. 96:1271-1279.

Foroud, N.A., Baines, D., Gagkaeva, T.Y., Thakor, N., Badea, A., Steiner, B., Bürstmayr, M., and Bürstmayr, H. 2019. Trichothecenes in cereal grains – an update. Toxins 11:634.

Frandsen, R.J., Schütt, C., Lund, B.W., Staerk, D., Nielsen, J., Olsson, S., and Giese, H. 2011. Two novel classes of enzymes are required for the biosynthesis of aurofusarin in *Fusarium graminearum*. J. Biol. Chem. 286:10419-10428.

Frandsen, R.J.N., Nielsen, N.J., Maolanon, N., Sørensen, J.C., Olsson, S., Nielsen, J., and Giese, H. 2006. The biosynthetic pathway for aurofusarin in *Fusarium graminearum* reveals a close link between the naphthoquinones and naphthopyrones. Mol. Microbiol. 61:1069-1080.

Frandsen, R.J.N., Rasmussen, S.A., Knudsen, P.B., Uhlig, S., Petersen, D., Lysøe, E., Gotfredsen, C.H., Giese, H., and Larsen, T.O. 2016. Black perithecial pigmentation in *Fusarium* species is due to the accumulation of 5-deoxybostrycoidin-based melanin. Sci. Rep. 6:26206.

Fujikawa, T., Kuga, Y., Yano, S., Yoshimi, A., Tachiki, T., Abe, K., and Nishimura, M. 2009. Dynamics of cell wall components of *Magnaporthe grisea* during infectious structure development. Mol. Microbiol. 73:553-570.

Fujioka, T., Mizutani, O., Furukawa, K., Sato, N., Yoshimi, A., Yamagata, Y., Nakajima, T., and Abe, K. 2007. MpkA-Dependent and -independent cell wall integrity signaling in *Aspergillus nidulans*. Eukaryot Cell 6:1497-1510.

Gaffoor, I., and Trail, F. 2006. Characterization of two polyketide synthase genes involved in zearalenone biosynthesis in *Gibberella zeae*. Appl. Environ. Microbiol. 72:1793-1799.

Gaffoor, I., Brown, D.W., Plattner, R., Proctor, R.H., Qi, W., and Trail, F. 2005. Functional analysis of the polyketide synthase genes in the filamentous fungus *Gibberella zeae* (anamorph *Fusarium graminearum*). Eukaryot Cell 4:1926.

Garcia-Rubio, R., de Oliveira, H.C., Rivera, J., and Trevijano-Contador, N. 2020. The Fungal Cell Wall: *Candida*, *Cryptococcus*, and *Aspergillus* species. Front. Microbiol. 10.

Garreau de Loubresse, N., Prokhorova, I., Holtkamp, W., Rodnina, M.V., Yusupova, G., and Yusupov, M. 2014. Structural basis for the inhibition of the eukaryotic ribosome. Nature 513:517-522.

Goswami, R.S., and Kistler, H.C. 2004. Heading for disaster: *Fusarium graminearum* on cereal crops. Mol. Plant Pathol. 5:515-525.

Goyal, R.K., Tulpan, D., Chomistek, N., González-Peña Fundora, D., West, C., Ellis, B.E., Frick, M., Laroche, A., and Foroud, N.A. 2018. Analysis of MAPK and MAPKK gene families in wheat and related Triticeae species. BMC Genom. 19:178.

Gray, J.V., Ogas, J.P., Kamada, Y., Stone, M., Levin, D.E., and Herskowitz, I. 1997. A role for the Pkc1 MAP kinase pathway of *Saccharomyces cerevisiae* in bud emergence and identification of a putative upstream regulator. EMBO J. 16:4924-4937.

Gu, Q., Zhang, C., Yu, F., Yin, Y., Shim, W.-B., and Ma, Z. 2015. Protein kinase FgSch9 serves as a mediator of the target of rapamycin and high osmolarity glycerol pathways and regulates multiple stress responses and secondary metabolism in *Fusarium graminearum*. Environ. Microbiol. 17:2661-2676.

Guerra-Castellano, A., Díaz-Moreno, I., Velázquez-Campoy, A., De la Rosa, M.A., and Díaz-Quintana, A. 2016. Structural and functional characterization of phosphomimetic mutants of cytochrome c at threonine 28 and serine 47. BBA, Biochim. Biophys. Acta - Bioenerg. 1857:387-395.

Hafez, M., Gourlie, R., Telfer, M., Schatz, N., Turkington, T.K., Beres, B., and Aboukhaddour, R. 2022. Diversity of *Fusarium* spp. associated with wheat node and grain in representative sites across the Western Canadian prairies. Phytopathology 112:1003-1015.

Hamel, L.-P., Nicole, M.-C., Duplessis, S., and Ellis, B.E. 2012. Mitogen-activated protein kinase signaling in plant-interacting Fungi: distinct messages from conserved messengers. The Plant Cell 24:1327-1351.

Hansen, F.T., Sørensen, J.L., Giese, H., Sondergaard, T.E., and Frandsen, R.J.N. 2012. Quick guide to polyketide synthase and nonribosomal synthetase genes in *Fusarium*. Int. J. Food Microbiol. 155:128-136.

Hansen, F.T., Gardiner, D.M., Lysøe, E., Fuertes, P.R., Tudzynski, B., Wiemann, P., Sondergaard, T.E., Giese, H., Brodersen, D.E., and Sørensen, J.L. 2015. An update to polyketide synthase and non-ribosomal synthetase genes and nomenclature in *Fusarium*. Fungal Genet. Biol. 75:20-29.

Harris, L.J., Balcerzak, M., Johnston, A., Schneiderman, D., and Ouellet, T. 2016. Host-preferential *Fusarium graminearum* gene expression during infection of wheat, barley, and maize. Fungal Biol. 120:111-123.

Harris, L.J., Desjardins, A.E., Plattner, R.D., Nicholson, P., Butler, G., Young, J.C., Weston, G., Proctor, R.H., and Hohn, T.M. 1999. Possible role of trichothecene mycotoxins in virulence of *Fusarium graminearum* on maize. Plant Dis. 83:954-960.

Harris, L.J., Alexander, N.J., Saparno, A., Blackwell, B., McCormick, S.P., Desjardins, A.E., Robert, L.S., Tinker, N., Hattori, J., Piché, C., Schernthaner, J.P., Watson, R., and Ouellet, T. 2007. A novel gene cluster in *Fusarium graminearum* contains a gene that contributes to butenolide synthesis. Fungal Genet. Biol. 44:293-306.

Harris, S.D. 2005. Morphogenesis in germinating *Fusarium graminearum* macroconidia. Mycologia 97:880-887.

Hayashi, M., and Maeda, T. 2006. Activation of the HOG pathway upon cold stress in *Saccharomyces cerevisiae*. J. Biochem. 139:797-803.

Hohn, T.M., and Vanmiddlesworth, F. 1986. Purification and characterization of the sesquiterpene cyclase trichodiene synthetase from *Fusarium sporotrichioides*. Arch. Biochem. Biophys. 251:756-761.

Hohn, T.M., and Beremand, P.D. 1989. Isolation and nucleotide sequence of a sesquiterpene cyclase gene from the trichothecene-producing fungus *Fusarium sporotrichioides*. Gene 79:131-138.

Holinsworth, B., and Martin, J.D. 2009. Siderophore production by marine-derived fungi. Biometals 22:625-632.

Hou, Z., Xue, C., Peng, Y., Katan, T., Kistler, H.C., and Xu, J.-R. 2002. A mitogen-activated protein kinase gene (MGV1) in *Fusarium graminearum* is required for female fertility, heterokaryon formation, and plant infection. Mol. Plant Microbe Interact. 15:1119-1127.

Ilgen, P., Maier, F.J., and Schäfer, W. 2008. Trichothecenes and lipases are host-induced and secreted virulence factors of *Fusarium graminearum*. Cereal Res. Commun. 36:421-428.

Inoue, S.B., Takewaki, N., Takasuka, T., Mio, T., Adachi, M., Fujii, Y., Miyamoto, C., Arisawa, M., Furuichi, Y., and Watanabe, T. 1995. Characterization and gene cloning of 1,3-beta-D-glucan synthase from *Saccharomyces cerevisiae*. Eur. J. Biochem. 231:845-854.

Irie, K., Takase, M., Lee, K.S., Levin, D.E., Araki, H., Matsumoto, K., and Oshima, Y. 1993. MKK1 and MKK2, which encode *Saccharomyces cerevisiae* mitogen-activated protein kinase-kinase homologs, function in the pathway mediated by protein kinase C. Mol. Cell. Biol. 13:3076-3083.

Iyer, V.R., Horak, C.E., Scafe, C.S., Botstein, D., Snyder, M., and Brown, P.O. 2001. Genomic binding sites of the yeast cell-cycle transcription factors SBF and MBF. Nature 409:533-538.

Jamai, A., Dubois, E., Vershon, A.K., and Messenguy, F. 2002. Swapping functional specificity of a MADS box protein: residues required for Arg80 regulation of arginine metabolism. Mol. Cell. Biol. 22:5741-5752.

Jansen, C., von Wettstein, D., Schäfer, W., Kogel, K.-H., Felk, A., and Maier, F.J. 2005. Infection patterns in barley and wheat spikes inoculated with wild-type and trichodiene synthase gene disrupted *Fusarium graminearum*. Proc. Natl. Acad. Sci. U.S.A. 102:16892.

Jarolim, K., Wolters, K., Woelflingseder, L., Pahlke, G., Beisl, J., Puntscher, H., Braun, D., Sulyok, M., Warth, B., and Marko, D. 2018. The secondary *Fusarium* metabolite aurofusarin induces oxidative stress, cytotoxicity and genotoxicity in human colon cells. Toxicol. Lett. 284:170-183.

Jenczmionka, N.J., Maier, F.J., Lösch, A.P., and Schäfer, W. 2003. Mating, conidiation and pathogenicity of *Fusarium graminearum*, the main causal agent of the head-blight disease of wheat, are regulated by the MAP kinase gpmk1. Curr. Genet. 43:87-95.

Jeon, J., Goh, J., Yoo, S., Chi, M.-H., Choi, J., Rho, H.-S., Park, J., Han, S.-S., Kim, B.R., Park, S.-Y., Kim, S., and Lee, Y.-H. 2008. A putative MAP Kinase Kinase Kinase, MCK1, is required for cell wall integrity and pathogenicity of the rice blast fungus, *Magnaporthe oryzae*. Mol. Plant Microbe Interact. 21:525-534.

Jia, L.-J., Tang, H.-Y., Wang, W.-Q., Yuan, T.-L., Wei, W.-Q., Pang, B., Gong, X.-M., Wang, S.-F., Li, Y.-J., Zhang, D., Liu, W., and Tang, W.-H. 2019. A linear nonribosomal octapeptide from *Fusarium graminearum* facilitates cell-to-cell invasion of wheat. Nature Communications 10:922.

Jia, L.J., and Tang, W.H. 2015. The omics era of *Fusarium graminearum*: opportunities and challenges. New Phytol. 207:1-3.

Jiang, C., Zhang, X., Liu, H., and Xu, J.-R. 2018. Mitogen-activated protein kinase signaling in plant pathogenic fungi. PLoS Pathog. 14:e1006875.

Jiang, J., Yun, Y., Yang, Q., Shim, W.-B., Wang, Z., and Ma, Z. 2011. A type 2C protein phosphatase FgPtc3 is involved in cell wall integrity, lipid metabolism, and virulence in *Fusarium graminearum*. PLoS One 6:e25311-e25311.

Johnson, G.L., and Lapadat, R. 2002. Mitogen-activated protein kinase pathways mediated by ERK, JNK, and p38 protein kinases. Science 298:1911-1912.

Jørgensen, S.H., Frandsen, R.J.N., Nielsen, K.F., Lysøe, E., Sondergaard, T.E., Wimmer, R., Giese, H., and Sørensen, J.L. 2014. *Fusarium graminearum* PKS14 is involved in orsellinic acid and orcinol synthesis. Fungal Genet. Biol. 70:24-31.

Jung, U.S., and Levin, D.E. 1999. Genome-wide analysis of gene expression regulated by the yeast cell wall integrity signalling pathway. Mol. Microbiol. 34:1049-1057.

Jung, U.S., Sobering, A.K., Romeo, M.J., and Levin, D.E. 2002. Regulation of the yeast Rlm1 transcription factor by the Mpk1 cell wall integrity MAP kinase. Mol. Microbiol. 46:781-789.

Kamada, Y., Jung, U.S., Piotrowski, J., and Levin, D.E. 1995. The protein kinase C-activated MAP kinase pathway of *Saccharomyces cerevisiae* mediates a novel aspect of the heat shock response. Genes Dev. 9:1559-1571.

Kamada, Y., Qadota, H., Python, C.P., Anraku, Y., Ohya, Y., and Levin, D.E. 1996. Activation of yeast Protein Kinase C by Rho1 GTPase. J. Biol. Chem. 271:9193-9196.

Ketela, T., Green, R., and Bussey, H. 1999. *Saccharomyces cerevisiae* Mid2p is a potential cell wall stress sensor and upstream activator of the PKC1-MPK1 Cell Integrity Pathway. J. Bacteriol. 181:3330-3340.

Khan, M., Rozhon, W., Bigeard, J., Pflieger, D., Husar, S., Pitzschke, A., Teige, M., Jonak, C., Hirt, H., and Poppenberger, B. 2013. Brassinosteroid-regulated GSK3/Shaggy-like kinases phosphorylate mitogen-activated protein (MAP) kinase kinases, which control stomata development in *Arabidopsis thaliana*. J. Biol. Chem. 288:7519-7527.

Kim, D.-W., Shin, Y.-K., Lee, S.-W., Wimonmuang, K., Kang, K.B., Lee, Y.-S., and Yun, S.-H. 2021. FgPKS7 is an essential player in mating-type-mediated regulatory pathway required for completing sexual cycle in *Fusarium graminearum*. Environ. Microbiol. 23:1972-1990.

Kim, J.-E., Han, K.-H., Jin, J., Kim, H., Kim, J.-C., Yun, S.-H., and Lee, Y.-W. 2005a. Putative polyketide synthase and laccase genes for biosynthesis of aurofusarin in *Gibberella zeae*. Appl. Environ. Microbiol. 71:1701-1708.

Kim, Y.-T., Lee, Y.-R., Jin, J., Han, K.-H., Kim, H., Kim, J.-C., Lee, T., Yun, S.-H., and Lee, Y.-W. 2005b. Two different polyketide synthase genes are required for synthesis of zearalenone in *Gibberella zeae*. Mol. Microbiol. 58:1102-1113.

Kimura, M., and Yamaguchi, I. 1999. The mystery of the trichothecene 3-O-acetyltransferase gene: Tri101 evolved independently of other trichothecene biosynthetic genes in the gene cluster. FEBS Lett. 55:372-374.

Kimura, M., Tokai, T., Takahashi-Ando, N., Ohsato, S., and Fujimura, M. 2007. Molecular and genetic studies of fusarium trichothecene biosynthesis: pathways, genes, and evolution. Biosci Biotechnol Biochem 71:2105-2123.

Kojima, K., Kikuchi, T., Takano, Y., Oshiro, E., and Okuno, T. 2002. The mitogen-activated protein kinase gene MAF1 is essential for the early differentiation phase of appressorium formation in *Colletotrichum lagenarium*. Mol. Plant Microbe Interact. 15:1268-1276.

Kong, L.-A., Yang, J., Li, G.-T., Qi, L.-L., Zhang, Y.-J., Wang, C.-F., Zhao, W.-S., Xu, J.-R., and Peng, Y.-L. 2012. Different chitin synthase genes are required for various developmental and plant infection processes in the rice blast fungus *Magnaporthe oryzae*. PLoS Pathog. 8:e1002526-e1002526.

Kramer, J., Özkaya, Ö., and Kümmerli, R. 2020. Bacterial siderophores in community and host interactions. Nat. Rev. Microbiol. 18:152-163.

Kumaraswamy, G.K., Kushalappa, A.C., Choo, T.M., Dion, Y., and Rioux, S. 2012. Differential metabolic response of barley genotypes, varying in resistance, to trichothecene-producing and -nonproducing (tri5−) isolates of *Fusarium graminearum*. Plant Pathol. 61:509-521.

Lai, S., and Pelech, S. 2016. Regulatory roles of conserved phosphorylation sites in the activation T-loop of the MAP kinase ERK1. Mol. Biol. Cell 27:1040-1050.

Lee, J.C., Laydon, J.T., McDonnell, P.C., Gallagher, T.F., Kumar, S., Green, D., McNulty, D., Blumenthal, M.J., Heys, J.R., Landvatter, S.W., Strickler, J.E., McLaughlin, M.M., Siemens, I.R., Fisher, S.M., Livi, G.P., White, J.R., Adams, J.L., and Young, P.R. 1994. A protein kinase involved in the regulation of inflammatory cytokine biosynthesis. Nature 372:739-746.

Lee, K.S., and Levin, D.E. 1992. Dominant mutations in a gene encoding a putative protein kinase (BCK1) bypass the requirement for a *Saccharomyces cerevisiae* protein kinase C homolog. Mol. Cell. Biol. 12:172-182.

Lee, K.S., Irie, K., Gotoh, Y., Watanabe, Y., Araki, H., Nishida, E., Matsumoto, K., and Levin, D.E. 1993. A yeast mitogen-activated protein kinase homolog (Mpk1p) mediates signalling by protein kinase C. Mol. Cell. Biol. 13:3067-3075.

Levin, D.E. 2011. Regulation of cell wall biogenesis in *Saccharomyces cerevisiae:* the cell wall integrity signaling pathway. Genetics 189:1145-1175.

Levy, R., Gregory, E., Borcherds, W., and Daughdrill, G. 2019. p53 Phosphomimetics Preserve Transient Secondary Structure but Reduce Binding to Mdm2 and MdmX 9:83.

Li, A., Zhang, M., Wang, Y., Li, D., Liu, X., Tao, K., Ye, W., and Wang, Y. 2014. PsMPK1, an SLT2-type mitogen-activated protein kinase, is required for hyphal growth, zoosporogenesis, cell wall integrity, and pathogenicity in *Phytophthora sojae*. Fungal Genet. Biol. 65:14-24.

Li, S., Hartman, G.L., and Gray, L.E. 1998. Chlamydospore formation, production, and nuclear status in *Fusarium solani* f. sp. glycines soybean sudden death syndrome-causing isolates. Mycologia 90:414-421.

Liu, J.-B., Wang, Y.-M., Peng, S.-Q., Han, G., Dong, Y.-S., Yang, H.-Y., Yan, C.-H., and Wang, G.-Q. 2007. Toxic effects of *Fusarium* mycotoxin butenolide on rat myocardium and primary culture of cardiac myocytes. Toxicon 50:357-364.

Liu, N., Fan, F., Qiu, D., and Jiang, L. 2013. The transcription cofactor FgSwi6 plays a role in growth and development, carbendazim sensitivity, cellulose utilization, lithium tolerance, deoxynivalenol production and virulence in the filamentous fungus *Fusarium graminearum*. Fungal Genet. Biol. 58-59:42-52.

Liu, R., Xu, C., Zhang, Q., Wang, S., and Fang, W. 2017. Evolution of the chitin synthase gene family correlates with fungal morphogenesis and adaption to ecological niches. Sci. Rep. 7:44527.

Liu, Z., Jian, Y., Chen, Y., Kistler, H.C., He, P., Ma, Z., and Yin, Y. 2019. A phosphorylated transcription factor regulates sterol biosynthesis in Fusarium graminearum. Nature Communications 10:1228.

Lodder, A.L., Lee, T.K., and Ballester, R. 1999. Characterization of the Wsc1 protein, a putative receptor in the stress response of *Saccharomyces cerevisiae*. Genetics 152:1487-1499.

Luo, X., Keyhani, N.O., Yu, X., He, Z., Luo, Z., Pei, Y., and Zhang, Y. 2012. The MAP kinase Bbslt2 controls growth, conidiation, cell wall integrity, and virulence in the insect pathogenic fungus *Beauveria bassiana*. Fungal Genet. Biol. 49:544-555.

Maeda, T., Wurgler-Murphy, S.M., and Saito, H. 1994. A two-component system that regulates an osmosensing MAP kinase cascade in yeast. Nature 369:242-245.

Maeda, T., Takekawa, M., and Saito, H. 1995. Activation of yeast PBS2 MAPKK by MAPKKKs or by binding of an SH3-containing osmosensor. Science 269:554-558.

Maier, F.J., Miedaner, T., Hadeler, B., Felk, A., Salomon, S., Lemmens, M., Kassner, H., and Schäfer, W. 2006. Involvement of trichothecenes in fusarioses of wheat, barley and maize evaluated by gene disruption of the trichodiene synthase (Tri5) gene in three field isolates of different chemotype and virulence. Mol. Plant Pathol. 7:449-461.

Malz, S., Grell, M.N., Thrane, C., Maier, F.J., Rosager, P., Felk, A., Albertsen, K.S., Salomon, S., Bohn, L., Schäfer, W., and Giese, H. 2005. Identification of a gene cluster responsible for the biosynthesis of aurofusarin in the *Fusarium graminearum* species complex. Fungal Genet. Biol. 42:420-433.

Mazur, P., Morin, N., Baginsky, W., el-Sherbeini, M., Clemas, J.A., Nielsen, J.B., and Foor, F. 1995. Differential expression and function of two homologous subunits of yeast 1,3-beta-D-glucan synthase. Mol. Cell. Biol. 15:5671-5681.

McCormick, S.P. 2009. Phytotoxicity of trichothecenes. Pages 143-155 in: Mycotoxin Prevention and Control in Agriculture, American Chemical Society.

McMullen, M., Bergstrom, G., De Wolf, E., Dill-Macky, R., Hershman, D., Shaner, G., and Van Sanford, D. 2012. A unified effort to fight an enemy of wheat and barley: Fusarium head blight. Plant Dis. 96:1712-1728.

Mead, J., Bruning, A.R., Gill, M.K., Steiner, A.M., Acton, T.B., and Vershon, A.K. 2002. Interactions of the Mcm1 MADS box protein with cofactors that regulate mating in yeast. Mol. Cell. Biol. 22:4607-4621.

Mehrabi, R., Ding, S., and Xu, J.-R. 2008. MADS-box transcription factor Mig1 is required for infectious growth in *Magnaporthe grisea*. Eukaryot Cell 7:791-799.

Mehrabi, R., van der Lee, T., Waalwijk, C., and Kema, G.H.J. 2006. MgSlt2, a cellular integrity MAP Kinase gene of the fungal wheat pathogen *Mycosphaerella graminicola*, is dispensable for penetration but essential for invasive growth. Mol. Plant Microbe Interact. 19:389-398.

Miller, J.D., and Blackwell, B.A. 1986. Biosynthesis of 3-acetyldeoxynivalenol and other metabolites by *Fusarium culmorum* HLX 1503 in a stirred jar fermentor. Canadian Journal of Botany 64:1-5.

Modi, V., and Dunbrack, R.L. 2019. Defining a new nomenclature for the structures of active and inactive kinases. Proc. Natl. Acad. Sci. U.S.A. 116:6818.

Nasmith, C.G., Walkowiak, S., Wang, L., Leung, W.W.Y., Gong, Y., Johnston, A., Harris, L.J., Guttman, D.S., and Subramaniam, R. 2011. Tri6 is a global transcription regulator in the phytopathogen *Fusarium graminearum*. PLoS Pathog. 7:e1002266.

Nguyen, T.T.X., Dehne, H.-W., and Steiner, U. 2016. Histopathological assessment of the infection of maize leaves by *Fusarium graminearum*, *F. proliferatum*, and *F. verticillioides*. Fungal Biol. 120:1094-1104.

Nonaka, H., Tanaka, K., Hirano, H., Fujiwara, T., Kohno, H., Umikawa, M., Mino, A., and Takai, Y. 1995. A downstream target of RHO1 small GTP-binding protein is PKC1, a homolog of protein kinase C, which leads to activation of the MAP kinase cascade in *Saccharomyces cerevisiae*. EMBO J. 14:5931-5938.

Nyvall, R.F. 1970. Chlamydospores of Fusarium roseum "Graminearum" as survival structures. Phytopathology 60:1175-1177.

O'Rourke, S.M., and Herskowitz, I. 1998. The Hog1 MAPK prevents cross talk between the HOG and pheromone response MAPK pathways in *Saccharomyces cerevisiae*. Genes Dev. 12:2874-2886.

O'Rourke, S.M., and Herskowitz, I. 2002. A third osmosensing branch in *Saccharomyces cerevisiae* requires the Msb2 protein and functions in parallel with the Sho1 branch. Mol. Cell. Biol. 22:4739-4749.

Onyilo, F., Tusiime, G., Tripathi, J.N., Chen, L.-H., Falk, B., Stergiopoulos, I., Tushemereirwe, W., Kubiriba, J., and Tripathi, L. 2018. Silencing of the Mitogen-Activated Protein Kinases (MAPK) Fus3 and Slt2 in *Pseudocercospora fijiensis* reduces growth and virulence on host plants. Front Plant Sci 9.

Orlean, P. 2012. Architecture and biosynthesis of the *Saccharomyces cerevisiae* cell wall. Genetics 192:775-818.

Perez-Nadales, E., and Di Pietro, A. 2015. The transmembrane protein Sho1 cooperates with the mucin Msb2 to regulate invasive growth and plant infection in *Fusarium oxysporum*. Mol. Plant Pathol. 16:593-603.

Pinto, V.F., Patriarca, A., and Pose, G. 2013. Mycotoxins associated to *Fusarium* species that caused Fusarium head blight in wheat in Latin-America. Pages 59-73 in: Fusarium Head Blight in Latin America, T.M. Alconada Magliano and S.N. Chulze, eds. Springer Netherlands, Dordrecht.

Prados Rosales, R.C., and Di Pietro, A. 2008. Vegetative hyphal fusion is not essential for plant infection by *Fusarium oxysporum*. Eukaryot Cell 7:162-171.

Pritsch, C., Muehlbauer, G.J., Bushnell, W.R., Somers, D.A., and Vance, C.P. 2000. Fungal development and induction of defense response genes during early infection of wheat spikes by *Fusarium graminearum*. Mol. Plant Microbe Interact. 13:159-169.

Proctor, R.H., Hohn, T.M., and McCormick, S.P. 1995a. Reduced virulence of *Gibberella zeae* caused by disruption of a trichothecene toxin biosynthetic gene. Mol. Plant Microbe Interact. 8:593-601.

Proctor, R.H., Hohn, T.M., McCormick, S.P., and Desjardins, A.E. 1995b. Tri6 encodes an unusual zinc finger protein involved in regulation of trichothecene biosynthesis in *Fusarium sporotrichioides*. Appl. Environ. Microbiol. 61:1923-1930.

Pucheta-Martínez, E., Saladino, G., Morando, M.A., Martinez-Torrecuadrada, J., Lelli, M., Sutto, L., D'Amelio, N., and Gervasio, F.L. 2016. An allosteric cross-talk between the activation loop and the ATP binding site regulates the activation of Src kinase. Sci. Rep. 6:24235.

Puri, K.D., and Zhong, S. 2010. The 3ADON population of *Fusarium graminearum* found in North Dakota is more aggressive and produces a higher level of DON than the prevalent 15ADON population in spring wheat. Phytopathology 100:1007-1014.

Qadota, H., Python, C.P., Inoue, S.B., Arisawa, M., and et al. 1996. Identification of yeast Rho1p GTPase as a regulatory subunit of 1,3-beta-Glucan synthase. Science 272:279.

Qi, Z., Wang, Q., Dou, X., Wang, W., Zhao, Q., Lv, R., Zhang, H., Zheng, X., Wang, P., and Zhang, Z. 2012. MoSwi6, an APSES family transcription factor, interacts with MoMps1 and is required for hyphal and conidial morphogenesis, appressorial function and pathogenicity of *Magnaporthe oryzae*. Mol. Plant Pathol. 13:677-689.

Qin, G., Yun, C., Ye, L., Chengqi, Z., and Zhonghua, M. 2015. The transmembrane protein FgSho1 regulates fungal development and pathogenicity via the MAPK module Ste50-Ste11-Ste7 in *Fusarium graminearum*. New Phytol. 206:315-328.

Raman, M., Chen, W., and Cobb, M.H. 2007. Differential regulation and properties of MAPKs. Oncogene 26:3100-3112.

Rampitsch, C., Subramaniam, R., Djuric-Ciganovic, S., and Bykova, N.V. 2010. The phosphoproteome of *Fusarium graminearum* at the onset of nitrogen starvation. Proteomics 10:124-140.

Rampitsch, C., Leung, W., Blackwell, B., and Subramaniam, R. 2011. Map kinase MGV1: a potential shared control point of butenolide and deoxynivalenol biosynthesis In *Fusarium graminearum*. Plant Breed. Seed Sci. 64:81-88.

Ray, L.B., and Sturgill, T.W. 1988. Insulin-stimulated microtubule-associated protein kinase is phosphorylated on tyrosine and threonine in vivo. Proc. Natl. Acad. Sci. U.S.A. 85:3753-3757.

Ridley, C.P., and Khosla, C. 2009. Polyketides. Pages 472-481 in: Encyclopedia of Microbiology (Third Edition), M. Schaechter, ed. Academic Press, Oxford.

Riquelme, M. 2013. Tip growth in filamentous Fungi: a road trip to the apex. Annu. Rev. Microbiol. 67:587-609.

Rossomando, A.J., Payne, D.M., Weber, M.J., and Sturgill, T.W. 1989. Evidence that pp42, a major tyrosine kinase target protein, is a mitogen-activated serine/threonine protein kinase. Proc. Natl. Acad. Sci. U.S.A. 86:6940-6943.

Roux, P.P., and Blenis, J. 2004. ERK and p38 MAPK-Activated Protein Kinases: a Family of Protein Kinases with Diverse Biological Functions. Microbiol. Mol. Biol. Rev. 68:320-344.

Schoental, R. 1994. Mycotoxins in food and the plague of Athens. J. Nutr. Med. 4:83-85.

Schwarz-Sommer, Z., Huijser, P., Nacken, W., Saedler, H., and Sommer, H. 1990. Genetic control of flower development by homeotic genes in *Antirrhinum majus*. Science 250:931-936.

Seong, K.-Y., Pasquali, M., Zhou, X., Song, J., Hilburn, K., McCormick, S., Dong, Y., Xu, J.-R., and Kistler, H.C. 2009. Global gene regulation by *Fusarium* transcription factors Tri6 and Tri10 reveals adaptations for toxin biosynthesis. Mol. Microbiol. 72:354-367.

Serajazari, M., Hudson, K., Kaviani, M., and Navabi, A. 2019. *Fusarium graminearum* chemotype–Spring wheat genotype interaction effects in type I and II resistance response assays. Phytopathology 109:643-649.

Shewry, P.R. 2009. Wheat. Journal of Experimental Botany 60:1537-1553.

Shore, P., and Sharrocks, A.D. 1995. The MADS-box family of transcription factors. Eur. J. Biochem. 229:1-13.

Shostak, K. (2020). Secret arsenal of a cereal killer - cryptic activation of secondary metabolite biosynthesis in *Fusarium graminearum* (Carleton University: Carleton University), pp. 161.

Sieber, C.M.K., Lee, W., Wong, P., Münsterkötter, M., Mewes, H.-W., Schmeitzl, C., Varga, E., Berthiller, F., Adam, G., and Güldener, U. 2014. The *Fusarium graminearum* genome reveals more secondary metabolite gene clusters and hints of horizontal gene transfer. PLoS One 9:e110311.

Sobrova, P., Adam, V., Vasatkova, A., Beklova, M., Zeman, L., and Kizek, R. 2010. Deoxynivalenol and its toxicity. Interdiscip. Toxicol. 3:94-99.

Somale, D., Di Nardo, G., di Blasio, L., Puliafito, A., Vara-Messler, M., Chiaverina, G., Palmiero, M., Monica, V., Gilardi, G., Primo, L., and Gagliardi, P.A. 2020. Activation of RSK by phosphomimetic substitution in the activation loop is prevented by structural constraints. Sci. Rep. 10:591.

Son, H., Lee, J., and Lee, Y.-W. 2012. Mannitol induces the conversion of conidia to chlamydospore-like structures that confer enhanced tolerance to heat, drought, and UV in *Gibberella zeae*. Microbiol. Res. 167:608-615.

Sørensen, J.L., Hansen, F.T., Sondergaard, T.E., Staerk, D., Lee, T.V., Wimmer, R., Klitgaard, L.G., Purup, S., Giese, H., and Frandsen, R.J.N. 2012. Production of novel fusarielins by ectopic activation of the polyketide synthase 9 cluster in *Fusarium graminearum*. Environ. Microbiol. 14:1159-1170.

Sørensen, J.L., Sondergaard, T.E., Covarelli, L., Fuertes, P.R., Hansen, F.T., Frandsen, R.J., Saei, W., Lukassen, M.B., Wimmer, R., Nielsen, K.F., Gardiner, D.M., and Giese, H. 2014. Identification of the biosynthetic gene clusters for the lipopeptides fusaristatin A and W493 B in *Fusarium graminearum* and *F. pseudograminearum*. J. Nat. Prod. 77:2619-2625.

Sridhar, P.S., Trofimova, D., Subramaniam, R., González-Peña Fundora, D., Foroud, N.A., Allingham, J.S., and Loewen, M.C. 2020. Ste2 receptor-mediated chemotropism of *Fusarium graminearum* contributes to its pathogenicity against wheat. Sci. Rep. 10:10770.

Subramaniam, R., Narayanan, S., Walkowiak, S., Wang, L., Joshi, M., Rocheleau, H., Ouellet, T., and Harris, L.J. 2015. Leucine metabolism regulates TRI6 expression and affects deoxynivalenol production and virulence in *Fusarium graminearum*. Mol. Microbiol. 98:760-769.

Sutton, J.C. 1982. Epidemiology of wheat head blight and maize ear rot caused by *Fusarium graminearum*. Can. J. Plant Pathol. 4:195-209.

Tag, A.G., Garifullina, G.F., Peplow, A.W., Ake, C., Phillips, T.D., Hohn, T.M., and Beremand, M.N. 2001. A novel regulatory gene, Tri10, controls trichothecene toxin production and gene expression. Appl. Environ. Microbiol. 67:5294-5302.

Tamburic-Ilincic, L., Wragg, A., and Schaafsma, A. 2015. Mycotoxin accumulation and *Fusarium graminearum* chemotype diversity in winter wheat grown in southwestern Ontario. Can. J. Plant Sci. 95:931-938.

Taylor, S.S., Wu, J., Bruystens, J.G.H., Del Rio, J.C., Lu, T.-W., Kornev, A.P., and Ten Eyck, L.F. 2021. From structure to the dynamic regulation of a molecular switch: A journey over 3 decades. J. Biol. Chem. 296:100746.

Turrà, D., Segorbe, D., and Pietro, A.D. 2014. Protein kinases in plant-pathogenic fungi: conserved regulators of infection. Annu. Rev. Phytopathol. 52:267-288.

Turrà, D., El Ghalid, M., Rossi, F., and Di Pietro, A. 2015. Fungal pathogen uses sex pheromone receptor for chemotropic sensing of host plant signals. Nature 527:521-524.

Valverde-Bogantes, E., Bianchini, A., Herr, J.R., Rose, D.J., Wegulo, S.N., and Hallen-Adams, H.E. 2020. Recent population changes of Fusarium head blight pathogens: drivers and implications. Can. J. Plant Pathol. 42:315-329.

van der Lee, T., Zhang, H., van Diepeningen, A., and Waalwijk, C. 2015. Biogeography of *Fusarium graminearum* species complex and chemotypes: a review. Food Additives & Contaminants: Part A 32:453-460.

Verna, J., Lodder, A., Lee, K., Vagts, A., and Ballester, R. 1997. A family of genes required for maintenance of cell wall integrity and for the stress response in *Saccharomyces cerevisiae*. Proc. Natl. Acad. Sci. U.S.A. 94:13804-13809.

Vitale, S., Di Pietro, A., and Turrà, D. 2019. Autocrine pheromone signalling regulates community behaviour in the fungal pathogen *Fusarium oxysporum*. Nat. Microbiol. 4:1443-1449.

Walkowiak, S., Rowland, O., Rodrigue, N., and Subramaniam, R. 2016. Whole genome sequencing and comparative genomics of closely related Fusarium Head Blight fungi: *Fusarium graminearum, F. meridionale* and *F. asiaticum*. BMC Genom. 17:1014.

Wang, C., Zhang, S., Hou, R., Zhao, Z., Zheng, Q., Xu, Q., Zheng, D., Wang, G., Liu, H., Gao, X., Ma, J.-W., Kistler, H.C., Kang, Z., and Xu, J.-R. 2011. Functional analysis of the kinome of the wheat scab fungus *Fusarium graminearum*. PLoS Pathog. 7:e1002460.

Wang, Y.M., Liu, J.B., and Peng, S.Q. 2009. Effects of *Fusarium* mycotoxin butenolide on myocardial mitochondria in vitro. Toxicol. Mech. Methods 19:79-85.

Wang, Z., An, N., Xu, W., Zhang, W., Meng, X., Chen, G., and Liu, W. 2018. Functional characterization of the upstream components of the Hog1-like kinase cascade in hyperosmotic and carbon sensing in *Trichoderma reesei*. Biotechnol Biofuels 11:97-97.

Ward, T.J., Clear, R.M., Rooney, A.P., O'Donnell, K., Gaba, D., Patrick, S., Starkey, D.E., Gilbert, J., Geiser, D.M., and Nowicki, T.W. 2008. An adaptive evolutionary shift in Fusarium head blight pathogen populations is driving the rapid spread of more toxigenic *Fusarium graminearum* in North America. Fungal Genet. Biol. 45:473-484.

Watanabe, Y., Irie, K., and Matsumoto, K. 1995. Yeast RLM1 encodes a serum response factor-like protein that may function downstream of the Mpk1 (Slt2) mitogen-activated protein kinase pathway. Mol. Cell. Biol. 15:5740-5749.

Watanabe, Y., Takaesu, G., Hagiwara, M., Irie, K., and Matsumoto, K. 1997. Characterization of a serum response factor-like protein in *Saccharomyces cerevisiae*, Rlm1, which has transcriptional activity regulated by the Mpk1 (Slt2) mitogen-activated protein kinase pathway. Mol. Cell. Biol. 17:2615-2623.

Wegulo, S.N., Baenziger, P.S., Hernandez Nopsa, J., Bockus, W.W., and Hallen-Adams, H. 2015. Management of Fusarium head blight of wheat and barley. Crop Prot. 73:100-107.

Wei, C.-M., and McLaughlin, C.S. 1974. Structure-function relationship in the 12, 13-epoxytrichothecenes novel inhibitors of protein synthesis. Biochem. Biophys. Res. Commun. 57:838-844.

Westphal, K.R., Wollenberg, R.D., Herbst, F.-A., Sørensen, J.L., Sondergaard, T.E., and Wimmer, R. 2018a. Enhancing the production of the fungal pigment aurofusarin in *Fusarium graminearum*. Toxins 10:485.

Westphal, K.R., Muurmann, A.T., Paulsen, I.E., Nørgaard, K.T.H., Overgaard, M.L., Dall, S.M., Aalborg, T., Wimmer, R., Sørensen, J.L., and Sondergaard, T.E. 2018b. Who needs neighbors? PKS8 is a stand-alone gene in *Fusarium graminearum* responsible for production of Gibepyrones and Prolipyrone B. Molecules 23:2232.

Westphal, K.R., Nielsen, K.A.H., Wollenberg, R.D., Møllehøj, M.B., Bachleitner, S., Studt, L., Lysøe, E., Giese, H., Wimmer, R., Sørensen, J.L., and Sondergaard, T.E. 2019. Fusaoctaxin A, an example of a two-step mechanism for non-ribosomal peptide assembly and maturation in Fungi. Toxins 11:277.

Woelflingseder, L., Del Favero, G., Blažević, T., Heiss, E.H., Haider, M., Warth, B., Adam, G., and Marko, D. 2018. Impact of glutathione modulation on the toxicity of the *Fusarium* mycotoxins deoxynivalenol (DON), NX-3 and butenolide in human liver cells. Toxicol. Lett. 299:104-117.

Xu, J.R., Staiger, C.J., and Hamer, J.E. 1998. Inactivation of the mitogen-activated protein kinase Mps1 from the rice blast fungus prevents penetration of host cells but allows activation of plant defense responses. Proc. Natl. Acad. Sci. U.S.A. 95:12713-12718.

Xu, L., Wang, M., Tang, G., Ma, Z., and Shao, W. 2019. The endocytic cargo adaptor complex is required for cell-wall integrity via interacting with the sensor FgWsc2B in *Fusarium graminearum*. Curr. Genet. 65:1071-1080.

Yin, Y., Wang, Z., Cheng, D., Chen, X., Chen, Y., and Ma, Z. 2018a. The ATP-binding protein FgArb1 is essential for penetration, infectious and normal growth of *Fusarium graminearum*. New Phytol. 219:1447-1466.

Yin, Y., Wu, S., Chui, C., Ma, T., Jiang, H., Hahn, M., and Ma, Z. 2018b. The MAPK kinase BcMkk1 suppresses oxalic acid biosynthesis via impeding phosphorylation of BcRim15 by BcSch9 in *Botrytis cinerea*. PLoS Pathog. 14:e1007285.

Yin, Z., Feng, W., Chen, C., Xu, J., Li, Y., Yang, L., Wang, J., Liu, X., Wang, W., Gao, C., Zhang, H., Zheng, X., Wang, P., and Zhang, Z. 2020. Shedding light on autophagy coordinating with cell wall integrity signaling to govern pathogenicity of *Magnaporthe oryzae*. Autophagy 16:900-916.

Yu, F., Gu, Q., Yun, Y., Yin, Y., Xu, J.-R., Shim, W.-B., and Ma, Z. 2014. The TOR signaling pathway regulates vegetative development and virulence in *Fusarium graminearum*. New Phytol. 203:219-232.

Yun, Y., Liu, Z., Zhang, J., Shim, W.-B., Chen, Y., and Ma, Z. 2014. The MAPKK FgMkk1 of *Fusarium graminearum* regulates vegetative differentiation, multiple stress response, and virulence via the cell wall integrity and high-osmolarity glycerol signaling pathways. Environ. Microbiol. 16:2023-2037.

Yun, Y., Liu, Z., Yin, Y., Jiang, J., Chen, Y., Xu, J.-R., and Ma, Z. 2015. Functional analysis of the *Fusarium graminearum* phosphatome. New Phytol. 207:119-134.

Zhang, C., Wang, J., Tao, H., Dang, X., Wang, Y., Chen, M., Zhai, Z., Yu, W., Xu, L., Shim, W.B., Lu, G., and Wang, Z. 2015. FvBck1, a component of cell wall integrity MAP kinase pathway, is required for virulence and oxidative stress response in sugarcane Pokkah Boeng pathogen. Front Microbiol 6:1096.

Zhang, G., Sun, Z., Ren, A., Shi, L., Shi, D., Li, X., and Zhao, M. 2017. The mitogen-activated protein kinase GlSlt2 regulates fungal growth, fruiting body development, cell wall integrity, oxidative stress and ganoderic acid biosynthesis in *Ganoderma lucidum*. Fungal Genet. Biol. 104:6-15.

Zhang, W., and Liu, H.T. 2002. MAPK signal pathways in the regulation of cell proliferation in mammalian cells. Cell Res. 12:9-18.

Zhao, P.B., Ren, A.Z., and Li, D.C. 2011. The FUS3/KSS1-type MAP kinase gene FPK1 is involved in hyphal growth, conidiation and plant infection of *Fusarium proliferatum*. J. Mol. Microbiol. Biotechnol. 21:110-119.

Zhao, X., Mehrabi, R., and Xu, J.-R. 2007. Mitogen-activated protein kinase pathways and fungal pathogenesis. Eukaryot Cell 6:1701-1714.

Zheng, D., Zhang, S., Zhou, X., Wang, C., Xiang, P., Zheng, Q., and Xu, J.-R. 2012. The FgHOG1 pathway regulates hyphal growth, stress responses, and plant infection in *Fusarium graminearum*. PLoS One 7:e49495.

Zheng, L., Campbell, M., Murphy, J., Lam, S., and Xu, J.-R. 2000. The BMP1 gene is essential for pathogenicity in the gray mold fungus *Botrytis cinerea*. Mol. Plant Microbe Interact. 13:724-732.

Zu, T., Verna, J., and Ballester, R. 2001. Mutations in WSC genes for putative stress receptors result in sensitivity to multiple stress conditions and impairment of Rlm1-dependent gene expression in *Saccharomyces cerevisiae*. Mol. Genet. Genom. 266:142-155.

Appendix A: supplementary information for chapter 2

Table of Contents

Supplementary Table 2.1. Name and accession number of genes used in this chapter.

Gene name	**Accession #**
β-TUBULIN	FGSG_09530
ELONGATION FACTOR-1α	FGSG_08811
MKK1	FGSG_07295
MGV1	FGSG_10313
RLM1	FGSG_09339
GPMK1	FGSG_06385
HOG1	FGSG_09612
CHITIN SYNTHASE 1A	FGSG_10116
CHITIN SYNTHASE 1B	FGSG_16273
CHITIN SYNTHASE 3	FGSG_10327
CHITIN SYNTHASE 4	FGSG_01272
CHITIN SYNTHASE 5	FGSG_01964
CHITIN SYNTHASE 6	FGSG_15914
FKS1	FGSG_07946
TRI5	FGSG_03537
TRI6	FGSG_03536
PKS12	FGSG_02324
GIP1	FGSG_02328
AURF	FGSG_02327
AURJ	FGSG_02326
AURR1	FGSG_02320
AURR2	FGSG_02323
KIN4	FGSG_11812

a)

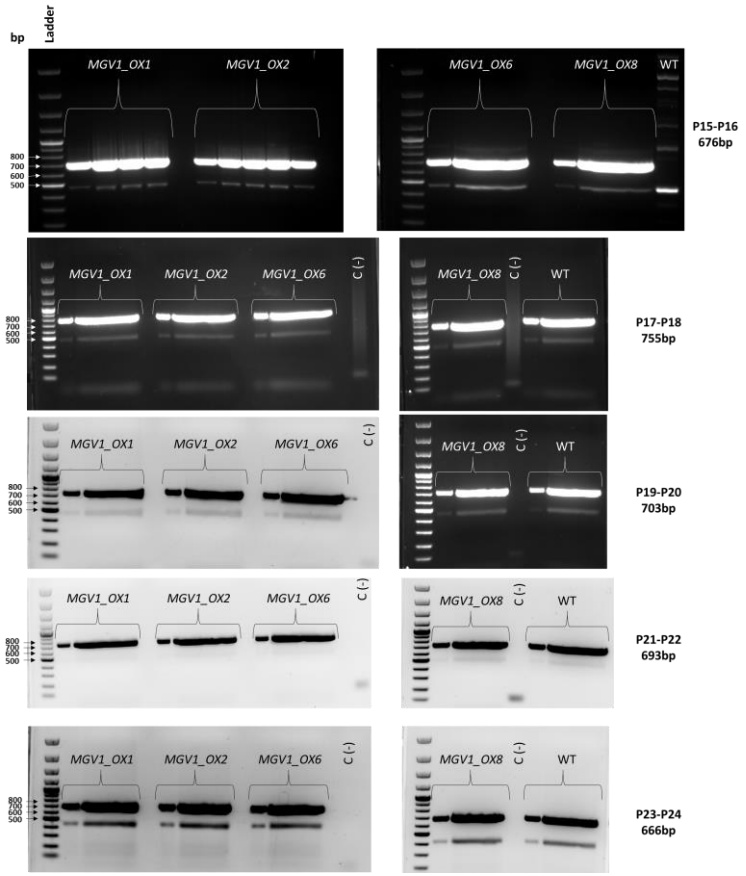

b)

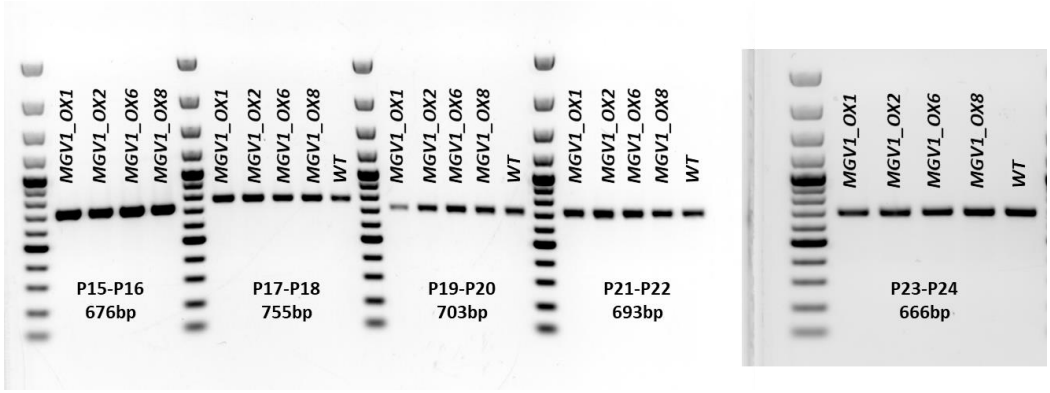

Supplementary Figure 2.1. Amplicons obtained with different set of primers that were used for sequencing the HU2E fragment inserted into the WT strain for generating *MGV1_OX* transformants. a) PCR result of *MGV1_OX* transformants and the WT strains. b) Purified amplicons sent for sequencing.

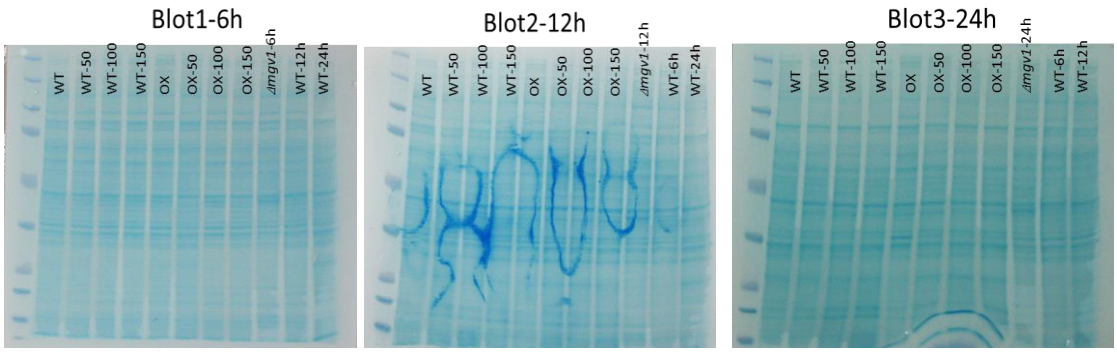

Supplementary Figure 2.2. Total protein detected in blots stained with Thermo Scientific™ Pierce™ reversible protein stain kit for PVDF membranes, corresponding to blots in Figure 2.26.

Appendix B: supplementary information for chapter 3

Table of contents

Supplementary Table 3.1. Name and accession numbers of genes used in Chapter 3.

Gene name	**Accession #**
β-TUBULIN	FGSG_09530
ELONGATION FACTOR-1α	FGSG_08811
MKK1	FGSG_07295
MGV1	FGSG_10313
GPMK1	FGSG_06385
HOG1	FGSG_09612
CHITIN SYNTHASE 1A	FGSG_10116
CHITIN SYNTHASE 5	FGSG_01964
CHITIN SYNTHASE 6	FGSG_15914
TRI5	FGSG_03537
TRI6	FGSG_16251
PKS12	FGSG_02324
GIP1	FGSG_02328
AURF	FGSG_02327
AURJ	FGSG_02326
AURR1	FGSG_02320
AURR2	FGSG_02323
KIN4	FGSG_11812

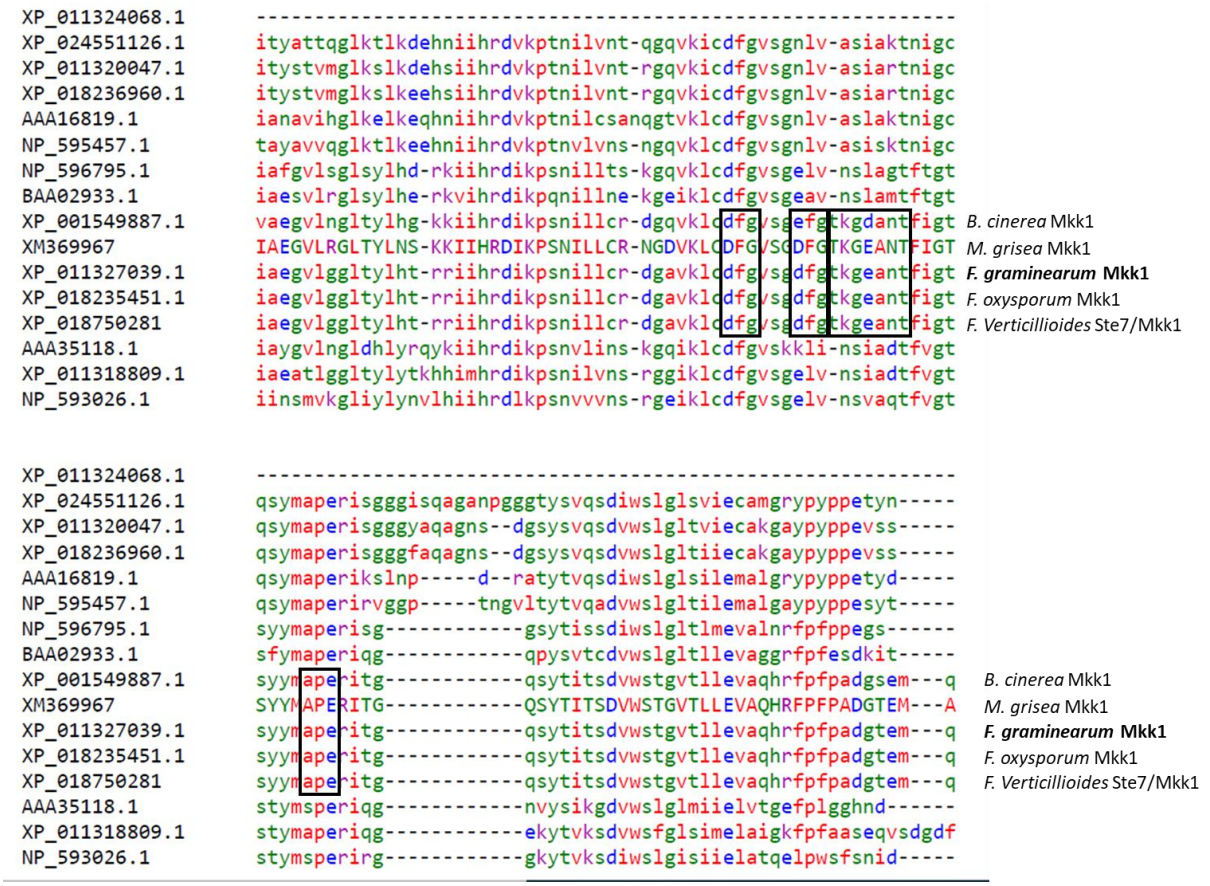

Supplementary Figure 3.1. Activation loop in *MAPKKs* from different fungal species. Activation loop motif starts with a conserved DFG motif (there are two putative motifs in boxes), continues with the T-X_5-T motif, and finishes with the APE motif.

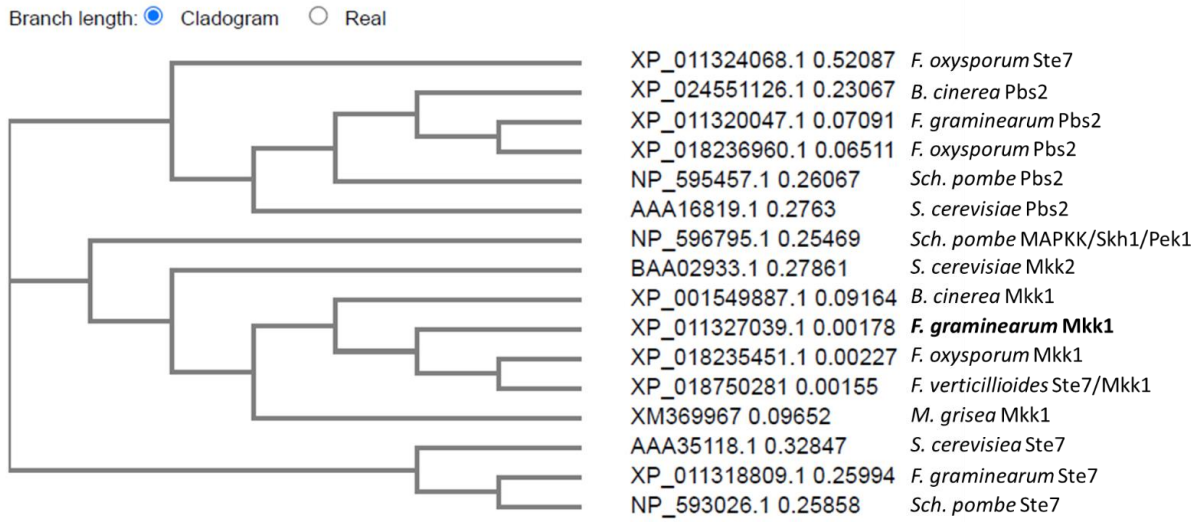

Supplementary Figure 3.2. Phylogenetic tree of *MAPKK* from different fungal species.

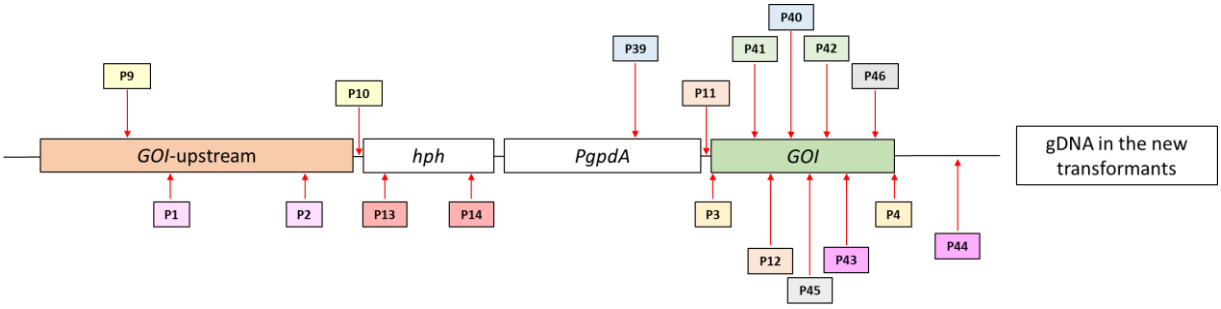

Supplementary Figure 3.3. Scheme representing the position of the primers in the *MKK1_OX* and *MKK1^{EE}_OX* strains. The regions between primers P1-P2 and P3-P4 were those amplified from the gDNA in the WT strain (in the case of *MKK1^{EE}_OX*, the region between P3 and P4 primers was synthesised to include the modification in the activation loop) that were inserted into the vector, and used for homologous recombination. Note that P9 and P4 are located outside of the inserted cassette, and the amplicons flanked by P9-P10 and P45-P46 confirm the right position of the insertion into the genome.

a)

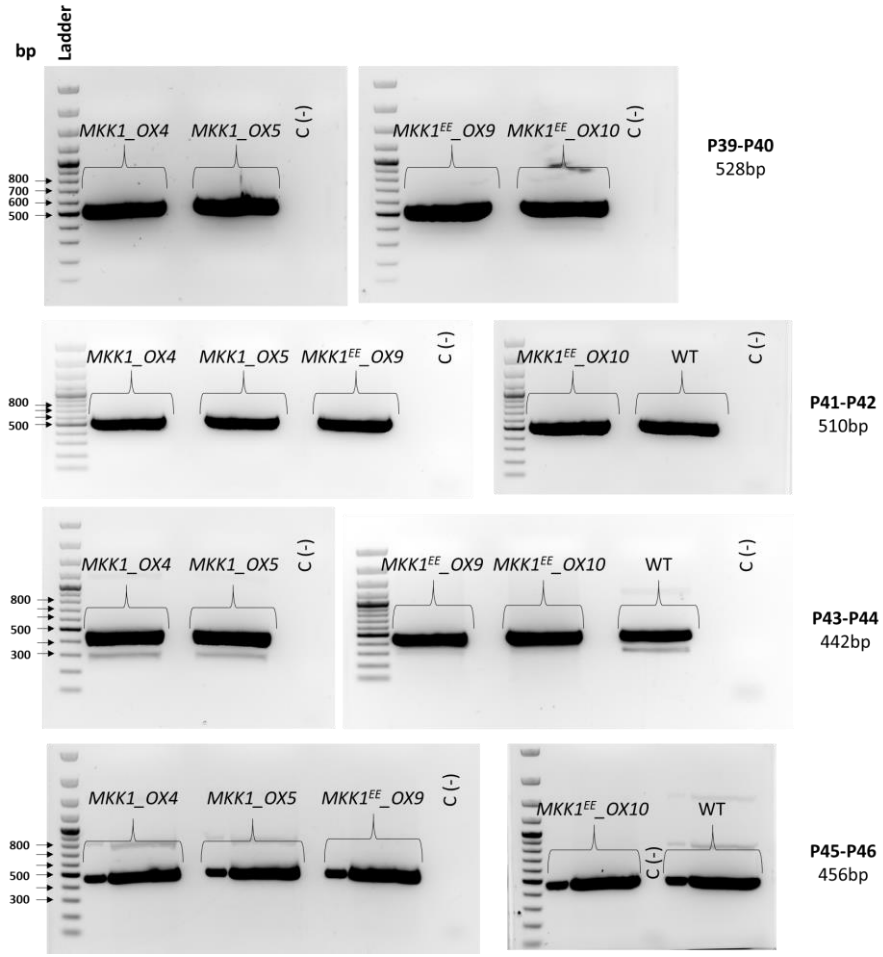

b)

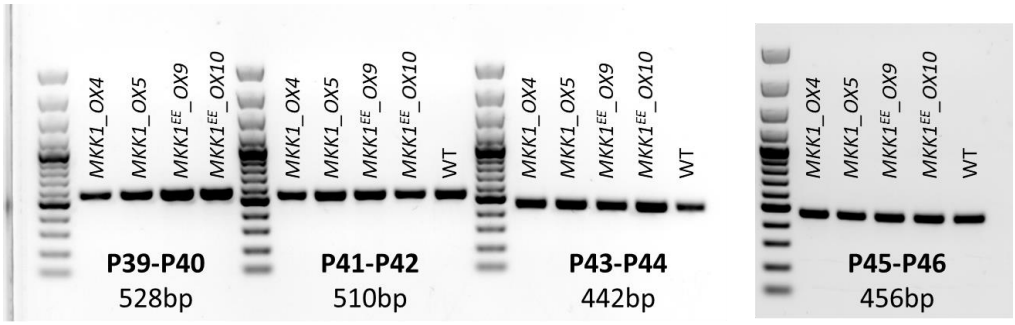

Supplementary Figure 3.4. Amplicons obtained with different set of primers were used for sequencing the HU2E fragment inserted into the WT strain for generating *MKK1_OX* and *MKK1^{EE}_OX* strains. a) PCR results of *MKK1_OX* and *MKK1^{EE}_OX* and the WT strains. b) Bands of purified amplicons sent for sequencing.

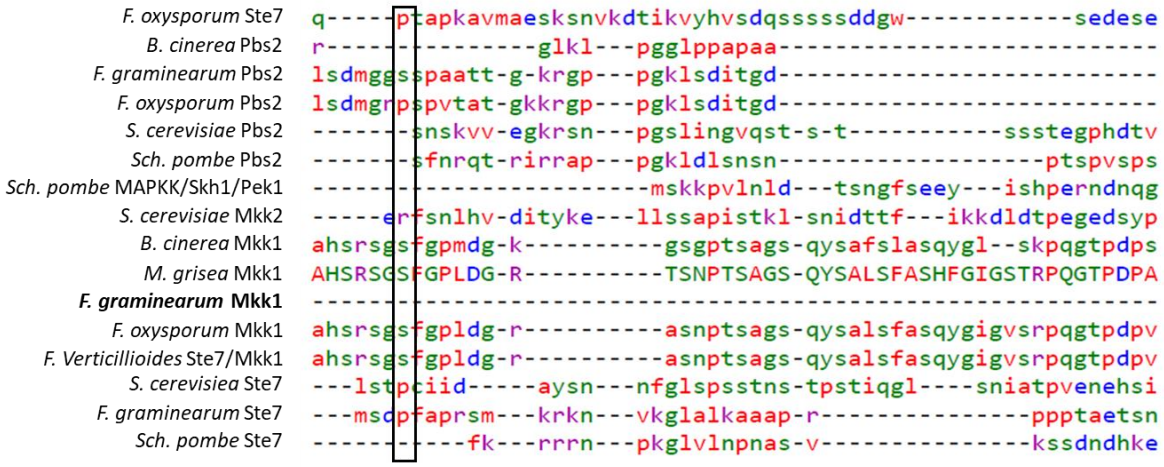

Supplementary Figure 3.5. Alignment of different fungal MAPKK sequences. The box contains the *M. grisea* Ser115 and how it aligns with other sequences. The references used for *M. grisea* (Fujikawa *et al*., 2009) and *M. oryzae* (Yin *et al*., 2020) had the same gene ID 2684637 on NCBI database. The name used in the alignment was *M. grisea*.

Appendix C: supplementary information for chapter 4

Table of contents

Supplementary Table 4.1. Selection of 30 (genes with the highest and lowest Log_2FC value) of the 838 genes differentially expressed when *MKK1* was overexpressed, at a power cut-off of 0.8.

Genes with the highest Log_2FC value

No	gene_id	Log_2FC	PValue	FDR
1	FGSG_03888	5.8750	0.0028	0.0361
2	FGSG_01789	4.0190	0.0001	0.0037
3	FGSG_10675	3.5844	0.0047	0.0479
4	FGSG_07295	3.5621	0.0000	0.0000
5	FGSG_03245	3.3316	0.0001	0.0042
6	FGSG_02036	2.9177	0.0000	0.0011
7	FGSG_09311	2.7265	0.0000	0.0011
8	FGSG_07775	2.6770	0.0000	0.0028
9	FGSG_06728	2.5538	0.0000	0.0023
10	FGSG_10606	2.4206	0.0001	0.0037
11	FGSG_07571	2.3426	0.0004	0.0118
12	FGSG_09041	2.2983	0.0000	0.0011
13	FGSG_08196	2.2954	0.0007	0.0160
14	FGSG_03658	2.2524	0.0007	0.0164
15	FGSG_04563	2.0806	0.0003	0.0095

Genes with the lowest Log_2FC value

No	gene_id	Log_2FC	PValue	FDR
1	FGSG_12204	-3.2999	0.0005	0.0128
2	FGSG_10612	-3.2850	0.0003	0.0089
3	FGSG_01513	-3.2728	0.0035	0.0408
4	FGSG_09051	-3.2571	0.0001	0.0044
5	FGSG_03901	-3.2380	0.0002	0.0066
6	FGSG_02328	-3.2214	0.0019	0.0294
7	FGSG_02111	-3.1946	0.0000	0.0037
8	FGSG_08795	-3.1853	0.0000	0.0022
9	FGSG_03706	-3.1728	0.0000	0.0011
10	FGSG_02327	-3.1422	0.0034	0.0399
11	FGSG_03445	-3.0803	0.0000	0.0015
12	FGSG_07710	-3.0460	0.0007	0.0164
13	FGSG_07988	-3.0216	0.0000	0.0030
14	FGSG_04583	-2.9831	0.0000	0.0015
15	FGSG_02329	-2.9801	0.0030	0.0370

Supplementary Table 4.2. Selection of 30 (genes with the highest and lowest Log_2FC value) of the 461 genes differentially expressed that have a $Log_2FC \geq 0.99$ or $Log_2FC \leq -0.99$, when *MKK1* was overexpressed.

Genes with the highest Log_2FC value

No	gene_id	Log_2FC	PValue	FDR
1	FGSG_03888	5.8750	0.0028	0.0361
2	FGSG_01789	4.0190	0.0001	0.0037
3	FGSG_10675	3.5844	0.0047	0.0479
4	FGSG_07295	3.5621	0.0000	0.0000
5	FGSG_03245	3.3316	0.0001	0.0042
6	FGSG_02036	2.9177	0.0000	0.0011
7	FGSG_09311	2.7265	0.0000	0.0011
8	FGSG_07775	2.6770	0.0000	0.0028
9	FGSG_06728	2.5538	0.0000	0.0023
10	FGSG_10606	2.4206	0.0001	0.0037
11	FGSG_07571	2.3426	0.0004	0.0118
12	FGSG_09041	2.2983	0.0000	0.0011
13	FGSG_08196	2.2954	0.0007	0.0160
14	FGSG_03658	2.2524	0.0007	0.0164
15	FGSG_04563	2.0806	0.0003	0.0095

Genes with the lowest Log_2FC value

No	gene_id	Log_2FC	PValue	FDR
1	FGSG_12009	-4.9342	0.0000	0.0004
2	FGSG_03531	-4.3636	0.0000	0.0005
3	FGSG_03583	-4.1444	0.0002	0.0071
4	FGSG_00260	-3.7878	0.0000	0.0011
5	FGSG_02324	-3.6049	0.0038	0.0420
6	FGSG_02112	-3.4450	0.0000	0.0026
7	FGSG_01512	-3.4367	0.0003	0.0103
8	FGSG_09093	-3.4209	0.0000	0.0011
9	FGSG_03817	-3.4060	0.0000	0.0022
10	FGSG_10613	-3.3168	0.0000	0.0035
11	FGSG_12204	-3.2999	0.0005	0.0128
12	FGSG_10612	-3.2850	0.0003	0.0089
13	FGSG_01513	-3.2728	0.0035	0.0408
14	FGSG_09051	-3.2571	0.0001	0.0044
15	FGSG_03901	-3.2380	0.0002	0.0066

Supplementary Table 4.3. Overview of secondary metabolite gene clusters differentially expressed in *MKK1_OX* and *MKK1*^{197E,203E}*_OX* strains. Heat maps of **(a)** Aurofusarin, **(b)** Butenolide, **(c)** Gramillins, **(d)** Trichothecene, **(e)** *NRPS*, **(f)** *PKS*. A gradient from red tones (lower Log_2FC values) to blue tones (higher Log_2FC values) is showed in the tables, where 0 values represent no change in the expression of the genes.

(a)

Aurofusarin cluster		**Log_2FC**	
Gene name	**gene_ID**	***MKK1_OX***	***MKK1*^{197E,203E}*_OX***
AURR1	FGSG_02320	0	0
AUR0	FGSG_02321	0	0
AURT	FGSG_02322	0	1.7
AURR2	FGSG_02323	0	1.6
PKS12	FGSG_02324	-3.6	0
AURZ	FGSG_02325	0	0
AURJ	FGSG_02326	-2.9	0
AURF	FGSG_02327	-3.1	0
GIP1	FGSG_02328	-3.2	0
AURS	FGSG_02329	-3.0	0
AURL2	FGSG_02330	0	0

b)

Butenolide cluster	**Log_2FC**	
gene ID	***MKK1_OX***	***$MKK1^{197E,203E}$_OX***
FGSG_08077	0	1.4
FGSG_08078	0	1.6
FGSG_08079	1.6	3.0
FGSG_08080	0	1.4
FGSG_08081	1.3	2.7
FGSG_08082	0	1.5
FGSG_08083	2.0	2.9
FGSG_08084	0	2.7

(c)

Gramillin cluster	**Log_2FC**	
gene_ID	***MKK1_OX***	***$MKK1^{197E,203E}$_OX***
FGSG_00036	0	0
FGSG_00039	0	1.1
FGSG_00043	0	0
FGSG_00044	0	0
FGSG_00045	0	0
FGSG_00046	0	0
FGSG_00047	0	0
FGSG_00048	0	0
FGSG_00049	0	0
FGSG_11653	0	0
FGSG_11656	0	0
FGSG_11657	0	-1.6
FGSG_11658	0	0
FGSG_15673	0	0
FGSG_15680	0	0

(d)

Trichothecene cluster		**Log$_2$FC**	
Gene name	**gene_ID**	***MKK1_OX***	***MKK1^{197E,203E}_OX***
TRI1	FGSG_00071	0	0
	FGSG_03527	0	-2.4
Uncharacterized protein with hydrolase activity, hydrolyzing O-glycosyl compounds. Cell wall localization	FGSG_03529	-1.8	-4.7
Tyrosinase_Cu-bd domain-containing protein with oxidoreductase activity	FGSG_03531	-4.4	-6.9
TRI8	FGSG_03532	0	-0.96
TRI7 MBOAT_2 domain-containing protein with O-acyltransferase activity	FGSG_03533	0	-1.8
TRI3 (15-O-Acetyltransferase)	FGSG_03534	0	0
TRI4 Trichodiene oxygenase (Cyt P450)	FGSG_03535	0	0
TRI6 hypothetical protein (transcription factor)	FGSG_03536	0	-0.96
TRI5 trichodiene synthase (sesquiterpene cyclase)	FGSG_03537	0	0
TRI10 hypothetical protein (transcription factor)	FGSG_03538	0	0
TRI9 hypothetical protein	FGSG_03539	0	-0.9
TRI11 Isotrichodermin C-15 hydrolase (Cyt P450 family)	FGSG_03540	0	0
TRI12 Efflux pump	FGSG_03541	0	0
TRI13 (Cyt P450)	FGSG_03542	-2.4	-4.1
TRI14	FGSG_03543	-0.9	0
hypothetical protein	FGSG_03544	-1.2	-1.3
TRI6 transcription factor	FGSG_16251	0	0

(e)

NRPS				**Log_2FC**	
Gene name	**gene_ID**	**cluster**	**Metabolite**	***MKK1_OX***	***$MKK1^{197E,203E}$_OX***
NRPS 1	FGSG_11026	C63	Malonichrome	0	0
NRPS 2	FGSG_05372	C33	Ferricrocin	0	0
NRPS 3	FGSG_10523			0	0
NRPS 4	FGSG_02315		Fusahexin	0	0
NRPS 5	FGSG_17487	C64	Fusaoctaxin A	0	0
NRPS 6	FGSG_03747	C21	Triacetylfusarinin	0	-1.3
NRPS 7	FGSG_08209	C47		0	-3.2
NRPS 8	FGSG_15673	C02	Gramillins	0	0
NRPS 9	FGSG_10990	C64	Fusaoctaxin A	-1.8	0
NRPS 10	FGSG_06507	C38		0	0
NRPS 11	FGSG_03245			3.3	5.2
NRPS 12	FGSG_17574			0	0
NRPS 13	FGSG_13153			0	-1.3
NRPS 14	FGSG_11395	C66		0	0
NRPS 15	FGSG_02394	C15		0	-1.7
NRPS 16	FGSG_15872	C06		0	0
NRPS 17	FGSG_10702			0	0
NRPS 18	FGSG_17386	C61		0	0
NRPS 19	FGSG_15676	C06		0	0

(f)

PKS				**Log$_2$FC**	
Gene name	**gene_ID**	**cluster**	**Metabolite**	***MKK1_OX***	***MKK1^{197E,203E}_OX***
PKS 1	FGSG_04694	C31		-1.2	-1.3
PKS 3	FGSG_17168	C53	Precursor of insoluble perithecial pigment	0	0
PKS 5	FGSG_17677	C34		0	0
PKS 7	FGSG_08795	C44		-3.2	-3.6
PKS 10	FGSG_07798	C42	FusarinC	0	-1.3
PKS 13	FGSG_03340	C26		0	0
PKS 21	FGSG_17387	C61		0	0
PKS 22	FGSG_17745	C15	Zearalenone	0	0
PKS 23	FGSG_08208	C47		0	-4.2
PKS 24	FGSG_10464	C60	Fusarielin	0	-1.1
PKS 25	FGSG_01790	C08		0	0
PKS 26	FGSG_02324	C13	Aurofusarin	-3.6	0
PKS 27	FGSG_15980	C15	Zearalenone	0	0
PKS 28	FGSG_03964	C18	Orcinol/orsellinic acid	0	-1.7
PKS 29	FGSG_04588	C16		0	0

Supplementary Table 4.4. Expression of main genes in the MAPK pathways and other genes associated with these cascades in the *MKK1_OX* and *MKK1^{197E,203E}_OX* strains compared to WT.

			Log$_2$ FC	
Pathway	**Gene name**	**gene_ID**	***MKK1_OX***	***MKK1^{197E,203E}_OXs***
CWI	*WSC1*	FGSG_03574	0.8	1.6
CWI	*WSC2*	FGSG_03884	0	0
CWI	*WSC2B*	FGSG_10787	0	0
CWI	*WSC3*	FGSG_10435	0	0
CWI	Protein with a WSC domain	FGSG_11097	-2.1	-2.4
CWI	*SHO1*	FGSG_09435	0	0
CWI	*PKC1*	FGSG_09660	0	0
CWI	*BCK1*	FGSG_06336	0	0
CWI	*MKK1*	FGSG_07295	3.6	3.6
CWI	*MGV1*	FGSG_10313	0	-
CWI	*RLM1*	FGSG_09339	-0.94	-1.5
CWI	*SWI6*	FGSG_04220	0	0
CWI	*KIN4*	FGSG_11812	0	0
CWI	*SCH9*	FGSG_00472	0	0
CWI	*RIM15*	FGSG_01312	0	0
CWI	*CHS1A*	FGSG_10116	0	0
CWI	*CHS1B*	FGSG_16273	0	0
CWI	*CHS3*	FGSG_10327	0	0
CWI	*CHS4*	FGSG_01272	0	0
CWI	*CHS4*	FGSG_15838	0	0
CWI	*CHS5*	FGSG_01964	-0.8	-1.1
CWI	*CHS6*	FGSG_15914	0	0
CWI	*CHS7*	FGSG_01949	0	0
CWI	Chitin synthase export chaperone	FGSG_02729	0	0
CWI	*FKS1*	FGSG_07946	0	0
CWI	*GEL1*	FGSG_09980	-1.1	-1.6
CWI	*PTC3*	FGSG_10239	0	0
CWI	*MSG5*	FGSG_06977	0	-1.0
CWI	Phosphatase	FGSG_10516	0	0
HOG	*MSB2*	FGSG_05633	0	0
HOG	*SSK2/SSK22*	FGSG_00408	0	0
HOG	*PBS2*	FGSG_08691	0	0
HOG	*HOG1*	FGSG_09612	0	0

Pathway	**Gene name**	**gene_ID**	***MKK1_OX***	***MKK1^{197E,203E}_OXs***
HOG	Phosphatase	FGSG_12867	0	0
GPMK1	*STE11*	FGSG_05484	0	0
GPMK1	*STE7*	FGSG_09903	0	0
GPMK1	*GPMK1*	FGSG_06385	0	0
GPMK1	*MCMI*	FGSG_08696	0	0
GPMK1	*APP* (Phosphatase)	FGSG_03333	1.1	1.6

Supplementary Table 4.5. Selection of 30 (genes with the highest and lowest Log_2FC value) of the 2,890 genes differentially expressed when *MKK1*^{197E,203E}*_OX* was overexpressed, at a power cut-off of 0.8.

Genes with the highest Log_2FC value

No	gene_id	Log_2FC	PValue	FDR
1	FGSG_03888	7.7143	0.0008	0.0057
2	FGSG_10675	6.4915	0.0000	0.0001
3	FGSG_03245	5.1600	0.0000	0.0004
4	FGSG_09311	4.8852	0.0000	0.0000
5	FGSG_02036	4.5265	0.0000	0.0004
6	FGSG_11391	4.3412	0.0011	0.0068
7	FGSG_04563	4.2216	0.0000	0.0000
8	FGSG_07152	4.1089	0.0074	0.0243
9	FGSG_03593	4.0728	0.0001	0.0017
10	FGSG_03592	4.0423	0.0008	0.0055
11	FGSG_08076	4.0144	0.0014	0.0080
12	FGSG_02852	4.0098	0.0030	0.0129
13	FGSG_09041	3.7193	0.0003	0.0033
14	FGSG_03244	3.7189	0.0000	0.0000
15	FGSG_08137	3.6391	0.0000	0.0008

Genes with the lowest Log_2FC value

No	gene_id	Log_2FC	PValue	FDR
1	FGSG_00260	-10.4455	0.0000	0.0000
2	FGSG_12009	-9.7847	0.0000	0.0000
3	FGSG_03586	-8.2049	0.0000	0.0002
4	FGSG_03445	-7.8838	0.0000	0.0000
5	FGSG_04583	-7.6856	0.0000	0.0000
6	FGSG_11517	-7.2073	0.0000	0.0000
7	FGSG_03531	-6.9230	0.0000	0.0003
8	FGSG_07988	-6.7277	0.0000	0.0000
9	FGSG_03211	-6.3317	0.0000	0.0003
10	FGSG_03637	-6.2178	0.0000	0.0003
11	FGSG_10212	-5.9365	0.0000	0.0000
12	FGSG_07710	-5.8472	0.0000	0.0002
13	FGSG_12203	-5.8015	0.0000	0.0012
14	FGSG_09051	-5.7082	0.0000	0.0008
15	FGSG_02112	-5.6013	0.0001	0.0014

Supplementary Table 4.6. Selection of 30 (genes with the highest and lowest Log_2FC value) of the 1,873 genes differentially expressed that have a $Log_2FC \geq 0.99$ or $Log_2FC \leq -0.99$, when *MKK1*^{197E,203E} was overexpressed.

Genes with the highest Log_2FC value

No	gene_id	logFC	PValue	FDR
1	FGSG_03888	7.7143	0.0008	0.0057
2	FGSG_10675	6.4915	0.0000	0.0001
3	FGSG_03245	5.1600	0.0000	0.0004
4	FGSG_09311	4.8852	0.0000	0.0000
5	FGSG_02036	4.5265	0.0000	0.0004
6	FGSG_11391	4.3412	0.0011	0.0068
7	FGSG_04563	4.2216	0.0000	0.0000
8	FGSG_07152	4.1089	0.0074	0.0243
9	FGSG_03593	4.0728	0.0001	0.0017
10	FGSG_03592	4.0423	0.0008	0.0055
11	FGSG_08076	4.0144	0.0014	0.0080
12	FGSG_02852	4.0098	0.0030	0.0129
13	FGSG_09041	3.7193	0.0003	0.0033
14	FGSG_03244	3.7189	0.0000	0.0000
15	FGSG_08137	3.6391	0.0000	0.0008

Genes with the lowest Log_2FC value

No	gene_id	logFC	PValue	FDR
1	FGSG_00260	-10.4455	0.0000	0.0000
2	FGSG_12009	-9.7847	0.0000	0.0000
3	FGSG_03586	-8.2049	0.0000	0.0002
4	FGSG_03445	-7.8838	0.0000	0.0000
5	FGSG_04583	-7.6856	0.0000	0.0000
6	FGSG_11517	-7.2073	0.0000	0.0000
7	FGSG_03531	-6.9230	0.0000	0.0003
8	FGSG_07988	-6.7277	0.0000	0.0000
9	FGSG_03211	-6.3317	0.0000	0.0003
10	FGSG_03637	-6.2178	0.0000	0.0003
11	FGSG_10212	-5.9365	0.0000	0.0000
12	FGSG_07710	-5.8472	0.0000	0.0002
13	FGSG_12203	-5.8015	0.0000	0.0012
14	FGSG_09051	-5.7082	0.0000	0.0008
15	FGSG_02112	-5.6013	0.0001	0.0014

Supplementary Table 4.7. Selection of 30 (genes with the highest and lowest Log_2FC value) of the 1,891 genes differentially expressed when *MKK1_OX* was compared to *MKK1*^{197E,203E}*_OX*, at a power cut-off of 0.8.

Genes with the highest Log_2FC value

No	gene_id	logFC	PValue	FDR
1	FGSG_00260	6.6347	0.0000	0.0000
2	FGSG_03586	5.4648	0.0000	0.0001
3	FGSG_12009	4.8766	0.0000	0.0000
4	FGSG_03445	4.8119	0.0000	0.0000
5	FGSG_04583	4.7873	0.0000	0.0000
6	FGSG_11517	4.5054	0.0000	0.0000
7	FGSG_02139	4.2342	0.0000	0.0001
8	FGSG_13756	3.8495	0.0000	0.0000
9	FGSG_07988	3.7568	0.0000	0.0000
10	FGSG_04335	3.6886	0.0000	0.0001
11	FGSG_03211	3.5212	0.0000	0.0000
12	FGSG_10212	3.4722	0.0000	0.0000
13	FGSG_08824	3.4375	0.0000	0.0005
14	FGSG_10998	3.4040	0.0000	0.0000
15	FGSG_03637	3.3963	0.0006	0.0038

Genes with the lowest Log_2FC value

No	gene_id	logFC	PValue	FDR
1	FGSG_12349	-5.1445	0.0000	0.0004
2	FGSG_01513	-4.9065	0.0000	0.0000
3	FGSG_03583	-4.0011	0.0000	0.0003
4	FGSG_11391	-3.7516	0.0003	0.0023
5	FGSG_09086	-3.4881	0.0001	0.0012
6	FGSG_01512	-3.4150	0.0000	0.0000
7	FGSG_02328	-3.1370	0.0001	0.0013
8	FGSG_04903	-3.1174	0.0000	0.0002
9	FGSG_09595	-3.0682	0.0004	0.0032
10	FGSG_02326	-3.0611	0.0001	0.0013
11	FGSG_02329	-3.0317	0.0001	0.0014
12	FGSG_07152	-3.0057	0.0012	0.0063
13	FGSG_02327	-2.9777	0.0003	0.0024
14	FGSG_02322	-2.9254	0.0000	0.0001
15	FGSG_10675	-2.8510	0.0002	0.0020

Supplementary Table 4.8. Selection of 30 (genes with the highest and lowest Log_2FC value) of the 854 genes differentially expressed that have a $Log_2FC \geq 0.99$ or $Log_2FC \leq -0.99$, when *MKK1_OX* was compared to *MKK1*^{197E,203E}*_OX*, at a power cut-off of 0.8.

Genes with the highest Log_2FC value

No	gene_id	logFC	PValue	FDR
1	FGSG_00260	6.6347	0.0000	0.0000
2	FGSG_03586	5.4648	0.0000	0.0001
3	FGSG_12009	4.8766	0.0000	0.0000
4	FGSG_03445	4.8119	0.0000	0.0000
5	FGSG_04583	4.7873	0.0000	0.0000
6	FGSG_11517	4.5054	0.0000	0.0000
7	FGSG_02139	4.2342	0.0000	0.0001
8	FGSG_13756	3.8495	0.0000	0.0000
9	FGSG_07988	3.7568	0.0000	0.0000
10	FGSG_04335	3.6886	0.0000	0.0001
11	FGSG_03211	3.5212	0.0000	0.0000
12	FGSG_10212	3.4722	0.0000	0.0000
13	FGSG_08824	3.4375	0.0000	0.0005
14	FGSG_10998	3.4040	0.0000	0.0000
15	FGSG_03637	3.3963	0.0006	0.0038

Genes with the lowest Log_2FC value

No	gene_id	logFC	PValue	FDR
1	FGSG_12349	-5.1445	0.0000	0.0004
2	FGSG_01513	-4.9065	0.0000	0.0000
3	FGSG_03583	-4.0011	0.0000	0.0003
4	FGSG_11391	-3.7516	0.0003	0.0023
5	FGSG_09086	-3.4881	0.0001	0.0012
6	FGSG_01512	-3.4150	0.0000	0.0000
7	FGSG_02328	-3.1370	0.0001	0.0013
8	FGSG_04903	-3.1174	0.0000	0.0002
9	FGSG_09595	-3.0682	0.0004	0.0032
10	FGSG_02326	-3.0611	0.0001	0.0013
11	FGSG_02329	-3.0317	0.0001	0.0014
12	FGSG_07152	-3.0057	0.0012	0.0063
13	FGSG_02327	-2.9777	0.0003	0.0024
14	FGSG_02322	-2.9254	0.0000	0.0001
15	FGSG_10675	-2.8510	0.0002	0.0020